Functional Characterization of the Human Hippocampal Long Axis Using Within-Individual Precision Neuroimaging

Citation

Angeli, Peter A. 2023. Functional Characterization of the Human Hippocampal Long Axis Using Within-Individual Precision Neuroimaging. Doctoral dissertation, Harvard University Graduate School of Arts and Sciences.

Permanent link

https://nrs.harvard.edu/URN-3:HUL.INSTREPOS:37378043

Terms of Use

Share Your Story

HARVARD UNIVERSITY
Graduate School of Arts and Sciences

DISSERTATION ACCEPTANCE CERTIFICATE

The undersigned, appointed by the

Division of Medical Sciences

Program in Neuroscience

have examined a dissertation entitled

Functional Characterization of the Human Hippocampal Long Axis Using Within-Individual Precision Neuroimaging

presented by Peter A. Angeli

candidate for the degree of Doctor of Philosophy and hereby certify that it is worthy of acceptance.

Signature: *Mark Andermann*
Mark Andermann (Jun 22, 2023 16:03 EDT)

Typed Name: Dr. Mark Andermann

Signature: *Elizabeth A. Phelps*
Elizabeth A. Phelps (Jun 23, 2023 14:04 EDT)

Typed Name: Dr. Elizabeth Phelps

Signature: *Amar Sahay*
Amar Sahay (Jun 22, 2023 12:18 EDT)

Typed Name: Dr. Amar Sahay

Signature: Chantal Stern

Typed Name: Dr. Chantal Stern

Date: June 13, 2023

Functional Characterization of the Human Hippocampal Long Axis Using Within-Individual

Precision Neuroimaging

A dissertation presented

by

Peter A. Angeli

to

The Division of Medical Sciences

in partial fulfillment of the requirements

for the degree of

Doctor of Philosophy

in the subject of

Neurobiology

Harvard University

Cambridge, Massachusetts

June 2023

Dissertation Advisor: Dr. Randy L. Buckner   Peter A. Angeli

Functional Characterization of the Human Hippocampal Long Axis Using Within-Individual

Precision Neuroimaging

Abstract

This dissertation describes my efforts towards a precise network-informed functional

characterization of the human hippocampal long axis, made possible by advances in within-

individual precision human neuroimaging. In the Introduction, I describe foundational work that

has proposed the differential involvement of hippocampal regions in diverse cognitive functions

including episodic memory, spatial reasoning, and assessing novelty. While a definitive account of

hippocampal function will remain elusive, I will argue it is both conceptually important and

experimentally useful to study the functional roles of the hippocampus in the context of associated

networks precisely estimated in cerebral cortex.

The first two chapters highlight the neuroimaging techniques necessary for precisely

estimating hippocampal network organization and function. These chapters focus on the

cerebellum, in part because that was my own introduction to these methods, but also because these

methods' success given the cerebellum's polysynaptic connectivity to cortex and fine structural

details strengthens the case for their use in the hippocampus. Chapter 1 uses functional

neuroimaging techniques to explore the organization of the human cerebellum based on network

functional connectivity. Chapter 2 applies within-individual neuroimaging of the cerebellum to

simple motor tasks. In both cases, exploring a small set of densely sampled individuals allowed all

analyses to respect each participant's idiosyncratic anatomy, improving resolution and allowing for the characterization of functional and organizational details that would have been missed using approaches which spatially average data across participants.

Chapter 3 applies these techniques to the hippocampal long axis across two independent sets of densely sampled individuals. We first demonstrate differential functional connectivity from the anterior and posterior hippocampus to distinct cerebral networks DN-A and SAL / PMN, respectively. Task data then reveals a double-dissociation: the anterior hippocampus is preferentially involved in the construction of mental scenes, while the posterior hippocampus displays transient activation in response to salient stimuli. These parallel dissociations in functional connectivity and cognitive function position the anterior and posterior hippocampus as separable components of broader brain networks and refines our understanding of hippocampal contributions to human cognition.

Table of Contents

Acknowledgments

The creation of this dissertation has relied heavily on an entire village of mentors, teachers, collaborators, friends, and friendly strangers. It strikes me as unfair that only my name is on the cover, so to make up for that I'll attempt here as best I can to thank everyone who has helped me develop as a scientist and person.

I'd like to start by thanking my advisor Randy Buckner, who has shown remarkable patience and insight guiding me through my graduate career. I will always be inspired by your dedication to scientific rigor, adherence to biological first principles, and fundamental respect for the privilege of being able to unravel Mother Nature's mysteries. I could not have asked for a better mentor to teach me to be scholarly, and to foster a community of respect, collaboration, and excitement about science.

Thank you to my dissertation advisory committee – Mark Andermann, Rick Born, and Dan Schacter – who have been nothing but supportive every step of the way, and whose intellectual generosity and kindness have been invaluable in helping me navigate this project. Thank you to my program advisors Roz Segal and John Assad for their advice, and for always assuring me that it'll all work out. Thank you to my undergraduate research mentor Michela Gallagher, and to all the mentors I've been fortune enough to work with along the way – Scott Boitano, Pawel Kiela, Nicholas Zachos, Kun Ping Lu, Amar Sahay, and Bob Datta.

To Lauren DiNicola, thank you for your endless enthusiasm, guidance, and friendship, which you've offered cheerfully from the very first moment I stepped in the lab. To the entire Buckner lab past and present – Arpi, Hannah, Emily, Aya, Kayla, Francesca, Stephanie, Joanna, Mark, Lindsay, Habib, Garth, Rod, Jingnan, Kevin, Noam, Max, Rim, Heather, Cony, Wendy, Alaric, Izzy, Katherine, Tobi, Sam – and everyone at CBS – Tammy, Ross, Caroline, Larry, Jenn – thank you for everything. Without your work and support, none of this would exist.

Introduction

The hippocampus, nestled along the medial portion of the temporal lobe, has been the subject of intense neurophysiological study for the better part of the last century. In that time, our understanding of the functional role of the human hippocampus had improved alongside the tools and methods we use to study it. The field has pushed towards increasingly nuanced views of both the hippocampus itself and its role within larger brain networks. In particular, significant support has emerged for differential connectivity and function along the hippocampal long axis, which runs from posterior to anterior in primates, as well as the homologous septo-temporal axis in rodents which runs from the dorsal (septal) to the ventral (temporal) pole. The work described in this dissertation builds upon the existing literature by leveraging recent advances in within-individual precision neuroimaging to robustly and extensively explore the functional specialization of the hippocampal long axis in humans.

Connections to the hippocampus from the vast majority of cerebral cortex first pass through portions of the parahippocampal region, which includes parahippocampal cortex (PHC), perirhinal cortex (PRC), and entorhinal cortex (EC). The EC in particular serves as the primary source of inputs for, and target of outputs from, the hippocampus: it receives connections from distributed portions of neocortex including PHC and PRC, and sends axons back to these same regions (Amaral and Witter 1989; Insausti et al. 1987; Suzuki and Amaral 1994; Witter 1993). Within the hippocampus, information flows through a trisynaptic circuit starting with projections from the EC to granule cells in the dentate gyrus (DG), which then send axons to the Cornus Ammonis 3 (CA3) subfield. From there, CA3 neurons synapse both onto other CA3 neurons as well as neurons in the CA1 subfield, which complete the loop by projecting back to the EC via the subiculum. This circuit is structured perpendicular to the long axis, and is present along the entire length of the hippocampus in all animals. The stereotyped connectivity of this circuit, along with its penchant for hyperactivity,

has long made the hippocampus an appealing target for electrophysiological study, and was eventually the structure in which long-term potentiation was first described (Bliss and Lømo 1973). Beyond that however, early work considered the hippocampus primarily in the context of the broader "limbic lobe" described by Paul Broca in 1878 (Broca 2015), hypothesized to be primarily concerned with olfaction (Green 1964)

Studies of hippocampal function began in earnest in the early 20th century, when Klüver and Bucy characterized a syndrome of impairments resulting from bilateral damage to the medial temporal lobe (including the hippocampus) in macaques (Klüver and Bucy 1939). The impairments, while consistent across animals, were unfortunately too broad to assign to any one common cause, or fully integrate into a cohesive view of medial temporal lobe function. Instead, the seminal breakthrough would come nearly 20 years later when Brenda Milner and colleagues characterized profound memory deficits in a patient called H.M. after a bilateral medial temporal lobe resection to treat his seizures (Milner et al. 1968; Scoville and Milner 1957). H.M.'s general intelligence appeared unchanged after the surgery, but he had impaired recall for events or facts from the years immediately before his operation, and a complete inability to form any new memories of this type. Scoville and Milner (1957) noted across additional patients that the degree of memory impairment seemed to correlate with the extent of hippocampal damage, suggesting a role for the hippocampus specifically in human memory. However, this view was complicated by the frequent damage in these individuals to the amygdala, located just anterior to the hippocampus, as well as the relatively less severe memory deficits observed in a patient with more focal damage restricted to hippocampal CA1 (Zola-Morgan et al. 1986).

The debate between the amygdala and the hippocampus as the seat of memory was the subject of intense study in the subsequent years, culminating in a series of precise lesion studies in macaques which identified the hippocampus and its surrounding cortical input regions (EC, PHC, and PRC), rather than the amygdala, as the critical portions of the medial temporal lobe memory

system (Squire 1992). Subsequent computational explorations of the hippocampal circuit revealed a system remarkably well suited for storing mnemonic information: granule cells in the DG are capable of producing sparse, unique representations for information, while neurons in CA3 are able to complete representations from partial information using the recurrent collaterals onto other CA3 neurons (Treves and Rolls 1994). Indeed, recent studies showing that optogenetic stimulation of DG granule cells appears to result in memory recall in rodents suggests these cells may be capable of storing a neural representation of a memory, or an "engram" (Liu et al. 2012; Ramirez et al. 2013).

In parallel with the lesion studies in humans and non-human primates described above, other researchers were exploring the sensitivity of the hippocampus to space through precise electrophysiological recordings. In 1971, O'Keefe and Dostrovsky found that some hippocampal neurons selectively fired when the animal was in specific portion of their enclosure, which they called the neuron's "place field" (O'Keefe 1976; O'Keefe and Burgess 1996; O'Keefe and Dostrovsky 1971). The location of a neuron's place field is generally stable, but can be shifted or warped if important features of the environment change (like the size of the enclosure, or the location of salient landmarks) (Muller and Kubie 1987; O'Keefe and Burgess 1996). This suggests that place fields likely rely on an internal model of the animal's environment, rather than only representing the animal's position in space using interoceptive motion cues. In addition, some neurons in the EC also show a stereotyped responsivity to space, this time with a pattern of firing that resembles a hexagonal grid tiling the entirety of the animal's environment (Fyhn et al. 2004; Hafting et al. 2005).

The diverse body of work exploring hippocampal function, including through the lens of memory, space, or even general novelty and expectation mismatch (Fyhn et al. 2002; Knight 1996; Rolls et al. 1989), presents several alternative paths for further explorations. One path, which may well be the end goal of the field, is to seek a unified model of hippocampal function that synthesizes the results across all these cognitive domains (e.g. Eichenbaum 2000; Eichenbaum and Cohen 2014;

Whittington et al. 2020). However, in many cases the more immediately tractable approach is to continue refining our understanding of not only which cognitive processes involve the hippocampus, but also the specific portions of the hippocampus they recruit. And as mentioned above, one notable spatial dimension along which the hippocampus has frequently been observed to vary in both connectivity and function is the long axis.

Evidence for Hippocampal Heterogeneity Along the Long Axis

Anatomical tracing studies in rat have found notable differences in the intrinsic and extrinsic connectivity of the dorsal and ventral hippocampus. Ipsilateral projections from neurons in the dorsal two-thirds of the hippocampus nearly exclusively terminate on other neurons in the dorsal two-thirds, while neurons in the ventral one-third similarly project primarily to other neurons in the ventral one-third (Fricke and Cowan 1978). In addition, connectivity from EC varies smoothly along the long axis. The ventral rodent hippocampus primarily receives inputs from the medial portion of lateral entorhinal cortex (LEC) and the rostral portion of medial entorhinal cortex (MEC), while the dorsal hippocampus receives inputs from the spatially opposite lateral LEC and caudal MEC, and the middle of the hippocampus sits in between and receives inputs from intermediate regions of both LEC and MEC (Dolorfo and Amaral 1998).

Research within macaques, which have hippocampal and parahippocampal anatomy more like humans, has further supported connectivity differences to the EC along the hippocampal long axis. The anterior hippocampus (homologous to the rodent ventral hippocampus) primarily receives projections from and sends projections to anterior-medial EC, while the posterior hippocampus (homologous to rodent dorsal) is preferentially connected to posterior-lateral EC (Witter et al. 1989; Witter and Amaral 2021). These results are particularly interesting when taken together with work showing that the anterior-medial and posterior-lateral EC receive connections

4

from different portions of cerebral cortex (Insausti and Amaral 2008), potentially suggesting differences in the cortical connectivity of the anterior and posterior hippocampus.

Evidence of Hippocampal Long Axis Specialization

While explorations of differential functional contributions along the long axis in non-human primates are limited, a rich literature in other mammals strongly supports the functional relevance of the observed anatomical heterogeneity in the hippocampus. On a purely cellular level, neurons in the dorsal and ventral hippocampus of cats and rats display markedly different firing properties in response to electrical or chemical stimulation meant to produce epileptiform activity (Elul 1964; Racine et al. 1977). In addition, rats with lesions in the dorsal hippocampus display more pronounced deficits in a spatial Morris water maze task than animals with ventral lesions, possibly indicating the preferential involvement of the dorsal hippocampus in representing space (Moser et al. 1993, 1995). While this view is consistent with O'Keefe and Dostrovsky's initial work which characterized place fields in specifically dorsal hippocampal neurons (O'Keefe 1976; O'Keefe and Dostrovsky 1971), subsequent work has identified neurons with place fields throughout the hippocampal long axis (Jung et al. 1994), suggesting that the ventral hippocampus may also be involved in spatial representations.

Importantly, this doesn't necessarily mean the dorsal and ventral hippocampus are involved in the same kinds of spatial processing. The place fields of neurons in the ventral hippocampus are larger than those of neurons in the dorsal hippocampus (Jung et al. 1994; Kjelstrup et al. 2008), indicating these two regions may be representing different spatial scales. Within the spatial domain, the differential involvement of the dorsal and ventral hippocampus is supported by results from complex tasks which include spatial elements. Rats with dorsal lesions are slower to learn a one-way active avoidance paradigm (Nadel 1968), but impairment on a spatial probability task only occurs in animals with ventral lesions (Stevens and Cowey 1973). Unfortunately, assessing the

extent to which these hippocampal differences in spatial processing apply to humans can be somewhat muddled by both the comparative lack of long axis functional characterizations in non-human primates, as well as the frequent use in rodent studies of an animal's movement through space as a given task's behavioral readout.

Using Neuroimaging to Study the Human Brain

In humans, we generally must rely on non-invasive measures in order to study the structure and function of the brain. Prominent among these methods, and the technique of choice for this thesis, is magnetic resonance imaging (MRI) which relies on a number of advancements in physics and engineering (Damadian 1971; Lauterbur 1973; Mansfield 1977; Rabi et al. 1938) to produce an anatomical image of the brain. Purely structural MRI is incredibly valuable for assessing damage to the brain or characterizing other broad structural features, but isn't able to measure cellular activity or inform discussions of connectivity beyond following the major fiber tracts that would be visible to naked eye in a dissected brain. To learn more, we can use a technique called functional MRI (fMRI) to indirectly measure neural activity via changes to the properties of blood in vessels near the activity (Kwong et al. 1992; Ogawa et al. 1992). When cells in the brain become more active, the circulatory system over-supplies the area of activation with oxygenated blood (Fox and Raichle 1986), and we can visualize that increase with a blood oxygenation level-dependent (BOLD) MRI contrast. This contrast produces a larger signal in oxygenated vs deoxygenated blood, due to the magnetic properties of deoxyhemoglobin (Ogawa et al. 1990).

Even considering the indirect nature of using the BOLD signal in fMRI as a measure for neural activity, its usefulness is immediately apparent especially when you consider the ability to measure this signal across the entire brain simultaneously. This whole-brain acquisition is the basis for functional connectivity, pioneered by Biswal and colleagues (1995), which correlates low frequency (<0.1Hz), spontaneous oscillations in BOLD signal across the brain (see also Buckner et

al. 2013; Fox and Raichle 2007; Murphy et al. 2013). This application of fMRI has proved to be particularly useful because it has been shown to be sensitive to actual anatomical connectivity. Several known patterns of polysynaptic connectivity have been recapitulated using functional connectivity, including connections between motor cortex and the contralateral cerebellum (Buckner et al. 2011; anatomical study: Kelly and Strick 2003), the hierarchical oculomotor pathway (Vincent et al. 2007; anatomical study: Maunsell and van Essen 1983), and differential cross-hemispheric connectivity in somatomotor cortex (Yeo et al. 2011; anatomical study: Pandya and Vignolo 1971). Further, in patients with damage to specific pathways, the functional connectivity correlations between regions connected by those pathways are reduced compared to controls (Johnston et al. 2008; Lu et al. 2011; Quigley et al. 2003), supporting the connection between functional and anatomical connectivity.

One appealing structure to highlight both the functional and anatomical relevance of fMRI is the cerebellum, particularly in the context of motor movements. Early work recording electrical responses in the cerebellum of cats and macaques after tactile stimulation or limb movement found a topographic map of the body in both the anterior and posterior lobe (Adrian 1943; Snider and Stowell 1944). Further work in macaques has noted that both these body maps form closed-loop, polysynaptic circuits with primary motor cortex via the pons and ventrolateral thalamus (Evarts and Thach 1969; Kelly and Strick 2003). Thus, the somatomotor cerebellum presents a compelling test case for the strengths of fMRI: an extensively studied and accepted polysynaptic circuit between spatially distant brain regions, with known functional properties. Indeed, fMRI studies have shown topographically-organized increases in BOLD signal in both the anterior and posterior lobes of the human cerebellum during movement (Grodd et al. 2001), and have replicated the two body maps based on functional connectivity to the body maps in primary motor cortex (Buckner et al. 2011).

Neuroimaging Studies of the Hippocampus

fMRI is an equally compelling tool for studying the hippocampus, given its polysynaptic connectivity to cortex and implication in complex cognition. Applied to the hippocampus, functional connectivity studies have found the anterior hippocampus (used here to include the head and the body of the hippocampus) is correlated with posterior lateral parietal and ventral medial prefrontal cortex (Barnett et al. 2021; Frank et al. 2019; Kahn et al. 2008), and some studies have shown anterior hippocampal correlations with retrosplenial cortex (Frank et al. 2019; Kahn et al. 2008) and a portion of dorsolateral prefrontal cortex (Barnett et al. 2021; Frank et al. 2019). These explorations of anterior hippocampal functional connectivity also identify correlations to a broad swath of antero-medial and -lateral temporal cortex, but these findings may be confounded by the proximity of anterior temporal cortex to the anterior hippocampus, along with signal dropout resulting in low signal-to-noise in these regions. Compared to the anterior hippocampus, functional connectivity analyses of the posterior hippocampus have been less convergent, but there is evidence for coupling of the posterior hippocampus to posterior and anterior cingulate cortex, as well as posteromedial cortex (Barnett et al. 2021)

Human fMRI studies on the functional specialization of the hippocampal long axis have, like similar studies in animals, characterized a wide range of dissociations (for review see Poppenk et al. 2013). Lesion case studies had already linked declarative memory and the hippocampus in humans (Milner et al. 1968; Scoville and Milner 1957; Zola-Morgan et al. 1986), so neuroimaging studies began looking for differential activation within the hippocampus for different components of declarative memory. A natural division within this research is between the initial exposure to the to-be-remembered item or event (encoding) and the subsequent use of the memory for that item or event (retrieval), but neuroimaging results supporting a mapping of this dissociation onto the hippocampal long axis have been mixed. One meta-analysis of early positron emission tomography (PET) studies showed activation primarily within the anterior hippocampus during encoding, and

within the posterior hippocampus during retrieval (Lepage et al. 1998). Not long after, however, an fMRI meta-analysis identified the opposite association, with preferential activation in the posterior hippocampus during memory encoding (Schacter and Wagner 1999). Further study has not cleared up this ambiguity: a more recent meta-analysis of fMRI studies covering several different types of encoding and retrieval identified left anterior hippocampal activity during both encoding and retrieval, but no clear pattern of activation in the posterior hippocampus (Spaniol et al. 2009), while in contrast structural imaging has found a positive correlation between the size of the posterior hippocampus and recollective memory performance (Poppenk and Moscovitch 2011).

Human MRI studies of the hippocampal long axis in relation to space and navigation have had some more success. A number of studies across both structural and functional MRI have suggested a larger role for the posterior than the anterior hippocampus in spatial reasoning and navigation (Maguire et al. 1997, 1998, 2000; Ryan et al. 2010). But, as in rodents, the division in spatial processing between the anterior and posterior hippocampus may be more a matter of degree than a sharp dissociation. Much of the structural evidence for a dissociation in spatial processing along the long axis comes from studies of taxis drivers in London, who are a required to pass a comprehensive test of London's roads prior to being granted a license. Compared to control individuals from the general populace, taxi drivers had larger posterior hippocampal volumes, and smaller anterior hippocampal volumes (Maguire et al. 2000). This structural change in the hippocampus seems to be a direct result of their studies and continued experience navigating London (Woollett and Maguire 2011), and comes with an interesting behavioral pattern on spatial memory tests. As expected, taxi drivers were significantly better than controls on tests of spatial relationships in London, but were surprisingly worse than controls on spatial association tasks not related to their expertise (Woollett and Maguire 2011, 2012).

This simultaneous behavioral and structural change is compelling evidence that the human hippocampus is differentially representing space. But measurements of brain activity, including

indirectly through fMRI, were necessary to implicate the anterior or posterior hippocampus specifically in a particular function. In that vein, fMRI studies have found evidence for a coarse-to-fine spatial gradient from anterior to posterior (Brunec et al. 2018; Hirshhorn et al. 2012), consistent with the observed differences in place fields along the rodent long axis. In addition, during a flexible navigation task in a familiar environment, trials where an individual accurately navigated showed increased posterior hippocampal activity compared to trials with less accurate navigation (Hartley et al. 2003). On the other hand, increased anterior hippocampal activity distinguished individuals that were generally better at flexible navigation from individuals with worse overall performance (Hartley et al. 2003). These results, along with those from taxi drivers, seem to indicate the involvement of the anterior hippocampus in large-scale or non-specific spatial processing, while the posterior hippocampus may be involved in more local or specific processing.

Contributions from the Whole Brain

Given the connectivity between the hippocampus and cerebral cortex, along with the differential connectivity of the anterior and posterior portions, it seems likely that the regions of the hippocampus function as part of a broader network. Early fMRI studies identified a broad set of cerebral regions that were active during successful retrieval in a memory task, notably including inferior parietal cortex near Brodmann's Area (BA) 39 or 40 (Dobbins et al. 2003; Kahn 2004; Konishi et al. 2000; Wagner et al. 2005; Wheeler and Buckner 2003), dorsolateral prefrontal cortex near BA 8 (Dobbins et al. 2003; Kahn 2004), and a large portion of the posterior midline including retrosplenial cortex (Wagner et al. 2005). Shortly after, functional connectivity studies described the coupling of the hippocampus to a topographically similar pattern of cortical regions (Greicius et al. 2004; Vincent et al. 2006), providing a potential connectivity link between this cerebral network and the hippocampus, in addition to a shared functional implication in memory.

Interestingly, both the hippocampus and the associated cortical regions described above are similarly engaged by both remembering our past and imagining our future (Addis et al. 2007; Okuda et al. 2003; Schacter et al. 2007). At least three frameworks have been proposed for understanding this similarity that each emphasize slightly different features of the experience of recollection and prospection (for review see Schacter et al. 2008). In my discussion below, I've chosen not to include the self-projection theory proposed by Buckner and Carroll (2007) because it, at least in part, is based off Theory of Mind tasks since shown to primarily recruit a cerebral network closely interdigitated with, but distinct from, the network involved in past and future thought (DiNicola et al. 2020).

One proposal from Dan Schacter and Donna Rose Addis is that the recombination of details from our relevant experienced past is the core common process supporting both our memory of the past and our simulation of the future (Schacter and Addis 2007a, 2007b). Indeed, that our memory of the past is constructive (rather than a more precise replay) seems disadvantageous until one considers the usefulness and flexibility of applying this same process to predicting outcomes in our own future. On the other hand, Demis Hassabis and Eleanor Maguire suggested the construction of coherent scenes ("scene construction") as the critical cognitive process, notably independent from the involvement of the self or temporal relation to the present (Hassabis and Maguire 2007). Critically, they found that patients with hippocampal lesions were impaired not only in remembering their past and imagining their future, but also in their ability to imagine completely fictitious scenes with no explicit temporal relation to the present (Hassabis et al. 2007b). Further, in individuals without hippocampal damage, imagining these types of fictious events produced activations in both the hippocampus and the core cortical network implicated in past and future thinking (Hassabis et al. 2007a).

In light of Hassabis and Maguire's scene construction proposal, as well as the extensive body of work described above implicating the hippocampus in spatial processing, it's valuable to

mention some of the data on the cortical areas involved in scene processing. Notably, Epstein, Kanswisher and colleagues found that a portion of the PHC, called the parahippocampal place area (PPA), responded more strongly when individuals viewed a scene than when they viewed objects or faces (Epstein et al. 1999; Epstein and Kanwisher 1998). Later work expanded scene-selective cortex into a potential network including not only PPA, but also retrosplenial cortex and posterior parietal cortex (Epstein 2008; Nasr et al. 2011). All three of these regions are situated just posterior to the regions which display functional connectivity to the hippocampus and are implicated in episodic simulation or scene construction. Interestingly, the PPA has been shown to be active even when individuals just imagine places (O'Craven and Kanwisher 2000), possibly indicating a bridge between scene perception and internal scene construction.

Keeping Analyses Within an Individual Improves Resolution

In the studies described above, the utility of fMRI in estimating neural connectivity and activity has always pushed up against the limitations of the technology, and in particular the issue of resolution. While at first approximation this may seem to be a purely technical barrier which requires improved MRI machines and acquisition parameters to overcome, there's also an important experimental component. Traditionally, fMRI studies focused on association cortex have often relied on collecting relatively small amounts of data from a large pool of subjects, and then averaging that data together to separate signal from noise. This approach has the advantage of minimizing the burden placed on each participant while also isolating the common features within a large sample, improving generalizability. But group averaging comes at a cost to resolution: even after registration to fit a common template, each individual will have idiosyncratic differences in anatomy, meaning an average taken at any given common template point will actually be averaging across slightly different portions of the brain.

To avoid this hit to resolution, studies focusing on cerebral networks have increasingly begun following the lead of researchers mapping early visual cortex (DeYoe et al. 1996; Engel et al. 1997; Tootell et al. 1998; Wandell et al. 2007) and localizing language (Fedorenko et al. 2010) by collecting enough data fully within individuals to no longer require group averaging to produce sufficient signal. Within-individual experimentation has allowed for improved resolution on the cerebral surface, resulting in more precise estimates of distributed cortical networks using functional connectivity (Laumann et al. 2015; Gordon et al. 2017; Braga and Buckner 2017). This improved precision led to the identification of two closely interdigitated networks within the bounds of the canonical default network, which have most likely been conflated in the group averaged data, called default network A (DN-A) and default network B (DN-B) (Braga and Buckner 2017). DN-A includes posterior parahippocampal cortex, immediately positioning it as a network of interest for the hippocampus, as well as retrosplenial, ventral medial prefrontal, inferior parietal, and a portion of dorsolateral prefrontal cortex. The topography of DN-A closely mirrors the pattern of activation previously associated with memory retrieval (e.g. Wagner et al. 2005), functional connectivity from the hippocampus generally (Greicius et al. 2004; Vincent et al. 2006), and correlations from the anterior hippocampus specifically (Barnett et al. 2021; Frank et al. 2019; Kahn et al. 2008), further supporting the relevance of DN-A in the study of the hippocampus.

Similar to DN-A, a within-individual approach has allowed us to recently identify a network which consists of regions within the previously described Salience Network (SAL, Seeley 2019; Seeley et al. 2007) and Parietal Memory Network (PMN, Gilmore et al. 2015), which we call SAL / PMN (Du et al. In Prep). SAL / PMN includes the anterior and posterior cingulate and dorsomedial prefrontal cortex, along with the anterior insula and posteromedial cortex. The grouping of these regions in group-averaged functional connectivity was highly inconsistent, likely because several networks were being blurred together (e.g. Doucet et al. 2011; Power et al. 2011; Shirer et al. 2012; Yeo et al. 2011). Functional connectivity within individuals, however, consistently identified SAL /

PMN as a unified network, rather than separate SAL and PMN, across two independent sets of data (Du et al. In Prep), while also dissociating it from the nearby Cingulo-Opercular Network (see Seeley 2019).

An improved understanding of cerebral cortical organization is, in and of itself, a valuable contribution of precision neuroimaging within individuals. But the power of this method becomes even more apparent when characterizing the preferential association of certain cognitive processes with these precisely defined networks. Following up on the networks identified by Braga and Buckner (2017), DiNicola et al. (2020) explored, within individuals, activity during episodic projection (or simulation) tasks and Theory of Mind tasks which involved inferring other's mental states. These tasks were chosen because they had been shown in group-averaged data to engage slightly different portions of broad cerebral regions which now, in individuals, show a close interdigitation of DN-A and DN-B (Andrews-Hanna et al. 2014; Rabin et al. 2010). Therefore, these episodic projection and Theory of Mind tasks were a compelling test for the functional relevance of these newly defined precise cerebral networks. Remarkably, DN-A and DN-B displayed a robust functional double-dissociation: the entirety of DN-A was preferentially recruited for episodic projection over Theory of Mind, while all of closely interdigitated DN-B was more active for Theory of Mind than episodic projection (DiNicola et al. 2020).

A Within-Individual, Network-Informed Approach to the Hippocampus

Recently, Zheng and colleagues made a theoretical and experimental breakthrough in our understanding of the human hippocampus (Zheng et al. 2021). Human fMRI studies often consider the hippocampus and surrounding areas in semi-isolation, much like the seminal lesion case studies in humans and electrophysiological work in rodents. Unfortunately, the limited resolution of fMRI makes these explorations difficult due to hippocampus' small size, proximity to cerebral cortex, and poor signal in the anterior portions. To offset these issues, Zheng et al. kept their analysis within the

individual, avoiding the loss of resolution which comes from averaging across multiple individuals with slightly different hippocampal anatomy. More critically, however, was their choice to approach the hippocampus from a broader network perspective, using networks estimated in cerebral cortex to gain leverage on the hippocampus.

Their exploration of the hippocampus began with identifying, in each individual, a set of networks covering nearly all of cerebral cortex using functional connectivity MRI. Two of these networks were not only prominently coupled to the hippocampus, but also differentially correlated with the anterior and posterior hippocampus. The anterior hippocampus correlated network closely resembles DN-A, and includes parahippocampal, retrosplenial, and ventromedial prefrontal cortex. They refer to the posterior hippocampus correlated network as the parietal memory network (PMN), which includes the posterior cingulate and retrosplenial cortex portions of the broader SAL / PMN network. This network-based division is a critical insight which parallels anatomical work done in non-human primates showing differential connectivity to cortical regions along the long axis (Insausti and Amaral 2008; Witter and Amaral 2021).

The functional roles of these hippocampal regions, however, require further study. Zheng et al. (2021) characterized larger task-induced deactivations in the anterior than the posterior hippocampus, and inferred from these results, along with the anterior hippocampal coupling to DN-A and weaker correlations to DN-B, that the anterior hippocampus is likely involved in the integration of internal, self-oriented information. In contrast, they were unable to probe the functional response of the posterior hippocampus, and so extrapolated a role in goal-directed processing based the on this region's primary coupling to PMN and weaker coupling to a Frontoparietal Control Network. Given the previously characterized functional specialization of DN-A on the cortical surface (DiNicola et al. 2020, 2023), and potential for SAL / PMN to display similar specialization, this leaves open the opportunity to precisely characterize the function of these

15

hippocampal regions with hypothesis-driven tasks, guided by each regions coupled cerebral network.

Brief Dissertation Overview

This dissertation is organized around three chapters, unified primarily by a common methodological push towards increasingly precise descriptions of human brain function and functional connectivity, made possible by an approach which densely samples a small number of individuals with fMRI. In **Chapter 1**, data from two individuals scanned over 31 separate MRI sessions is used to precisely map out the functional connectivity between the cerebellum and cerebral networks, and lays a framework for future explorations of the human cerebellum (Xue et al. 2021). **Chapter 2** leverages the improved resolution afforded by a within-individual fMRI study to characterize a third set of regions in the cerebellum which are active during body movements (Saadon-Grosman et al. 2022).

The culmination of my graduate work is described in **Chapter 3**, where we apply the cerebral network-informed functional connectivity approach of **Chapter 1** and the improved resolution for functional characterizations demonstrated in **Chapter 2** to study dissociations along the long axis of the human hippocampus. This chapter describes the application of our within-individual network identification to the hippocampus, inspired by the results from Zheng and colleagues described above and done with two goals in mind. First, we sought to replicate the dissociation between the anterior and posterior hippocampus via their coupling to distinct, distributed cerebral networks (DN-A and SAL / PMN). Our next goal was to directly probe the function of the anterior and posterior hippocampal regions using a battery of cognitive tasks, guided by hypotheses derived from the functional properties of each hippocampal region's coupled cerebral network (e.g. sensitivity to scene construction within DN-A coupled anterior hippocampus). To ensure rigorous hypothesis testing, and allow for exploratory tests of SAL / PMN

function, we completed all analyses in an initial data set first, then performed a prospective

replication in independent data. This approach allowed us to leverage fMRI to characterize

hippocampal functional specialization precisely and robustly on the level of the individual.

Chapter 1. The Detailed Organization of the Human Cerebellum Estimated by Intrinsic Functional Connectivity within the Individual

Contribution: *My contributions were primarily in the early stages of this project, where I mapped in two densely sampled participants the functional connectivity to the cerebellum from cerebral motor regions and higher-order networks such as default networks A and B. Later, I contributed to the writing and revision of the manuscript. M.C.E led data collection, A.X., R.K., Q.Y., R.L.B, and B.T.T.Y led analyses beyond my contribution, and A.X, R.K., R.L.B., and B.T.T.Y. led writing.*

Abstract

Distinct regions of the cerebellum connect to separate regions of the cerebral cortex forming a complex topography. Although cerebellar organization has been examined in group-averaged data, study of individuals provides an opportunity to discover features that emerge at a higher spatial resolution. Here, functional connectivity MRI was used to examine the cerebellum of two intensively sampled individuals (each scanned 31 times). Connectivity to somatomotor cortex showed the expected crossed laterality and topography of the body maps. A surprising discovery was connectivity to the primary visual cortex along the vermis with evidence for representation of the central field. Within the hemispheres, each individual displayed a hierarchical progression from

the inverted anterior lobe somatomotor map through to higher-order association zones. The hierarchy ended at Crus I/II and then progressed in reverse order through to the upright somatomotor map in the posterior lobe. Evidence for a third set of networks was found in the most posterior extent of the cerebellum. Detailed analysis of the higher-order association networks revealed robust representations of two distinct networks linked to the default network, multiple networks linked to cognitive control, as well as a separate representation of a language network. Although idiosyncratic spatial details emerged between subjects, each network could be detected in both individuals, and seed regions placed within the cerebellum recapitulated the full extent of the spatially specific cerebral networks. The observation of multiple networks in juxtaposed regions at the Crus I/II apex confirms the importance of this zone to higher-order cognitive function and reveals new organizational details.

New & Noteworthy: Stable, within-individual maps of cerebellar organization reveal orderly macroscale representations of the cerebral cortex with local juxtaposed zones representing distinct networks. In addition, individuals reveal idiosyncratic organizational features.

Introduction

Within its finely organized folia, the human cerebellum possesses a surface area that is 4/5th the size of the cerebral cortex (Sereno et al. 2020). Regions of the cerebral cortex project to specific zones of the cerebellum that, in turn, project back to the same regions of the cortex (Schmahmann and Pandya 1997; Strick et al. 2009). Although historical focus has been on motor function, the cerebellum is now known to contain major portions linked to cognitive and affective functions (Strick et al. 2009; Leiner et al. 1986; Leiner et al. 1989; Leiner et al. 1993; Schmahmann and

Sherman 1998; Buckner 2013; Karen-Happuch et al. 2014; Schmahmann et al. 2019; Diedrichsen et al. 2019). Over the past decade, the field has moved forward to explore the organization of cerebellar association zones with an increasing level of detail (Stoodley and Schmahmann 2009; Buckner et al. 2011; Guell et al. 2018a; King et al. 2019), including novel tools for visualization on the surface (Diedrichsen and Zotow 2015; Guell et al. 2019). What is converged upon is that between the anterior and posterior somatomotor representations is a large region linked to multiple cerebral association networks. The present work builds on these foundations by exploring the detailed organization of the human cerebellum within intensively sampled individuals.

A major challenge arising in the study of cerebrocerebellar organization is that there are no direct monosynaptic connections between the cerebellum and the cerebral cortex. The afferent inputs connect via the pons and the efferents project through the deep cerebellar nuclei and thalamus (Schmahmann and Pandya 1997; Strick et al. 2009). This creates a formidable barrier: cerebrocerebellar circuits cannot be mapped by the mainstay historical technique of systems neuroscience—monosynaptic retrograde and anterograde tract tracing. Polysynaptic tracing techniques allowed for a breakthrough that revealed a closed-loop architecture between the cerebrum and cerebellum that included parallel motor and prominent prefrontal connections in the macaque (e.g., Middleton and Strick 2001; Kelly and Strick 2003).

Human functional connectivity MRI based on spontaneous correlation provides another critical approach to map cerebrocerebellar organization (Biswal et al. 1995; Fox and Raichle 2007). For its many weaknesses and caveats (Buckner et al. 2013; Murphy et al. 2013; Smith et al. 2013; Power et al. 2014), functional connectivity MRI is powerful for mapping cerebellar organization because it is sensitive to polysynaptic circuitry and also because it allows for a wide field of view that can cover the entire brain. Numerous cerebral locations can be simultaneously mapped to numerous cerebellar locations. Use of functional connectivity MRI for cerebrocerebellar mapping has been supported by demonstrating 1) sensitivity, in detecting the well-established (Adrian 1943;

Snider and Stowell 1944) anterior and posterior somatomotor representations (Habas et al. 2009; Krienen and Buckner 2009); 2) specificity, by mapping the orderly topography of the inverted and upright body maps (Buckner et al. 2011); 3) sufficiency, by establishing cerebral stimulation can evoke a polysynaptic cerebellar response in nonhuman primates (Matsui et al. 2012); and 4) dependency, on intact anatomical circuits via analysis of hemipons lesions that disrupt the crossing cerebrocerebellar projections (Lu et al. 2011). Functional connectivity MRI is the basis of the present investigations.

A second challenge arises because of the small size of the human cerebellum and the limited sensitivity and resolution of human neuroimaging approaches. Most prior studies of the human cerebellum relied on group-averaging of data to boost signal-to-noise at the expense of resolution (e.g., Stoodley and Schmahmann 2009; Buckner et al. 2011; Guell et al. 2018a; King et al. 2019). What has emerged is a rough topographic organization of the cerebellum including multiple representations of sensory-attention networks and higher-order networks between the anterior and posterior lobe representations of the somatomotor map. The region surrounding the Crus I/II border is particularly intriguing because it contains representations of multiple distinct association networks. However, the detailed organization of the cerebellum, including mapping in relation to recently resolved higher-order association networks in the cerebral cortex, has been limited because spatial features are blurred together in group-averaged data (e.g., Fedorenko et al. 2012; Laumann et al 2015; Huth et al. 2016; Braga and Buckner 2017; Gordon et al. 2017; Braga et al. 2019; Gordon et al. 2020).

Of particular relevance to the present investigations are the higher-order association networks that have been mapped within individuals in great detail for the cerebral cortex. Multiple parallel networks have been discovered and replicated that possess neighboring regions that are often closely juxtaposed on the same sulcus (e.g., Braga et al. 2019). These multiple distinct juxtaposed networks are hypothesized to support functions related to remembering, social

inferences, and language—some of the most advanced forms of human thought (e.g., Fedorenko et al. 2012; Gordon et al. 2020; Buckner and DiNicola 2019; DiNicola et al. 2020; Braga et al. 2020). The present work focuses on these higher-order association networks within the individual by first identifying them in the cerebral cortex and then using the detailed characterization to map the cerebellum.

Providing a foundation, Marek et al. (2018) recently mapped the functional organization of the cerebellum from an openly available data resource of 10 highly sampled individuals (Gordon et al. 2017). This work illustrates the opportunity and challenges of precision cerebellar mapping. First, they found considerable variability between individuals that likely represents a combination of neuroanatomical variance as well as technical variance attributed to mapping at the edge of resolution and sensitivity limits. Second, they discovered organizational details that would be difficult to appreciate in group-averaged data. For example, they identified large representations of cognitive-control networks as well as attentional networks that have been underemphasized in prior group-averaged analyses. Finally, their individualized analyses confirmed the complexity of the cerebellar apex near the Crux I/II border with multiple association networks converging near to one another in most individuals.

Here, we extend precision cerebellar mapping to investigate the detailed functional organization of the cerebellum in two intensively sampled individuals. Particular focus is placed on the higher-order association networks that have been recently disentangled in the cerebral cortex including multiple parallel networks linked to the default network (Braga and Buckner 2017; Braga et al. 2019; DiNicola et al. 2020) and also their separation from a juxtaposed left-lateralized language network (Braga et al. 2020). Although not an original intent of our explorations, the high-resolution mapping within the individual yielded evidence for a visual representation near the vermis as predicted by van Es and colleagues (van Es et al. 2019).

Methods

Overview

The present explorations characterized the functional organization and topography of the cerebellum of two intensively studied individual subjects using data from 31 resting-state functional MRI (fMRI) sessions. Many of the analyses recapitulated strategies used previously to examine cerebellar organization in group-averaged data (Buckner et al. 2011), applied here to the individual. First, we examined the cerebrocerebellar functional connectivity of the somatomotor cortex to detect the well-established contralateral connectivity (establishing sensitivity) and topographic organization of the body representations (establishing specificity). Next, we estimated individual-specific cerebral parcellations using a Bayesian hierarchical approach (Kong et al. 2019) with data from the cerebellum blinded. We then used the cerebral network estimates as the anchor to comprehensively map the topographic organization of the cerebellum. All critical analyses were replicated between independent datasets within the same individual and generalized between the two individuals. Having established estimates of within-individual cerebellar organization using a cerebral-driven approach, we reversed the analysis strategy to validate the findings using a cerebellar-driven approach. Small seed regions were defined within the cerebellum, and the functional connectivity patterns were visualized in the cerebral cortex to determine whether the cerebellar regions were coupled to the cerebral cortex with spatially specific patterns. This same approach was also used to determine whether the multiple cerebellar representations would display the same patterns. As a final analysis, we explored in detail a surprising observation surrounding the identification of a zone of the cerebellar vermis that was linked to early retinotopic visual cortex.

Participants

The two subjects in this study were healthy, right-handed adult women (age, 22 yr and 23 yr) recruited from the greater Boston community and screened to exclude a history of neurological and psychiatric illness or ongoing use of psychoactive medications. The data from this study have been previously utilized in another study that focused on the cerebral cortex (Braga et al. 2019). The study was approved by the Institutional Review Board of Harvard University. Participants provided written informed consent.

MRI Data Acquisition

The resting-state fMRI data were collected at the Harvard Center for Brain Science on a Siemens Prisma-Fit 3-T MRI scanner using the vendor's 64-channel phased-array head-neck coil (Siemens, Erlangen, Germany). For both participants, 31 MRI sessions were collected with at least two resting-state blood oxygenation level-dependent (BOLD) runs included in each session. In total, 63 runs were obtained for each participant within 40 wk. Each run lasted 7 min and 2 s. Foam padding on the top and side of the head helped immobilize the head and reduce motion. Participants were instructed to remain still, stay awake, and maintain fixation on a centrally presented black crosshair with a light gray background viewed through a mirror. The scanner room was illuminated to enhance alertness.

BOLD fMRI (Kwong et al. 1992; Ogawa et al. 1992) data were acquired using a multiband gradient-echo echo-planar pulse sequence (Stesompop et al. 2012): repetition time (TR) = 1,000 ms, echo time (TE) = 32.6 ms, flip-angle = 64°, 2.4mm isotropic voxels, matrix 88 x 88 x 65, multislice 5 x acceleration, 422 frames for each run (with 4 frames then removed for T1 equilibration). The custom sequence was generously provided by the Center for Magnetic Resonance Research (CMRR) at the University of Minnesota as implemented for the Human Connectome Project (HCP; Xu et al. 2012; Van Essen et al. 2013). Signal dropout was minimized by automatically selecting a slice plane 25° from the anterior-posterior commissural plane toward the

coronal plane (van der Kouwe et al. 2005; Weiskopf et al. 2006; Mennes et al. 2014). A T1-weighted

structural image was obtained in each session using a rapid multiecho magnetization-prepared

rapid gradient echo (MPRAGE) three-dimensional sequence (van der Kouwe et al. 2008): TR =

2,200 ms, TE = 1.57, 3.39, 5.21, 7.03 ms, TI = 1,100 ms, flip-angle = 7°, voxel size 1.2 mm, matrix

192 x 192 x 176, in-plane generalized auto-calibrating partial parallel acquisition (GRAPPA)

acceleration 4 (see Nielsen et al. 2019 for analysis of this rapid variant). A dual gradient-echo B0

field map was acquired to correct for susceptibility-induced gradient inhomogeneities: TE = 4.45,

6.91 ms with slice prescription/spatial resolution matched to the BOLD sequence (Braga et al.

2019).

There were two exclusion rules for quality control of the BOLD data: 1) maximum absolute

motion more than 2 mm and 2) slice-based temporal signal-to-noise ratio ≤ 130. Following these

rules, one run was excluded for subject 1, and two runs were excluded for subject 2. Overall, 62

runs were usable for subject 1 and 61 runs for subject 2 [thereby recovering some data that failed

processing in the work by Braga et al. (2019)].

Data Processing

Data were processed through an in-house preprocessing pipeline ("iProc"; Braga et al.

2019) that combined tools from FreeSurfer (Fischl 2012), FSL (Jenkinson et al. 2012), and AFNI

(Cox 1996; 2012). A key goal of this processing pipeline is to align data within an individual across

runs and sessions with a single interpolation (to minimize blurring) and to high-resolution final

targets (1 mm). The two participants were processed independently. For each participant, a mean

BOLD template was created by taking the mean of all fieldmap-unwarped middle volumes after

registration to an upsampled (1.2-mm), unwarped mid-volume template. Five different

transformation matrices were calculated to align each BOLD image volume: 1) a motion correction

matrix for each volume to the run's middle volume, 2) a matrix for fieldmap-unwarping the run's

middle volume, 3) a matrix for registering the fieldmap-unwarped middle volume to the mean

BOLD template, 4) a matrix for registering the mean BOLD template to the subject's 1-mm native

space T1 image, and 5) a matrix for registering the native space T1 to the MNI152 1-mm atlas. The

first four transformation matrices were composed into one single matrix, and all five

transformation matrices into another. The composed matrices were used to project, in parallel,

each original BOLD volume to the native space T1 or to MNI space, each in a single interpolation to

reduce spatial blur (Braga and Buckner 2017; Braga et al. 2019).

Motion nuisance parameters, whole brain, ventricular, and deep white matter signal were

calculated and regressed out from the native space and MNI-space-projected data. A 0.01–0.1-Hz

bandpass filter was applied to the data. In the case of the cerebral cortex, the native space data

were projected to the fsaverage6 standardized cortical surface mesh with 40,962 vertices per

hemisphere (Fischl et al. 1999). A 2-mm full width at half-maximum (FWHM) kernel was used for

surface smoothing. In the case of the cerebellum, the volumetric data in MNI space were smoothed

with a 4-mm FWHM kernel. A manually corrected mask was used to extract the cerebellum (Fig.

1.1).

Visualization on the Cerebellar Surface

For many analyses, the cerebral data are visualized on the cerebral surface and the

cerebellar data within the cerebellar volume. In addition to volume representation within the

cerebellum, we also adopted a modeled projection of the data onto an estimated cerebellar surface.

More specifically, the volumetric parcellations were projected to a cerebellar flatmap using the

spatially unbiased infratentorial template (SUIT) toolbox

(http://www.diedrichsenlab.org/imaging/suit_ fMRI.htm). An outer (gray-matter) cerebellar

surface and inner (white-matter) cerebellar surface were defined by Diedrichsen and Zotow
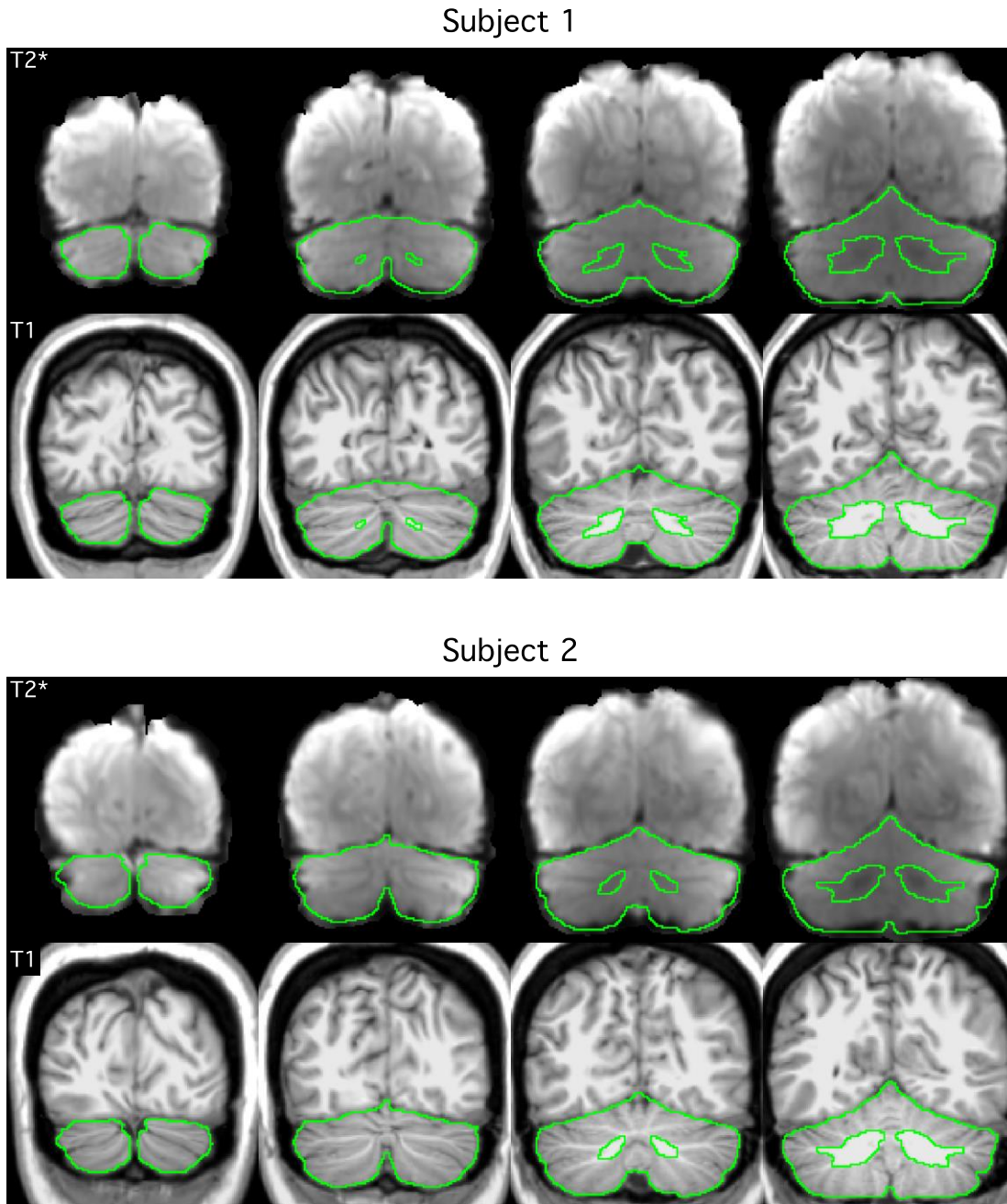
Subject 1

Subject 2

Figure 1.1 Extracted cerebellar boundaries for subjects 1 and 2 in MNI152 atlas space. The top row of each panel displays the T2 blood oxygenation level-dependent (BOLD) images. The bottom row of each panel shows the T1-weighted images. The green line shows the boundary of the cerebellum mask manually delineated based on each individual subject's T1-weighted image. There is good agreement between the green line and the cerebellum in the T2 images, suggesting good T1–T2 alignment. Imperfections in the BOLD data are also visible, e.g., signal dropout near the green cerebellar boundary.

(2015). Each vertex on the flatmap has a corresponding vertex on the outer surface and a corresponding vertex on the inner surface. To project the parcellations from the volume to the flatmap, each vertex on the flatmap was assigned to the most frequent network of the voxels along the line connecting the corresponding vertices on the outer and inner surfaces. Given the current resolution, the cerebellar surfaces are unable to reflect the highly fine cerebellar folia. Therefore, the flatmap is not a true unfolding of the cerebellar cortex. Nevertheless, based on our manual inspection, the flatmap was able to capture the main parcellation features.

Discovery and Replication Datasets

For each individual subject, the 31 sessions were divided into discovery and replication sets based on odd and even sessions. There were 16 sessions in the discovery set and 15 sessions in the replication set. For subject 1, there were 32 runs in the discovery set and 30 runs in the replication set. For subject 2, there were 32 runs in the discovery set and 29 runs in the replication set.

Motor Hand Region Functional Connectivity

To establish that our analysis procedures are sensitive to detect known organizational features of the cerebellum, we computed functional connectivity between cerebral motor regions positioned within or near the hand representation and the cerebellum. We estimated the motor hand region seed region location from the work by Buckner et al. (2011) defined in MNI152 space. More specifically, we considered 6mm-radius seed regions centered at MNI152 coordinates ($x = 41$, $y = 20$, $z = 62$) for the left-hand region and ($41, 20, 62$) for the right-hand region. For each run of each subject, we computed the Pearson's correlation (i.e., functional connectivity) between the time courses of the seed regions and all cerebellar voxels. The functional connectivity values were averaged across all runs after Fisher's r-to-z transformation. We then computed the difference

between the functional connectivity maps of the left-hand and right-hand seed regions for each

individual [paralleling the strategy established by Krienen and Buckner (2009)].

Foot, Hand, and Tongue Representations

To establish specificity to detect spatially separate features within the cerebellum, we

explored the topography of the different body parts in each individual's cerebellum by leveraging

their long-established spatial arrangement (Adrian 1943; Snider and Stowell 1944) and previous

identification in group-level cerebellar analyses in people (e.g., Buckner et al. 2011; Diedrichsen

and Zotow 2015). The group-level coordinates from the study by Buckner et al. (2011) did not work

well for the foot and tongue representations, potentially due to interindividual differences not

captured at the group level. Therefore, we considered a strategy of picking individual-specific seed

regions. More specifically, we manually picked single vertices representing hand, foot, and tongue

regions on the fsaverage6 surface based on functional connectivity within the discovery set. The

original MNI152 coordinates of foot, hand, and tongue regions (Buckner et al. 2011) were used to

guide our selection. Functional connectivity was then computed using the replication set. For each

run of each subject within the replication set, we computed the Pearson's correlation between the

time series of the motor seed regions and all cerebellar voxels. We then binarized the functional

connectivity maps for each body part and overlaid them to visualize the somatomotor organization.

Thresholds were set at z ≥ 0.1 for foot, z ≥ 0.2 for hand, and z ≥ 0.1 for tongue.

Individual-Specific Parcellation of the Cerebral Cortex

Having established that functional connectivity was able to detect and map the

somatomotor topography within each individual's cerebellum, we moved on to characterize the

individual-specific organization of cerebrocerebellar coupling across the entire cerebral cortex. We

started by estimating the individual-specific cerebral cortical parcellations of the two individuals

based on the connectivity profiles of each cortical region (vertex). Following our previous study

(Yeo et al. 2011), the connectivity profile of a cortical vertex was defined

as its functional coupling to 1,175 regions of interest (ROIs). These ROIs consist of single vertices

uniformly distributed across the surface meshes. For each participant, the Pearson's correlation

was computed between the fMRI time series at each vertex (40,962 vertices per hemisphere) and

the 1,175 ROIs. The 40,962 x 1,175 correlation matrix of each hemisphere was then binarized by

keeping the top 10% of the correlations to obtain the functional connectivity profiles (Yeo et al.

2011).

A multisession hierarchical Bayesian model (MS-HBM) was then utilized for estimating

cortical networks in the two individuals (Kong et al. 2019). The MS-HBM was initialized with a 10-

network group-level parcellation estimated from the HCP S900 data release using the group-level

clustering algorithm from Yeo and colleagues (Kong et al. 2019; Yeo et al. 2011). We note that the

cerebral cortex is organized in a hierarchical fashion, so there is no single optimal resolution in

terms of the number of networks (Yeo et al. 2011; Power et al. 2011). In this study, we consider the

10-network resolution because the network topography within the cerebellum was difficult to

interpret with more networks. However, the 10-network resolution was sufficiently fine to

distinguish default network A from default network B as well as to identify the distinct language

network, which were critical targets (Braga and Buckner 2017; Braga et al. 2020; Kong et al. 2019).

Thus, this choice reflected a balance to detect known target networks but also to limit the

dimensionality of the solution to a tractable level.

To test the reliability of the individual-specific cerebral cortical parcellations, the MS-HBM

algorithm was independently applied to the discovery and replication sets. Once reliability was

established, we obtained the best estimate of the cerebral cortical parcellations for each individual,

by applying the MS-HBM to all resting-state fMRI sessions [similar to the study by Yeo et al. 2011].

Individual-Specific Cerebellar Parcellation

The individual-specific cerebral cortical parcellations (from the previous section) were used to estimate individual-specific cerebellar parcellations using a winner-takes-all algorithm (Buckner et al. 2011; Marek et al. 2018). To test the reliability of the individual-specific cerebellar parcellations, the same procedure was independently repeated for the discovery and replication sets. Finally, to obtain the best estimate of the cerebellar parcellations for each individual, the procedure was also applied to all resting-state fMRI sessions.

Specifically, focusing on the analysis as applied to the discovery set, for each run of each subject, we computed the functional connectivity (i.e., Pearson's correlation) between the time courses of all cerebellar voxels and all cerebral cortical vertices. The functional connectivity values were averaged across all runs for each subject within the discovery set. For each cerebellar voxel, we identified the top 400 cerebral cortical vertices with the strongest correlations with the voxel's fMRI time course. Recall that all cortical vertices had been assigned to a cerebral cortical network by the HS-HBM analysis (see Individual-Specific Parcellation of the Cerebral Cortex section). The cerebellar voxel was then assigned to the cerebral cortical network that was most frequently present among the 400 vertices. Experiments (not reported) using different number of vertices (100 to 1,000 vertices) yielded highly similar cerebellar parcellations, so here we will focus on the parcellations generated with 400 vertices. The procedure was applied to the replication set independent of data from the discovery set and then, after establishing reliability, was applied to all of the data simultaneously to obtain the best estimate of the cerebellar parcellation [similar to the study by Buckner et al. 2011].

Cerebellar-Initiated Functional Connectivity

The above analyses yield cerebellar parcellations that are dependent on the assumptions of the cerebral network parcellation, including the decision of how many distinct networks to

estimate in the MS-HBM. To provide an alternative approach anchored directly from the

cerebellum, we also explored the cerebral correlation patterns when beginning the analyses with

small seed regions placed in the cerebellum. Such a strategy allows the specificity of the cerebral

pattern to be observed without a priori assumptions about the distributed organization within the

cerebrum or the number of networks in the parcellation solution. Positive evidence that the

parcellations reflect stable organizational properties arises if the cerebral networks generated from

small cerebellar seed regions recapitulate the estimated cerebral networks in an anatomically

specific manner. Negative evidence is obtained when the generated networks are orthogonal or

nonspecific. Moreover, multiple representations of the same network can be examined in the

cerebellum to explore whether the multiple candidate networks zones do, in fact, each

independently correlate specifically with the same cerebral network.

Our first analysis tested the specificity of default networks A and B by selecting separate

pairs of seed regions in the anterior and posterior cerebellar representations of the two distinct

networks. In this manner, specificity between the networks could be established independently

within the anterior and posterior representations (e.g., lobule HIX default network A vs. lobule HIX

default network B), and also the similarity or dissimilarity compared for the anterior and posterior

regions of the same network (e.g., Crus I/II default network A vs. lobule HIX default network A). The

second analysis tested the spatial specificity of the language network by selecting separate seed

regions across multiple cerebellar representations of the language network. The language network

is of particular interest because of its complex topography in the cerebellum including close

adjacency to larger networks in multiple regions of the cerebellum. Thus, targeted analysis allowed

the multiple representations of the language network to be verified and their specificity to be

established for each of multiple spatially discontinuous cerebellar representations. To confirm

individual differences in cerebellar network parcellations, the third analysis considered cerebellar

seed regions with identical MNI152 coordinates assigned to different network representations

between the two participants. In this manner, the specificity of the networks in each participant could be established while simultaneously illustrating how individual differences in topographic positioning of networks can lead to the inability to generalize the specific spatial details from one individual to the next. The fourth analysis sought to illustrate the uncommon failure modes of the parcellation algorithm due to the winner-takes-all nature of the approach.

We note that across all analyses, to further remove bias from this set of confirmation analyses, seed regions were manually selected based on functional connectivity within the discovery set. The final set of functional connectivity maps were computed using the replication set.

Estimation of V1 from Histology and Functional Connectivity Gradients

As the results will reveal, a surprising finding was a region of the cerebellar vermis that was associated with the visual network linked to early retinotopic visual cortex. To explore the details of this finding further, we estimated the location of primary visual cortex (V1) within each subject using both histology and functional connectivity gradients. The V1 histology was performed by the Juelich group (Amunts et al. 2000) and then projected to FreeSurfer fsaverage space (Fischl et al. 2008). Functional connectivity gradients were used to detect abrupt local changes in functional connectivity. Previous studies have suggested the feasibility of functional connectivity gradients to localize the V1 boundary in vivo (Laumann et al. 2015; Wig et al. 2014; Gordon et al. 2016).

Quantitative Relationship between Cerebral and Cerebellar Network Representations

Our previous study (Buckner et al. 2011) suggested that larger cerebral cortical networks have larger representations within the cerebellum at the group level, with some hints of disproportionate representation of certain networks (e.g., the frontoparietal control network). Marek et al. (2018) performed an extensive analysis of the relationship between cerebral and cerebellar network representations within individuals revealing evidence for disproportionate

33

frontoparietal representation. Motivated by these prior analyses, we conducted a similar analysis here but, unlike the previous work, explicitly included a clear candidate language network as well as separately calculated the relationship for the left and right cerebellar hemispheres, given the known laterality differences for certain networks (e.g., language). Specifically, for each cerebellar hemisphere, we computed the percentage of voxels assigned to each network within the cerebellar mask in MNI space and the percentage of vertices assigned to each network on the contralateral cerebral surface. We then compared the percentage of cortical surface dedicated to each network with the percentage of cerebellar volume dedicated to the same network in the contralateral hemisphere.

Code and Map Availability

The cerebral cortical parcellation code is publicly available here (https://github.com/ThomasYeoLab/CBIG/tree/master/ stable_projects/brain_parcellation/Kong2019_MSHBM). The cerebellum parcellation code is publicly available here (https:// github.com/ThomasYeoLab/CBIG/tree/master/stable_projects/ brain_parcellation/Xue2021_IndCerebellum). The parcellations and unthresholded brain maps can be found at https://balsa. wustl.edu/study/show/7q3ZP.

Results

Cerebral Motor Regions Show Robust Functional Connectivity with the Contralateral Cerebellum within the Individual

Subtraction of functional connectivity seed maps between the left-hand and the right-hand cerebral cortical seed regions revealed contralateral connectivity of the motor representations in
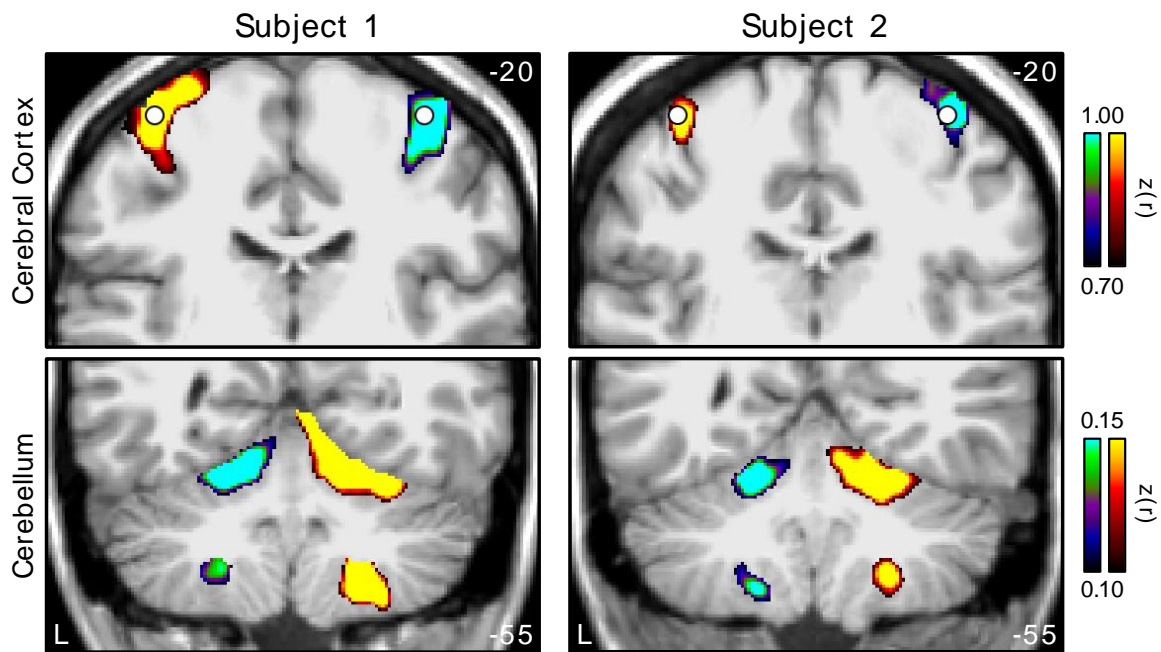
Figure 1.2. Functional connectivity of the cerebral cortical motor hand regions reveals contralateral somatomotor representations in the cerebellum of individual subjects. Coronal sections (top: y = 20; bottom: y = 55) display differences between functional connectivity of seed motor regions for each individual subject. Seed locations at or near the left- and right-hand motor representations are indicated by white circles. Warm colors show the connectivity of the right seed region subtracted from the connectivity of the left seed region. Cool colors represent the reverse subtraction. Color bars indicate correlation strength [z(r)]. The left hemisphere is displayed on the left (L). These results suggest that functional connectivity possesses sensitivity to detect known somatomotor representations within the individual.

35

the cerebellum for both individuals (Fig. 1.2). Both primary and secondary hand-region

representations in the anterior and posterior lobes of the cerebellum were evident.

Somatomotor Topography of the Cerebellum Is Evident within the Individual

Consistent with previous work on population-level cerebellar functional connectivity maps

(Buckner et al. 2011; Diedrichsen and Zotow 2015), individual-specific functional connectivity

maps of cerebral seed regions in estimated foot, hand, and tongue representations showed an

inverted topography in both individuals in the anterior lobe and a separate upright topography in

the posterior lobe (Fig. 1.3). Although the size and location of these binarized individual

representations were not exactly the same, the expected topographic ordering was consistent

across both participants (see also Marek et al. 2018).

A small detail was further noted. There was a spatial gap between the estimated hand and

foot representations for both the anterior and posterior lobe maps. This gap, which is less evident

in group-based analyses, may reflect portions of the cerebellar map associated with portions of the

body between the hand and foot that are not captured fully by our limited sampling of body parts

(see Saadon-Grosman et al. 2015).

Cerebral Cortical and Cerebellar Parcellations Are Reliable within Individuals

For each subject, the 31 sessions were split into discovery and replication sets based on odd

and even sessions. The MS-HBM (Kong et al. 2019) was applied to the discovery and replication

sets independently to derive 10-network cerebral cortical parcellations (Fig. 1.4). The parcellations

within each subject were highly similar across discovery and replication sets. In subject 1, 91.4% of

cortical vertices were assigned to the same networks across discovery and replication sets. In

subject 2, 90.2% of cortical vertices were assigned to the same networks across discovery and

replication sets. By contrast, overlaps between the cortical parcellations of subjects 1 and 2 were

Subject 1

## Subject 2
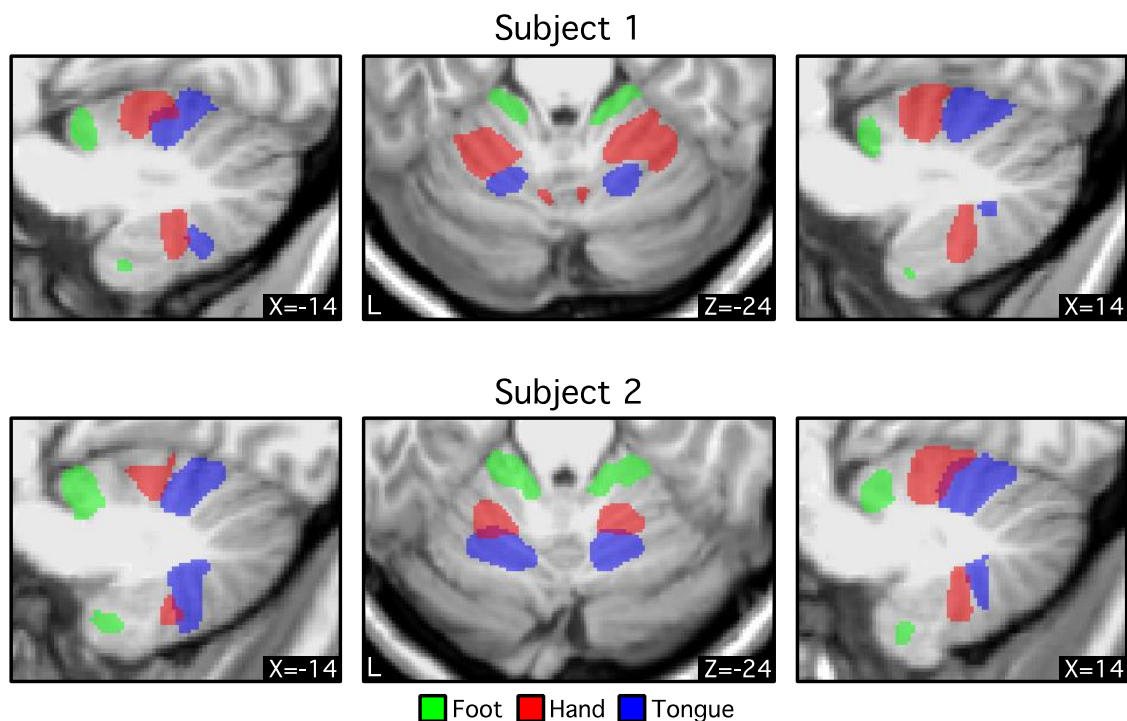
Foot   Hand   Tongue

Figure 1.3. Foot-hand-tongue representation in the cerebellum revealed by functional connectivity for individual subjects. Three different bilateral cortical regions were selected on the cerebral surface based on the discovery set (Table 1.1). Functional connectivity of these regions was computed using the replication set. Thresholds were set at $z \geq 0.1$ for foot, $z \geq 0.2$ for hand, and $z \geq 0.1$ for tongue. Green, red, and blue colors represent foot, hand, and tongue, respectively. Coordinates at the bottom right indicate the section level in MNI152 space. In both individuals, the order of the somatomotor representation in the anterior lobe is foot-hand-tongue, whereas the order in the posterior lobe is inverted. Note the consistent spatial gap between the foot and hand representations that may reflect the intervening body representation. These results suggest that functional connectivity possesses specificity to detect the known spatial topography of somatomotor representations within the individual.

	Subject 1	Subject 2
Left hemisphere		
Foot	2,110	24,883
Hand	5,768	5,768
Tongue	32,897	32,897
Right hemisphere		
Foot	34,531	17,843
Hand	6,167	6,167
Tongue	12,417	12,417

The number represents the index of each hemisphere on the fsaverage6 surface. Note that vertex index starts from 1 (rather than 0).

Table 1.1. Locations of seed regions used to create somatomotor topography.
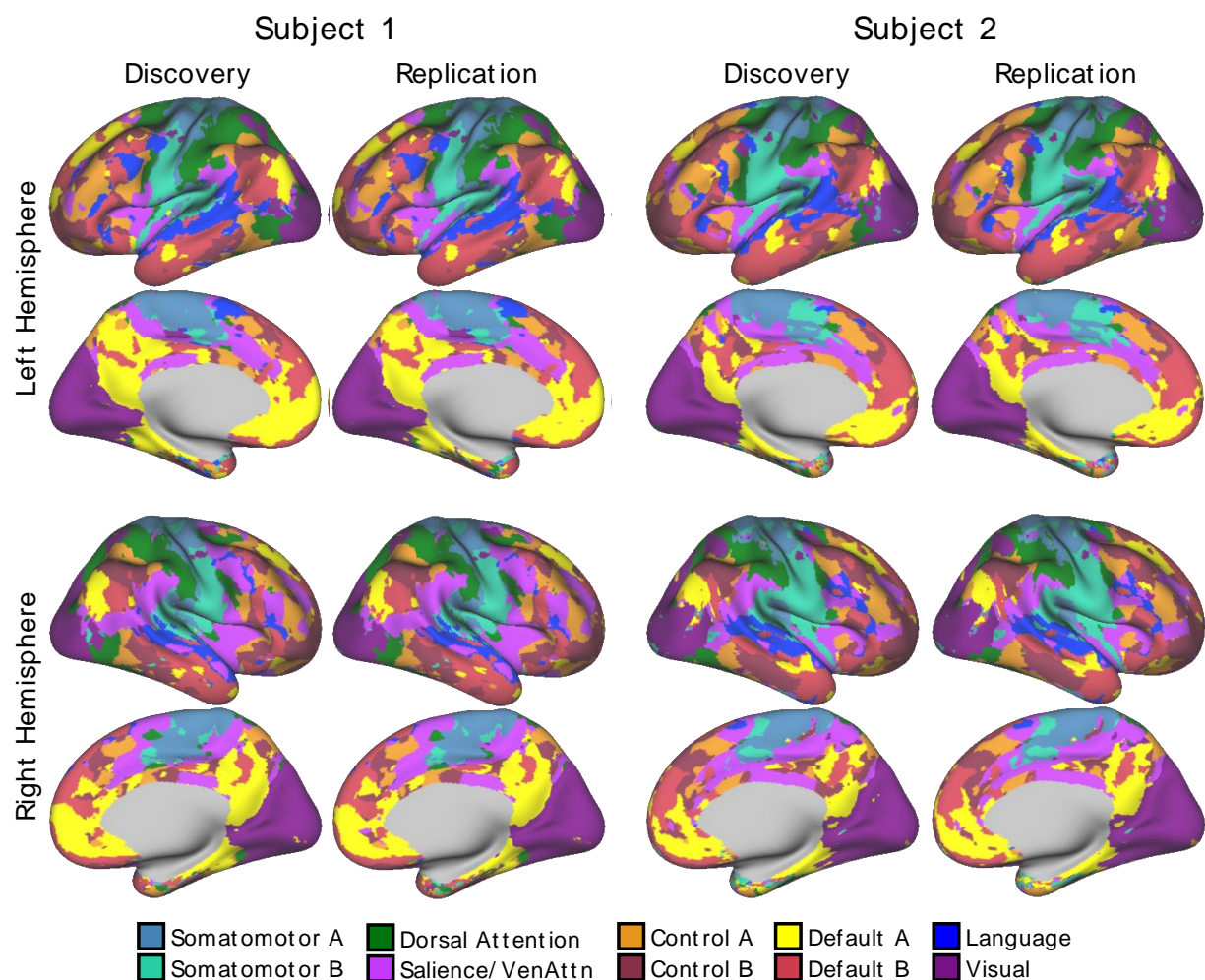
Figure 1.4. Cerebral cortical network parcellations were highly reliable across discovery and replication sets within individuals. 10-network individual-specific cerebral network parcellations were estimated by applying a multisession hierarchical Bayesian model (Kong et al. 2019) to the discovery (16 sessions) and replication (15 sessions) datasets independently. The individual-specific cortical parcellations were replicable within subjects. In subject 1, 91.4% cortical vertices were assigned to the same networks across discovery and replication datasets. In subject 2, 90.2% cortical vertices were assigned to the same networks across discovery and replication datasets. Networks are colored as labeled in the bottom legend using network names common in the literature for convenience. The names should not be taken to mean that networks code solely for functions associated with their assigned names, which are often derived from an evolving literature.
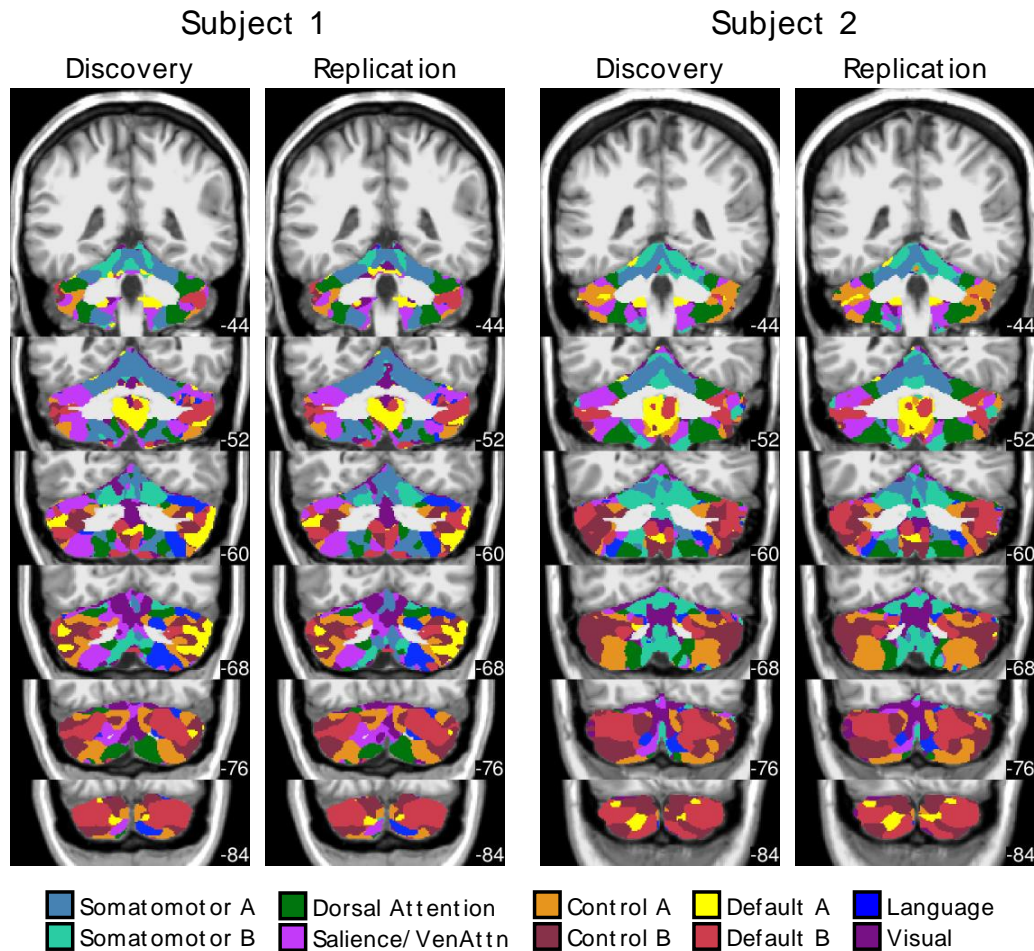
Figure 1.5. Cerebellar network parcellations were highly reliable across discovery and replication sets within individuals. Individual-specific cerebellar parcellations were estimated using discovery (16 sessions) and replication (15 sessions) datasets independently. Each cerebellar voxel was assigned to the most frequent cortical network among 400 cortical vertices with the strongest correlation (functional connectivity) with the voxel. Individual-specific cerebral parcellations were replicable within subjects. In subject 1, 83.8% voxels were assigned to the same networks across discovery and replication datasets. In subject 2, 84.2% voxels were assigned to the same networks across discovery and replication datasets. Networks are colored as labeled in the bottom legend.

59.8% in the discovery set and 60.4% in the replication set. Thus, between-subject variability was substantially greater than within-subject variability.

For the cerebellar parcellation, we applied a winner-takes-all algorithm (Buckner et al. 2011; Marek et al. 2018) based on the functional connectivity between the cerebral cortex and the cerebellum. Cerebellar parcellations were estimated from the discovery and replication sets independently (Fig. 1.5). The cerebellar parcellations within each subject were highly similar across discovery and replication sets. Overlap between parcellations in the discovery and replication sets were 83.8% for subject 1 and 84.2% for subject 2. By contrast, overlaps between the cerebellar parcellations of subjects 1 and 2 were 42.8% in the discovery set and 42.8% in the replication set. Thus, between-subject variability was substantially greater than within-subject variability for the cerebellum as well as cerebral cortex.

Complete Cerebellar Maps within Individuals

Results above indicate that we were able to derive reliable functional maps within the cerebellum of individuals. To obtain the best estimate of cerebellar maps within each individual, we applied our approach to map the full topography of the cerebellum by using all 62 runs for subject 1 and all 61 runs for subject 2. We first estimated the cerebral networks using the MS-HBM approach and then the cerebellar map using a winner-takes-all algorithm.

Figures 1.6 and 1.7 show the individual-specific cerebral cortical parcellations of subjects 1 and 2, respectively. The 10-network cortical parcellations shared some common features as well as clear individual differences across the two subjects. For example, in both participants, default networks A and B (yellow/red) were distributed across multiple zones of the cerebral cortex, including the inferior parietal lobule, ventromedial prefrontal cortex, posterior cingulate cortex, lateral temporal cortex, and other locations, consistent with previous work showing the same broad topography across individuals but with anatomical details varying (Braga and Buckner 2017; Braga
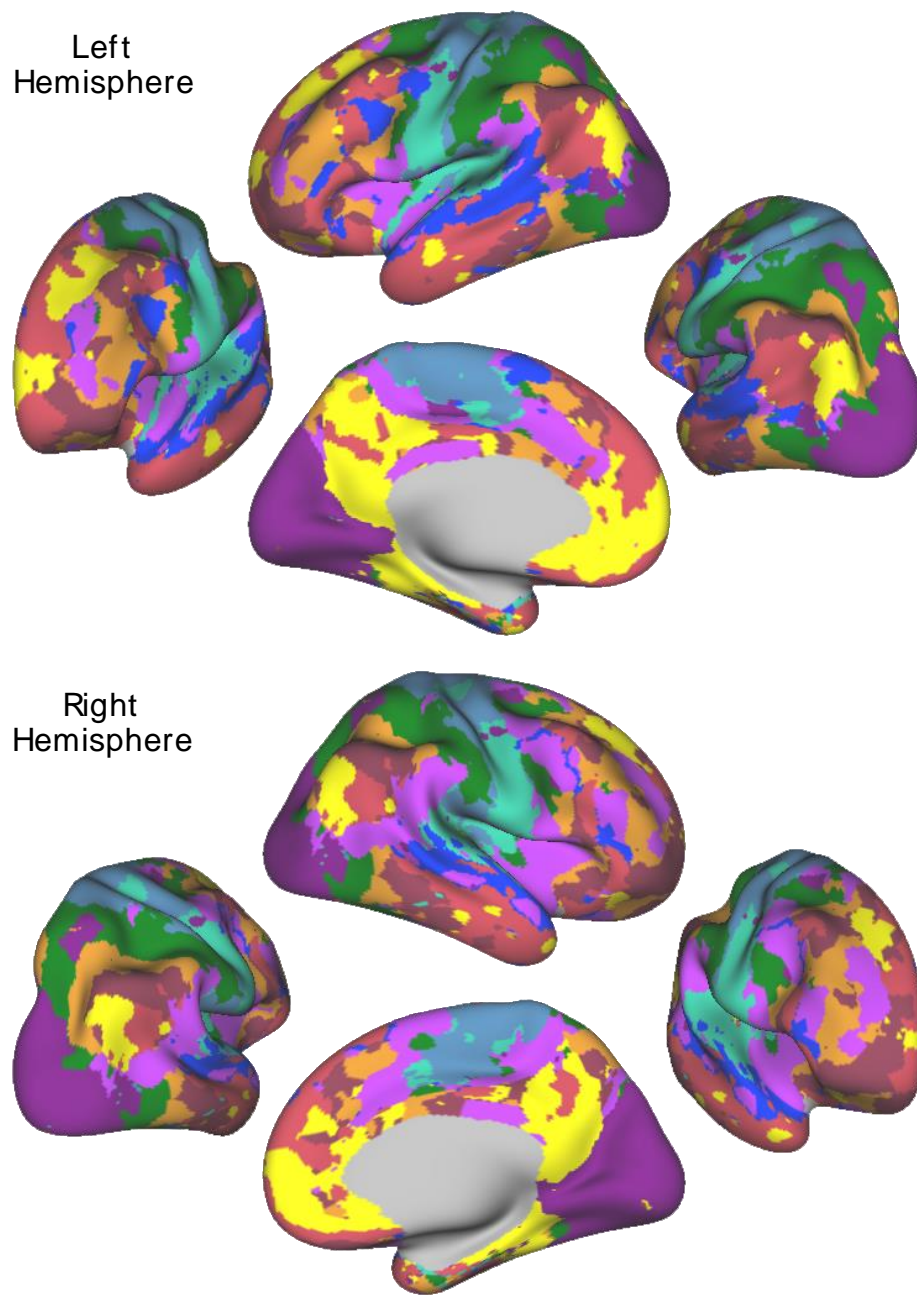
Figure 1.6. The best estimate of 10-network cerebral cortical parcellation of subject 1.
Multiple views for each hemisphere are provided to show the details of the parcellation. This parcellation represents the best estimate of cortical network organization using the present approach applied to all available data (62 runs from 31 independent sessions). Colors use the network labels as shown in Fig. 1.4. Note the presence of juxtaposed interdigitated networks in high-order association cortex that include default network A (yellow) and default network B (red), a candidate language network (blue), and cognitive control networks (orange and brown).
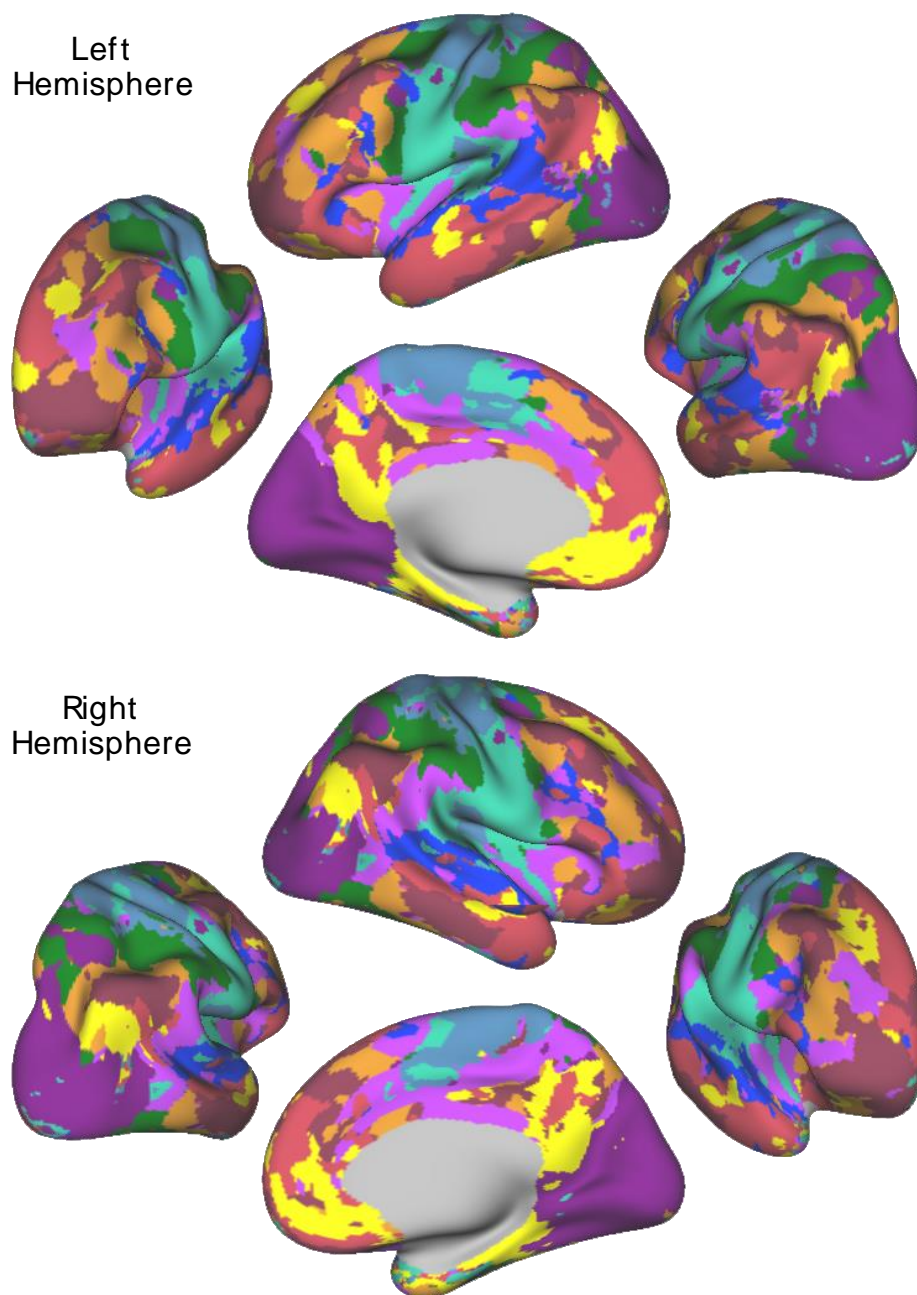
Figure 1.7. The best estimate of 10-network cerebral cortical parcellation of subject 2.
Multiple views for each hemisphere are provided to show the details of the parcellation. This
parcellation represents the best estimate of cortical network organization using the present
approach applied to all available data (61 runs from 31 independent sessions). Colors use the
network labels as shown in Fig. 1.4. Note the presence of juxtaposed interdigitated networks in
high-order association cortex that include default network A (yellow) and default network B (red),
a candidate language network (blue), and cognitive control networks (orange and brown).

et al. 2019; DiNicola et al. 2020). Similarly, a candidate language network was found in both individuals respecting broad topographic properties that have been well established (e.g., Fedorenko et al. 2012; Braga et al. 2020; Mineroff et al. 2018) but with variability between individuals. In this instance, subject 1 displayed a more left-lateralized network representation than subject 2.

Figures 1.8 and 1.9 show the individual-specific cerebellar parcellations of subjects 1 and 2 in the volume, and Fig. 1.10 shows the parcellations on the cerebellar surface. Like the cerebral cortex, the cerebellar parcellations of the two subjects displayed common as well as individual-specific features. First, for both subjects, the somatomotor regions in the anterior and posterior lobes were mapped to somatomotor networks in lobules IV–VI and lobule VIIIb. More specifically, foot and hand regions were assigned to two fractionated networks, provisionally labeled somatomotor network A (blue) and somatomotor network B (aqua). Of note, the two separate somatomotor network assignments capture features of the body map topography observed in targeted analyses (e.g., Fig. 1.3) but not all of the organization. Second, for both subjects, the majority of the cerebellum was mapped to cerebral association networks, including Crus I/II, lobule IX, lobule X, and part of lobules VI, VIIb, and VIIIa. However, the size and location of the association networks were different between the two subjects. For example, similar to the cerebral cortex, the language network representation within the cerebellum was more lateralized in subject 1 than in subject 2. Thus, although the language network had generally similar organizational features between the two subjects (note the clear parallels between the multiple distributed representations in the right cerebellar hemisphere), there were also differences that suggest individual variations in exact spatial locations as well as laterality.

Figure 1.8. The best estimate of 10-network cerebellar parcellation of subject 1. Each cerebellar voxel was assigned to the most frequent cortical network among the 400 cortical vertices with the strongest correlation (functional connectivity) with the voxel. The 10 cerebral networks of subject 1 are shown at the bottom for reference. Colors use the network labels as shown in Fig. 1.5. The three sections display sagittal (left), coronal (middle), and axial (right) views. L, left; R, right; A, anterior; P, posterior; S, superior; and I, inferior. The left hemisphere is displayed on the left. Coordinates at the bottom right of each panel indicate the section level in MNI152 space. Each network identified in the cerebral cortex has multiple representations in the cerebellum. The organization is broadly symmetric between the cerebellar hemispheres, with asymmetries paralleling the cerebral network asymmetries. For example, the language network (blue) shows a markedly expanded representation in the right hemisphere consistent with the leftward asymmetry in the cerebral cortex.
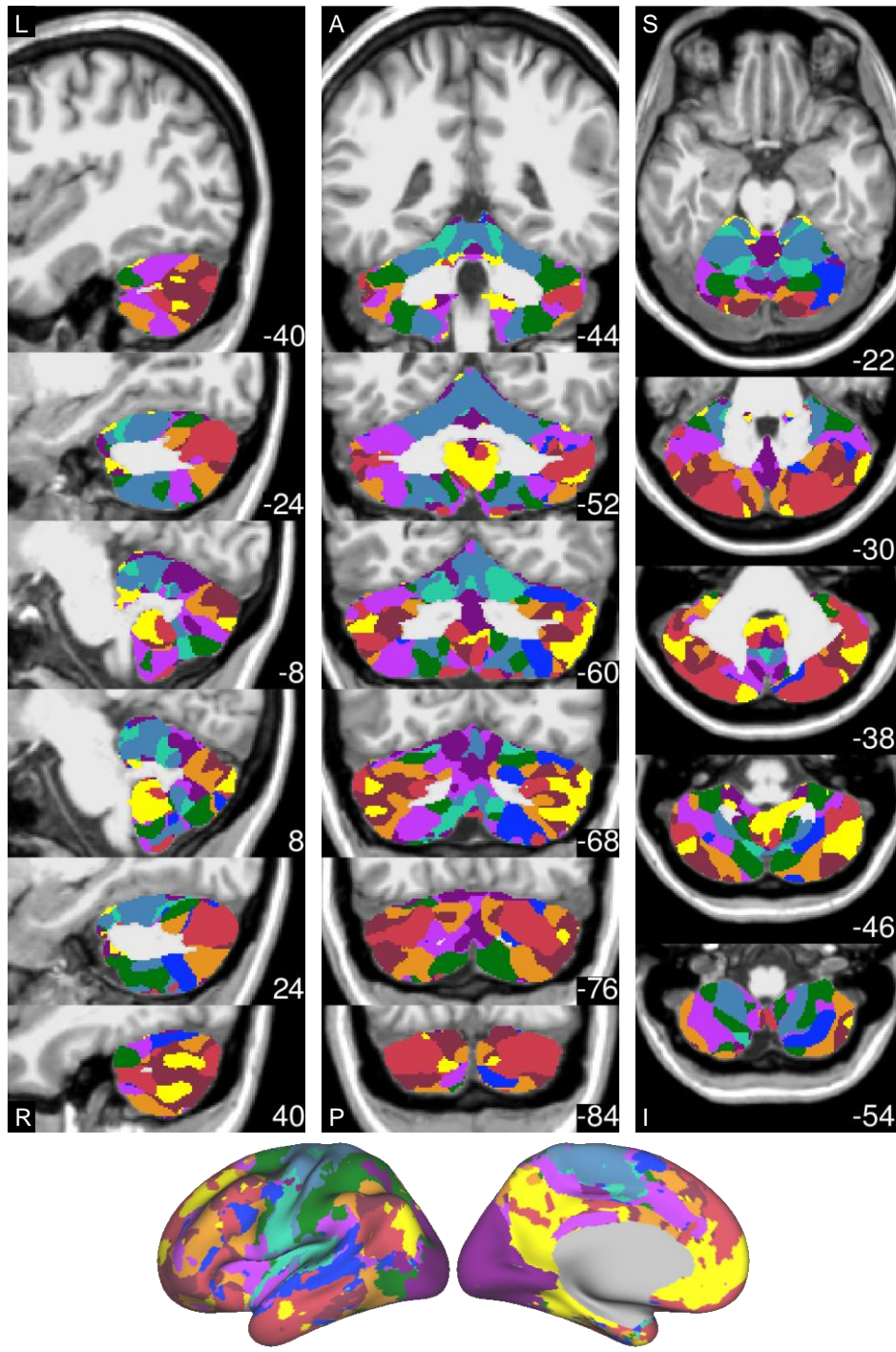
Figure 1.8 (Continued)

Figure 1.9. The best estimate of 10-network cerebellar parcellation of subject 2. Each cerebellar voxel was assigned to the most frequent cortical network among the 400 cortical vertices with the strongest correlation (functional connectivity) with the voxel. The 10 cerebral networks of subject 2 are shown at the bottom for reference. Colors use the network labels as shown in Fig. 1.5. The three sections display sagittal (left), coronal (middle), and axial (right) views. L, left; R, right; A, anterior; P, posterior; S, superior; and I, inferior. The left hemisphere is displayed on the left. Coordinates at the bottom right of each panel indicate the section level in MNI152 space. Each network identified in the cerebral cortex has multiple representations in the cerebellum.
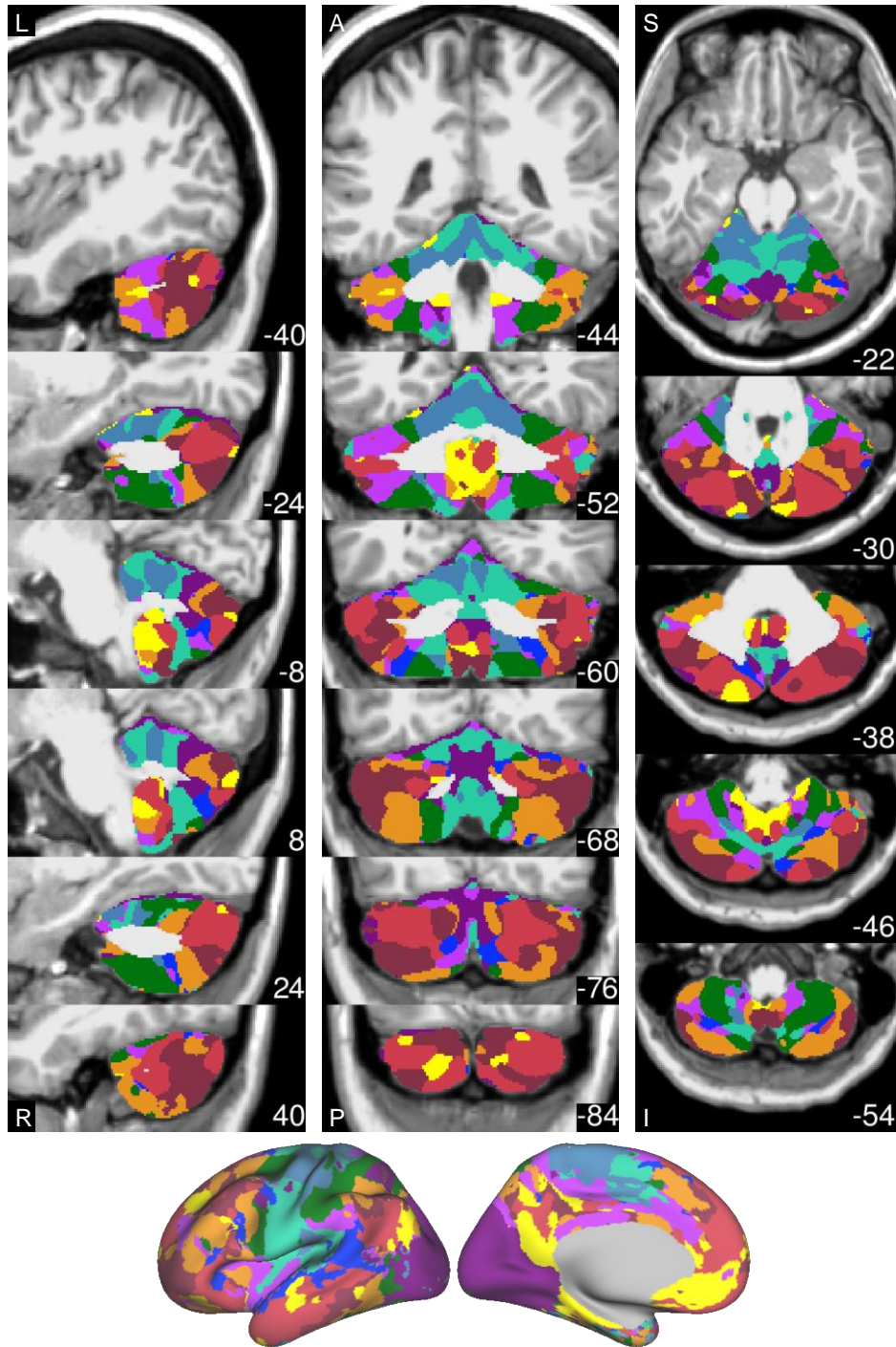
Figure 1.9 (Continued).

Individual Cerebellar Topography Includes Multiple Representations of the Cerebrum

Our previous explorations suggested that at the group level, the cerebellum contains three

representations of the cerebral cortex (Buckner et al. 2011; see also Guell et al. 2018a). Despite the

complex topography of individual-specific cerebellar parcellations, the three representations could

also be observed in both subjects (Figs. 1.10 and 1.11). Figure 1.11 shows the three representations

in different sagittal sections. The three representations are also marked on the left side of the

flatmaps in Fig. 1.10.

The primary map began with the somatomotor networks at the anterior lobe and ended

with the default networks A and B at Crus I/II. The remaining association networks were

sandwiched in between the somatomotor and default networks A and B. Association networks that

are more involved in sensory perception (i.e., dorsal and ventral attention networks) were

positioned adjacent to the somatomotor networks, whereas association networks involved in

cognitive control and language were positioned adjacent to the default networks A and B. Default

network A was juxtaposed to default network B in multiple locations in both individuals.

The secondary map began with default networks A and B at Crus I/II and ended with

somatomotor networks at lobule VIIIb. The ordering of the networks in the primary and

secondary maps was basically in an inverse order but with some variation. The tertiary map was

present in lobules VIIb, IX, and X. Not all association networks were independently observed in the

smaller tertiary map, but default networks A and B were particularly robust and distinct (Fig. 1.12).

Thus, the broad hierarchical ordering that has been previously highlighted in relation to cerebral

network organization (Braga and Buckner 2017; Margulies et al. 2016) reveals a parallel

macroscale organization in the cerebellum with a primary, secondary, and likely tertiary map of the

network set. However, the exact details of the adjacencies also show variability between subjects

and complex juxtapositions, especially among the higher-order association networks. This is

evident near the Crus I and II border. Specifically, in both individuals, the default networks A and B
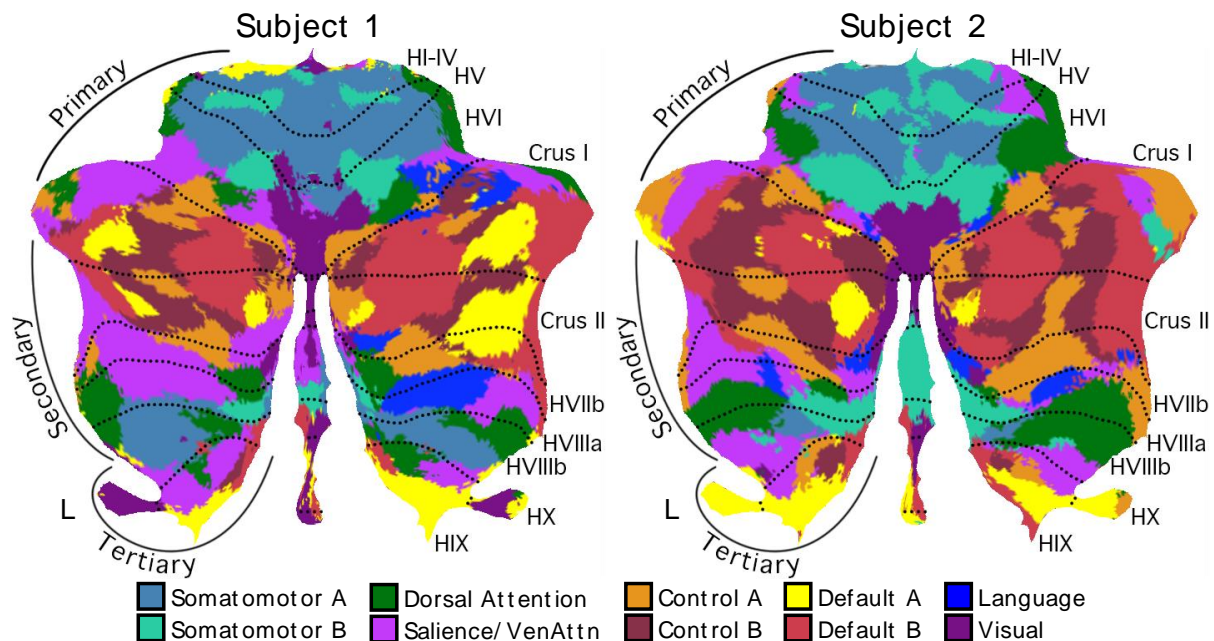
Figure 1.10. Cerebellar network parcellations within individuals are shown on flatmaps. The individual-specific parcellations were generated using all sessions for each subject projected using the SUIT toolbox (Diedrichsen and Zotow 2015). Dotted lines indicate lobular boundaries. L indicates left cerebellar hemisphere. Different lobules are marked on the right side. Networks are colored as labeled at bottom. Despite the complex topography, the cerebellum contained three representations of the cerebral cortex labeled as the putative primary, secondary, and tertiary maps. The primary map begins with the anterior lobe somatomotor representation, passes through dorsal attention and salience/ventral attention networks, and ends in the apex association networks centered at the Crus I/II border, including clear representation of default networks A and B. The secondary map then progresses in reverse through to a second somatomotor representation in the posterior lobe (within HVIIIb). Evidence for the tertiary map is the final representation of networks between HVIIIb and HIX that possesses representation of default networks A and B in HIX.

Subject 1

Subject 2

🟦 Somatomotor A	🟩 Dorsal Attention	🟧 Control A	🟨 Default A	🟦 Language
🟩 Somatomotor B	🟪 Salience/VenAttn	🟥 Control B	🟥 Default B	🟪 Visual
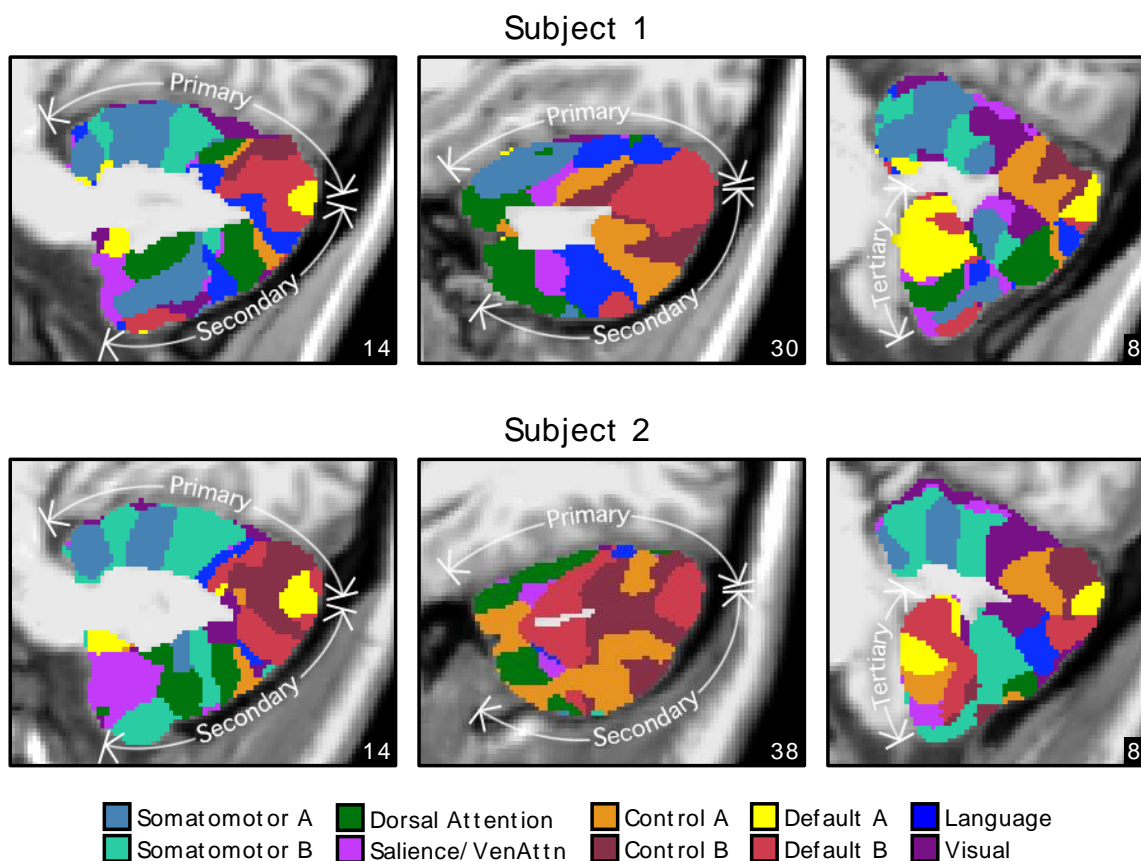
Figure 1.11. Cerebellar network parcellations within individuals shown in the volume to reveal multiple repeating maps. The topographic ordering of the cerebral networks from Fig. 1.10 is illustrated for three sagittal sections of the right cerebellum. Three distinct representations are observed for both subjects, labeled as primary, secondary, and tertiary. Each map is a roughly duplicated ordering of the adjacent map (with some variation).

Figure 1.12. Evidence for specificity of default networks A and B. Top: seed regions from default networks A (DN-A) and B (DN-B) were selected within the discovery set (plotted as white circles). Note two pairs of seed regions were selected, centered on adjacent default network A and B representations separately for the Crus I/II representation and the spatially distant HIX representation. This allowed the network topography of each separated cerebellar map to be examined in the cerebral cortex. Bottom: functional connectivity maps from the cerebellar seed regions were estimated for the cerebral cortex using the replication set. Black lines indicate boundaries of individual-specific default network A or B from the original cerebral parcellation (Fig. 1.4, replication set). Each pair of juxtaposed cerebellar seed regions yielded the full, distributed cerebral networks associated with the separate default network A or B; seed regions from the same networks in Crus I/II and lobule IX exhibited highly similar functional connectivity patterns. These results illustrate remarkable specificity of the cerebellar parcellations.
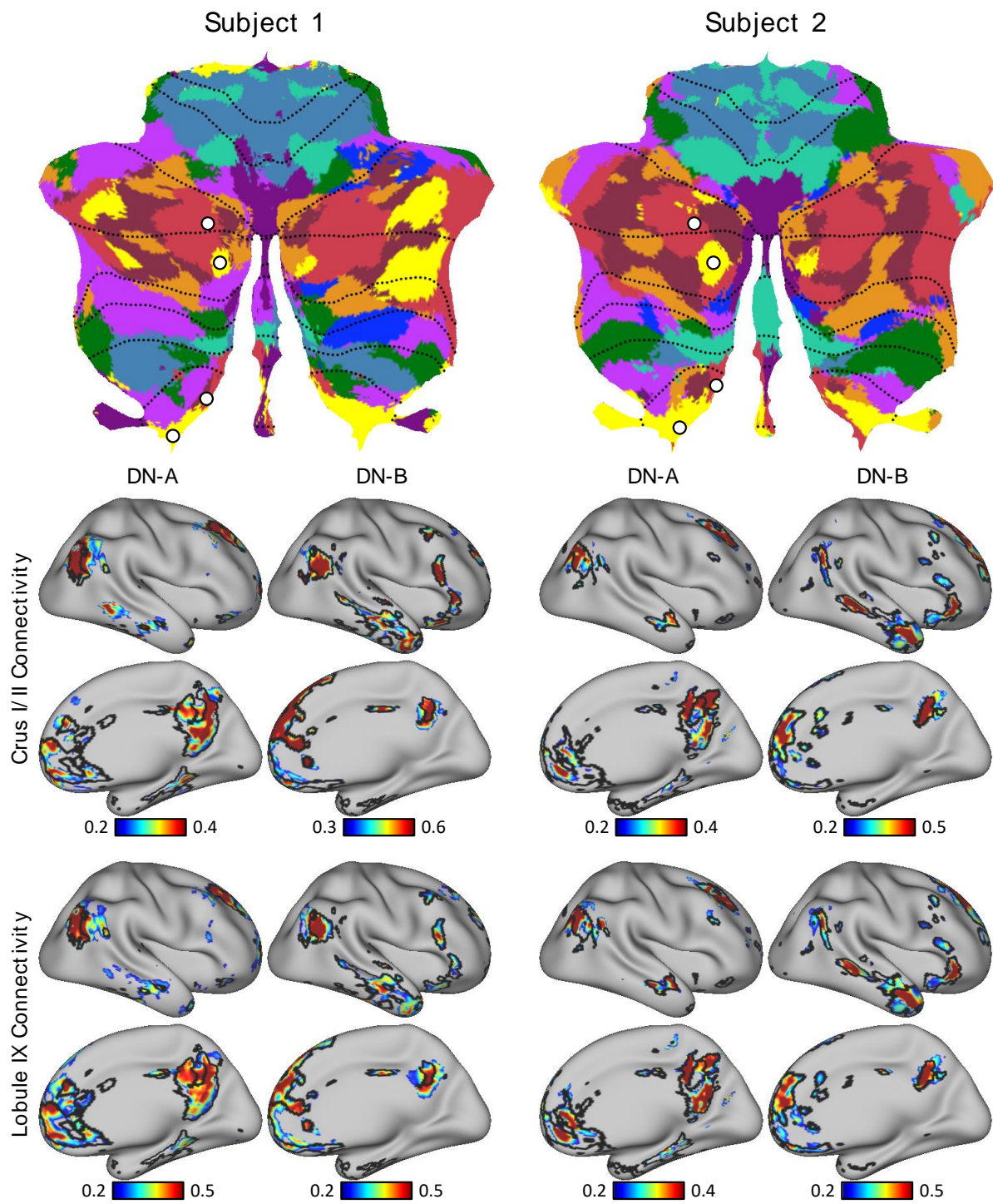
Subject 1   Subject 2

DN-A   DN-B   DN-A   DN-B

Crus I/II Connectivity

Lobule IX Connectivity

Figure 1.12 (Continued).

52

lie side by side adjacent to other higher-order association networks including control networks A and B and the language network. This complex topography in the cerebellum is reminiscent of the complex interdigitations of networks that exist in the multiple association zones of the cerebral cortex (e.g., Fedorenko et al. 2012; Braga and Buckner 2017; Gordon et al. 2017; Braga et al. 2019; Gordon et al. 2020). Despite this complex topography between the higher-order association networks, the broad hierarchical ordering was largely preserved with the default networks A and B at the apex in both subjects. Representations of the dorsal attention network were distant from the apex networks in both the anterior and the posterior lobe, and the somatomotor representations were the farthest. One unexpected exception to this hierarchical arrangement, concerning a novel representation of early visual cortex in the cerebellum, will be reported in detail in a later section.

Seed-Based Functional Connectivity Demonstrates Specificity of Cerebrocerebellar Circuits

The detailed and complex organization of the cerebellum described under Individual Cerebellar Topography Includes Multiple Representations of the Cerebrum relies on several assumptions including the use of a winner-takes-all parcellation algorithm that could give an appearance of specificity with nonspecific features and spatial blurring de-emphasized. The methods also assume there is a direct relationship between the cerebral networks and the cerebellar networks. If a cerebellar region exhibited a different connectivity pattern in the cerebral cortex, it would still be assigned to the best-fitting network. For this reason, like in our original efforts to identify network organization in averaged subject groups (Buckner et al. 2011; Yeo et al. 2011), we examined cerebellar organization using an independent method that made few assumptions about the spatial details of cerebral network organization. The basic idea here is that all analysis methods are biased and true features of organization should be robust to multiple, distinct analysis strategies.

For these analyses, we selected seed regions in the cerebellum using the discovery set and visualized their functional connectivity patterns in the cerebral cortex in the replication dataset for each individual. Across seed pairs, we asked a series of questions to test whether dissociations existed between nearby cerebellar regions as well as to test whether distributed regions in the multiple cerebellar representations link to the same cerebral network as hypothesized. Due to variability in the range of functional connectivity values, the visualization thresholds were not the same across the panels. Unthresholded maps are available on the BALSA repository (https://balsa.wustl.edu/study/show/7q3ZP).

To confirm default network representation within the cerebellum, we selected four cerebellar seed regions in each subject. To capture primary/secondary representations, two seed regions were selected in Crus I/II: one in default network A and one in default network B. To capture tertiary representations, two seed regions were selected in lobule IX: one in default network A and one in default network B. In both subjects, the resulting cerebrocerebellar functional connectivity maps were in strong agreement with individual-specific default network boundaries in the cerebral cortex (Fig. 1.12). This is a critical result that simultaneously shows the spatial specificity of the distinct default network A and B representations and that the specific representations in spatially discontinuous zones of the cerebellum converge on the same cerebral networks.

Similarly, the functional connectivity patterns of seed regions in the cerebellar language representations showed agreement with individual-specific language boundaries in the cerebral cortices of both subjects (Fig. 1.13). Although both subjects exhibited three representations of the cerebral cortex within the cerebellum, there were individual differences in the network topography. Of interest, the differences suggesting idiosyncratic spatial positions of the language network based on the winner-takes-all parcellation (the multiple blue zones in the flat maps) were confirmed by seed-based functional connectivity. Each of the three representations of the language

54

Figure 1.13. Evidence for specificity of the language network. Top: cerebellar seed regions from the language network were selected using the discovery set. Three separate seed regions were selected within each individual that included representations in the spatially distant HVI and HVIIIa regions. Bottom: functional connectivity maps of these seed regions were estimated using the replication set. Black lines indicate boundaries of the individual-specific language network and highlight agreement between the network estimates from each of the three cerebellar representations.
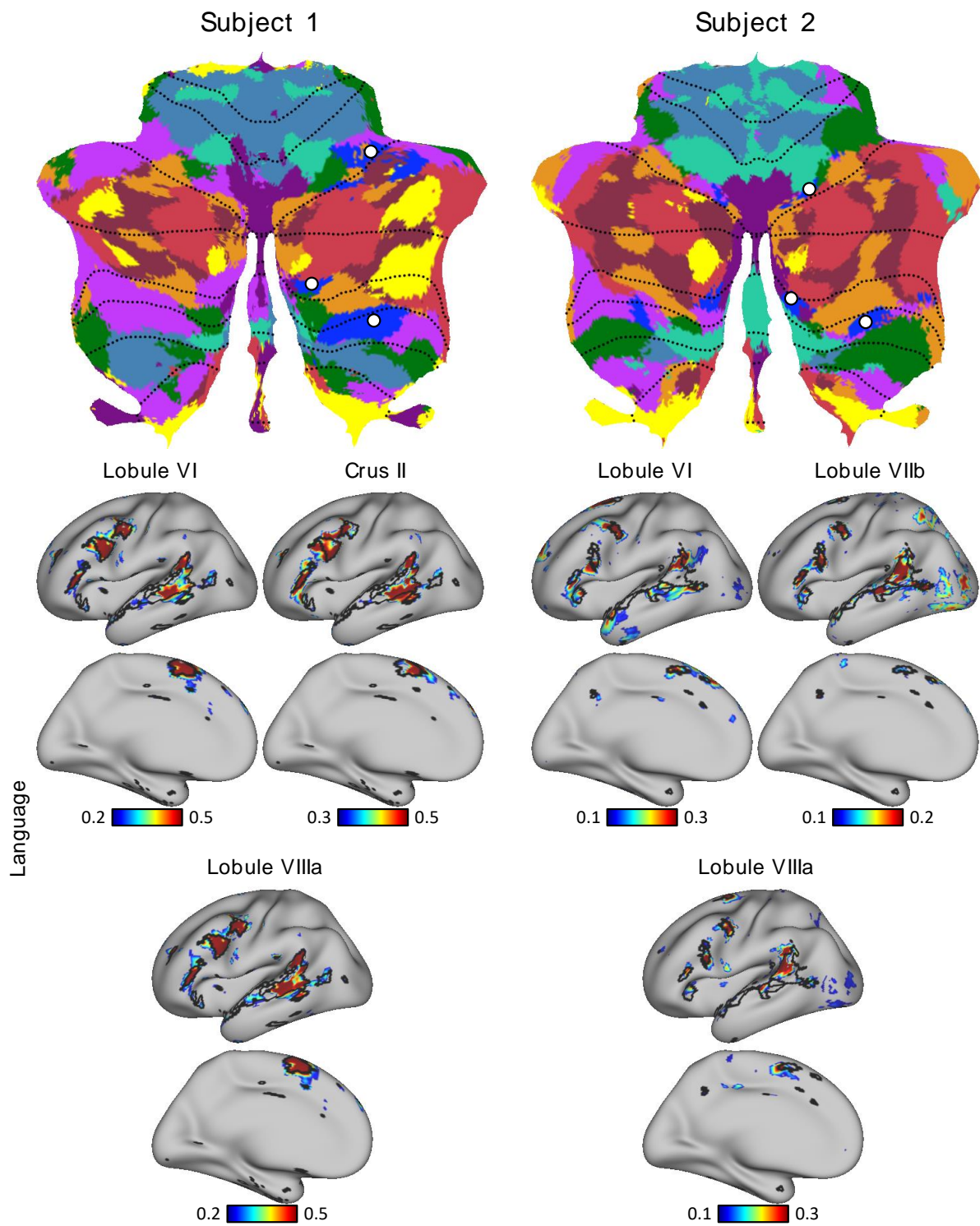
Figure 1.13 (Continued).
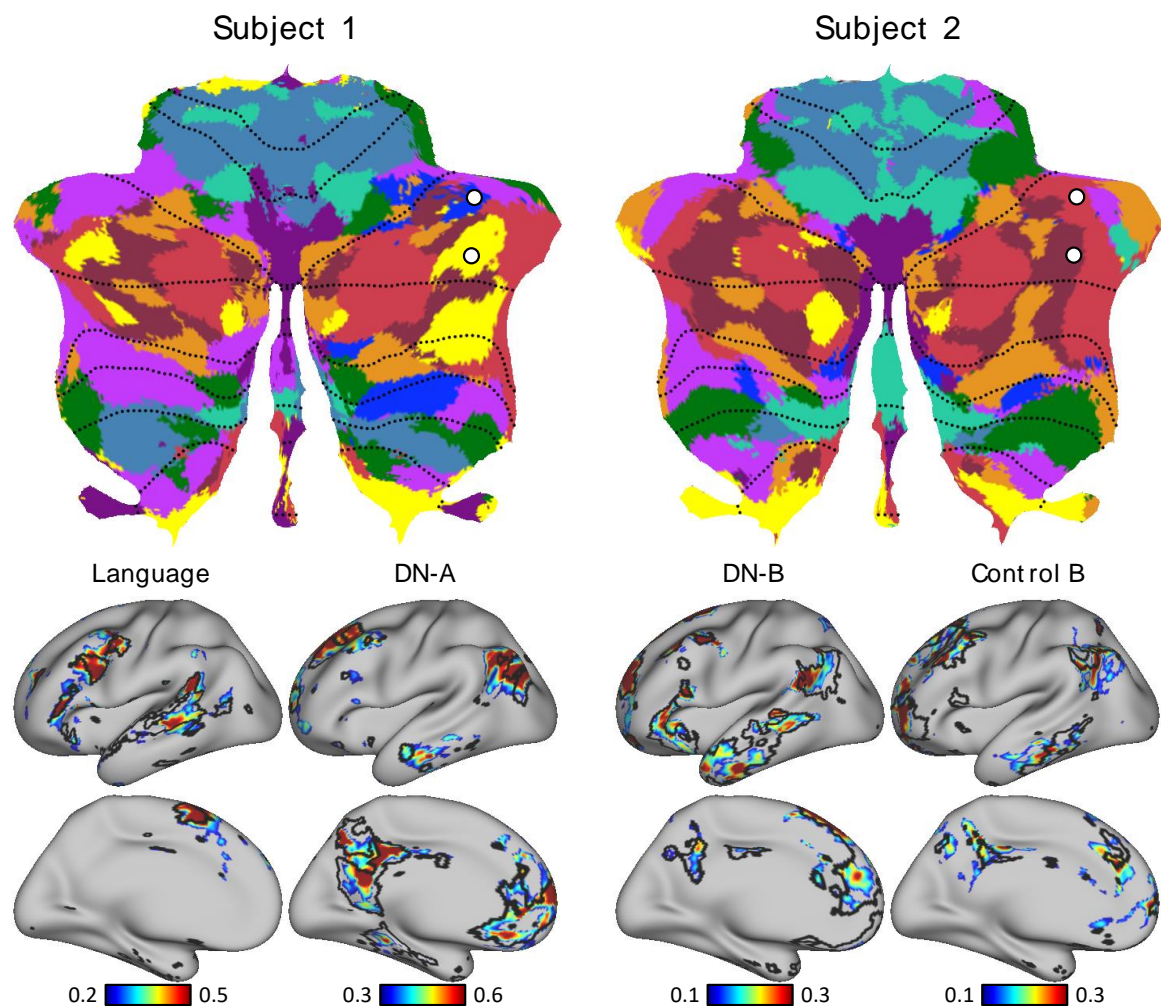
Figure 1.14. Differences in cerebellar topography between individuals were supported by seed-based functional connectivity. Top: pairs of seed regions were selected in the discovery dataset to highlight topographic differences between the two individuals. To make this point most clear, seed regions were selected for the same MNI coordinates in both subjects, with the corresponding networks they aligned to differing between subjects. The first cerebellar seed region was within the language network in subject 1 and within the default network B in subject 2. The second cerebellar seed region was within default network A in subject 1 and within control network B in subject 2. Bottom: functional connectivity maps of these seed regions were estimated using the replication sets. Black lines indicate boundaries of corresponding individual-specific networks and highlight strong agreement with functional connectivity maps. These results demonstrate how zones of the cerebellum that are located in similar volumetric positions between individuals can correspond to starkly different functional networks.

network in the right cerebellar hemisphere in each individual yielded a complete map of the spatially specific language network in each subject (Fig. 1.13).

Distinctions between networks were also confirmed. As an example, Fig. 1.14 shows the functional connectivity patterns of two pairs of cerebellar seed regions assigned to different networks by the winner-takes-all algorithm. One seed region was located in the language network in subject 1 and default network B in subject 2. The second seed region was located in default network A in subject 1 and control network B in subject 2. The functional connectivity patterns of these seed regions agreed well with individual-specific cerebral cortical network boundaries (Fig. 1.14).

An additional feature of the winner-takes-all parcellation was examined that surrounded seemingly "ectopic" network representations. In subject 2, there was a zone in the lateral right cerebellar hemisphere assigned to somatomotor cortex, surrounded by zones of higher-order association cortex. An intriguing possibility is that such a zone might emerge as a local ectopic specialized region of the cerebellum with a discontinuity from neighboring networks, at least as conceived in a hierarchical organizational framework. We did not find support for this possibility. Figure 1.15 shows a seed region placed in the candidate ectopic somatomotor representation. Unlike the dissociations described earlier in this section, where clear spatially specific network patterns emerged, here a noisy cerebral network pattern emerged. These discrepancies might be due to low signal-to-noise or biological origins that our approach was unable to capture.

Visual Representation within the Cerebellum of Individuals

Analyses of the cerebellum in humans and nonhuman primates have suggested that early retinotopic visual areas do not have a representation in the cerebellum, although recent analysis of high-resolution human data have suggested candidate zones that respond to retinotopic visual stimuli (van Es et al. 2019). The cerebellar maps in both individuals analyzed here support the
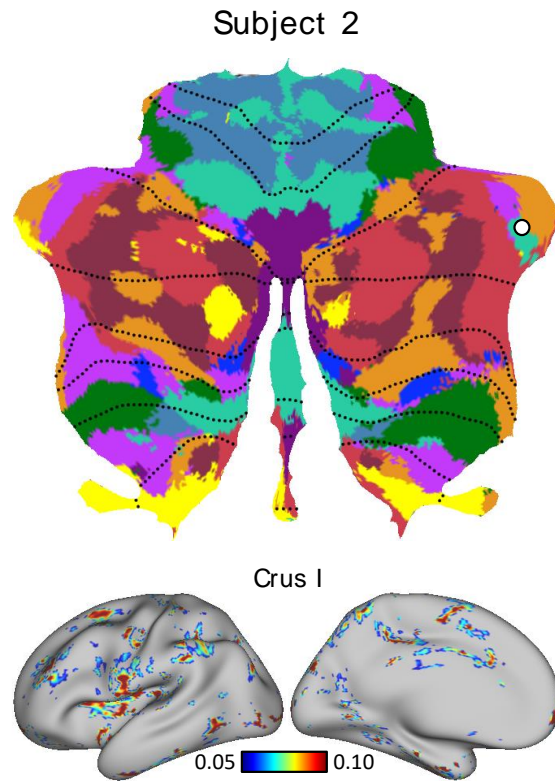
Figure 1.15. A failed test of an ectopic cerebellar functional zone. Top: a cerebellar seed region was selected using the discovery set in a region that showed an ectopic network assignment. The region was assigned to a somatomotor network in a zone of the lateral hemisphere near Crus I that is otherwise surrounded by higher-order association networks. Bottom: the functional connectivity map of the seed region estimated using the replication set reveals a distributed, noisy pattern. This pattern is not easily interpreted and may either represent an alternative biological arrangement or experimental noise that we presently do not understand. Failures of this type were rare.

existence of cerebellar representation of early retinotopic visual cortex. This visual representation was mainly present in the vermis with some extension to other lobules (mainly lobule VI) as can be seen in both subjects in the volume (Figs. 1.8 and 1.9) and flatmap (Fig. 1.10), corresponding near to the oculomotor vermis (OMV) representation of van Es et al. (2019). Functional connectivity maps of cerebellar seed regions were in agreement that these regions coupled to early visual cortex in both individual subjects, and further that they could be dissociated from higher-order visual representations linked to the dorsal attention network (Fig. 1.16).

We note that a small visual region inside the vermis was also present in our previous group-level cerebellar parcellation (Fig. 1.17; Buckner et al. 2011). Red voxels in the middle of the vermis were assigned to visual network B (Yeo et al. 2011). Comparing the group-level parcellation (Fig. 1.17) with our individual-specific parcellations (Figs. 1.8–1.10), the visual representation within the group-level parcellation was limited to the vermis.

Further exploration of seed regions within the vermis suggested that different seed locations exhibited preferential functional connectivity with central and peripheral locations of visual cerebral cortex (Fig. 1.18). To ensure that the visual representation was not an artifact of signal blurring between the cerebral cortex and cerebellum, we selected seed regions from the visual cerebral cortices (Fig. 1.19, left) and computed their functional connectivity in the volume (Fig. 1.19, right). The bright correlated regions within the cerebellum (white circles in Fig. 1.19) were clearly distant from the occipital lobe for both subjects, suggesting that the visual representation within the vermis was unlikely to be an artifact of signal blurring.

The Cerebellum Is Proportionately Mapped to the Cerebral Cortex

The final analysis explored the relationship between the extent of each network representation in the cerebral cortex to that of its representation in the cerebellum (paralleling Bucker et al. 2011; Marek et al. 2018). For this analysis, the networks were analyzed separately for

Figure 1.16. Evidence for specificity of a visual network representation in the cerebellum. Top: cerebellar seed regions were selected using the discovery set within a region of the vermis assigned to the visual network (purple) and a spatially separate region assigned to the dorsal attention network. Bottom: functional connectivity maps of these seed regions were estimated using the replication set. Black lines indicate boundaries of individual-specific visual and dorsal attention networks and highlight agreement with functional connectivity maps. The functional connectivity maps support the existence of early visual representation within the vermis of the cerebellum. Of note, the cerebral cortical regions coupled to the cerebellar vermis included early retinotopic visual cortex at or near V1.
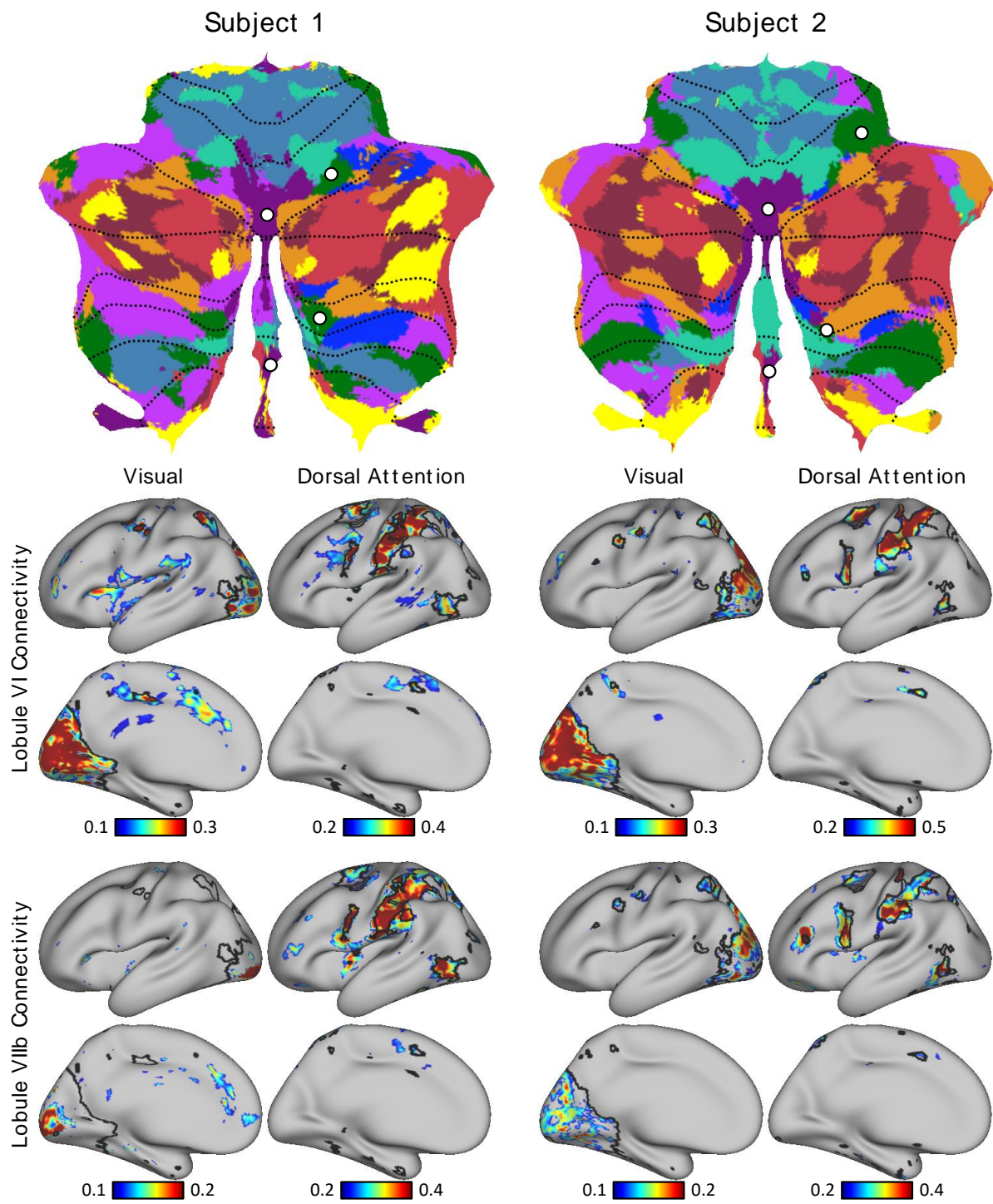
Figure 1.16 (Continued).
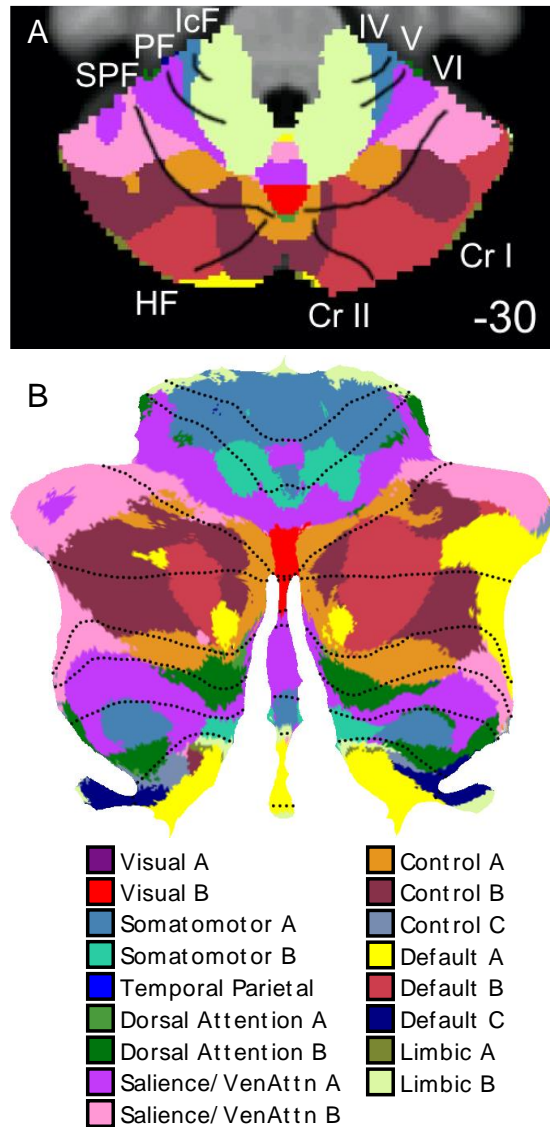
Figure 1.17. Evidence for visual network representation in group-averaged data. Group-level 17-network cerebellar parcellation from Buckner et al. 2011 also revealed visual representation (visual B in red) in the vermis. A: an axial section shows visual network B in the vermis. B: the same data projected to a flatmap. The visual region appeared in roughly the same location in both the group-level and individual-specific cerebellar parcellations (see Fig. 1.16). Cr I, Crus I; Cr II, Crus II; HF, horizontal fissure; IcF, intraculminate fissure; IV, lobule IV; PF, primary fissure; SPF, superior posterior fissure; V, lobule V; VI, lobule VI.

Figure 1.18. Evidence for central and peripheral visual representations coupled to primary visual cortex within the cerebellum. Top row: V1 is estimated in each individual based on projected histology (green line) and within-individual functional connectivity gradients (red-yellow lines). Histological estimates are derived from the Juelich atlas in FreeSurfer (Amunts et al. 2000; Fischl et al. 2008). The functional connectivity gradient maps (Laumann et al. 2015; Gordon et al. 2016) show sharp transitions in functional connectivity patterns across the cerebral cortex and align with the histological V1 boundaries. Middle rows: cerebral functional connectivity maps are displayed from seed regions placed in the visual zone of the cerebellar vermis. Histological V1 and V2 boundaries from the Juelich atlas in FreeSurfer are overlaid in black. Note that functional connectivity patterns strongly overlap with the estimate of primary visual cortex (V1). Separate regions are associated more with the peripheral and central visual zones, particularly evident for subject 1. Bottom row: the locations of the cerebellar seed regions are displayed in sagittal sections.
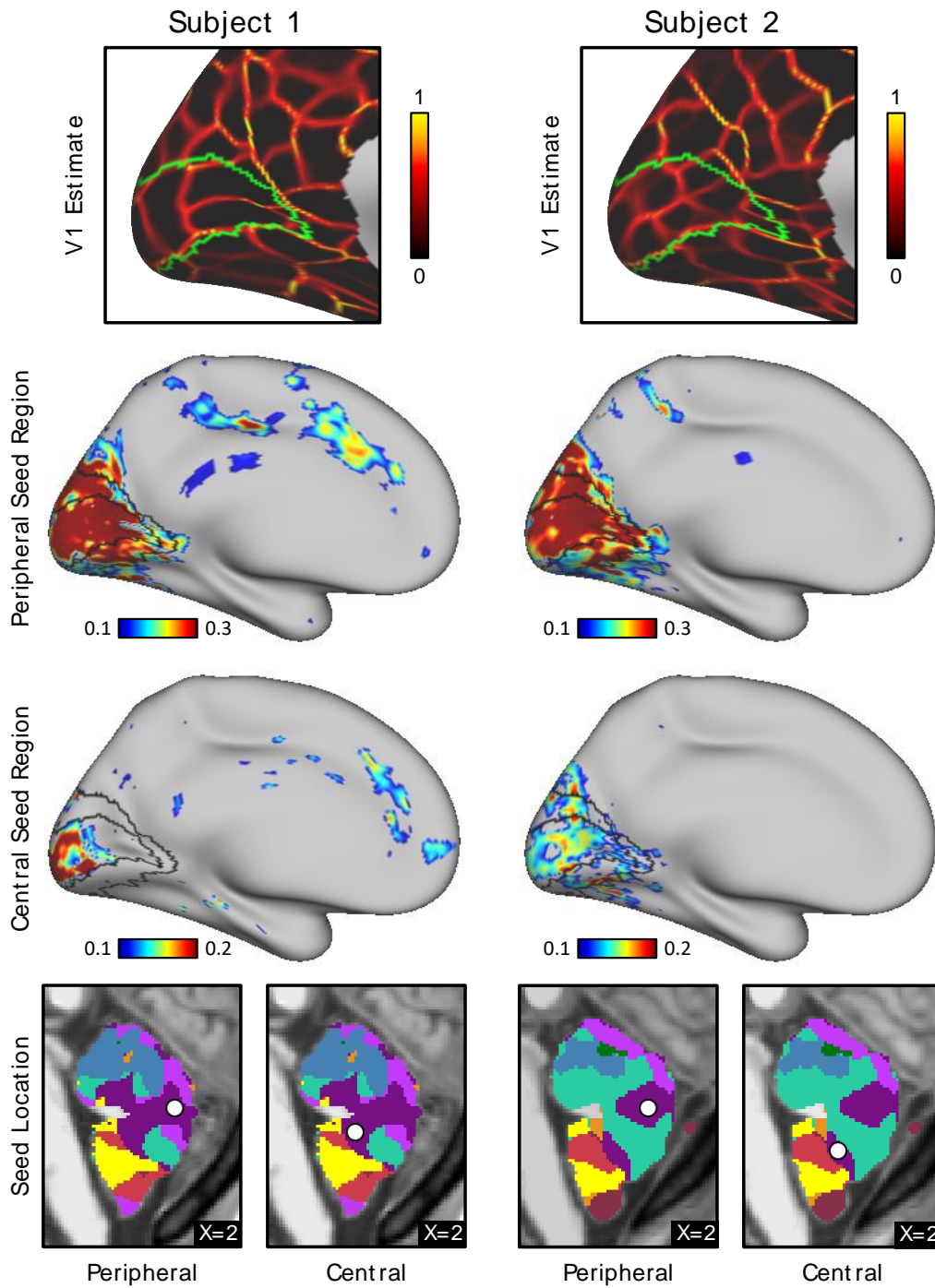
Figure 1.18 (Continued).
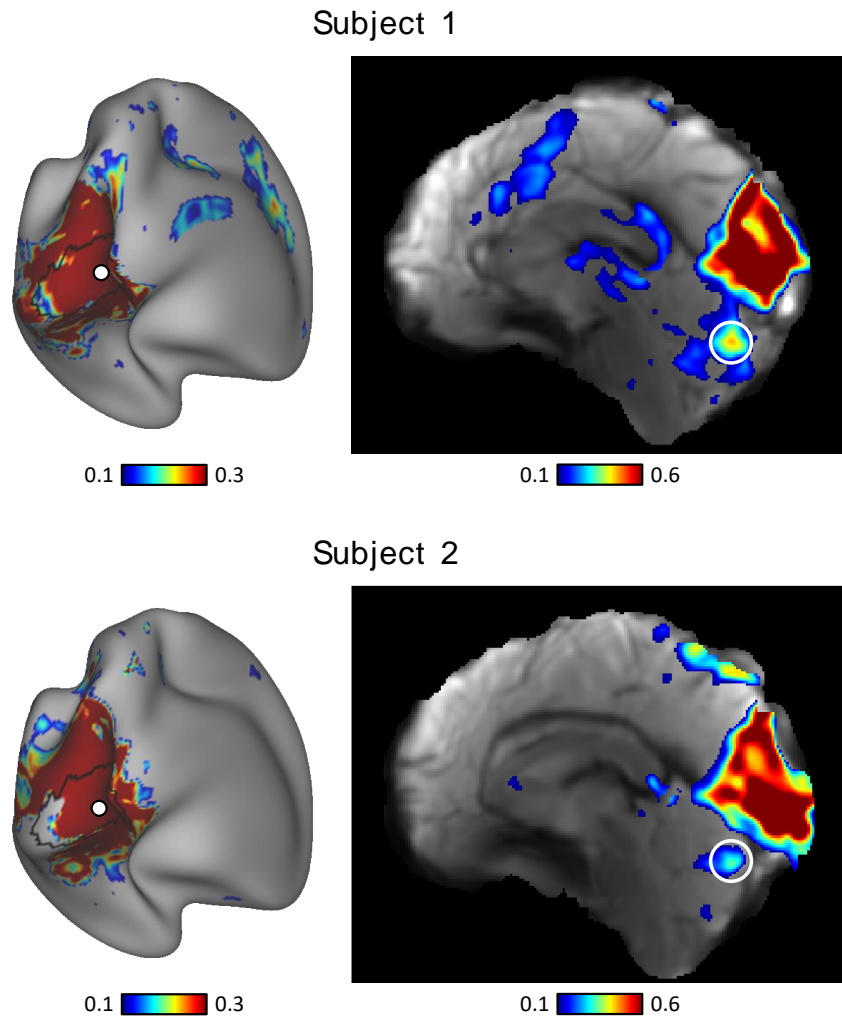
Figure 1.19. Primary visual cortex connectivity reveals selective representation in the cerebellum within individuals. Seed regions were selected in the visual cerebral cortex in the discovery set. The seeds regions are shown as white circles in the left panels. Functional connectivity maps of the seed regions were computed in the volume using the replication dataset and shown in the right panels. Cerebellar islands (white circles) show high connectivity with cortical visual regions that are separate from the correlation within and around the seed region in the cerebral cortex (the large region above), suggesting that the visual representation within the vermis is unlikely to be the result of signal leakage from the occipital lobe.
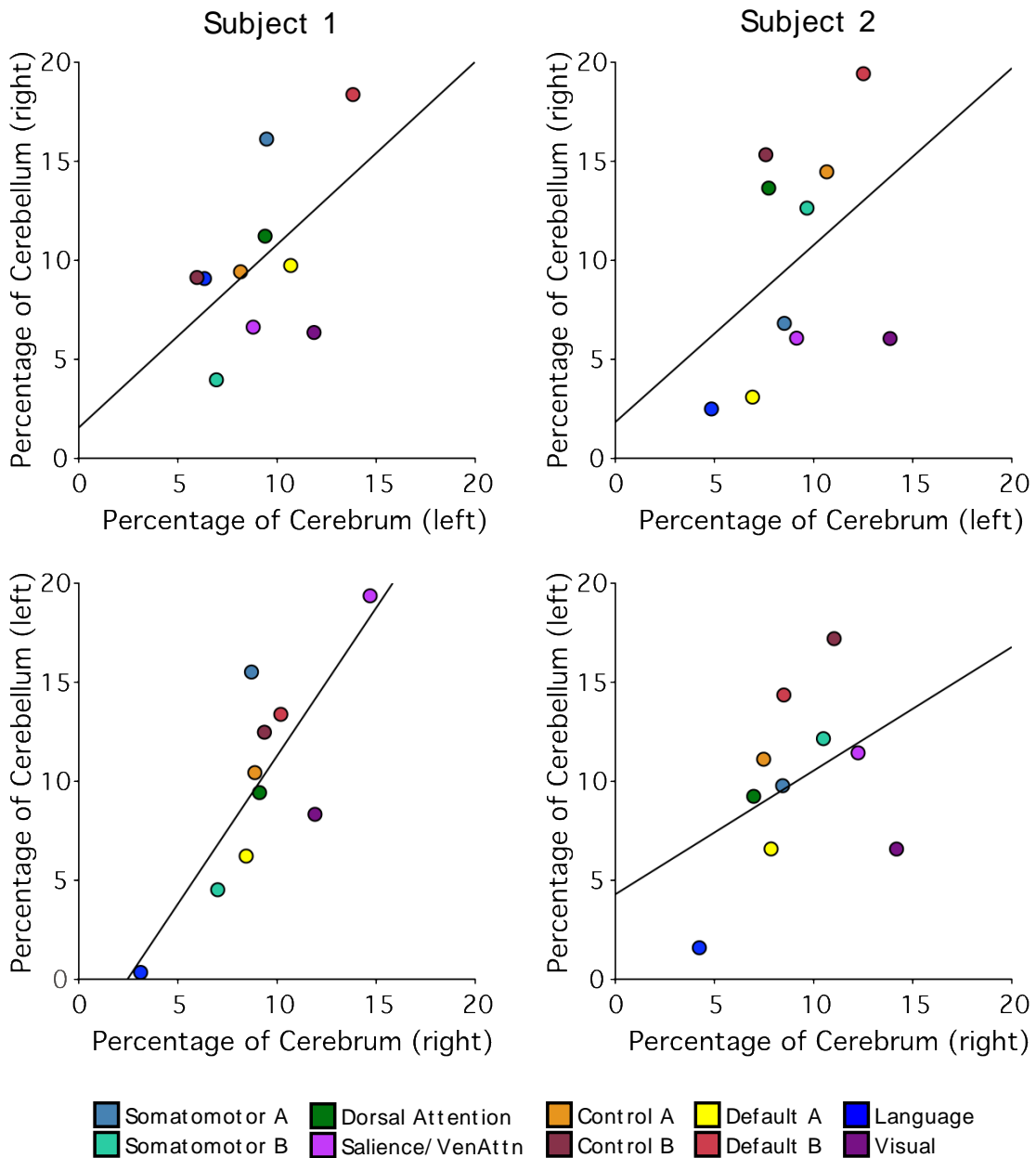
Figure 1.20. Relationship between the extent of cerebral and contralateral cerebellar cortices assigned to distinct functional networks. Each colored circle represents a different network as labeled at bottom. The x-axis shows the percentage of cortical vertices assigned to each network. The y-axis shows the percentage of cerebellar voxels assigned to each network in the contralateral hemisphere. The black lines indicate best-fit regression lines.

the left and right hemispheres so as to allow lateralized networks to reveal their organization fully. Figure 1.20 shows the relationship between the extent of cerebral and contralateral cerebellar cortices assigned to distinct functional networks.

In general, networks occupying larger proportions of the cerebral cortex possessed larger cerebellar representations. Across the two subjects and including both hemispheres, the relationships ranged from r = 0.41 to 0.81. The results did not reveal any consistent pattern that might suggest disproportionate representation of a single association network in the cerebellum. In particular, the two networks associated with cognitive control were represented as expected in the cerebellum, with no clear disproportionate relationship as compared with the default networks A and B, the language network, or the dorsal attention network.

Discussion

Detailed analysis of cerebellar organization reveals a macroscale organization. Within this broad macroscale organization are additional reproducible topographic features that include separation of distinct higher-order association networks linked to the default network, language, and cognitive control.

A Macroscale Organization Is Present in the Cerebellum despite Individual Differences

A key result of the present findings is that a conserved topographic organization of the cerebellum emerges reproducibly between individuals despite a complex topography and individual differences. Both intensively sampled individuals analyzed here demonstrated the same broad macroscale organization. These findings support the hypothesis that, just as the cerebral cortex demonstrates a broad macroscale organization, the topography of the cerebellum is likely

driven by developmental constraints—a conserved Bauplan—that is expressed between individuals despite differences in idiosyncratic anatomical features.

In many ways this result is expected. Global organizational features such as the double somatomotor map with its inverted orientation in the anterior lobe and upright orientation in the posterior lobe are conserved between distantly related mammalian species including cats and monkeys (Adrian 1943; Snider and Stowell 1944) and detected using direct physiological methods (Adrian 1943; Snider and Stowell 1944), task-based functional MRI (Buckner et al. 2011; Diedrichsen and Zotow 2015; Grodd et al. 2001; Wiestler et al. 2011; Boillat et al. 2020), and intrinsic functional connectivity (Buckner et al. 2011; Marek et al. 2018). The present data extend these observations to suggest that the general spatial arrangements of the cerebellar association zones are conserved between individuals. Specifically, the network organization in the cerebellum follows a hierarchical macroscale gradient paralleling recent observations in the cerebral cortex (Braga and Buckner 2017; Buckner and DiNicola 2019; Margulies et al. 2016; Huntenburg et al 2018).

The primary cerebellar hierarchy begins in the anterior lobe, progressing from the primary somatomotor zone to first-order association networks linked to sensory-motor processes (the dorsal attention and salience/ventral attention networks) and then to higher-order association networks (cognitive control and default networks A and B). The hierarchy reverses and progresses through the same set of networks in opposite order, ending in the secondary somatosensory zone in VIIIa/VIIIb. This major gradient is consistent with that proposed by Guell et al. (2018b). Like the cerebral hierarchy, the cerebellar zones progress from networks involved in processing and acting on the external sensory environment to anatomically distant zones linked to networks involved in constructive aspects of cognition. Why there are major gradients in the cerebellum and why they show an inverted topography mirrored on either side of the Crus I/II border are open questions

that will likely be informed by better understanding of developmental mechanisms that specify early projection patterns.

Evidence for a third hierarchical representation situated in the most posterior extent of the cerebellum is also provided, as hypothesized based on group data (Buckner et al. 2011; Guell et al. 2018b). In both individuals, clear representations of default networks A and B were present in IX, surrounded by representations of the cognitive control network anteriorly and then the dorsal attention and salience/ventral attention networks before the prominent somatomotor representations in VIIIa/VIIIb. The posterior representations of default networks A and B in IX, when seeded with small regions, were each sufficient to reproduce the full distributed extents of the separate association networks (Fig. 1.12). The possibility of a posterior representation of cognitive networks was anticipated by the polysynaptic tracing observations by Kelly and Strick (2003), who observed projections to and from the prefrontal cortex to lobule IX/X in the monkey (see their Fig. 11). Here, we reveal that these posterior zones, when analyzed within the individual, possess distinct localized representations of the multiple association networks.

A Cerebellar Language Network Can Be Distinguished from Adjacent Association Networks

One of the earliest observations suggesting the involvement of the cerebellum in cognition was that the right lateral cerebellum was active during cognitive demands of a speech production task (Petersen et al. 1989). Despite this origin, multiple published estimates of the cerebellar organization based on group functional connectivity MRI (Buckner et al. 2011) and individual functional connectivity MRI (Marek et al. 2018) do not identify a clear language network in the cerebellum. A contributing reason for this omission is likely that networks important to language are adjacent to the largest association network identified with functional connectivity (the default network) and are blurred together in many functional connectivity analyses (for discussion, see Braga et al. 2020).

Recent cerebellar mapping efforts explicitly using tasks demanding language processing yield clear responses at or near the Crus I/II border (King et al. 2019; see also Guell et al. 2018a). For example, using a covert verb generation task similar to that originally used by Petersen and colleagues, King et al. (2019) demonstrated a large region of response near right Crus I/II that overlapped the response observed during a theory-of-mind task (see their Fig. 1). These prior studies make clear that networks important to language are represented in the cerebellum but also that the location of the regions and their separation from other networks is challenging. Within the cerebrum, specialized regions involved in language are finely juxtaposed next to distinct higher-order association regions involved in cognitive control and default networks A and B (Fedorenko et al. 2012; Braga et al. 2020).

Here, we found clear representation of a language network in the cerebellum that is spatially separate from nearby association networks. In both individuals, the language network abutted the major Crus I/II zones linked to default network B and cognitive control network A, echoing their proximity in the cerebral cortex (Braga et al. 2020). The network was strongly right lateralized in one individual and more bilateral in the other, reflecting variation in lateralization that is well known in the cerebrum (and provisionally established for the cerebellum; Wang et al. 2013). These findings suggest the presence of multiple discrete cerebellar zones that are components of a network specialized for language. The cerebellar language network regions fall within a larger zone of multiple, specialized association networks, as discussed in the next section.

The Crus I/II Apex Possesses Juxtaposed Zones That Participate in Specialized Networks

Beyond the broad gradient evident in both individuals, at the Crus I/II border, which forms the apex of the cerebellum, multiple association networks were juxtaposed next to one another with idiosyncratic spatial patterns between individuals. The flatmap visualization in Fig. 1.10 displays this feature. Virtually all networks have multiple representations that fall along the medial

to lateral extent of the cerebellum, which are interdigitated with distinct association networks. Detailed analyses of the focal zones in Figs. 1.12–1.14 support that most of these local cerebellar zones are specific for a single cerebral network rather than a technical artifact of a winner-takes-all parcellation. For example, the cerebellar zones that are associated with the language network possess multiple representations at the edges of the Crus I/II association cluster. Each of these representations, when seeded in the cerebellum, yields the distributed cerebral association network linked to language function (Fig. 1.13) and can be dissociated from nearby zones (Fig. 1.14). As another example, the local cerebellar zones that are linked to default networks A and B (Braga and Buckner 2017; Braga et al. 2019; DiNicola et al. 2020) show multiple dissociated representations in the cerebellum, including separate medial and lateral components (Fig. 1.12). The organization of these multiple and interdigitated representations of networks within the Crus I/ II association region was not revealed in earlier group-averaged analyses of cerebellar topography and does not appear to reflect a simple linear gradient.

The complex organization within individuals raises several issues to consider for future studies. First, description of the detailed organization of the cerebellum requires high resolution, almost certainly better than that achieved here or in the field to date. Features of functional organization are missed when group-averaged or lower-resolution estimates are obtained. Second, there are translational implications of the present results. The Crus I/II apex is the closest portion of the cerebellum to the scalp (~15 mm), approximately half the distance to the estimated somatomotor representations in lobule V (~30–35 mm). Given that the cerebellum has emerged as a neuromodulatory target for neuropsychiatry (e.g., Brady et al. 2019) and transcranial magnetic stimulation (TMS) can alter cognitive domains (Desmond et al. 2005; Esterman et al. 2017; Sheu et al. 2019), detailed modeling of stimulation effects on distinct networks at and around the Crus I/II apex will become increasingly relevant. The juxtaposition of network regions and individual variation will be important considerations.

Finally, the complex interdigitation of association networks—as an anatomical feature—is itself a target for understanding. Similar to the cerebral cortex, the cerebellum possesses a broad macroscale organization (see also Buckner et al. 2011; Guell et al. 2018a). Within that organization is a set of fractionated zones linked to distinct cerebral networks, supporting specialized cognitive functions. At the Crus I/II apex, there are zones linked to cerebral networks involved in language, remembering, and aspects of social cognition. Zones of the cerebellum supporting these advanced forms of cognition and the boundaries between them seem unlikely to be fully specified by innate molecular gradients. Rather, paralleling what has been hypothesized for cerebral organization (e.g., Buckner and DiNicola 2019; DiNicola et al. 2020), cerebellar development may be influenced by protracted activity-dependent sculpting that differentiates these interdigitated zones within an earlier-specified broad gradient. A hierarchical developmental sequence might explain the broad macroscale organization that is observed across individuals (and even species) as well as the interdigitated and varied organization that exists within regions including the Crus I/II apex (see also Marek et al. 2018).

The Cerebellar Vermis Represents the Central Field of Primary Visual Cortex

Visual topography at or near the vermis has not widely been discussed in prior studies of human cerebellar organization, including in our own work (e.g., Buckner et al. 2011). However, motivated by the present work, we revisited our earlier group-averaged cerebellar parcellations and did find that the vermis was coupled to a visual network representing peripheral visual eccentricities (Fig. 1.17). More recently, in a thorough and detailed analysis of the vermis using visually evoked task data from the HCP, van Es and colleagues (2019) reported strong evidence that the vermis maps to topographically organized visual space. The present results provide convergent evidence that the vermis is coupled to a cerebral visual network and further reveals that the

mapping 1) is linked to primary visual cortex and 2) possesses representation of the central visual field.

An additional feature of the vermis mapping is that it can be distinguished from a nearby but separate cerebellar representation of the dorsal attention network (Fig. 1.16). The two sets of regions within the cerebellum are coupled to nonoverlapping networks in the cerebral cortex. The vermis is coupled to early retinotopic cortex that includes central V1; distributed zones that include prominent representations in lateral VI and VIIb/VIII are coupled to the dorsal attention network, consistent with the observations of Brissenden and colleagues (2018).

Boillat and colleagues (2020) recently generated human task-based somatomotor maps in the cerebellum at high resolution within the individual through instructed movement of body parts, including the eyes. In their eye movement task, a dot jumped back and forth across the screen and the subjects followed it. Their analysis revealed an eye-selective response within the vermis (see also King et al. 2019). As van Es et al. (2019) note in their detailed analysis of the vermis, maps based on retinotopic stimulation while subjects are fixating cannot unambiguously distinguish among retinotopic (eye-centered), head-centered, and world-centered spatial mapping. It is thus of particular interest that the present results identify the vermis of the cerebellum through its functional coupling to early retinotopic visual cortex, in the cerebellar region that has also been identified in studies of eye movement.

Work in nonhuman primates has long suggested that the cerebellar vermis participates in spatially mapped oculomotor function including adaptive response to saccadic errors (Optican and Robinson 1980; Sparks and Mays 1990; Herzfeld et al 2015; Soetedjo et al. 2019). For this reason, the region has often been labeled the oculomotor vermis or OMV (e.g., van Es et al. 2019; Yamada and Noda 1987). Focus of OMV's role in saccade error correction has most often highlighted signals originating from the superior colliculus and on aspects of motor-control related to saccadic adjustment. The present results suggest OMV, directly or indirectly, represents information coupled

to primary visual cortex (Figs. 1.16–1.19). The finding that OMV is coupled to primary visual cortex, while incompletely understood at this time, may be relevant to understanding how motor predictions are integrated with their perceptual outcomes.

Limitations and Caveats

A key limitation of the present results is that they are based on correlations between cerebral and cerebellar signals. Future work will be required to verify the functional-anatomical details through differential task-induced responses of the cerebellar subzones proposed to be distinct via the present findings. In this light, the detailed maps of the cerebellum generated here within individual subjects should be considered hypotheses, much like our earlier work on group-averaged data (Buckner et al. 2011) and those from other efforts (Stoodley and Schmahmann 2009; Guell et al. 2018a; King et al. 2019; Marek et al. 2018). The present work adds to this progressing endeavor by describing new details around the Crus I/II border where multiple, previously undistinguished zones are demonstrated to couple to distinct interdigitated cerebral networks.

A further limitation of the present work, that also applies to prior functional neuroimaging work on the human cerebellum, pertains to resolution. The folia of the cerebellum are organized like a fine-folded accordion that, if unraveled, are ~1m long and 10cm wide (Sereno et al. 2020; see also Diedrichsen and Zotow 2015; Sultan and Braitenberg 1993; Van Essen 2002). Small errors in localization in the volume can translate into differences of centimeters on the modeled cerebellar surface. Our functional data collected here at 2.4-mm resolution and smoothed during processing falls far short of what would be required to resolve the cerebellar cortex [Sereno et al. (2020) used < 0.2 mm voxels to reconstruct the cerebellar surface]. For the foreseeable future, functional analyses within individuals will be based on probabilistic relationships to the details of surface geometry. The present analyses likely miss (or distort) topographic features of functional anatomy (for discussion, see Sereno et al 2020; Diedrichsen and Zotow 2015).

One technical point to mention for future experimentalists is that the present results were not our first attempt to map within-individual organization of the cerebellum. Beginning shortly after our initial efforts to map the cerebellum in the group (Buckner et al. 2011), we attempted several times to map the detailed organization, especially the hypothesized third map near the posterior lobe [the 7 T reported by Braga et al. (2019) was originally analyzed for such a purpose]. In each instance, while aspects of cerebrocerebellar topography could be mapped using functional connectivity (e.g., the representation of the default network in Crus I/II), other aspects needed for validation failed (e.g., the detection and reversal of the body maps as illustrated here in Fig. 1.3). The clear patterns presented in this paper only emerged when we collected extremely large quantities of data within the same individual, thereby boosting signal-to-noise significantly. We do not yet know the boundary conditions of what amount of data are required to explore within-individual anatomy at high resolution and how alternative analytical approaches might improve the situation, but we have been struck by the need to acquire far more data than was necessary for our parallel analyses of the cerebrum. For more detailed discussion of group-level versus individual-level analyses, we refer the reader to the growing literature on this topic (Fedorenko et al. 2012; Laumann et al. 2015; Braga and Buckner 2017; Gordon et al. 2017).

Conclusions

The human cerebellum possesses a topographic representation of multiple higher-order association networks. Separate cerebellar zones can be shown to couple selectively to distinct networks that are finely interdigitated in the cerebral cortex, including networks hypothesized to support advanced functions related to remembering, making social inferences, and language.

Endnote

Chapter 2. A Third Somatomotor Representation in the Human Cerebellum

__Contribution:__ I contributed to the data collection along with L.M.D, and also assisted N.S-G. with task creation, data processing and analyses, and interpretation where needed. I later provided input on writing and revisions. N.S-G. and R.L.B led study design, interpretation, and writing.

Abstract

Seminal neurophysiological studies in the 1940s discovered two somatomotor maps in the cerebellum – an inverted anterior lobe map and an upright posterior lobe map. Both maps have been confirmed in the human using non-invasive neuroimaging with additional hints of a third map within and near to the cerebellar vermis. Here we sought direct evidence for the third somatomotor map by using intensive, repeated functional MRI (fMRI) scanning of individuals performing movements across multiple body parts (tongue, hands, glutes and feet). An initial discovery sample (N=4, 4 sessions per individual including 576 separate blocks of body movements) yielded evidence for the two established cerebellar somatomotor maps, as well as evidence for a third discontinuous foot representation within the vermis. When the left versus right foot movements were directly contrasted, the third representation could be clearly distinguished from the second representation in multiple individuals. Functional connectivity from seed regions in the third somatomotor representation confirmed anatomically-specific connectivity with the cerebral cortex, paralleling

the patterns observed for the two well-established maps. All results were prospectively replicated

in an independent dataset with new individuals (N=4). These collective findings provide direct

support for a third somatomotor representation in the vermis of the cerebellum that may be part of

a third map. We discuss the relations of this candidate third map to the broader topography of the

cerebellum as well as its implications for understanding the specific organization of the human

cerebellar vermis where distinct zones appear functionally specialized for somatomotor and visual

domains.

New and Noteworthy: A third somatomotor representation exists in the vermis of the human

cerebellum. Evidence for this elusive representation arises specifically from mapping the foot.

Separate foot representations distinguish the third from the nearby second somatomotor

representation. A third somatomotor map in the posterior vermis supports a large scale

organization hypothesis in which the cerebellum possesses three full sets of homotopic

representations of the full cerebrum.

Introduction

A somatomotor topography was first described in the anterior lobe of the cerebellum by

Edgar Adrian (Adrian 1943). In cats and monkeys, Adrian recorded afferent discharges reaching the

cerebellum following electrical stimulation to the cerebral cortex, tactile stimulation, movements of

joints and stretching of muscles. He discovered that body parts are topographically organized in an

inverted fashion beginning with the hindlimb represented in lobules III and HIII, the forelimb in

lobules IV, V and HIV and HV, and the face in lobules VI and HVI at the posterior border of the

anterior lobe. A year after Adrian's seminal observations, Snider and Stowell (1944) confirmed the

anterior lobe somatomotor topography and discovered a second discontinuous body map in the posterior lobe that was upright rather than inverted (Snider and Stowell 1944). They recorded cerebellar evoked potentials, also in cats and monkeys, following tactile stimulation. In the paramedian lobule (lobules HVII, HVIII), the hindlimb representation was found posteriorly, the face anteriorly and the forelimb in between (Snider and Stowell 1944; see also Snider and Eldred 1952).

A half century after their discovery, the anatomical basis of the two separate somatomotor maps was revealed using transneuronal viral tracing techniques. A barrier to measuring anatomical connectivity between the cerebral cortex and the cerebellum was that the pathways are polysynaptic and did not yield to traditional monosynaptic anatomical tracing techniques (Evarts and Thach 1969; Strick 1985; Schmahmann and Pandya 1997). Using polysynaptic tracing techniques based on specific strains of herpes and rabies viruses, Strick and colleagues (Zemanick et al. 1991; Middleton and Strick 1994; Kelly and Strick 2003) demonstrated that the hand region of the monkey's cerebral motor cortex projects to and receives input from cerebellar lobules V-VI in the anterior lobe and HVIIb-HVIII in the posterior lobe, consistent with the two well-established somatomotor maps.

The two distinct somatomotor maps have been repeatedly observed in humans using non-invasive neuroimaging techniques evoked by movements (Nitschke et al. 1996; Rijntjes et al. 1999; Grodd et al. 2001; Buckner et al. 2011; Diedrichsen and Zotow 2015; Guell et al. 2018a) and through tactile stimulation (Fox et al. 1985, Bushara et al. 2001; Takanashi et al. 2003). Functional connectivity between cerebral motor regions and the cerebellum in task-free data also reveals the two maps (Buckner et al. 2011; Guell et al. 2018b; Xue et al. 2021). Thus, multiple approaches have converged to suggest that the cerebellum possess two distinct somatomotor body maps. Beyond these two established somatomotor body maps, we have also postulated the existence of a third, smaller body map in the posterior extent of the cerebellum within and near to the vermis

80

(Buckner et al. 2011). There are multiple motivations for this hypothesis. In comprehensive mapping efforts that have explored both somatomotor and non-somatomotor regions of the cerebellum, an orderly progression of zones is found along the anterior-to-posterior axis of the cerebellum variably described as a sequence of networks or a gradient (Buckner et al. 2011; Buckner 2013; Guell et al. 2018b; Xue et al. 2021). The progression begins with the inverted somatmotor map in the anterior lobe of the cerebellum and then progresses through multiple sensory-motor and higher cognitive networks ending at the Crus I / II border. The progression of networks inverts at the Crus I / II border and proceeds in mirror-reversed order through the posterior lobe of the cerebellum ending on the well-established upright somatomotor map. While these two gradients alone capture many features of the observed organization of the cerebellum, they fail to explain a key feature.

Specifically, cerebral networks associated with higher-order functions display representations in the posterior lobe of the cerebellum near lobule IX, which would be expected if there was a third gradient, including somatomotor representation. In particular, the network referred to in the human literature as the default network possesses a robust representation in lobule IX (Buckner et al. 2011; Xue et al. 2021; Habas et al. 2009; Krienen and Buckner 2009;). Tasks targeting social inferences, which increase response in the default network, also reveal a response in lobule IX (Diedrichsen and Zotow 2015; Guell et al. 2018a; King et al. 2019). Furthermore, in their seminal work, Kelly and Strick (2003) noted that Crus I / II receive prefrontal projections but also described a smaller group of neurons in lobules IX / X. The labelled neurons fall within the region of the suggested tertiary association map in the posterior end of the cerebellum [see Figure 1 in Guell et al. 2018a]. One possibility is that a third map represents cognitive networks but not motor networks, or what Guell et al. (2018a) refer to as the "double motor/triple nonmotor representation hypothesis." The alternative possibility is that the cerebellum possesses a third somatomotor map that is small and challenging to identify.

Hints of a third somatomotor representation exist in the literature. In an early electrophysiological study, Dow and Anderson (1942) documented responses to tactile stimulation in the pyramis (part of the posterior vermis) of rats. With transneuronal viral tracing techniques, Coffman et al. (2011) showed that the cerebellar vermis is a target of projections from motor regions in the cerebral cortex of monkeys . More broadly, this finding challenged longstanding concepts about functional organization of the cerebellum. The vermis is considered part of the "spino-cerebellum" as it is the target of ascending spinal pathways while the lateral cerebellar cortex is part of the "cerebro-cerebellum" due to dense interconnections with the cerebral cortex. Coffman et al. (2011) showed that the density of projections from motor regions in the cerebral cortex to the vermis is as great as the density of projections to the lateral cerebellar cortex.

In humans, one of the first studies to use fMRI to map the cerebellum noted that there might be a third somatomotor representation in the vermis (Rijntjes et al. 1999). However, this suggestion was made with caution due to the small sample size and mixed results. In our prior well-powered, group-averaged study, a small medial region within and near to the vermis of the cerebellum was linked to cerebral somatomotor networks (see the transverse section at Z = -38 and the coronal section at Y=-68 in Fig. 8 of Buckner et al. 2011). But the representation in the vermis could not be disambiguated from the adjacent zones of the cerebellum attributed to the established second somatomotor map. Similarly, Guell et al. (2018a) noted a candidate motor representation of the foot near the vermis but with sufficient location uncertainty to downplay the result.

A definitive demonstration of a third somatomotor map, if one exists, faces multiple challenges. First, the hypothesized map is expected to be found in a small area within the already small cerebellum. Second, the inferior portions of the cerebellum near the vermis have low signal-to-noise ratio (SNR) in fMRI compared to the cerebral cortex.[1] Finally, a third somatomotor map is

---

[1] Within our own work we have previously looked for a third map using functional connectivity fMRI both at high-field, high-resolution 7T Braga et al. 2019) and within intensively studied individuals at 3T (Xue et al. 2021). These efforts yielded equivocal results. Considering also

expected to be found in close spatial proximity to the second map, making it difficult to dissociate between the two posterior lobe representations.

In the present work we took a number of steps to overcome these challenges. First, we acquired a substantial amount of data within individual participants during task-based motor movements to boost SNR. Each participant was scanned on four days with six motor runs per day, for a total of 576 separate blocks of motor movements (96 blocks for each of six separate motor conditions). Second, to avoid between-individual spatial blurring, each participant was analyzed separately (Xue et al. 2021; Marek et al. 2018). Third, we employed an experimental paradigm that targeted movement across the body parts, including the hands and feet on both sides. Given the orientation of the second somatomotor map, one but not both of the hand and foot representations should juxtapose one another, allowing the other body part to demonstrate separation of the second and hypothesized third maps. As the results will reveal, we were able to identify a clear third map representation in most of the individuals studied, with movements of the feet being the critical condition to differentiate the second and third somatomotor maps.

Methods

Participants

Eight healthy adults, aged 19-25 [mean= 22.4 yr (SD= 2.6), 2 men, 7 right-handed], were recruited from the Boston area. Four participants contributed data to the initial Discovery sample, and 4 participants contributed data to the Replication sample. All participants were screened to exclude a history of neurological and psychiatric illness or ongoing use of psychoactive medications.

Buckner et al. (2011) the present effort is our fourth attempt to find evidence for a third somatomotor map.

Participants provided written informed consent through a protocol approved by the Institutional Review Board of Harvard University.

MRI data acquisition

Scanning was conducted at the Harvard Center for Brain Science using a 3T Siemens Magnetom Prisma-fit MRI scanner and a 64-channel phased-array head-neck coil (Siemens Healthcare, Erlangen, Germany). Inflatable padding provided comfort and helped immobilize the head. Participants viewed a rear-projected display through a mirror attached to the head coil. Before each session, the screen presentation was adjusted so that the center point could be comfortably viewed without any eye strain. Participants' eyes were monitored and video-recorded using the Eyelink 1000 Core Plus with Long-Range Mount (SR Research, Ottawa, Ontario, Canada), and alertness was scored during each functional run.

All participants were scanned across 4 MRI sessions on separate non-consecutive days. Six task-based runs were acquired each day where participants made active movements (motor runs) as well as 2 runs where participants fixated on a centrally presented black crosshair on a light grey background (fixation runs). In total, each participant had 24 motor and 8 fixation runs. 3 participants (S5-S7) were scanned in an additional session not used here.

Functional data employed a multiband gradient-echo echo-planar pulse sequence sensitive to blood oxygenation level-dependent (BOLD) contrast (Moeller et al. 2010; Feinberg et al. 2010; Setsompop et al. 2012; Xu et al. 2013), generously provided by the Center for Magnetic Resonance Research (CMRR) at the University of Minnesota. The 4 Discovery sample participants (S1-S4) were scanned with two different spatial resolutions: 1.8mm (2 sessions) and 2.4mm (2 sessions) isotropic voxels (order of sessions was balanced across participants). All sessions of the 4 Replication sample participants (S5-S8) were scanned with 2.4mm isotropic voxels. Acquisition parameters for 1.8mm resolution: TR = 2000ms, TE = 30ms, flip-angle = 80°, matrix 122 × 122 × 87

(FOV-220×220), multislice 3× acceleration. 211 volumes were acquired for each fixation run and 214 volumes for each motor run. Acquisition parameters for 2.4mm resolution: TR = 1000ms, TE = 33ms, flip-angle = 64°, matrix 92 × 92 × 65 (FOV = 221×221), multislice five times acceleration. 422 volumes were acquired for each fixation run and 428 volumes for each motor run. The two resolutions in the Discovery sample were acquired to explore the possibility of higher (1.8mm) resolution disambiguating functional details better than lower (2.4mm) resolution. For the present purposes, the two resolutions were combined and smoothed with a uniform kernel. The first 2 sessions of S5 and the first session of S6 were acquired in a different FOV (211×211); therefore, the matrix for both BOLD runs and field maps was: 88 × 88 × 65 and BOLD TE = 32.6ms. The change in FOV, which occurred to accommodate larger heads, did not affect the quality of registration or impact the analyses in any way we could detect.

A T1-weighted structural image was obtained in each session using a rapid multiecho magnetization-prepared rapid gradient echo (MPRAGE) three-dimensional sequence (van der Kouwe et al. 2008): TR = 2200ms, TE = 1.57, 3.39, 5.21, 7.03ms, TI = 1100ms, flip-angle = 7°, voxel size 1.2mm, matrix 192 × 192 × 176, in-plane generalized auto-calibrating partial parallel acquisition (GRAPPA) 4× acceleration. In each session two dual gradient-echo B0 field maps were also acquired to correct for susceptibility-induced gradient inhomogeneities with slice spatial resolution matched to the BOLD sequence (1.8mm or 2.4mm). Other field map parameters included: 1.8mm resolution – TE = 4.73ms, 7.19ms, TR = 806ms, flip angle = 55°; 2.4mm resolution – TE = 4.45ms, 6.91ms, TR = 295ms, flip angle = 55°.

Exclusion criteria included a maximum absolute motion of no more than 1.8 mm. 1 motor run was excluded for S3, 2 motor runs for S4, 1 motor and 2 fixation runs for S6 and 1 fixation run for S8 due to motion. One border case motor run of S4 (with maximum absolute motion of 1.88mm) was included as the motion estimate was mostly the result of a linear drift. In 3 motor runs of S3, an artifact in the form of a peak translation (in the z axis and to a lesser extent in the y axis) was

spotted in approximately the same time point across these 3 runs. Maximum absolute motion did not exceed the set threshold for these runs (0.72, 1.01, 0.85mm), but we conservatively excluded them from analysis. Runs were excluded based on BOLD data quality prior to examination of task response patterns to avoid bias.

Motor task

Participants performed a blocked-task paradigm consisting of 6 types of movements that targeted four separate parts along the anterior-posterior body axis: (1) *Tongue*: participants moved their tongue from right to left, touching their upper premolar teeth, (2,3) *Right and Left Hands*: participants moved their fingers alternating between tapping the thumb with the index finger and the thumb with the middle finger, (4) *Glutes*: participants contracted and relaxed their gluteal muscles, and (5,6) *Right and Left Feet*: participants alternated dorsiflexion and plantarflexion of their toes.

Each movement was performed repeatedly in 10s active movement blocks. Prior to a movement block, a visual cue of a drawn body part with a text label was presented for 2s, informing the participant to initiate one of the six movement types. Then, the fixation crosshair was presented with a black circle surround that repeatedly flashed on and off to pace the movements (1s on then 1s off). The onset of the black circle cued movement of the tongue to the right, thumb to index, glutes contraction and toes plantarflexion. The black circle turning off cued movement of the tongue to the left, thumb to middle, glutes relaxation and toes dorsiflexion. The word 'End' was presented for 1s at the end of each movement block to instruct the participant to stop, and there was a 1s fixation gap before the onset of the next movement cue.

Twenty-four movement blocks (4 per body part) occurred within each motor run, with 16s blocks of passive fixation providing a break after each set of 6 movement blocks. All runs began and ended with fixation yielding 5 fixation blocks per run. Six separate runs with distinct orders of

86

movement conditions were performed on each day. Counterbalancing of the movement conditions across the 6 runs on each day ensured that each condition appeared exactly once in each of the run positions.

Participants extensively practiced the intended movements before the first scanning session. First, participants practiced remotely during a consent and training session, after watching a video demonstrating how to execute the movements. Emphasis was placed on how to localize each movement in a subtle way to avoid head motion. Next, when participants arrived for their first session, they practiced again while lying on the scanner bed outside of the bore and then a final time inside the bore. To further reduce extraneous motion, participants' legs were supported in a semiflexed position using an ergonomic knee-to-ankle cushion.

Data processing

A custom analysis pipeline for individualized data processing was used as described in detail in Braga et al. (2019). Briefly, the pipeline combines tools from FreeSurfer (Fischl 2012), FSL (Jenkinson et al. 2012) and AFNI (Cox 1996) to align data within an individual across runs and sessions to a high-resolution output target (1mm isotropic) using a single interpolation to minimize spatial blurring. Five different registration matrices were combined for the single interpolation: (1) a motion correction matrix for each volume to the run's middle volume (linear registration, 12 degrees of freedom (DOF); MCFLIRT, FSL), (2) a matrix for field-map-unwarping the run's middle volume (FUGUE, FSL), (3) a matrix for registering the field-map-unwarped middle volume to a mean BOLD template (12 DOF; FLIRT, FSL), (4) a matrix for registering the mean BOLD template to the participant's native space T1 image (6 DOF; using boundary-based registration, FSL) and (5) a matrix for registering the native space T1 to the MNI152 1mm atlas (nonlinear registration; FNIRT, FSL). The mean BOLD template was created by taking the mean of all field-map-unwarped middle volumes after registration to an upsampled (1.2mm), unwarped mid-volume template (temporary

target, selected from a low motion run acquired close to a field map). The native space template was one of the participant's T1 structural images, upsampled to 1mm isotropic resolution. Given that multiple structural images were available for each individual, a single reference image was chosen that possessed a robust estimate of the pial and white-matter boundaries (as constructed by FreeSurfer recon-all).

Data were checked for registration errors. In cases of sub-optimal registration, a different mid-volume temporary template was chosen, or a different/additional field map was used for unwarping (since two field maps were acquired in each session). Before the calculation of these matrices, for each BOLD run, the first 12 volumes were discarded for T1 equilibration (6 volumes in 1.8mm resolution). For the participants (S1-S4) that had two spatial resolutions (two sessions with 1.8mm isotropic voxels and two sessions with 2.4mm isotropic voxels), each resolution was processed separately and then combined. All functional data were smoothed in the volume with a 3mm full width at half maximum (FWHM) kernel.

Data were analyzed in the standard space of the MNI152 atlas within each participant individually. Thus, all idiosyncratic details within the individual were preserved. The use of the atlas space allowed the separate participants to be examined in a spatially registered framework and also allowed their data to be projected to a flat representation of the cerebellar cortex to aide visualization of patterns.

Visualization on the cerebellar surface

To visualize the spatial extent of maps in the cerebellum, the data were projected onto flat and inflated representations of the cerebellar surface [similar to our prior work in Xue et al. 2021]. This representation was created by Diedrichsen and Zotow (2015) and utilized within the spatially unbiased infratentorial template (SUIT) toolbox [http://www.diedrichsenlab.org/imaging/suit_fMRI.htm]. The projection method uses an

approximate surface of the grey and white matter defined on the SUIT template (here specifically,

MNI152, normalized by FSL). The vertices on the two surfaces come in pairs. When projecting, the

algorithm samples the data along the line connecting the two vertices and then takes the mean of

these numbers to determine the value of the vertex.

The surface representation was used for display purposes only. The surface is not unique to

each individual. In addition, the flat surface may not be optimal for the cerebellar vermis. To enable

flattening, a cut was made between the posterior vermis and lobules HVII-HIX which can introduce

distortions to the vermal region. Nonetheless, the surface representation can display the individual

participant's topographic details in a uniform, comprehensive display framework. To avoid

ambiguities in anatomical localization, key findings were also displayed across multiple slices

through the cerebellar volume, including the vermis.

Motor task analysis

Motor run data in MNI152 atlas space were analyzed within each individual separately. A

high-pass filter with a 100s (0.01 Hz) cut-off was applied to remove low-frequency drifts within

each run. Run specific general linear model (GLM, using FEAT; FSL) analyses were performed,

including the six movement conditions as regressors of interest. The onsets of the six movement

blocks were modeled 1s before the initiation of movement (1s after the appearance of the visual

cue). The duration of each event block was set to 10s. Events were modeled with a canonical

hemodynamic response function (double-Gamma) along with its temporal derivative. GLM analyses

resulted in voxel-level β values for each movement.

Somatomotor topography

Initial analyses focused on estimating the somatomotor map across the four body parts in

the cerebral cortex and separately in the cerebellum. A contrast map was computed for each

movement by subtracting all other movements' β values (weighted so that the target movement β map was balanced with the subtracted movements, here achieved by multiplying the target movement β map by 5 before subtracting the 5 other β values). This was done in each motor run separately and then averaged across runs (including averaging across resolutions in S1-S4). To visualize somatomotor topography, a winner-take-all map was generated. Each voxel was assigned with the highest β value across all movement contrasts (one versus all the others) and was colored with the color of the corresponding movement: tongue-red, right and left hand-yellow, glutes-green, and right and left foot-blue. In this visualization, right and left representations were not distinguished. Maps were visualized separately for each individual in the volume and also projected onto the SUIT flatmap template of the cerebellum. Maps were thresholded within individuals to best capture somatomotor topography, separately for the cerebrum and for the cerebellum.

Focus on the hand and foot representations

A critical aspect of the design is the ability to contrast left and right movements separately for the hands and feet. This enables direct contrast of the left and right movements within each body part, allowing a clean estimate of the representation of the body part because non-specific noise and other features of the data are largely nulled [paralleling the strategy we have repeatedly used in group-averaged functional connectivity data (Buckner et al. 2011; Krienen and Buckner 2009)]. Contrast maps were averaged across runs (and across resolutions in S1-S4). Contrast maps were projected onto a flatmap template of the cerebellar surface and thresholded within individuals.

Seed based functional connectivity analysis

To assess representations' specificity, we conducted a seed based functional connectivity analysis. This analysis should not be considered independent as we utilized all available data,

including the motor task runs used to make the contrast maps. Specifically, in addition to the 24 motor runs (across 4 sessions) of each individual, we used the 8 fixation runs (2 per session), resulting in 32 possible runs. After quality control exclusions, S3 had 28 runs (193.3min), S4 had 30 runs (207.2min), S6 had 29 runs (200.5min) and S8 had 31 runs (214.2min). All other participants utilized all 32 runs (221.1min). Note that unlike purely task-free data, the present data included substantial modulation due to active task demands.

Pre-processing included all steps as used for the prior task-based analyses but also regression of nuisance variables (3dTproject, AFNI) as is typical in functional connectivity analysis (whole brain, ventricular, and deep cerebral white matter mean signals, as well as six motion parameters, and their temporal derivatives). The residual BOLD data were then band-pass filtered at 0.01–0.1 Hz and smoothed with a 3mm FWHM kernel paralleling the task-based analysis.

Seed regions were defined in the right and left primary, secondary and tertiary somatomotor cerebellar representations. For each seed region, an MNI152 coordinate was selected in the volume to best capture the center of the representation in the right versus left hand and foot contrast maps. In one individual, S8, we selected right and left foot tertiary coordinates to be similar to the ones of other individuals given the lack of detectable representations.

Seed regions were defined with a 2mm-radius centered at the selected MNI152 coordinate (33 voxels). For each run, the Pearson's correlation was computed between the averaged time course of the seed region and that of all other voxels. The functional connectivity values were averaged across all runs (and resolutions for S1-S4) after being Fisher's r-to-z transformed.

Discovery and replication

A key aspect of our methods was prospective replication. Data from the initial four participants were fully analyzed and graphed (Discovery sample, S1-S4) before any analysis was attempted on the second, independent group of participants (Replication sample, S5-S8).

Results

Somatomotor topography is detected within the primary motor cortex

The body map in the primary motor cortex (M1, precentral gyrus) is well established. The anterior (head) to posterior (foot) axis is topographically organized as one moves from the lateral extent of the motor strip to the midline (Penfield and Boldrey 1937). Data from each individual revealed the full M1 body topography: tongue-hand-glutes-foot, lateral to medial as expected (Fig. 1, top). Although not common in the literature, contraction and relaxation of the gluteal muscles was included to evoke a representation of the trunk. As predicted by the body topography, representation of the glutes fell between the hand and the foot. The observed M1 motor topography validates the experimental paradigm and the processing methods applied.

Somatomotor topography is detected in both of the established maps within the cerebellum

The two well-established cerebellar somatomotor maps were apparent in all participants (Fig. 2.1, middle and bottom). The ordering of body parts was inverted between the two maps. In the anterior lobe the foot was anterior to the tongue and in the posterior lobe the tongue was anterior to the foot (Fig. 2.1 bottom, highlighted in S2). In both maps, the glutes representation falls between the hand and foot filling in a gap often observed in motor body maps [e.g., Xue et al. 2021, their Fig. 3], although more apparent in the primary map than the secondary, and more clean for some participants (S1 and S2) than others (S3 and S4). The current data thus reveal strong and reliable evidence for the anterior lobe and posterior lobe somatomotor maps.

One other aspect of the results (Fig. 2.1 bottom) is that the tongue movements induced noise centered outside of the cerebellum (but extending into the cerebellum). Given the sensitivity

92
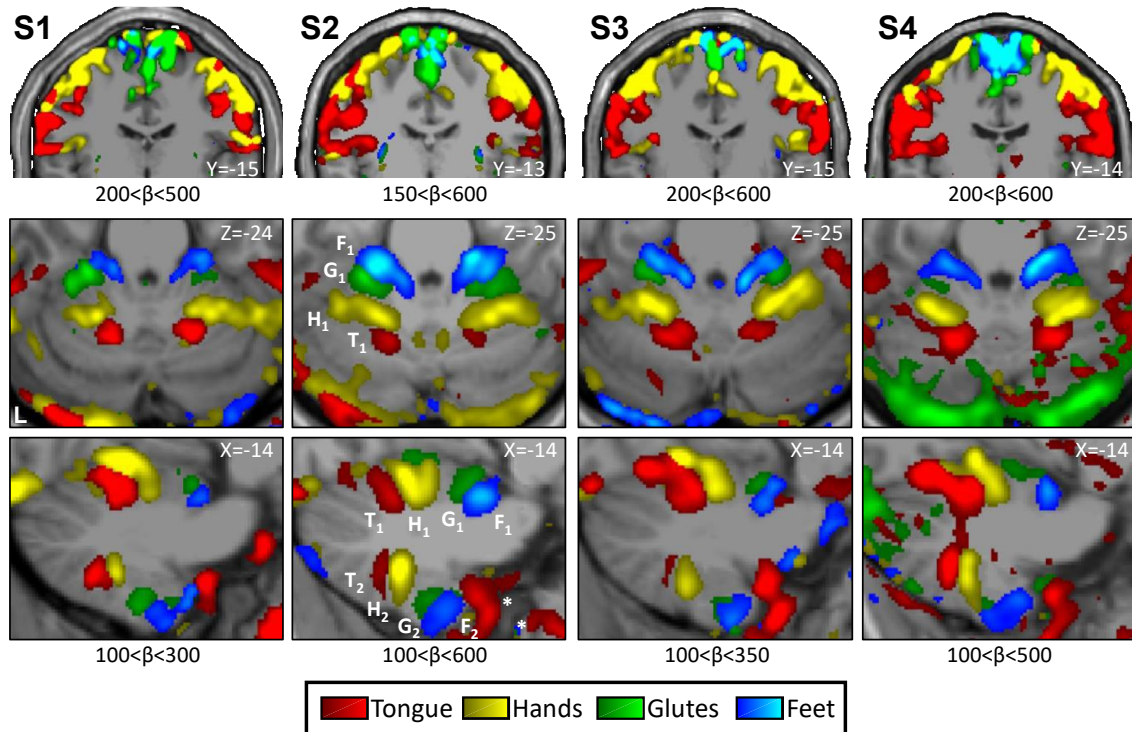
Figure 2.1. Somatomotor topography in the cerebral cortex and cerebellum is evident in individual participants. Winner-take-all maps of active movements are displayed for 4 body parts along the anterior-posterior body axis: tongue (red), right and left hands (yellow), glutes (green) and right and left feet (blue). Each column displays a separate participant (S1-S4). B values are thresholded to best capture topography, separately for the cerebral cortex and cerebellum. In each participant a clear body topography is evident by the order tongue-hand-glutes-foot in the primary motor cortex, M1 (lateral to medial, top row), cerebellar anterior lobe (middle and bottom rows) and in the cerebellar posterior lobe (bottom row). The primary cerebellar representation (T1-H1-G1-F1) is inverted to the secondary representation as labelled in S2 (T2-H2-G2-F2). Note the tongue assignment anterior to the secondary representation (in all participants, marked with an asterisk in S2) is outside the cerebellum and likely results from a motion artifact. Also note that the cerebral coronal sections also include parts of the supplementary motor area (SMA) along the midline, which are continuous to M1 (foot and glutes). Coordinates indicate the section level in the space of the MNI152 atlas. The color bars represent β values. L indicates left.

of fMRI to motion artifact, it is not surprising that movements within the field of view produce artifact. Fortunately, the predicted tongue representation is spatially distant from the region of artifact and thus easy to distinguish.

To visualize the entirety of the somatomotor cerebellar topography, maps with representations of the four body part movements were projected onto a flatmap view of the cerebellum (Fig. 2.2). In this view, the inversion of the two map representations is clear. Note that the second map evolves also over the medial-lateral axis, with anterior-medial (close to the vermis) tongue representation distant from the posterior-lateral foot representation.

Figure 2.2 also shows provisional evidence for a third map within and near to the vermis. The hand representation in all four participants extends into the region of the vermis, as does the foot and glutes representations in S2 and S3. This feature is consistent with the hypothesized third (tertiary) somatomotor map of the cerebellum. However, idiosyncrasies in the data, variability across participants and the adjacency to the secondary representation make it uncertain. To further explore the possibility of a third map, we focused specifically on hand and foot movements where direct contrasts between the right and left movements were possible.

The hand representation in the cerebellum is consistent with, but does not differentiate, a third somatomotor map

Contrasting right and left hand movements yielded robust responses in the cerebellum for all participants (Fig. 2.3). The primary and secondary representations were clear and distinct. In addition, all four individuals possessed bilateral hand representations on the edges of the vermis, medially and anteriorly to the second representation, potentially a component of the hypothesized third map. Specifically, in S1 and S2 there were two distinct representations for the second and the candidate third map. In S3 and S4 the two representations appeared as one continuous cluster. Consequently, it is still ambiguous as to whether the medial representation is a distinct third

94
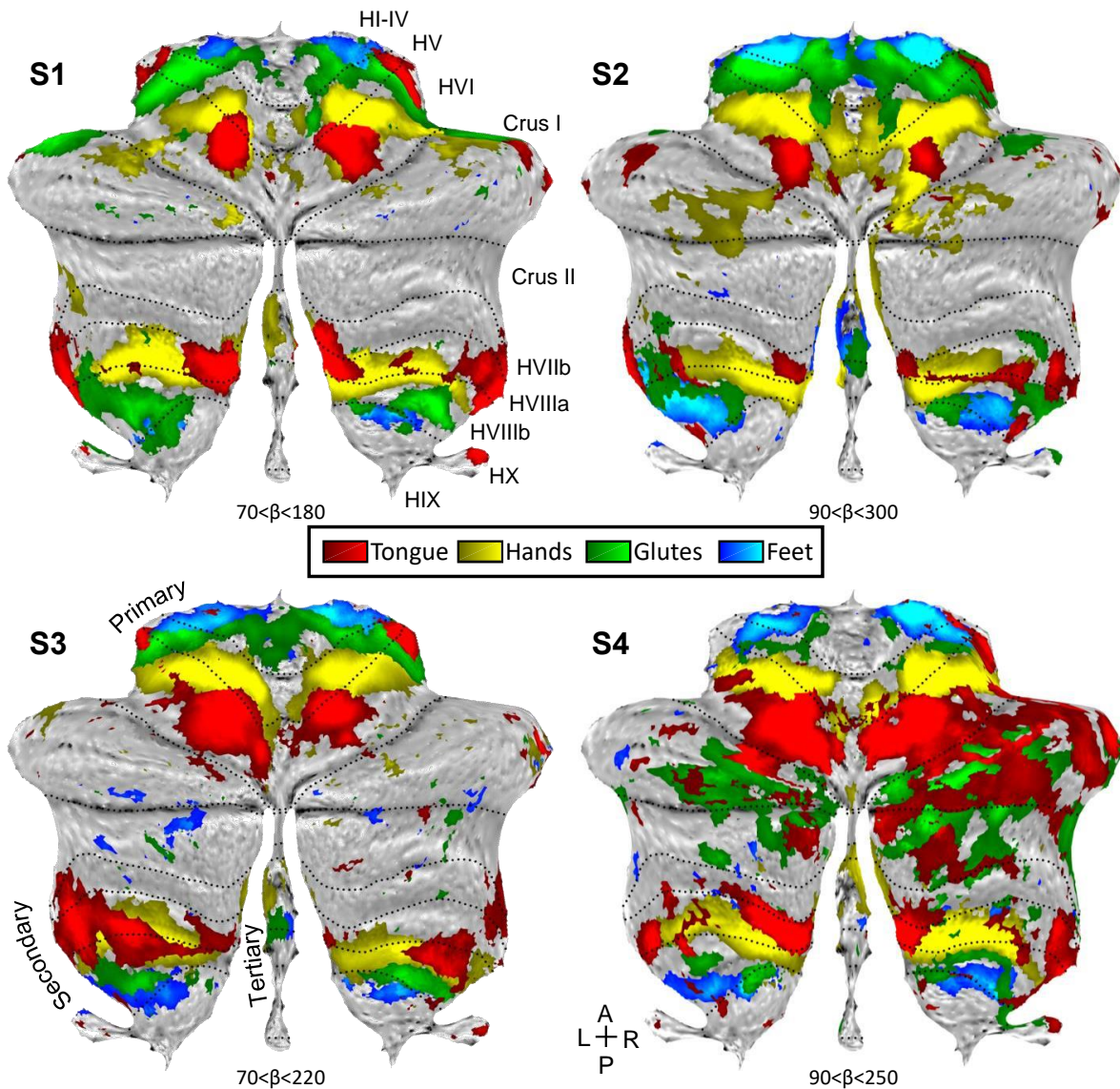
Figure 2.2. Somatomotor topography projected onto a flatmap of the cerebellum reveals details. Winner-take-all maps of active movements are displayed for 4 body parts along the anterior-posterior body axis projected onto flatmaps using the SUIT toolbox: tongue (red), right and left hands (yellow), glutes (green) and right and left feet (blue). Each panel displays a separate participant (S1-S4). In each participant, the primary and secondary somatomotor maps are apparent in the anterior and posterior lobes of each hemisphere corresponding to the anterior-posterior body axis. Also note the medial representations within the vermis (glutes and feet in S2 and S3, and hands in all four individuals). These may be hints for the hypothesized tertiary body representation in the cerebellum. Glutes and tongue responses in the Crus I / II of S4 are likely due to motion artifacts that are more common during these movements. Dotted lines indicate approximate lobule boundaries with lobules labelled for S1. L: Left; R: Right; A: Anterior; P: Posterior.
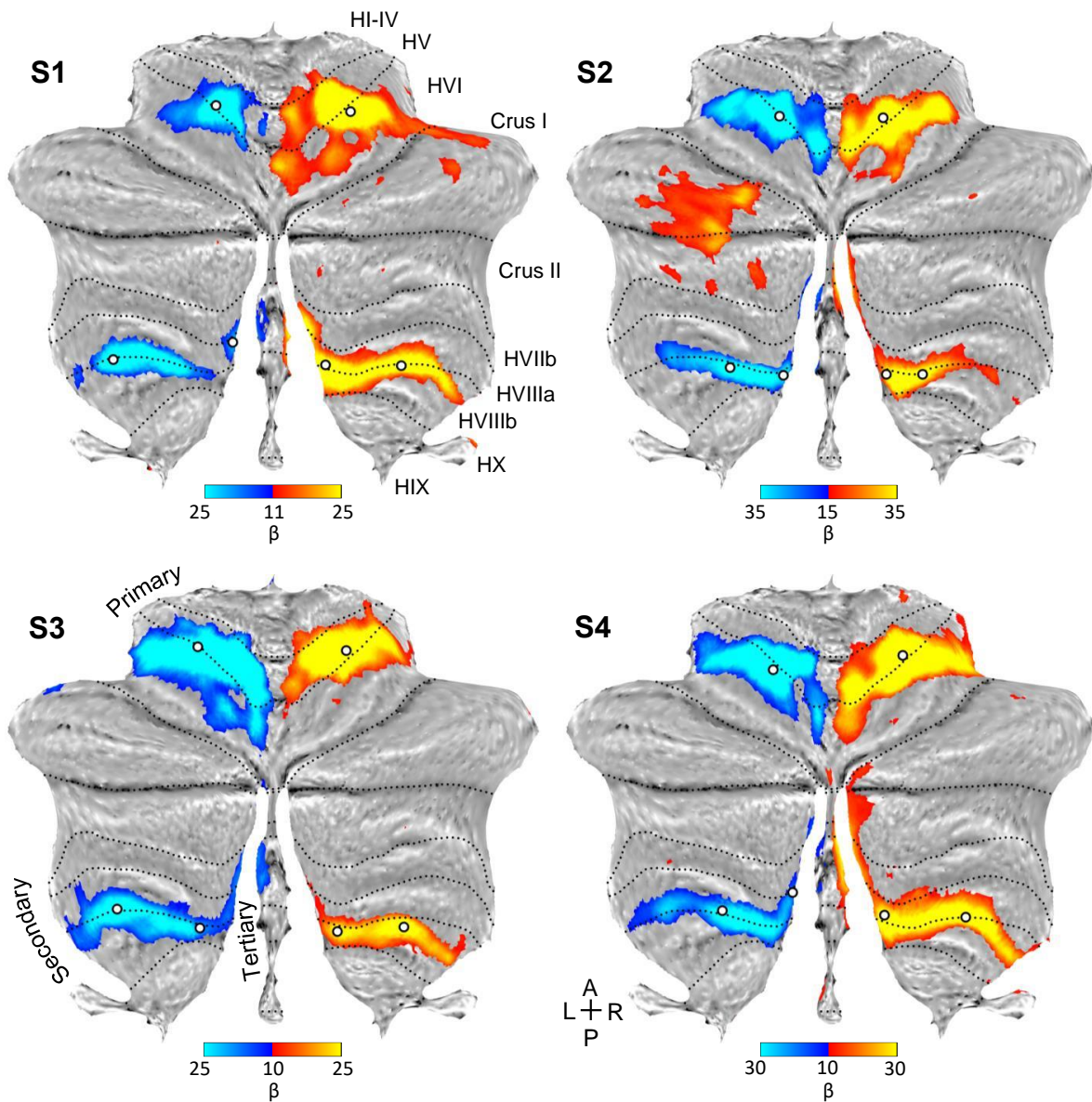
Figure 2.3. Direct contrast of left and right hand movements isolates representations of the body part. Contrast maps of right (red) versus left (blue) hand movements are projected onto flatmaps. Each panel displays a separate participant (S1-S4). In each participant, the hand representation is robust in both the anterior and posterior lobes. On the vermis, medial to the second representation, there is a bilateral hand representation in all participants. This extension of the hand representation may be a component of the tertiary representation, but it is ambiguous because there is no discontinuity. The white circles display the positions of seed regions that were used for analyses displayed in Fig. 2.5 (see text). Dotted lines indicate approximate lobule boundaries with lobules labelled for S1. L: Left; R: Right; A: Anterior; P: Posterior. Color bars indicate β values.

representation or simply a continuation of the second representation. It seems that even if there is a third map, the hand representation is not positioned to provide clear evidence for dissociation. Therefore, we repeated the same analyses focused on the foot representation.

The foot representation in the cerebellum differentiates the third somatomotor map

Contrasting right and left foot movements yielded robust responses that included a representation in the vermis medial to the second representation in multiple participants (Fig. 2.4). Unlike the hand representation (Fig. 2.3), where the posterior lobe representation was continuous, the two representations associated with movement of the foot were spatially distinct (Fig. 2.4). One large representation was centered in lobule HVIIIb where the established second map's upright topography begins. The smaller (newly) detected foot representations were medial and discontinuous with the known second somatomotor map. The presence of an independent foot representation in the vermis of the posterior lobe directly supports a third somatomotor map.

The third cerebellar somatomotor map shows anatomically-specific coupling to cerebral motor cortex

Another way to refute or support the presence of independent cerebellar maps is to examine the specificity of cerebellar functional connectivity to the cerebral cortex. The positioning of the second and third somatomotor maps is such that (1) the spatially separate cerebellar foot representations should both couple to the same midline cerebral zone (see Fig. 2.1), and (2) the hand representations, which sit between the two foot representations in the cerebellum, should couple to a distinct cerebral zone near the hand knob of the precentral gyrus (see Fig. 2.1).

To explore these hypotheses, we first examined the specificity of the hand representations by applying seed-based functional connectivity analysis to the cerebellum and examining the correlation pattern in the cerebral cortex. Three sets of right and left seed regions were defined in the primary, secondary and candidate tertiary representations (white dots, Fig. 2.3). Given that the
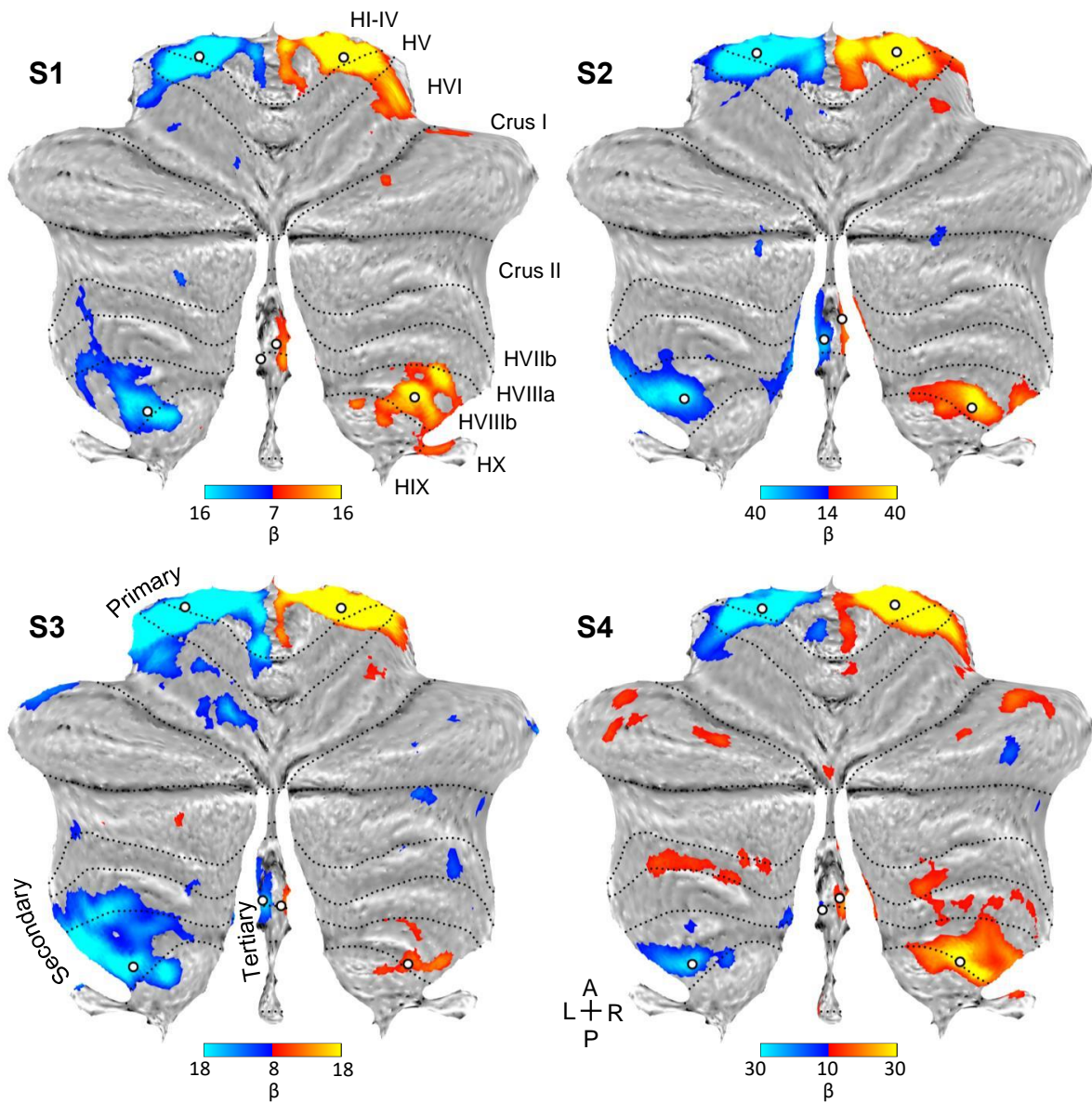
Figure 2.4. Direct contrast of left and right foot movements isolates three spatially discontinuous representations of the body part. Contrast maps of right (red) versus left (blue) foot movements are projected onto flatmaps. Each panel displays a separate participant (S1-S4). In each participant, the foot representation is detected in the anterior lobe and also the posterior lobe near to where the beginning of the secondary map is localized (laterally in lobule HVIIIb). Within the vermis, there is a distinct representation of the foot in each participant that is particularly clear in S2 and S3. This spatially discontinuous representation is evidence for a third somatomotor map. The white circles display the positions of seed regions that were used for analyses displayed in Fig. 2.6 (see text). Dotted lines indicate approximate lobule boundaries with lobules labelled for S1. L: Left; R: Right; A: Anterior; P: Posterior. Color bars indicate β values.

98

obtained posterior lobe hand representation does not possess a discontinuity to separate the second from the third maps, the seed regions were estimated to be at or near the transitions to the foot representations, but still within the hypothesized hand representation.

In all individuals, functional connectivity for all three seed region pairs revealed spatially-specific cerebral regions at or near the hand region of M1 (Fig. 2.5). Right cerebellar seed regions correlated with the left cerebral hand region and left seed regions with the right. The results for the tertiary seed regions were found to be the weaker but possessed the same, spatially-convergent pattern.

Applying a parallel analysis to the foot representations revealed a distinct pattern (Fig. 2.6). Unlike the hand representations, the seed region pairs for the second representation and candidate third representation of the foot are spatially discontinuous. Functional connectivity for all three seed region pairs revealed cerebral regions at or near the foot region of M1 that were distinct from the hand region. Of note, the hypothesized third foot cerebellar representation when seeded was, in isolation, able to recapitulate the selective cerebral motor pattern. This is important evidence because the zone of the cerebellum between the second and third maps is coupled to the cerebral hand region. The second and third foot representations are thus functionally selective and robustly dissociated from the cerebellar zone between them.

To appreciate the discontinuity of the second and third somatomotor maps, the locations of the seed regions used in the above analyses were plotted on each individual's structural volume image of their cerebellum. Seed regions for the second and third foot representations are on either side of the seed regions for the hand representation (Fig. 2.7). This observation alleviates concerns that the discontinuity could be an artifactual byproduct of the surface projection.

Figure 2.5. Seed based functional connectivity of cerebellar hand representations reveals the contralateral hand region in M1. Coronal sections display functional connectivity patterns for hand seed regions in the right (red) and left (blue) cerebellum. In each column of three panels, an individual participant's data are shown for separate sets of right versus left hand region contrasts that are independently seeded in the three cerebellar representations. The locations of the seed regions are illustrated by white circles in Fig. 2.3. In each individual, functional connectivity resulting from the estimated primary, secondary and candidate tertiary cerebellar representations reveals M1's contralateral hand region, demonstrating specificity. Note how, despite differences in correlation strength, the pattern revealed by the tertiary representation's seed regions recapitulates the same pattern as the seed regions placed in the primary and secondary representations. Coordinates indicate the section level in the space of the MNI152 atlas. The color bars indicate correlation strength [z(r)]. L indicates left.
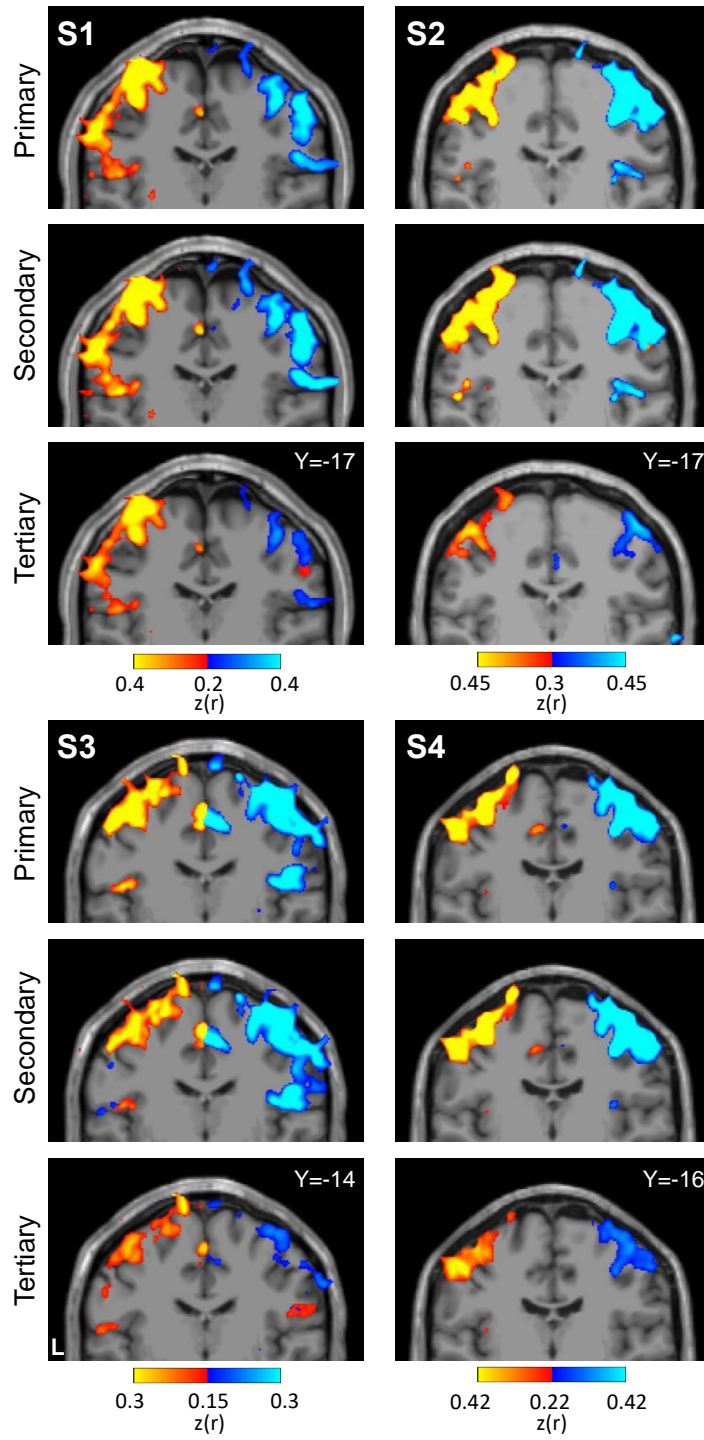
Figure 2.5 (Continued).

Figure 2.6. Seed based functional connectivity of cerebellar foot representations reveals the contralateral foot region in M1, including for the spatially discontinuous tertiary representation. Coronal sections display functional connectivity patterns for foot seed regions in the right (red) and left (blue) cerebellum. In each column of three panels, an individual participant's data are shown for separate sets of right versus left foot region contrasts that are independently seeded in the three cerebellar representations. The locations of the seed regions are illustrated by white circles in Fig. 2.4. In each individual, functional connectivity resulting from the estimated primary, secondary and candidate tertiary cerebellar representations reveals M1's contralateral foot region, demonstrating specificity. Note the pattern revealed by the tertiary representation's seed regions recapitulates the same pattern as the seed regions placed in the primary and secondary representations despite being spatially discontinuous. Coordinates indicate the section level in the space of the MNI152 atlas. The color bars indicate correlation strength [z(r)]. L indicates left.
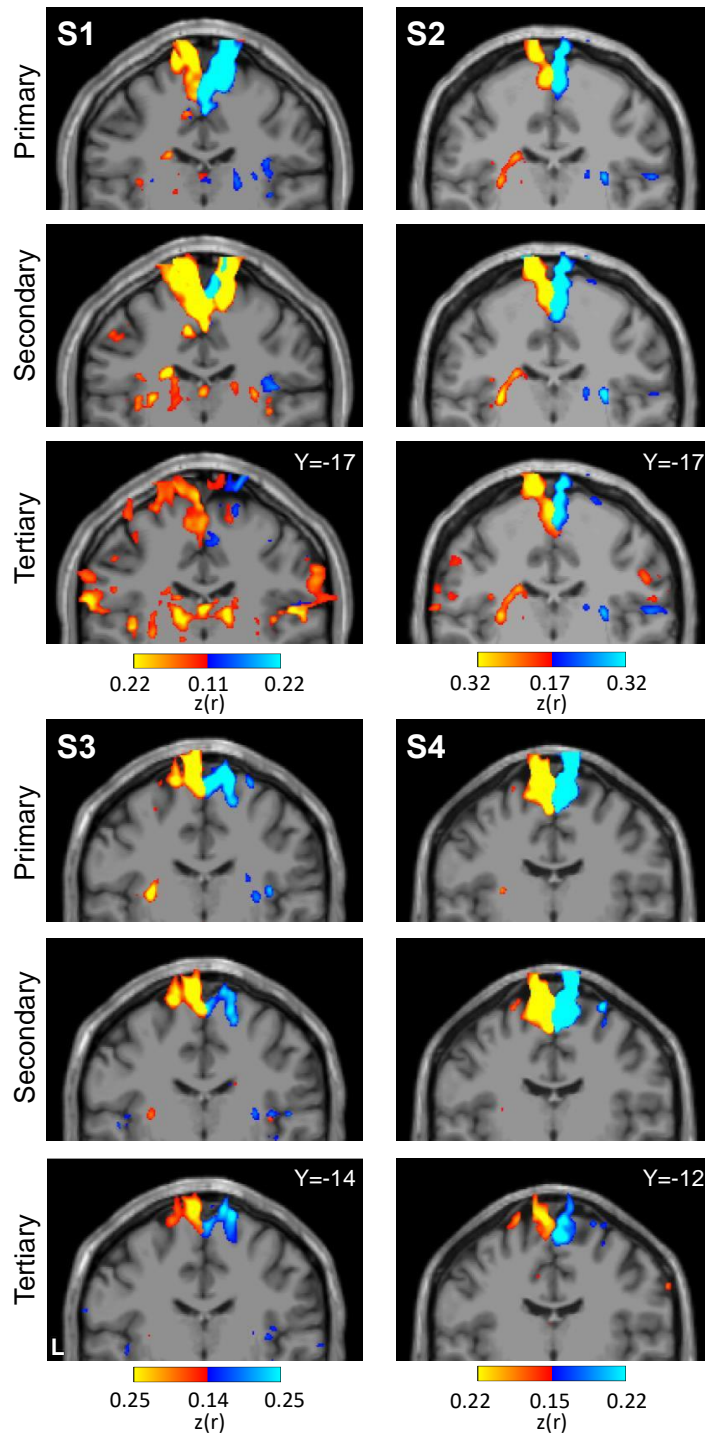
Figure 2.6 (Continued).
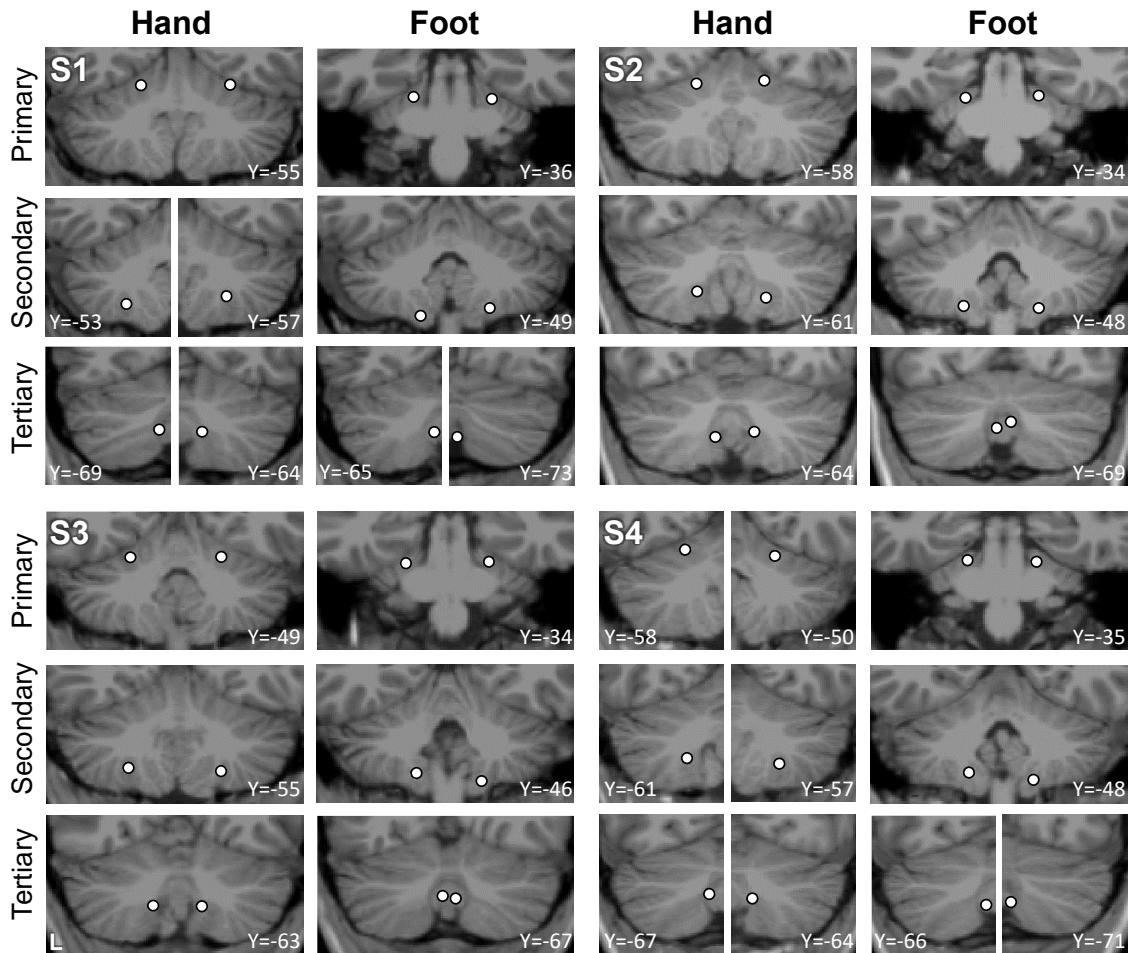
Figure 2.7. Visualization of seed region locations in the volume. Seed region locations of the right and left primary, secondary and tertiary representations (white circles) are plotted on coronal sections of the T1 structural image for each participant. Sections presented are of the seed region's center or within 1mm of the center. For each individual, hand and foot seed region locations are presented. Note how the tertiary foot location is medial to the hand representation in each participant. Coordinates indicate the section level in the space of the MNI152 atlas. L indicates left.

Prospective replication of the third cerebellar somatomotor map

The findings above reveal strong evidence for a third somatomotor map in the cerebellum. Given the importance of this observation and also that we have previously failed to find clear evidence for a third map[1], we sought to replicate all of the above observations in an independent set of new participants. Critically, none of the Replication sample data (S5 to S8) were processed until all of the analyses on the initial Discovery sample (S1 to S4) were completed and plotted.

In the Replication participants, we again found evidence for full body topography in M1 (Fig. 2.8, top) and in the cerebellar anterior lobe of all four individuals with the expected order of the tongue-hand-glutes-foot (Fig. 2.8, top and middle rows, Fig. 2.9). The second cerebellar map in the posterior lobe was also found with its full topography in S6 and S7. S5 and S8 were missing clear representation of the glutes. In participants S5, S6 and S7, responses consistent with a third map were also evident with foot representations present within the vermis (Fig. 2.9).

Contrasting right and left hand movements again yielded robust responses in the cerebellum (Fig. 2.10). The maps of the hand representations were present in all participants. Repeating the same analysis for foot movements yielded evidence for the third somatomotor map with discontinuous representation of the foot within the vermis (Fig. 2.11). S5 and S6 were particularly clean examples in the Replication sample, similar to the S2 and S3 in the prior Discovery sample. S8 showed a great deal of non-specific noise throughout the cerebellum and also lacked a clear foot representation within the vermis. Thus, across the two studies, there were multiple robust demonstrations of the third foot representation, but also the occasional ambiguous result and one clear failure (S8), consistent with prior studies of within-individual precision mapping that do not always achieve robust results in every individual [e.g., see Braga and Buckner 2017; DiNicola et al. 2020].

Placing seed regions within each of the three cerebellar maps again revealed the expected anatomically-specific correlation patterns with cerebral motor zones (Figs. 2.12 and 2.13). High
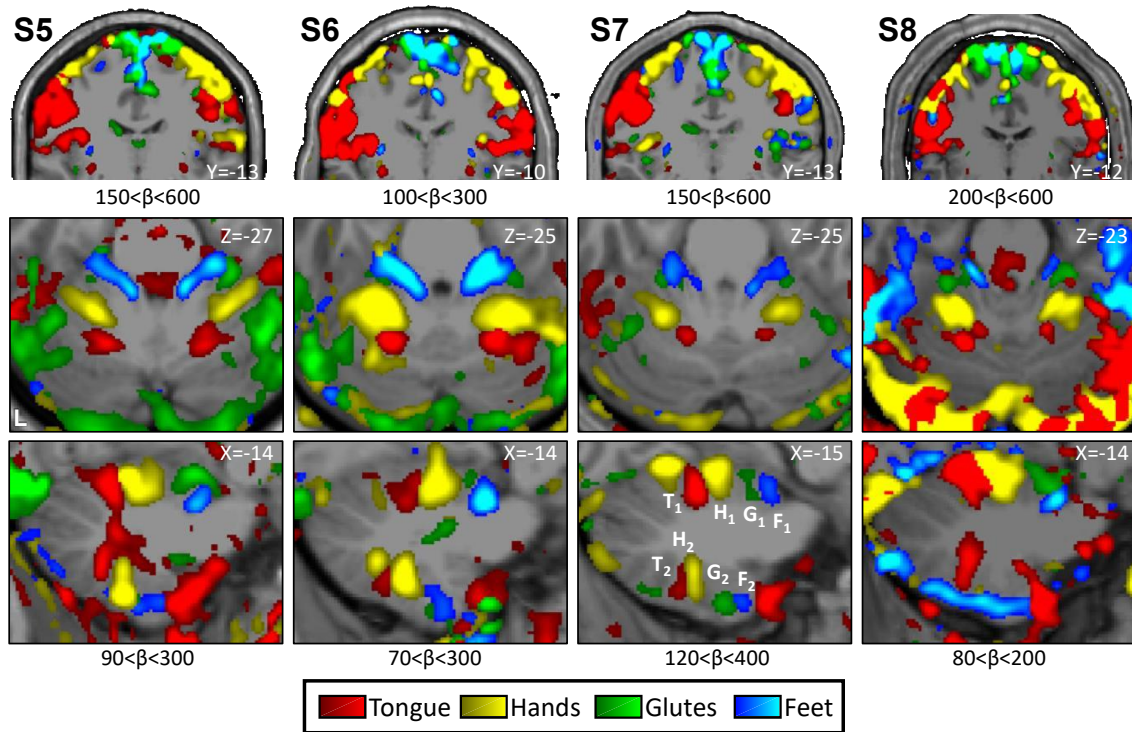
Figure 2.8. Replication of somatomotor topography in the cerebral cortex and cerebellum.
Winner-take-all maps of active movements are displayed for 4 body parts along the anterior-
posterior body axis: tongue (red), right and left hands (yellow), glutes (green) and right and left feet
(blue). Each column displays a separate participant from the Replication sample (S5-S8). Analysis
and plotting of these participants occurred after the results of the Discovery cohort were finalized.
β values are thresholded to best capture topography, separately for the cerebral cortex and
cerebellum. In each participant a clear body topography is evident by the order tongue-hand-
glutes-foot in the primary motor cortex, M1 (lateral to medial, top row), and cerebellar anterior
lobe (middle and bottom rows). The primary cerebellar representation (T1-H1-G1-F1) is inverted
to the secondary representation as labelled in S2 in Fig. 2.1 (T2-H2-G2-F2). S6 and S7 show a full
topography also in the cerebellar posterior lobe (bottom row) while a partial topography is
observed in S5 and only the tongue representation in S8. Coordinates indicate the section level in
the space of the MNI152 atlas. The color bars represent β values. L indicates left.
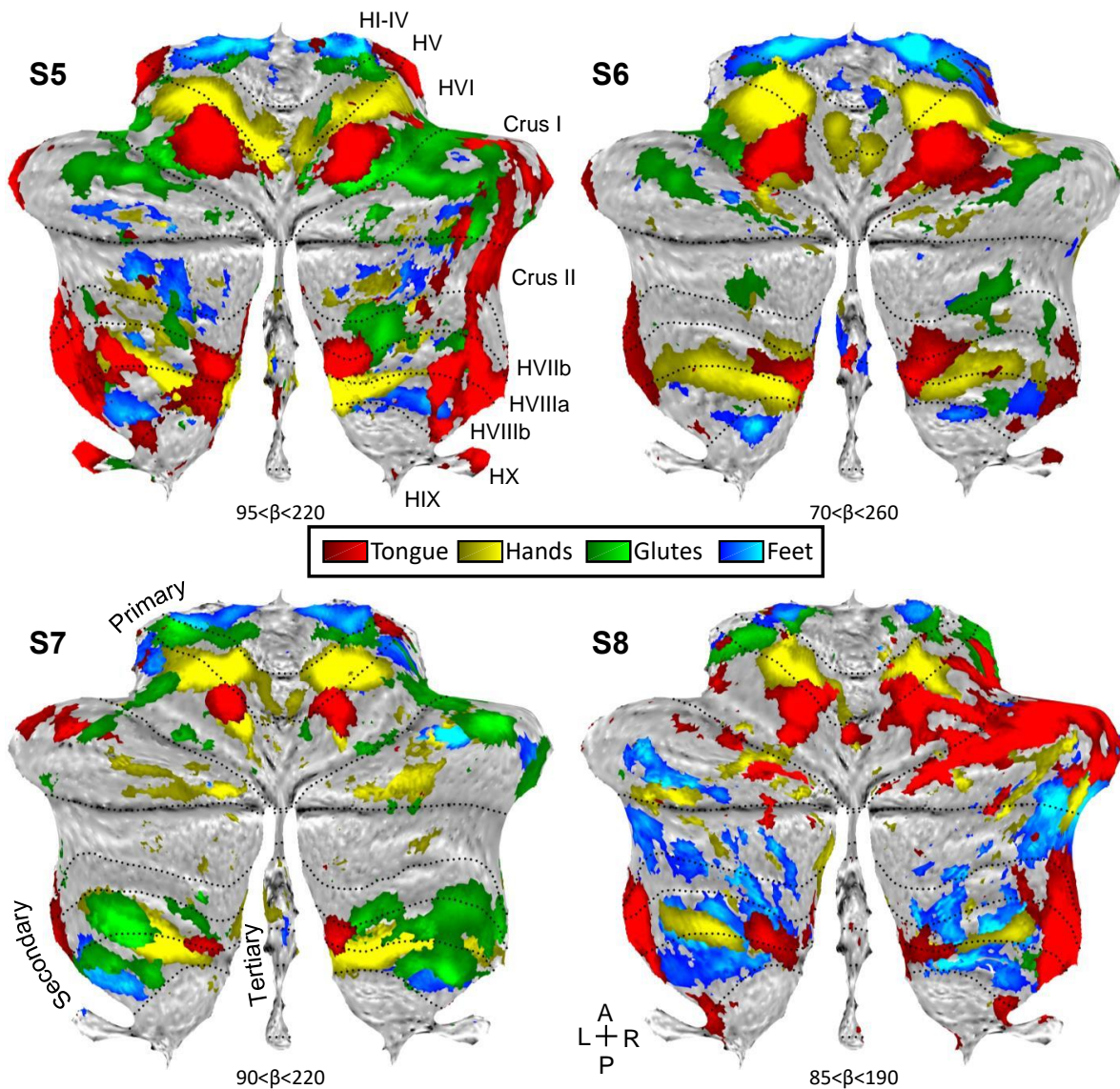
Figure 2. 9. Replication of somatomotor topography projected onto a flatmap. Winner-take-all maps of active movements are displayed for 4 body parts along the anterior-posterior body axis projected onto flatmaps using the SUIT toolbox: tongue (red), right and left hands (yellow), glutes (green) and right and left feet (blue). Each panel displays a separate participant from the Replication sample (S5-S8). In participants S5-S7, the primary and secondary somatomotor maps are apparent in the anterior and posterior lobes of each hemisphere corresponding to the anterior-posterior body axis. The experiment largely failed in S8 (the primary map is apparent but the secondary map is ambiguous). Also note the medial representations within the vermis of S5-S7. These may be hints for the hypothesized tertiary body representation in the cerebellum. Dotted lines indicate approximate lobule boundaries with lobules labelled for S5. L: Left; R: Right; A: Anterior; P: Posterior.
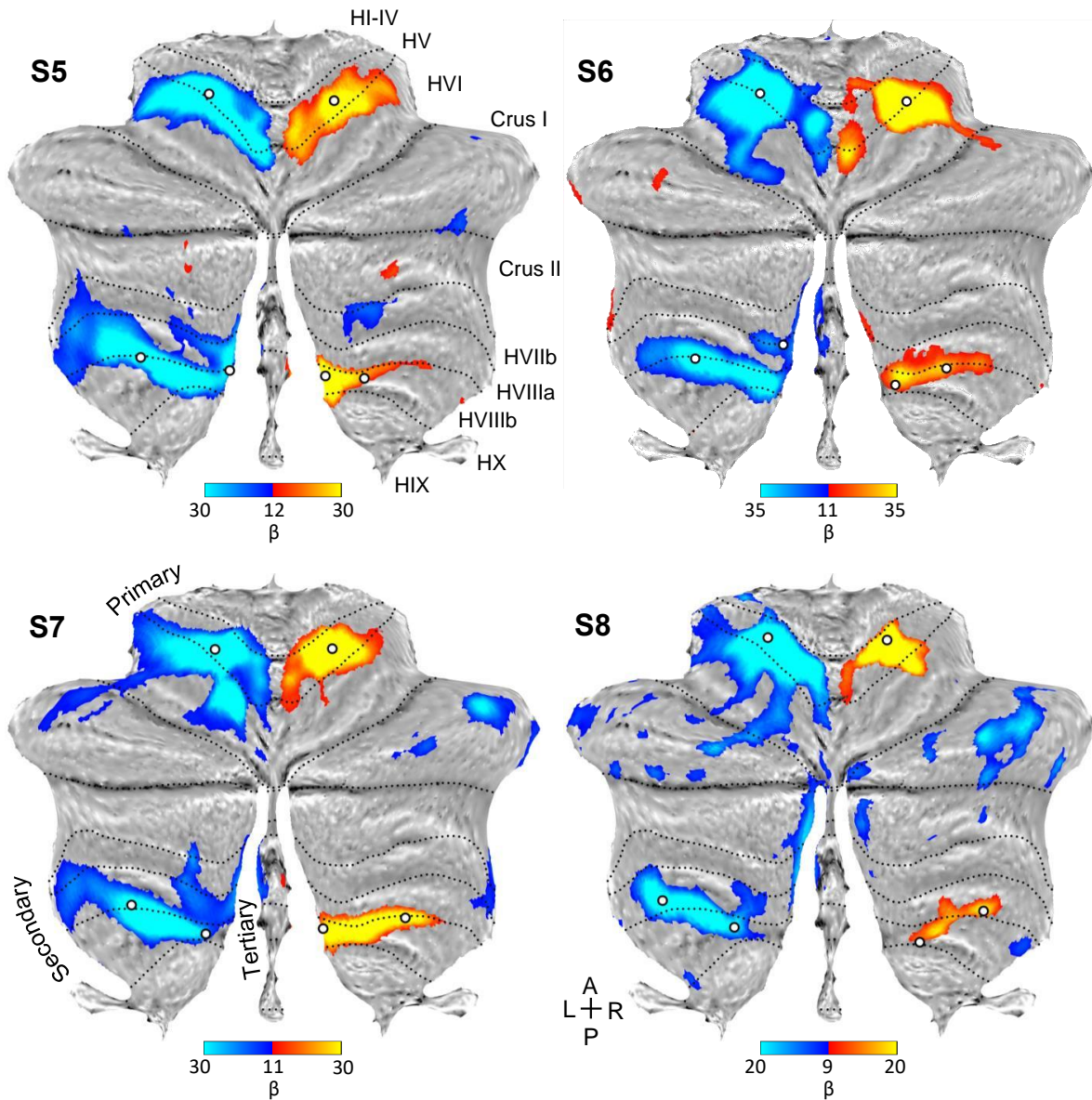
Figure 2.10. Replication of the hand representations. Contrast maps of right (red) versus left (blue) hand movements are projected onto flatmaps. Each panel displays a separate participant from the Replication sample (S5-S8). In each participant, the hand representation is robust in the anterior and the posterior lobes. The white circles display the positions of seed regions that were used for analyses displayed in Fig. 2.12 (see text). Dotted lines indicate approximate lobule boundaries with lobules labelled for S5. L: Left; R: Right; A: Anterior; P: Posterior. Color bars indicate β values.
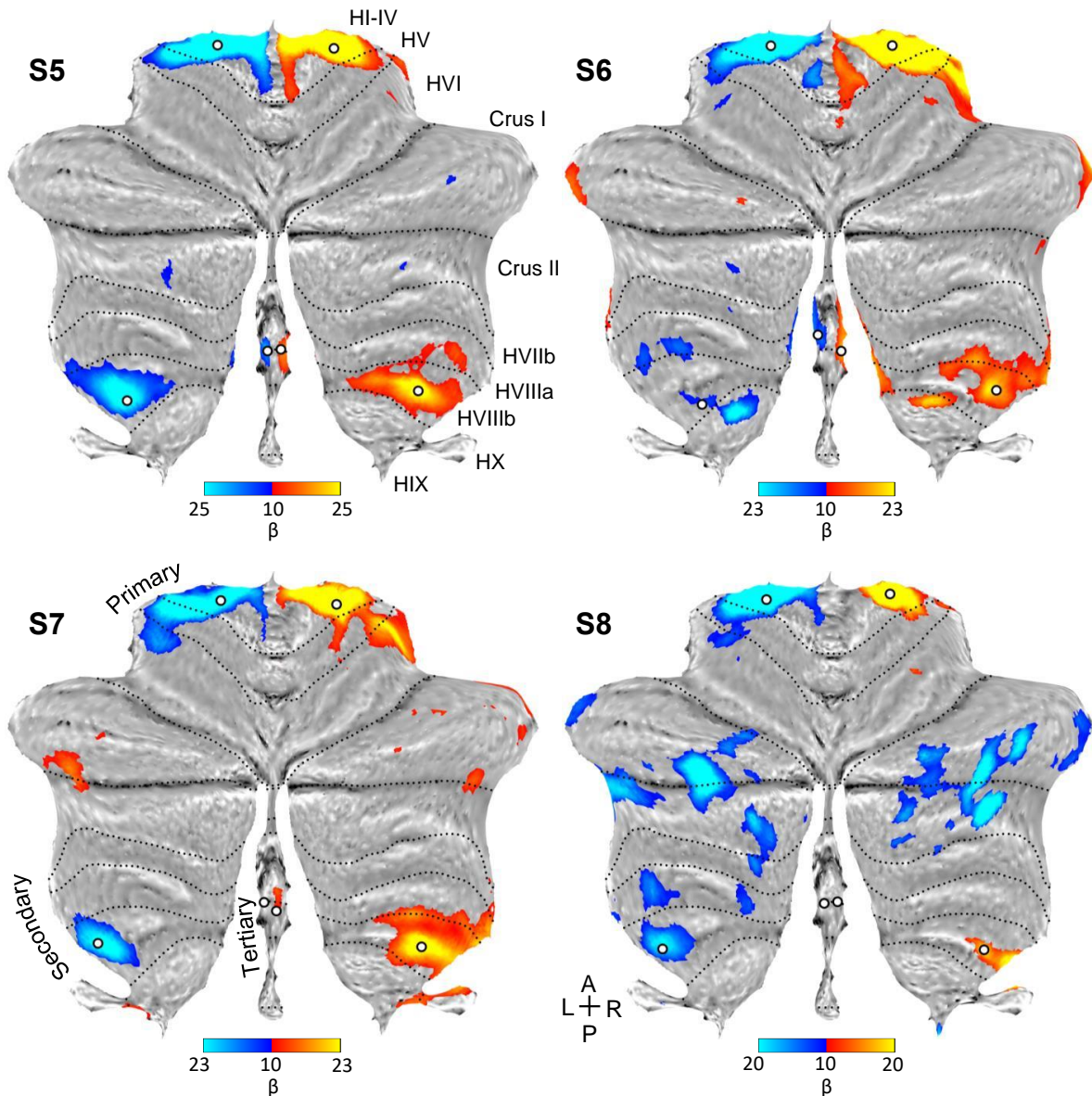
Figure 2.11. Replication of three spatially discontinuous foot representations. Contrast maps of right (red) versus left (blue) foot movements are projected onto flatmaps. Each panel displays a separate participant from the Replication sample (S5-S8). In three individuals, three separate foot representations can be identified - right and left primary, secondary and a tertiary representation in the vermis (only right in S7). In S8, a tertiary representation was not detected. The spatially discontinuous representation within the vermis replicates evidence for a third somatomotor map. The white circles display the positions of seed regions that were used for analyses displayed in Fig. 2.13 (see text). Dotted lines indicate approximate lobule boundaries with lobules labelled for S5. L: Left; R: Right; A: Anterior; P: Posterior. Color bars indicate β values.

Figure 2.12. Replication of seed based functional connectivity from cerebellar hand representations. Coronal sections display functional connectivity patterns for hand seed regions in the right (red) and left (blue) cerebellum. In each column of three panels, an individual participant's data from the Replication sample are shown for separate sets of right versus left hand region contrasts that are independently seeded in the three cerebellar representations. The locations of the seed regions are illustrated by white circles in Fig. 2.10. Functional connectivity resulting from the estimated primary, secondary and candidate tertiary cerebellar representations reveal M1's contralateral hand region in all participants, demonstrating specificity. Note how, despite differences in correlation strength, the pattern revealed by the tertiary representation's seed regions again recapitulate largely the same pattern as the seed regions placed in the primary and secondary representations. Coordinates indicate the section level in the space of the MNI152 atlas. The color bars indicate correlation strength [z(r)]. L indicates left.
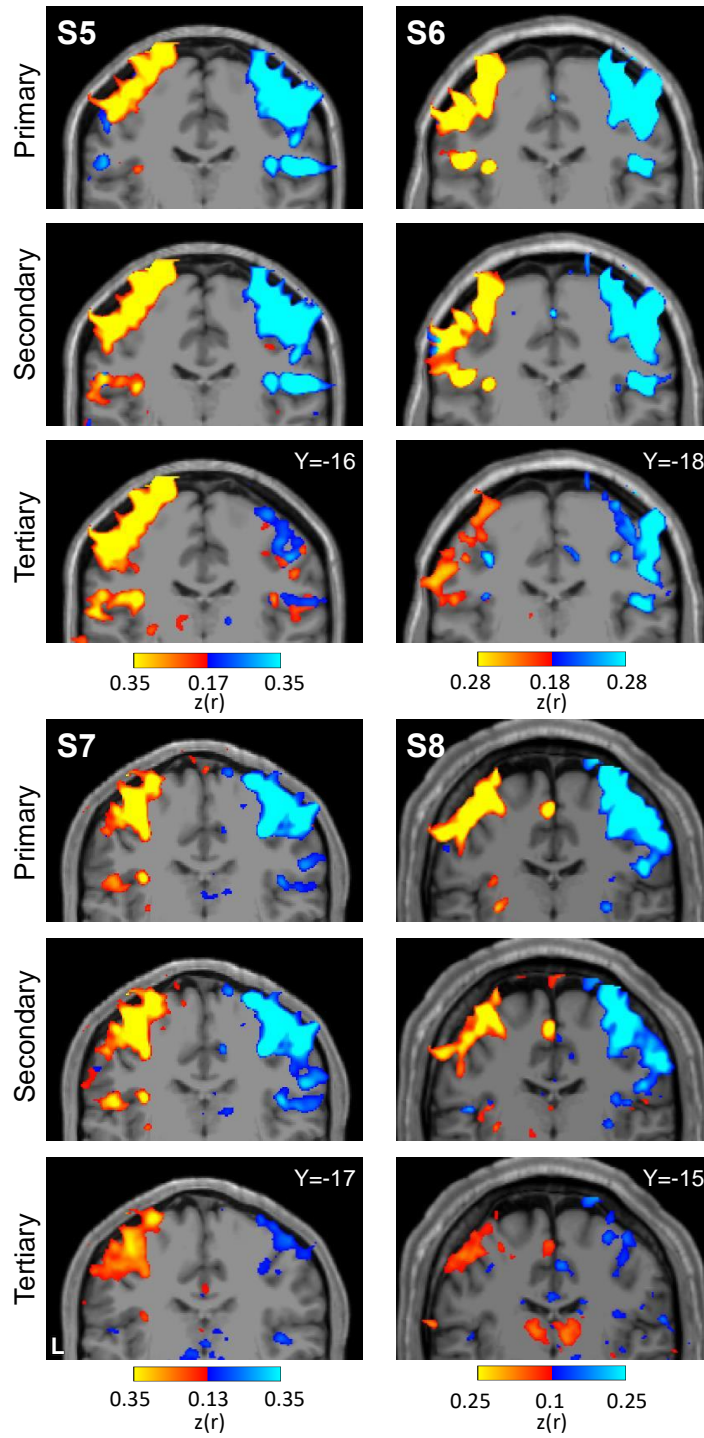
Figure 2.12 (Continued).

Figure 2.13. Replication of seed based functional connectivity from cerebellar foot representations. Coronal sections display functional connectivity patterns for foot seed regions in the right (red) and left (blue) cerebellum. In each column of three panels, an individual participant's data from the Replication sample are shown for separate sets of right versus left foot region contrasts that are independently seeded in the three cerebellar representations. The locations of the seed regions are illustrated by white circles in Fig. 2.11. In three individuals (S5-S7), functional connectivity of seed regions in the primary, secondary, and candidate tertiary cerebellar representations reveal M1's contralateral foot region (with S5 and S6 clearer than S7). The pattern is absent in S8. Coordinates indicate the section level in the space of the MNI152 atlas. The color bars indicate correlation strength [z(r)]. L indicates left.
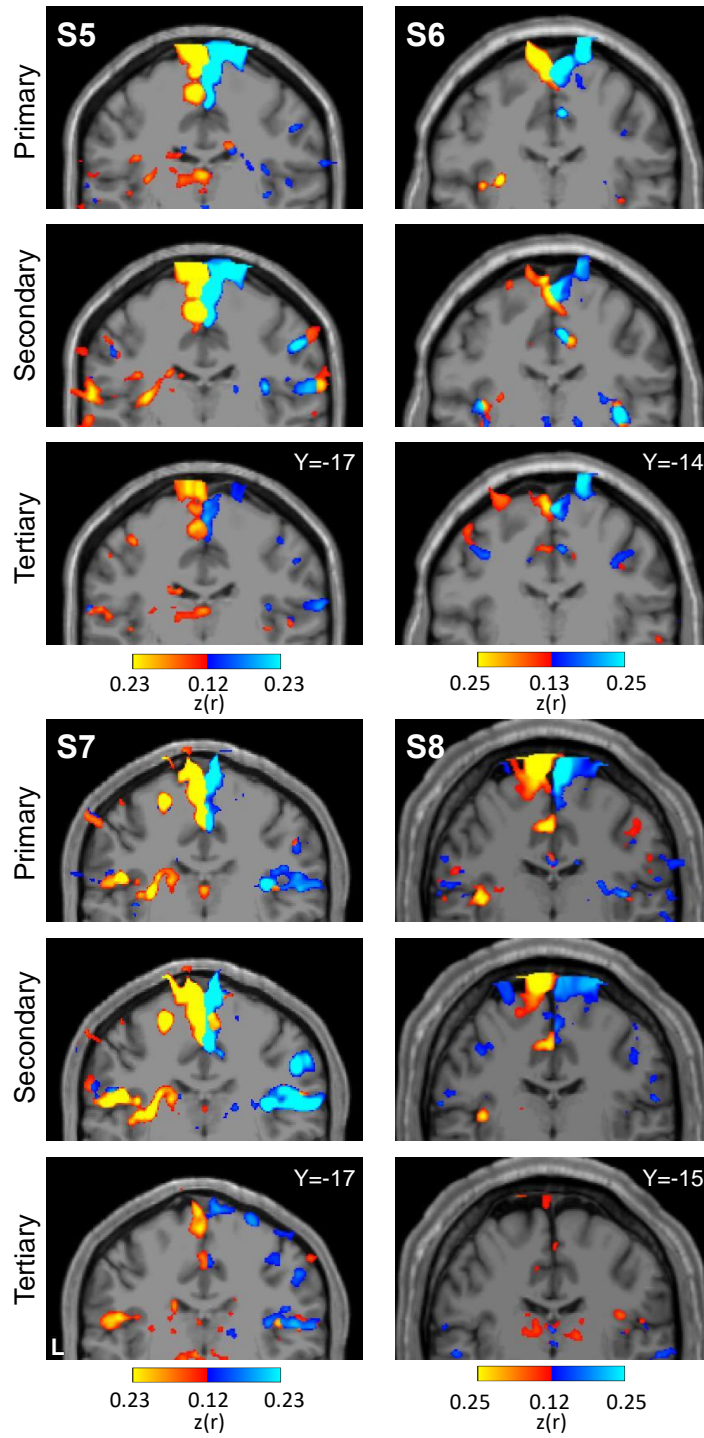
Figure 2.13 (Continued).
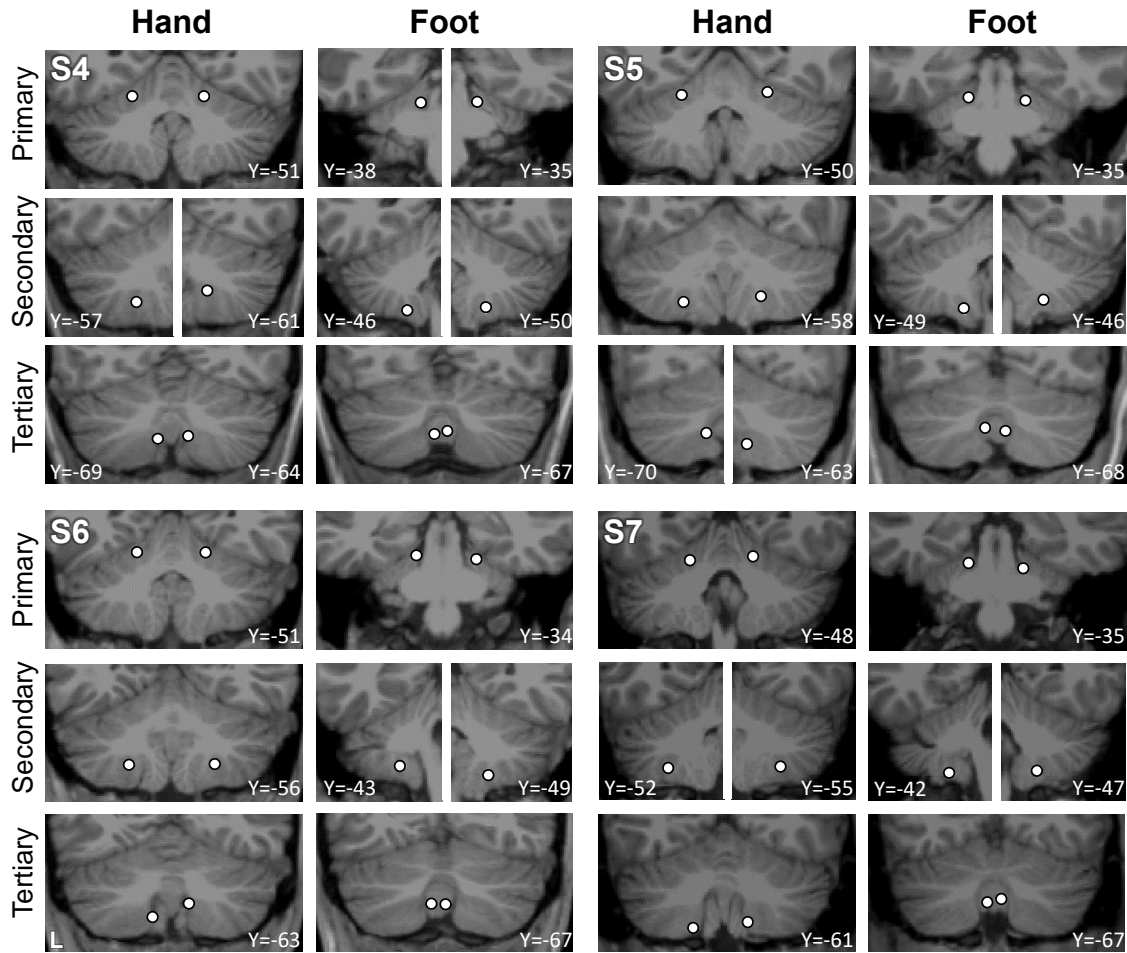
Figure 2.14. Visualization of seed region locations in the volume for S5 to S8. Seed region locations of the right and left primary, secondary and tertiary representations (white circles) are plotted on coronal sections of the T1 structural image for each participant in the Replication sample. Sections presented are of the seed region's center or within 1mm of the center. For each individual, hand and foot seed region locations are presented. Note how the tertiary foot location is medial to the hand representation in each participant. Coordinates indicate the section level in the space of the MNI152 atlas. L indicates left.

specificity was found in the three individuals for all three representations. S8's connectivity pattern showed M1's bilateral foot region from the primary and secondary seed regions (to lesser extent) but failed to demonstrate evidence for a tertiary representation. The locations of the seed regions are displayed in the volume (Fig. 2.14).

The three somatomotor maps are evident when examined at the group level

While our studies were designed with the goal of preserving idiosyncratic anatomical details within the individual, the results suggested that there may be sufficient positional stability of the three somatomotor maps to examine the data at the group level. Figure 2.15 (top) shows the full somatomotor topography across all 8 individuals (combining all data from the Discovery and Replication samples). A winner-take-all map was generated after averaging each movement contrast across individuals and projected onto flat map (left) and inflated cerebellar pial surface (right) visualizations. The primary and secondary somatomotor maps clearly present inverted and upright body topography correspondingly, suggesting that averaging data across participants can be effective. The posterior vermis shows hints of the tertiary map, clearer on the inflated surface, with the foot representation separated from the two others.

Figure 2.15 (bottom) also shows the left versus right contrasts of the hand and foot movements averaged across all individuals. Critically, the small discontinuous responses linked to the right and left foot movements are evident within the vermis as would be expected from the analyses of the individuals. Once the location is known, it is now possible to see evidence in the group data. Figure 2.16 illustrates the location of the third representation of the foot in the group-averaged volume (marked by F_3) along with the primary (F_1) and secondary (F_2) representations. The positioning and small size of the response also suggest why the third map representation is challenging to detect (and notice) as separate. We will return to this point in the discussion where the existing literature was reexamined for prior overlooked evidence for the third map.

115

Figure 2.15. The three somatomotor representations are detected in the group-averaged maps projected onto the cerebellar surface. Top: Group winner-take-all maps of active movements, generated after averaging contrasts across all 8 individuals are displayed for 4 body parts projected onto a flatmap (left) and inflated pial surface (right): tongue (red), right and left hands (yellow), glutes (green) and right and left feet (blue). The top inflated surface shows a dorsal/anterior view of the cerebellum and the bottom surface shows the ventral/posterior view. The primary inverted body map is apparent in the anterior lobe and the secondary map in the posterior lobe. Note candidate tertiary foot representations within the vermis, specifically in the ventral/posterior view of the inflated surface. Bottom left: A contrast map of right (red) versus left (blue) hand movements, averaged across participants, is projected on a cerebellar flatmap. The map is the mean contrast map of all 8 participants including 192 separate runs collected during active movements. Dotted lines indicate lobular boundaries as labelled in Fig. 2.2. Note the robust separation of the primary and secondary representation of the hand, with the secondary representation extending to the vermis. Bottom right: A parallel contrast map of right (red) and left (blue) foot movements is displayed. Note that there are three separate representations of the foot, with a tertiary representation falling within the vermis. The tertiary representation is spatially discontinuous with the secondary representation. The color bar represents the mean β values. L: Left; R: Right; A: Anterior; P: Posterior.

Somatomotor Topography
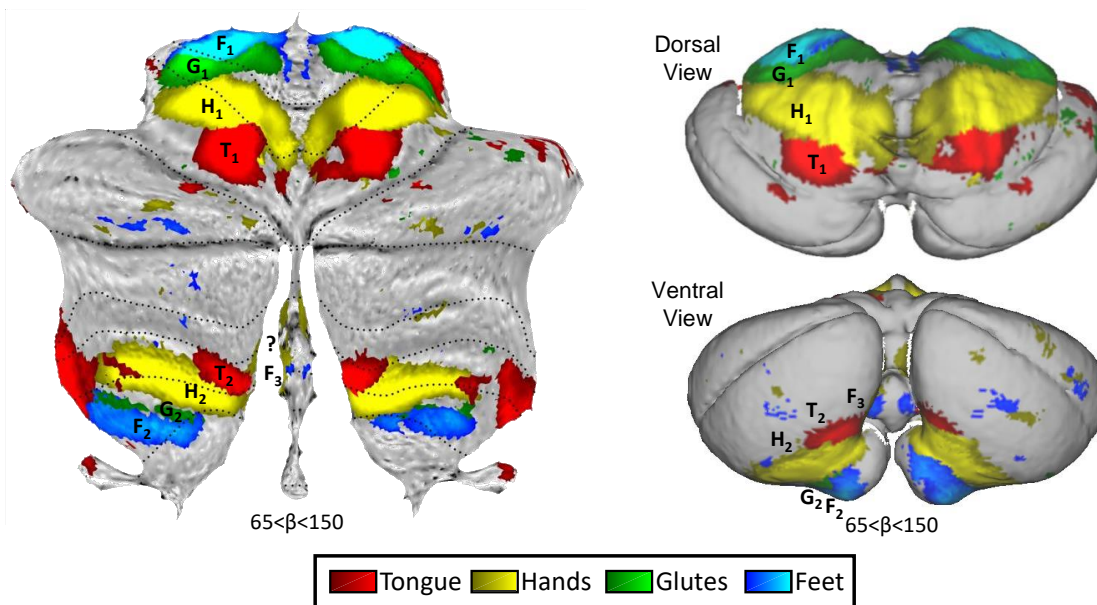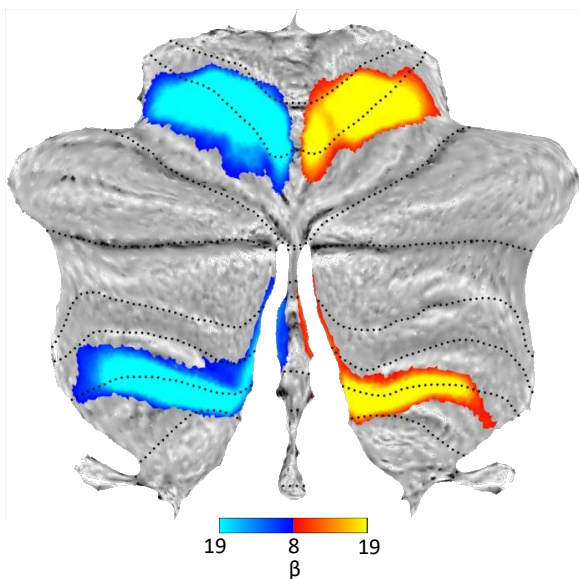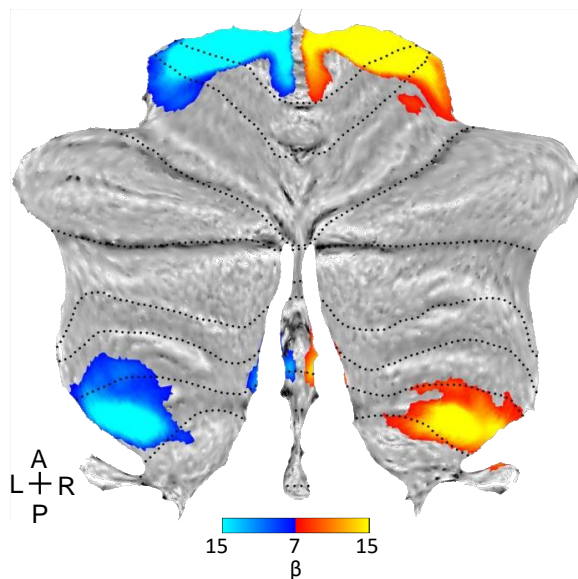
Figure 2.15 (Continued).

117
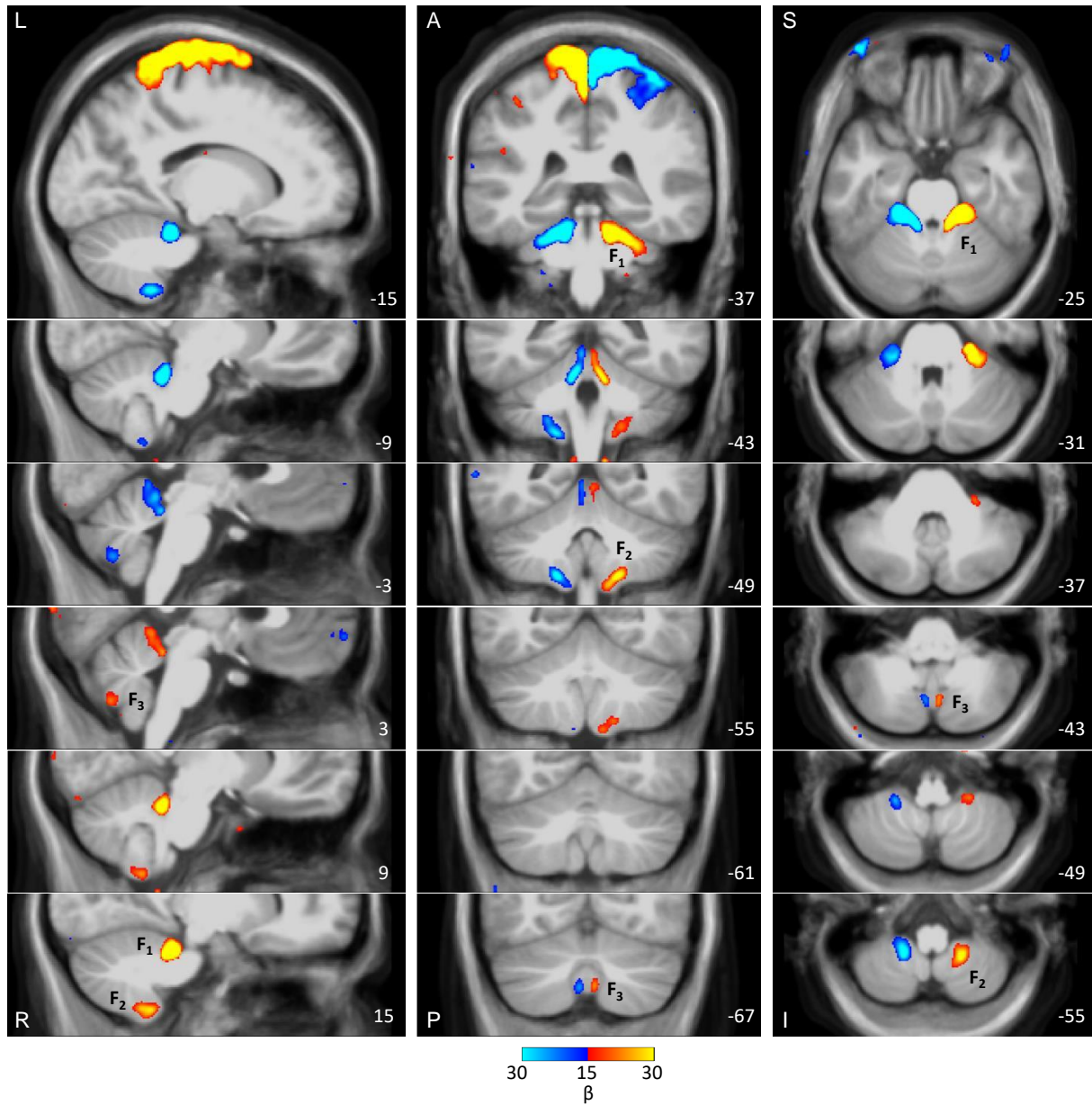
Figure 2.16 The three somatomotor representations of the foot are anatomically distinct in the group-averaged map, overlaid on the volume of the cerebellum. The three columns display sections in sagittal (Left), Coronal (Middle), and transverse (Right) orientation. In each orientation, the third foot representation is detected and anatomically separated from the second foot representation. The right primary, secondary and tertiary representations are marked by F_1, F_2 and F_3. Note that the third representation is smaller in size as compared to the other two representations. The anatomical backdrop is the average volume from the 8 participants contributing the functional data. In the middle and right columns, left is displayed on the left. Coordinates at the bottom right of each panel indicate the section level in the space of the MNI152 atlas. The color bar represents the mean β values. L: Left; R: Right; A: Anterior; P: Posterior; S: Superior; I: Inferior.

Figure 2.17 Relative location of hand and foot representations in the candidate tertiary map. The three columns display sections in sagittal (Left), Coronal (Middle), and transverse (Right) orientation. Right versus left contrasts show hand and foot primary (H_1, F_1), secondary (H_2, F_2) and tertiary (H_3, F_3) representations. Note that the tertiary hand representation is superior and lateral to the foot. It is unclear what the definitive orientation of the tertiary body map is since the secondary and tertiary hand representations are continuous. Nonetheless, these data are consistent with an upright map. The anatomical backdrop is the average volume from the 8 participants contributing the functional data. In the middle and right columns, left is displayed on the left. Coordinates at the bottom right of each panel indicate the section level in the space of the MNI152 atlas. The color bar represents the mean β values. L: Left; R: Right; A: Anterior; P: Posterior; S: Superior; I: Inferior.

Hands ▮ 15<β<25 ▮ Feet
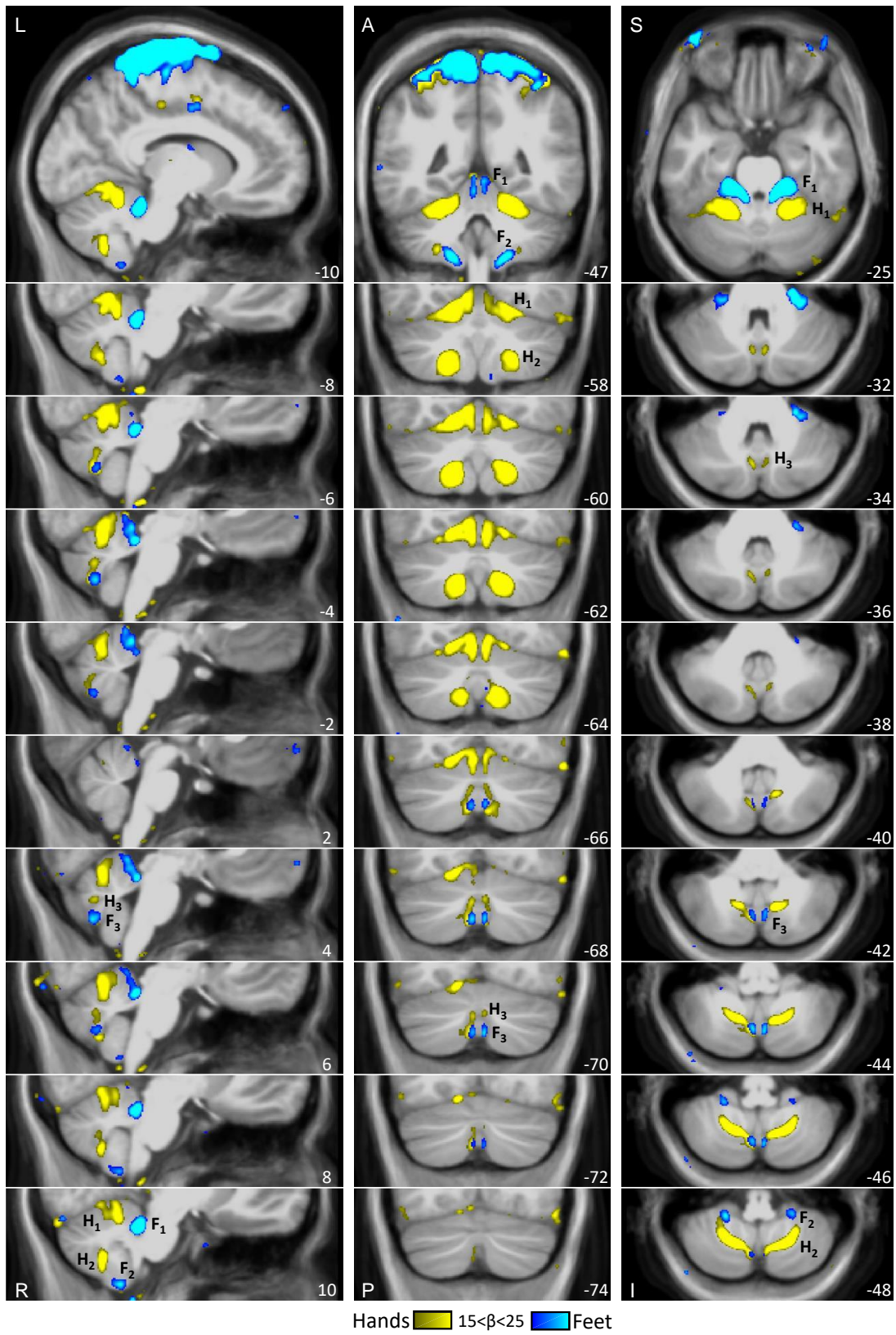
Figure 2.17 (Continued).

For another perspective on the relative location of the hand and the foot of the tertiary map, Figure 2.17 shows a group averaged contrasts across multiple 2mm-spaced slices. The tertiary hand representation appears superior and lateral to the foot. Still, because the secondary and tertiary hand representations are spatially continuous, we do not have sufficient information to definitively determine the third body map orientation. Nonetheless, the orientation of the hand and foot representations in Figure 2.17 and suggestive of an upright map.

Discussion

Our data provide evidence for a third somatomotor map representation within and near to the vermis of the human cerebellum. Unlike the two well-established somatomotor maps that can be distinguished as separate by exploring the hand, foot or other body parts bilaterally, the linchpin for detecting the separation between the second map and candidate third map was examining the multiple representations of the foot. When left and right foot movements were contrasted, a response was detected in the cerebellar vermis that was spatially discontinuous from the known second map. Moreover, the region of the posterior cerebellum between the two foot representations was associated selectively with the hand, providing evidence that the two foot representations are parts of spatially- and functionally-distinct maps. All findings were detected in multiple independent participants and replicated in a second, prospectively analyzed cohort. We discuss these observations in the context of what they reveal about the broad topography of the cerebellum as well as implications for the specific organization of the vermis.

Evidence for the elusive third cerebellar somatomotor map

While two somatomotor maps within the cerebellum have long been established (Adrian 1943; Snider and Stowell 1944; Snider and Eldred 1952; for review see Manni and Petrosini 2004), it has been difficult to find clear evidence for a third map[1]. Guell et al. (2018a, 2018b) hypothesized that a third somatomotor map may not exist, suggesting an organizational distinction between how motor zones of the cerebellum are represented in contrast to nonmotor zones. By their "double motor / triple nonmotor representation hypothesis", the most posterior zones of the cerebellum are occupied only by regions associated with higher-order cognitive and affective functions. The present results suggest that three distinct somatomotor maps may be present in the cerebellum, with the third falling at or near the third representation of nonmotor networks.

There are multiple possible reasons why the third map representation has been challenging to identify. First, it is small and buried in a difficult to access and hard to image region of the cerebellum. Second, studies using human neuroimaging have tended to focus on hand and finger movements and less on direct contrasts of foot movements. For example, the recent work by King and colleagues that produced detailed, comprehensive maps of cerebellar functional zones in both groups and individuals included only finger movement paradigms and did not include foot movements (King et al. 2019). We suspect if detailed analyses of foot movements had been more common in the field, consensus about the representation may have already emerged.

A third challenge deserving deeper discussion is that task-free functional connectivity estimates of cerebellar somatomotor representations have been surprisingly equivocal. As one example from our own recent work where we explored two individuals each scanned across 31 sessions, the somatomotor organization was the weakest aspect of the data. Even after revisiting that data based on the present findings, we cannot clearly establish the second map by contrasting left and right motor regions linked to the cerebral foot representations, despite there being little debate about the existence of the second map. The third map, being smaller than the second, is not detected. As another example, in our studies at high field (e.g., see Braga et al. 2019) we were not

able to detect robust functional connectivity between cerebral motor zones and the cerebellum in the face of clear functional connectivity from higher-order networks including the default network. In the recent work of Marek et al. (2018) that examined within-individual estimates of cerebellar organization from extensive functional connectivity data, the second somatomotor map is variably absent. This can be seen in individuals but also in their averaged flatmap representation (see Fig. S2 in Marek et al. 2018). While there is a clear inverted topography in the anterior lobe, posterior lobe cerebellar regions within the vicinity of the established second somatomotor map are assigned to higher-order cognitive networks including the default network. We suspect functional connectivity between the cerebral cortex and the cerebellum, as examined in our multiple earlier studies and also in these other studies in the literature, is yielding an incomplete estimate of somatomotor organization. We do not fully understand the origins of this limitation but have been perplexed previously on multiple occasions[1].

In this light it is interesting to revisit the results reported in Guell et al. (2018a) because their study is one of the few to examine cerebellar organization using both task-free functional connectivity and also task-evoked active motor movements. Using data from the Human Connectome Project (Van Essen et al. 2013), the study is well-powered, including data from 787 participants with the ability to directly contrast left and right active foot movements. What is notable is that the group-averaged task-evoked estimates in Guell et al. (2018a, see Fig. 4) are highly similar to our present group-averaged map (Fig. 2.15), with a spatially-discontinuous representation of the foot in the posterior vermis. The estimate of the foot representation from the task-free data does not show the same pattern as the task-evoked estimate. Thus, when examined closely, the present results converge with earlier studies that have examined task-evoked somatomotor topography.

Contextualizing the third somatomotor map within the broader organization of the cerebellum

The cerebellum possesses multiple roughly homotopic representations of the full cerebrum (Buckner et al. 2011b; Guell et al. 2018b; Xue et al. 2021; Buckner 2013). Two sets of somatomotor, cognitive and affective networks are found that begin in the anterior lobe and progress along the anterior-to-posterior axis. A primary representation spans from the anterior extent of the cerebellum to Crus I / II, and a secondary representation spans from Crus I / II to the posterior extent of the somatomotor representation[2]. Yet, a parsimonious account of cerebellar organization as multiple repeating cerebral representations encounters an inconsistency.

Evidence for a third partial representation of cerebral networks has been found posterior to the second somatomotor representation (Buckner et al. 2011; Guell et al. 2018a; Xue et al. 2021; King et al. 2019). The third representation includes cognitive and affective regions, but the expected somatomotor component that would complete the representation has been missing. The present finding of a third foot representation, localized to the posterior vermis (Figs. 2.15 and 2.16), is consistent with the possibility that the cerebellum possesses three separate representations of the full cerebrum each including a topographic representation of somatomotor cortex.

The location of the third map within the vermis is particularly intriguing because this region has been understudied in humans despite being a major focus or work in animal models (e.g., see Peters and Monjan 1971; Optican and Robinson 1980; Yamada and Noda 1987; Takagi et al. 1998; Herzfeld et al. 2015; Huang and Liu 1991). Recently, van Es and colleagues (2019) demonstrated that the human cerebellar vermis responds to visual stimuli. Detailed within-individual analysis

---

[2] We heuristically term the somatomotor / body maps as primary, secondary, and tertiary. As discussed by Guell et al. (2018a), this terminology is a heuristic for convenience and should not be taken to imply a known relation between the representations such as exists in primary and secondary visual cortical areas where direct thalamic input goes to the earlier (primary) area in a hierarchy of anatomically-connected areas. The ordering of the somatomotor maps in the cerebellum reflects the order in which the representations were discovered, not a functionally meaningful hierarchy.

confirmed this observation and further noted that the region is coupled to primary retinotopic

visual cortex. The third foot somatomotor representation is spatially near to the visual and auditory

representations within the vermis, suggesting that multiple sensory and motor maps may be

proximal to one another in this small buried region of the cerebellum, and also near to

representations of non somatomotor cerebral networks, including those important to affective

function (e.g., see Schmahmann and Sherman 1998; Stoodley and Schmahmann 2009). This

juxtaposition of sensory and motor maps between domains is not predicted by a simple model in

which all aspects of cerebellar topography are understood within a continuous homotopic mapping

of the cerebrum, as visual cortex is distant from somatosensory and motor cortices in the cerebrum.

Further study of the organization and functional importance of the human vermis is thus of great

interest.

A gap remains

Our data provide direct evidence for three separate discontinuous representations of the

foot. Based on the relative location of the hand and foot within the vermis, we speculate that the

tertiary body map is mostly upright, similar to the secondary map, where the hand representation

is anterior to the foot. Unlike the secondary representation hand representation appears lateral to

the foot. However, despite mapping four body parts extensively within each individual participant,

our results do not provide definitive evidence for the orientation of the third map. There are

multiple possible reasons for this gap. First, the tertiary representation is likely smaller than the

other two. It is possible that the spatial resolution used here is not sufficient for mapping the full

topography, especially given the complex surface topology of the cerebellum (Sereno et al. 2020).

Second, the tongue and the glutes are more susceptible to head motion, and therefore the

corresponding representations are noisier than the ones for the hands and feet, which also allow

direct subtraction of left and right movements. Future explorations with intensive within-individual

sampling at higher resolution will be informative. In addition, exploring a somatosensory paradigm where lateralized stimulation (right versus left) can be administered repeatedly across multiple body parts along the anterior-posterior axis may provide a path forward.

In the current study, we used a task of simple motor movements to assess the cerebellar somatomotor maps. It was previously suggested that complex movements (e.g., sequences of individual digits flexion and extension) can result in a different pattern of cerebellar activity and engage regions that are not activated during simple movements (Schlerf et al. 2010). The present paradigm is not able to map response related to complex movements or speculate about a specific functional role of the tertiary map. Future explorations might benefit from including complex movements in the experimental paradigm.

Conclusions

We provide reliable evidence that the human cerebellum possesses three spatially-distinct representations of the foot. The location of the third foot representation is in the vermis, consistent with a third somatomotor map continuous with the tertiary representations of cognitive and affective networks. The third map's small size and location may have contributed to its evasiveness in past explorations, and suggests examination at high spatial resolution will be necessary to fully understand the third map's spatial orientation and its relation to functionally-distinct zones of the vermis.

Chapter 3. Human Hippocampal Specialization Along the Long Axis Revisited

Abstract

Functional specialization along the long axis of the hippocampus has long been studied in rodents, non-human primates, and humans. The well-characterized connectivity of the hippocampal formation to distributed cerebral regions, along with recent advances for precision estimation of networks within individuals, present an opportunity to better understanding functional differences within the hippocampus. Building on the recent discovery of differential functional connectivity from the anterior and posterior hippocampus to cerebral networks, we characterized individuals from two independent functional MRI cohorts with the goal of exploring specialization of the long axis (N = 9 and N = 11). Functional connectivity analyses revealed and replicated that cerebral Default Network A (DN-A) was primarily correlated with the anterior hippocampus, while the Salience Network / Parietal Memory Network (SAL / PMN) was preferentially correlated with the posterior hippocampus. Functional characterization using task data discovered an unexpected double dissociation between the anterior and posterior hippocampal regions. DN-A and the anterior hippocampal region were sensitive to task demands related to scene construction, while SAL / PMN and the associated posterior hippocampal region were not. Motivated by the SAL / PMN network's historical role in responding to salient events, *post-hoc* analysis of available task data revealed the posterior hippocampus responded to the transitions between task blocks. To explicitly test the involvement of the posterior hippocampus in salience processing, we prospectively explored a visual oddball task. The posterior hippocampus displayed transient responses to salient targets, consistent with its coupling to the SAL / PMN network, yet contrary to expectations from several current models of hippocampal function. These

findings suggest a functional dissociation along the long axis of the hippocampus with the anterior hippocampus responding during scene processing, and the posterior hippocampus responding to transient, salient events.

Introduction

The hippocampus in non-human primates is connected to cerebral cortex via the entorhinal cortex (EC, Amaral and Witter 1989), which receives direct connections from distributed cerebral regions (Insausti et al. 1987; Insausti and Amaral 2008). The EC in turn is interconnected with parahippocampal (PHC) and perirhinal (PRC) cortices, which also receive inputs from regions throughout cerebral cortex (Suzuki and Amaral 1994). Functional connectivity analyses in humans converge with these results, showing coupling in both the PHC and the hippocampus proper to distributed cerebral networks including the network called the default network in the human neuroimaging literature (Fox et al. 2005b; Fransson 2005; Greicius et al. 2004; Vincent et al. 2006). We can leverage this hippocampal-cortical connectivity to effectively study functional differences along the long axis of the human hippocampus by anchoring our functional explorations to the functional properties of coupled cerebral networks,

Anatomical and functional heterogeneity along both the primate long axis and the homologous septo-temporal axis in rodents inspires the present work. Along the rat hippocampus, which runs from the dorsal to the ventral pole, internal projections from the dorsal two-thirds terminate almost exclusively within that same region of the long axis, and intrinsic connections in the ventral one-third of the hippocampus are similarly restricted (Fricke and Cowan 1978). Extrinsic connections to the hippocampus are also heterogenous, with the dorsal and ventral hippocampus receiving inputs from spatially distinct portions of the entorhinal cortex (EC) (Dolorfo and Amaral 1998). Differences in extrinsic connectivity also exist along the long axis of the macaque

hippocampus, which runs from posterior to anterior along the medial aspect of the temporal lobe. The anterior hippocampus sends outputs to and receives projections from mainly antero-medial EC, while the posterior hippocampus is primarily connected with postero-lateral EC (Amaral and Witter 1989; Witter and Amaral 2021). These regions of EC in turn receive projections from different portions of higher order association cortex (Insausti and Amaral 2008). This suggests the anterior and posterior hippocampus, via the EC, may be receiving inputs from different cerebral networks, or at minimum different portions of the broader hippocampal-cortical network.

In humans, functional MRI (fMRI) can be leveraged to explore whole brain network organization through functional connectivity analysis, which identifies regions with correlated fluctuations in spontaneous activity (Biswal et al. 1995; Fox and Raichle 2007). While there are limitations to indirect fMRI connectivity methods (Buckner et al. 2013; Murphy et al. 2013; Power et al. 2014), functional connectivity has recapitulated many features of anatomical connectivity (Buckner et al. 2011; Buckner and Margulies 2019; Matsui et al. 2012; Vincent et al. 2007; Yeo et al. 2011), and is sensitive to damage which severs anatomical connections (Johnston et al. 2008; Lu et al. 2011; Quigley et al. 2003). Functional connectivity has been employed to explore networks coupled to the hippocampus and immediately adjacent interconnected cortical structures.

Across multiple studies, functional connectivity from the hippocampal formation converges on a distributed network consisting of retrosplenial cortex / posterior cingulate, caudal posterior parietal cortex, ventromedial prefrontal cortex, and additionally often the dorsolateral prefrontal cortex, and the temporal pole (Barnett et al. 2021; Frank et al. 2019; Greicius et al. 2004; Kahn et al. 2008; Vincent et al. 2006). Many studies which did not explicitly segment the hippocampus tended to focus on the larger anterior hippocampal zones or immediately adjacent cortical structures including the entorhinal cortex and parahippocampal gyrus (e.g., Greicius et al. 2004; Vincent et al. 2006), so there has been comparatively less work characterizing the specific functional connectivity of the posterior hippocampus. Among the work that has been done there is variability in the pattern

of correlations, likely driven in part by differences in how the posterior hippocampus was defined (e.g. tractography based parcellation versus anatomical segmentation based on the uncal apex). However, there is some convergence across studies showing hippocampal functional connectivity to a portion of the midline posterior to retrosplenial cortex (Barnett et al. 2021; Przeździk et al. 2019).

The Long Axis of the Hippocampus Displays Functional Heterogeneity

In addition to organizational heterogeneity, the hippocampus also displays functional heterogeneity along its long axis. In 1971, John O'Keefe and Jon Dostrovsky first identified neurons in the dorsal hippocampus of rats which fired when animals were in a particular portion of their enclosure (O'Keefe 1976; O'Keefe and Dostrovsky 1971). The locations in which these neurons preferentially fire is termed their "place field," and are stable unless certain features of the environment change (e.g. a change to the enclosure size, or the movement of orienting landmarks) (Muller and Kubie 1987; O'Keefe and Burgess 1996). Subsequent work has found neurons with place fields along the full extent of the septo-temporal axis, and by mapping those place fields characterized a gradual expansion in place field size from dorsal to ventral neurons (Jung et al. 1994; Kjelstrup et al. 2008). Interestingly, animals with dorsal and ventral hippocampal lesions display different behavioral phenotypes across a variety of spatial tasks. For example, lesions to the dorsal hippocampus preferentially disrupt spatial learning in Morris water maze (Moser et al. 1993, 1995) and one-way active avoidance paradigms (Nadel 1968), but impairments on a spatial probability task only occur after a ventral lesion (Stevens and Cowey 1973).

Human neuroimaging studies have also explored dissociations along the long axis motivated by varied theories of hippocampal function (for review see Poppenk et al. 2013). In line with work linking declarative memory deficits to hippocampal damage (Milner et al. 1968; Scoville and Milner 1957; Zola-Morgan et al. 1986), some positron emission tomography (PET) and fMRI

studies have suggested the anterior hippocampus is primarily involved in memory encoding while the posterior hippocampus supports memory retrieval (Lepage et al. 1998; Poppenk and Moscovitch 2011), but others have found minimal effect in the posterior hippocampus (Spaniol et al. 2009) or even the opposite dissociation (Schacter and Wagner 1999).

Meanwhile, other studies have taken inspiration from rodent neurophysiology to explore the involvement of the human hippocampus in the representation of space. This work implicates the posterior hippocampus in spatial reasoning and navigation (Maguire et al. 1997, 1998, 2000; Ryan et al. 2010; Woollett and Maguire 2011, 2012) in contrast to the coarser representations in the anterior hippocampus (Brunec et al. 2018; Hirshhorn et al. 2012), a dissociation paralleling the observed differences in rodent place field size. This diversity in functional dissociation motivates further exploration of human hippocampal function.

A goal of the present paper is to revisit the functional specialization of the long axis of the hippocampus motivated by the response properties of the networks the regions interact with. As will be shown, such a starting point – anchored on response properties of cortical regions – converges with ideas about the hippocampus's role in spatial processing, and raises the possibility of an unexpected role for certain sub-regions in the processing of transient, salient events.

Within-individual MRI Improves the Precision of Functional Characterization

Functional characterizations of the human hippocampus has been limited by the resolution of neuroimaging methods. Several approaches to tackle the challenge of limited resolution have focused on anatomical strategies to segment the hippocampal formation and / or align it across participants using substructure landmarks (Carr et al. 2010; Ekstrom et al. 2009; Miller et al. 2005; Small et al. 2000; Stark and Okado 2003; Zeineh et al. 2000, 2001). Anchoring off seminal investigations on the visual system (DeYoe et al. 1996; Engel et al. 1997; Tootell et al. 1998; Wandell et al. 2007), collecting sufficient data within individual participants to avoid spatial

blurring (via between-subject averaging) has resulted in improved precision for estimating

distributed cerebral functional networks (Braga et al. 2019; Braga and Buckner 2017; Gordon et al.

2017; Laumann et al. 2015; Xue et al. 2021) and task-based functional characterization of

association regions (Braga et al. 2020; DiNicola et al. 2020, 2023; Fedorenko et al. 2010; Saadon-

Grosman et al. 2022; Tootell et al. 1998).

Recently, within-individual precision approaches have explored networks coupled to the

hippocampal formation, in particular the network identified as default network A (DN-A), so named

because it falls within the bounds of the canonical group estimated default network (Braga and

Buckner 2017). DN-A includes the portions of the default network functionally coupled to the

extended hippocampal region including the posterior parahippocampal, retrosplenial, ventromedial

prefrontal, posterior parietal, and dorsolateral prefrontal cortices (Barnett et al. 2021; Frank et al.

2019; Greicius et al. 2004; Kahn et al. 2008; Vincent et al. 2006). Within-individual selective

targeting of the subiculum within the hippocampus proper yielded the full distributed cerebral DN-

A network in a high resolution study at high (7T) field (Braga et al. 2019). The present paper will

use within-individual intensive sampling to explore hippocampal function along the long axis.

Off particular relevance to the present investigations, Zheng and colleagues recently made a

breakthrough in our understanding of human hippocampal organization by characterizing

hippocampal heterogeneity within individuals using functional connectivity to cerebral networks

(Zheng et al. 2021). Specifically, they found two networks with prominent and differential coupling

to the anterior and posterior hippocampus. The first network correlated with the anterior

hippocampus is topographically similar to DN-A, and included retrosplenial, ventromedial

prefrontal, and parahippocampal cortex. In contrast, the posterior hippocampus correlated

network was distinct and linked to what they described as the parietal memory network

(PMN)(Gilmore et al. 2015). The PMN resembles another network heavily studied in the literature

generally referred to as the Salience Network (Seeley 2019; Seeley et al. 2007). Their anterior /

posterior hippocampal dissociation thus affords a novel approach to explore functional differences along the hippocampal long axis, while the complexity of the networks identifies raises the need for direct targeted functional explorations to disambiguate possible functional roles of the identified regions.

Here we expand on the work of Zheng and colleagues (2021) to first replicate and explore in detail the candidate dissociation between anterior and posterior hippocampal regions. Then using targeted task-based functional characterizations, we explored functional response properties with a particular focus on processes related to scene construction (Hassabis and Maguire 2007) and transient responses to salient events (Dosenbach et al. 2006; Fox et al. 2005a; Konishi et al. 2001) motivated by the recruitment of cerebral DN-A and SAL / PMN for these processes. To avoid the potential for bias, all functional connectivity analyses identified cerebral networks and regions of the hippocampus prior to functional characterization, and included multiple replications and generalizations. This rigorous approach to data analysis within the individual, coupled with a grounding in cerebral networks, allowed for a precise and robust characterization of human hippocampal function.

Methods

Overview

Our exploration of the hippocampus used two independent data sets, both published previously as part of work characterizing networks in cerebral cortex within individuals [Experiment 1, N = 9 (DiNicola et al. 2020). Experiment 2, N =11 (Du et al. In Prep)]. Both data sets included extensive resting-state fixation and task data for every participant, which were used for hippocampal region identification and functional exploration of those regions, respectively. Hippocampal region identification used previously identified cerebral networks and proceeded

identically in both Experiments. Functional task responses were first interrogated at the level of

task runs. This was followed by an analysis that considered each trial of a task separately, which

has been shown to allow for more detailed investigations of cognitive tasks when paired with trial-

level estimates of cognitive strategy use (e.g. DiNicola et al. 2023). Finally, we visualized transient

responses that were difficult to separate using run- and trial-level analyses using raw percent

change in blood oxygenation level-dependent (BOLD) signal.

Experiment 1: Initial Exploration

MRI Participants

Twelve healthy adult participants ages 18-25 were recruited from the Boston area, with the

goal of acquiring 4 neuroimaging sessions each (S7-S18 in DiNicola et al. 2020, contains S1-S10 in

DiNicola et al. 2023). All paid participants were native English speakers screened to exclude

neurological or psychiatric illness, and were provided with written informed consent through a

protocol approved by the Harvard University Intuitional Review Board (IRB). Two participants (S9

and S13) completed only two of the planned four scanning sessions and were excluded from

analyses. One additional subject (S8) was excluded after functional connectivity analyses but prior

to task analysis due to difficulty in conclusively identifying SAL / PMN (see Data Processing below).

The final cohort of 9 participants had a mean age of 21.3 yr (SD = 2.1 yr) with 8 right-handed

participants, 7 who identified as female, and 3 individuals (33%) who self-reported as non-white

and/or Hispanic. Experiment 1 participants are labelled from S8 to S18, remaining consistent with

the previous report on this data (DiNicola et al. 2020).

MRI Data Acquisition

All scanning was done at the Harvard Center for Brain Science using a 3T Siemens Magnetom Prisma-fit MRI scanner and a 64-channel phase-arrayed head-neck coil (Siemens Healthcare, Erlangen, Germany) with foam padding on the back and sides of the head for comfort and to help with head motion. Stimuli were presented on a rear projected display which participants viewed while supine using a mirror attached to the head coil. Participants were instructed to remain as still and alert as possible throughout each scanning session. Alertness was assessed and scored by monitoring a live view of the participant's eyes (Eyelink 100 Core Plus with Long Range Mount, SR Research, Ottawa, Ontario, Canada), and real-time movement during functional runs was assessed using FIRMM (Framewise Integrated Real-time MRI Monitoring, Dosenbach et al. 2017).

Each scan session included acquisition of a rapid T1-weighted structural image, using a multi-echo magnetization prepared rapid acquisition gradient echo (ME-MPRAGE, van der Kouwe et al. 2008) sequence (1.2mm isotropic voxels, TR=2200ms, TE=1.57, 3.39, 5.21, 7.03ms, TI=1100ms, 176 slices, flip angle=7°, matrix=192 x 192 x 176, in-plane GRAPPA acceleration=4). BOLD data were acquired using a multi-band gradient-echo echo-planar pulse sequence (see Feinberg et al. 2010; Moeller et al. 2010; Setsompop et al. 2012; Xu et al. 2013), provided by the Center for Magnetic Resonance Research at the University of Minnesota (2.4 mm isotropic voxels, TR=1000ms, TE=32.6ms, flip-angle=64°, matrix=88 x 88, 65 slices covering cerebral cortex and cerebellum).

MRI Task Paradigms

MRI participants completed a battery of tasks including passive fixation, an episodic projection task, Theory of Mind (ToM) tasks, and a working memory task. Additional tasks not discussed here were also included in the neuroimaging battery (see Braga et al. 2020).

FIXATION. During passive fixation (11 runs, 7min 2s each, 77min 22s total), participants

were asked to fixate on a black plus sign in the center of a light grey background while staying still

and alert. Data from each individual's fixation runs were used to identify that subject's cerebral

networks using functional connectivity analysis, prior to and independently from any task analyses

(see Individualized Cerebral Surface Parcellation below).

EPISODIC PROJECTION AND THEORY OF MIND. The episodic projection (6 runs, 10min 12s

each, 61min 12s total) and ToM (8 runs, 5min 18s each, 42min 24s total) tasks are described in

detail in DiNicola et al. 2020. The episodic projection task asked participants to answer questions

spanning combinations of self-relevance (Self vs Non-Self) and temporal orientation (Past, Present,

Future), e.g. Past Self or Future Non-Self, after carefully considering the question's details (10s

trials, 10s ISI). Each run had 5 unique questions for each condition, and questions were not

repeated, resulting in 180 unique questions over 6 runs. In the ToM tasks, participants were

similarly instructed to answer, after careful consideration (15s trial, 15s ISI), questions relating to:

emotional and physical pain (Pain, 4 runs); characters with potentially false beliefs and objects with

potentially false information (Belief, 4 runs).

WORKING MEMORY. The working memory task (10 runs, 1min 48s each, 18min total) was a

2-back only version of an N-back task. Large upper-case consonants were presented in blocks, each

presented for 1s with a 1s ISI, with 12 presentations per block. For each presented letter,

participants were instructed to indicate whether that letter matched the letter shown 2

presentations earlier. In each block, among the 10 trials that could be matches (the first two

presentations could never be matches), 4 were target 2-back matches, while 3 were non-target 1-

back lures. Each run consisted of 24s of fixation, two 24s task blocks with 18s of fixation between,

and a final 18s of fixation after the final task block.

MRI Exclusion Criteria and Quality Control

All data was examined for quality prior to analysis. Run-level exclusion criteria for functional BOLD runs included: (1) maximum absolute motion exceeding 2 mm, (2) slice-based signal-to-noise ratio less than or equal to 135 and, (3) eyes closed during skipped or incorrect task trials. All exclusions were finalized prior to task analysis to avoid potential bias. Across all Experiment 1 participants 16 fixation runs were excluded due to motion, and the number of usable fixation runs per participant ranged from 5 (S14 and S16) to the maximum of 11. In addition, two participants (S11 and S12) had one run of the Pain ToM task excluded each due to a presentation error.

MRI Data Processing

A custom analysis pipeline designed to preserve within-individual details ("iProc", see Braga et al. 2019; DiNicola et al. 2020) was used to process all data. In brief, this pipeline consists of registering each participant's data to either their own 1mm-isotropic T1 template or the MNI ICBM 152 1mm atlas through a single interpolation. In each case, a participant's interpolation includes matrices for motion, field map unwarping, alignment to a mean BOLD template image derived from that participant's data, and registration to the participant specific T1 template. The MNI interpolation includes an additional matrix registering the individual participant's T1 template to the MNI template.

T1-aligned BOLD fixation data used for functional connectivity analysis had additional nuisance variables regressed (6 motion parameters as well as whole-brain, ventricular, and white matter signals and their temporal derivatives), and were bandpass filtered at 0.01-0.10 Hz (using AFNI v2016.09.04.1341; Cox 1996, 2012). For analyses of responses within the hippocampus during tasks, whole-brain signal was regressed (see DiNicola et al. 2020) from the MNI-aligned BOLD data before extracting the hippocampus as described below. Task analysis on the cerebral surface used whole-brain regressed T1-aligned data resampled to the fsaverage6 cortical surface

mesh (using trilinear interpolation; Fischl et al. 1999) and smoothed on that surface mesh using a 2mm full-width at half-maximum (FWHM) Gaussian kernel.

Online Behavioral Participants

300 participants aged 20-28 were recruited through Amazon Mechanical Turk using Cloud Research (Litman et al. 2017) and paid for their participation. Respondents who self-reported age as young as 18 were included. Participants were all English-speakers located within the United States with high ratings for completion and performance (90%+ approval rating with at least 100 prior tasks approved). Each participant provided informed consent through a Harvard University IRB-approved online protocol. The study was administered using Harvard University's Qualtrics platform.

Online Question and Strategy Probe Format

Mirroring the neuroimaging protocol, online behavioral questions asked about either a real-world experience or general knowledge and featured three possible answer choices. The questions themselves were the same as the scanned task, except for a few questions that required minor wording changes to be applicable to online participants. Participants were asked to respond to the question within 10s, after which time participants received a reminder to answer the question. After answering each individual question, the participants reported the cognitive strategies they used when answering the question by giving a number from 1 (not used at all) to 7 (used extensively) for each of 16 strategies (see DiNicola et al. 2023, adapted from Andrews-Hanna et al. 2010). Only after completing this reflection was the participant able to move forward and view the next question. The included strategies probed the extent a given question: asked about a personally significant topic (Significance); prompted them to think about their personal feelings (Pers_Feelings); evoked emotions (Emotions); asked them to rely on personal past experiences

138

(Pers_Past_Exper); lead them to imagine a sequence of event unfolding (Sequence_Events); lead them to envision the locations of mentioned objects or places (Loc_Obj_Places); lead them to envision the physical locations of other people (Loc_People); lead them to speculate about others feelings (Others_Feelings); made them consider general moral principles (Moral_Principles); required them to think about their relationships to other people (Relationships); made them consider the personality traits of appearances of other people (Others_Personality); evoked visual imagery (Visual_Imagery); evoked thoughts that had recently been on their mind (Recent_Thoughts). Participants were also asked to rate how difficult a question was (Difficulty), how much they relied on facts when answering (Facts), and how specific their thoughts were (Specificity).

Each participant was given a subset of the questions presented to MRI participants to alleviate the burden of rating many strategy probes. The subset of trials presented to participants was rotated such that 50 online participants provided strategy ratings for each in-scanner trial. As a control, 5 questions were presented to every participant to test for potential cohort effects, and 2 additional questions were included as attention checks (one probed whether participants were reading the questions while another targeted task focus).

Online Behavioral Exclusion Criteria and Quality Control

Extensive quality control measures were used to ensure only participants who fully engaged with the task were included. Participants were excluded if they failed on measures of compliance, such as spending too little time on the survey, responding incorrectly to attention check questions, or having particularly stereotyped response patterns (full details in DiNicola et al. 2023). 62 participants were excluded through this process, leaving 238 participants in the final set, with 37 or more participant responses for each question. Participant ages ranged from 18 to 25 (mean age = 22.5 yr (SD = 1.9 yr), 61% identifying as female), and completed the tasks in between

38.1 and 46.6 min (mean = 42.5 min). Analysis of the ratings for questions included for all participants revealed no cohort effect across the 6 acquisition groups ($F(5,570) = 0.26$, $p = 0.94$).

Strategy Clustering

The collected strategies were clustered to create robust composite scores for every episodic projection trial. For each trial, strategy ratings for the presented question were averaged across all online participants, and the subsequent trial-specific average was z-scored within a given strategy. The correlation structure of the resulting 16 x 180 matrix (strategies x trials) was calculated and visualized, before using hierarchical clustering to estimate strategy groupings (hclust function and ward.D2 amalgamation procedure in R v3.5.1). This resulted in 5 clusters: Difficulty (Facts and Difficulty strategies); Scene Construction (Loc_Obj_Places and Visual_Imagery strategies); Autobiographical (Pers_Past_Experiences and Sequence_Events strategies); Others-Relevant (Others_Feelings and Other_Personality strategies); Self-Relevant (Significance, Recent_Thoughts, Pers_Feelings, and Emotions strategies). Composite ratings were calculated by summing the average z-scored ratings for strategies within each cluster.

Individualized Cerebral Surface Parcellation

Whole-brain networks were precisely estimated on the cerebral surface of each individual participant using functional connectivity analyses on fixation data, using a k-means algorithm for clustering (see Braga et al. 2020; DiNicola et al. 2020). Cerebral networks were identified manually based on diagnostic features (Braga and Buckner 2017) at k values ranging from 10 to 20. For every individual, the smallest k solution resulting in differentiation of 6 a priori notable networks was chosen. These networks were: Default Network A (DN-A) and B (DN-B), Language Network (LANG), Frontoparietal Network A (FPN-A) and B (FPN-B), and the Cingular-Opercular Network (CG-OP). Other networks of interest were identified where possible, including the Salience Network /

Parietal Memory Network (SAL / PMN) and Dorsal Attention Network (dATN). As SAL / PMN was

not considered when initially identifying the appropriate parcellation, in one participant (S8) the

chosen k did not dissociate this network. A larger k value would have dissociated SAL / PMN but

would have also changed the assignments for other networks used in previous analyses. Because

SAL / PMN was the network hypothesized to be correlated the posterior hippocampus, the choice

was made prior to any task analyses to exclude this participant from the present work.

Individualized Hippocampal Functional Connectivity and Region Creation

Individual specific hippocampal regions were defined based on functional connectivity to

cerebral networks while respecting each individual's idiosyncratic hippocampal anatomy (Fig. 3.1).

For each fixation run, the mean BOLD signal was extracted within DN-A and SAL / PMN on the

cerebral surface smoothed to 2mm FWHM. Each network's mean time course on the surface was

correlated with the time-course of every voxel in that run's MNI111-registered BOLD data, resulting

in two whole-brain correlation maps: one to cerebral DN-A, the other to cerebral SAL / PMN. These

two maps were compared across the entire brain, and every voxel was assigned to the cerebral

network with which it was most correlated.

To isolate hippocampal voxels, each individual's hippocampus was first identified using the

Freesurfer automated parcellation (Fischl et al. 2002, 2004). The Freesurfer-based mask was then

binarized and warped to MNI space using the same individual-specific matrix used in "iProc"

preprocessing. After warping, ambiguous voxels along the edge of the hippocampal region (value of

less than 1) were removed. The temporal signal to noise ratio (tSNR) was calculated for each

hippocampal voxel by dividing the mean time course across all fMRI runs by its standard deviation.

Voxels with a tSNR below 50 (between 7.65% and 38.03% of hippocampal voxels) were removed to

minimize the inclusion of regions with signal dropout. Signal dropout was particularly notable near

to and within the anterior pole of the hippocampus (e.g. Fig. 3.2). The resulting individual-specific

141
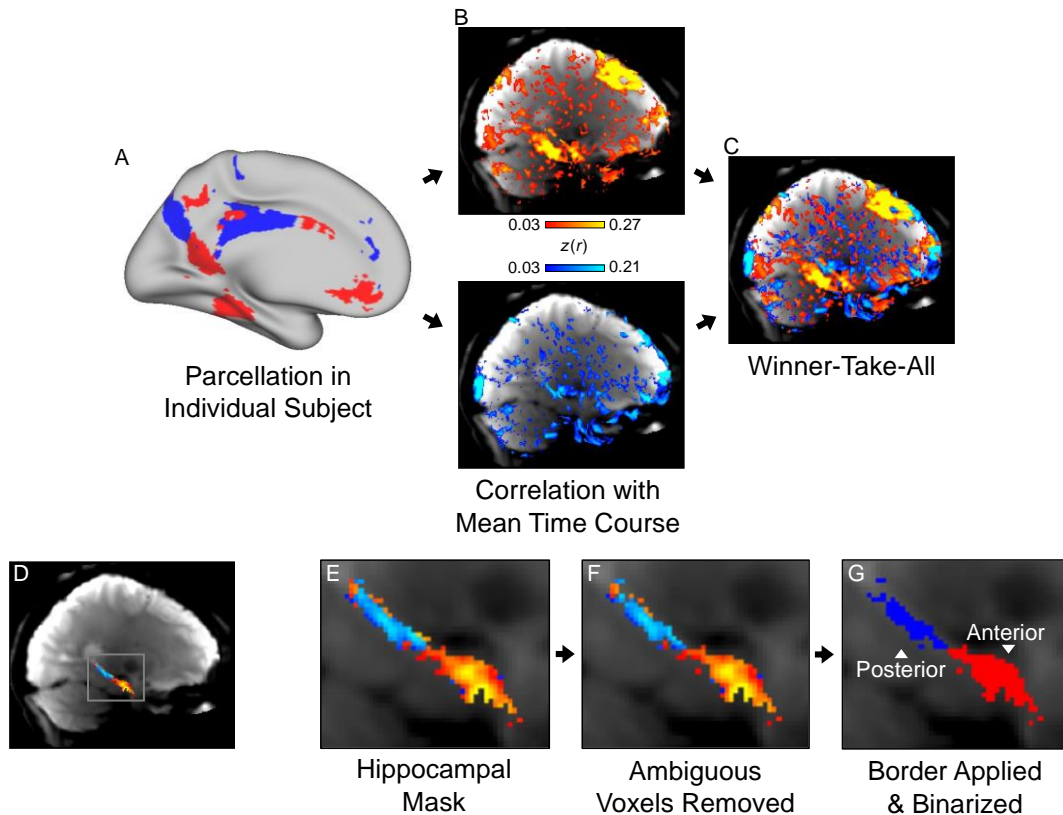
Figure 3.1 Procedure for defining hippocampal regions based on functional connectivity with cerebral networks. In each participant, networks of interest (Default Network A, DN-A, red; Salience Network / Parietal Memory Network, SAL / PMN, blue) were identified on the cortical surface (A) using k-mean clustering in Experiment 1 or multi-session hierarchical Bayesian modeling in Experiment 2. The mean BOLD time-course within each network's boundaries was extracted and correlated with the BOLD time-course of every voxel in the brain volume (B). Volume voxels were assigned to the network with which they were more correlated (C), masked for the hippocampus using each individual's Freesurfer parcellation after excluding voxels with a signal-to-noise ratio below 50 (D, E). Within this region, ambiguous voxels with comparable correlations to both networks ($|z(r)_{DN-A} - z(r)_{PMN}/z(r)_{DN-A} + z(r)_{PMN}| < 0.1$) were removed (F), and a single network was assigned to define the anterior or posterior region. Only voxels assigned to the anterior-defining network were kept and binarized anterior to a defined border, and similarly for the posterior-defining network (G). The border position was defined as the MNI Y coordinate which left an equal proportion of DN-A voxels anterior to the border and SAL / PMN voxels posterior, as well as vice-versa. The network with > 50% of its assigned voxels anterior to border was chosen as the anterior-defining network, while the network with > 50% of assigned voxels posterior to the defined border was chosen as the posterior-defining network. In this representative participant the border was defined at MNI coordinate Y = -26, and ~77% of DN-A and SAL / PMN defined the anterior and posterior regions, respectively.

hippocampal mask was applied to the winner-take-all correlation map described above, leaving only voxels within the hippocampus. The network-assigned voxels within the hippocampus were further refined by removing low correlation voxels ($z(r) < 0.03$) and voxels with similar correlation values to both cerebral networks, defined as having a normalized correlation difference of less than 0.1 ($|z(r)_{DN-A} - z(r)_{SAL/PMN}/z(r)_{DN-A} + z(r)_{SAL/PMN}| < 0.1$).

An MNI Y coordinate was chosen as the anterior / posterior border for each individual subject, and voxels assigned to each network were quantified posterior to or anterior to that border (voxels within border were included in the anterior region). The border location was chosen such that the proportion of DN-A assigned voxels in the anterior region and proportion of SAL / PMN assigned voxels in the posterior region would be equal, and vice-versa (DN-A assigned voxels posterior and SAL / PMN voxels anterior). In practice, this identified the coordinate where, moving along the long axis, one network's assigned voxels began to be more prevalent while the other network's assigned voxels began to be less prevalent. Following border assignment, DN-A and SAL / PMN were assigned as the defining network for whichever side of the border contained the majority of that network's assigned voxels. Voxels belonging to the non-assigned network were removed in both the anterior and posterior regions, and the remaining voxels were binarized to produce masks for the hippocampal regions (Fig. 3.2).

To evaluate the selectivity of these regions' connectivity to the cerebral surface without the constraints imposed during region creation, for each fixation run the mean BOLD time course within each hippocampal region (whole brain regressed and bandpass filtered as described above) was correlated with the BOLD time course of every vertex on the surface projected data (whole brain regressed, bandpass filtered, and smoothed to 2mm FWHM). These correlation values were Fischer z transformed, the resulting z-value for each surface vertex was averaged across all of a participant's fixation runs, and finally visualized on the cerebral surface. To quantify the specificity of the correlations from each participant's anterior and posterior hippocampal regions, we

143
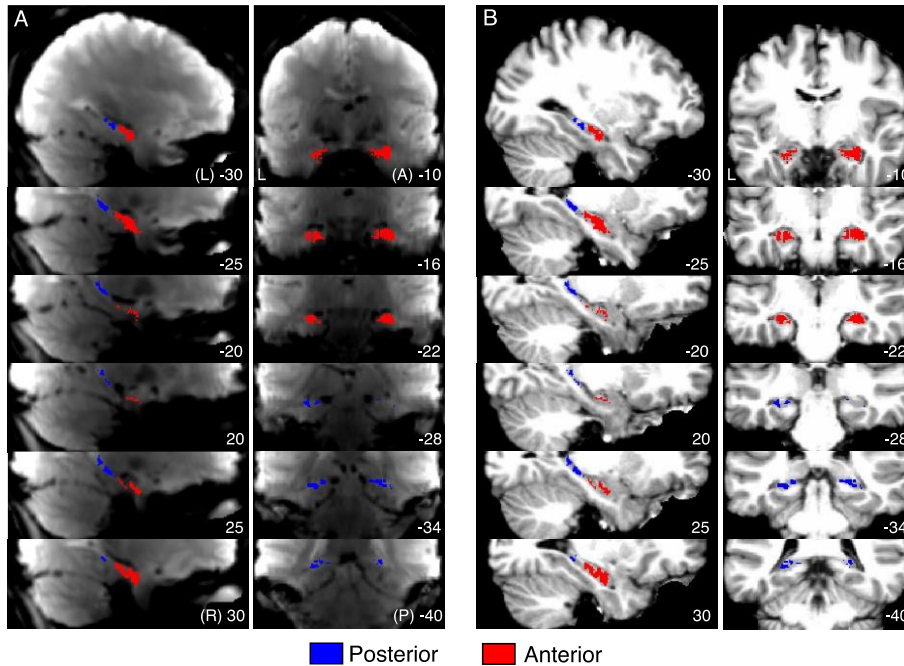
Figure 3.2 Hippocampal functional connectivity to DN-A and SAL / PMN can be used to define bilateral anterior and posterior hippocampal regions. In this representative participant, the posterior hippocampus contained the majority of SAL / PMN correlated voxels while the anterior hippocampus consisted almost entirely of DN-A correlated voxels. The region creation process (Fig. 3.1) resulted in anterior (red) and posterior (blue) regions defined by high correlations to DN-A and SAL / PMN respectively, with a border at MNI Y = -26. These regions are displayed both this participant's mean T2*-weighted image (A) and T1-weighted structural image (B) to show their adherence to individual-specific hippocampal anatomy. Note the significant loss of signal in the T2* image within the anterior and medial parahippocampal gyrus, highlighting the difficulty in imaging this region. MNI X and Y coordinates are given in the bottom right of each sagittal and coronal slice, respectively.

averaged the *z*-values across all the vertices contained within the boundaries of each of that individual's cerebral networks. The mean *z*-values for each identified network were then averaged across participants to create a group-level estimate of the anterior and posterior hippocampal regions' selectivity to cerebral networks, and significance was assessed using a one-tail t-test (H_o: μ = 0, H_a: $\mu > 0$).

Task Analysis

RUN-LEVEL. For task analyses, run-specific general linear models (GLMs) were created with regressors for task conditions (implemented through FSL v5.0.4 first-level FEAT, Jenkinson et al. 2012). GLMs were run separately for each hemisphere of the cortical surface (using whole-brain regressed data, smoothed to 2mm FWHM) and the MNI111-registered volume (whole-brain regressed, not smoothed) which included the hippocampus. Task contrasts were created separately for each task run by subtracting the β-values for conditions within a contrast for each voxel. This contrast β-value was converted to a *t*-value by dividing by its standard error, and finally converted to a *z*-value. *Z*-value maps for each contrast were averaged across runs to create an average task contrast, and these average values were extracted within each participant's individualized cerebral networks and hippocampal regions for quantification.

TRIAL-LEVEL. The episodic projection task was additionally analyzed using a GLM with separate regressors for every trial (e.g. DiNicola et al. 2023; Hassabis et al. 2014). Trial-specific β-values were converted to *z*-values as described above, then extracted and averaged from within individual-specific cerebral networks and hippocampal regions. This yielded a trial-level readout of each participant's network and hippocampal region recruitment for a given episodic projection question (for additional detail see DiNicola et al. 2023). To further explore how network and hippocampal activity is driven by the cognitive strategies used to answer each trial's question, the average value for a given trial within a network or hippocampal region was averaged across

145

participants, producing a single group-estimate of network / region activity during that trial. This allowed for extremely stable estimates for each of the episodic projection trials while also continuing to respect each individual's idiosyncratic anatomy.

Experiment 2: Prospective Replication

In the interest of rigorous hypothesis testing, data acquisition, processing, and analysis were deliberately kept as similar as possible between Experiments 1 and 2. Any relevant differences in Experiment 2 are outlined below, with more extensive details provided in Du et al. (In Prep).

MRI Participants

Fifteen healthy native English-speaking adults (ages 18-35), without neurological or psychiatric illness, were recruited from the Boston area and completed 8-11 neuroimaging sessions each (P1-P15 in Du et al. In Prep). All participants were paid and provided with written informed consent according to a protocol approved by the Harvard University IRB. One participant was excluded due to an idiosyncratic error in registration to the fsaverage6 surface (see MRI Data Processing), and three participants were excluded for low quality episodic projection task performance (see MRI Data Processing). The final set of 11 participants had a mean age of 22.4 yr (SD = 4.1; 11 right-handed; 8 identifying as female; 7 (64%) self-reported non-white and/or Hispanic). These independent participants are labelled P1-P15 to remain consistent with previous work (Du et al. In Prep) and distinguish them from Experiment 1 participants.

MRI Data Acquisition

Experiment 2 data was collected on the same scanner as Experiment 1 with a 32-channel phase-arrayed head-neck coil (Siemens Healthcare, Erlangen, Germany). Padding on the side of the head was achieved using inflatable pads rather than foam padding. Participant alertness and real-time motion were assessed during acquisition as in Experiment 1.

Each scan session included acquisition of 2 rapid T1-weighted ME-MPRAGE structural images with the same parameters as Experiment 1, except for a slightly different field of view (FOV, matrix = 192 x 192 x 144). An additional higher resolution T1-weighted ME-MPRAGE was also acquired (0.8mm isotropic voxels, TR=2500ms, TE=1.81, 3.6, 5.39, 7.18ms, TI=1000ms, 208 slices, flip angle=8°, matrix=320 x 320 x 208, in-plane GRAPPA acceleration=2) along with a matched T2-weighted structural scan using a sampling perfection with application-optimized contrasts using different flip angle evolution (SPACE, Siemens Healthcare, Erlangen, Germany) sequence (0.8mm isotropic voxels, TR=3200ms, TE=564ms, 208 slices, matrix=320 x 320 x 208, in-plane GRAPPA acceleration=2). BOLD data acquisition was unchanged except for a larger FOV (matrix = 92 x 92 x 65).

MRI Task Paradigms

MRI participants completed a battery of tasks including passive fixation (22 runs, 7min-2s each, 154min 44s total), an episodic projection task (10 runs, 10min 17s each, 102min 50s total), ToM tasks (8 runs, 5min 18s each, 42min 24s total), a visual motor task (8 runs, 3min 24s each, 27min 12s total), and a visual oddball task (5 runs, 5min 50s each, 29min 10s total). Additional tasks not discussed here were also included as part of data acquisition, including: a language localizer, a retinotopic mapping task, a working memory task, a motor task, and a reward task (see Du et al. In Prep for additional details).

The acquired episodic projection task was an expanded version of the task acquired in Experiment 1 and included all 180 original questions, as well as an additional 120 questions

targeting new categories of interest. These new questions were split across 4 conditions, each with 30 new questions: Spatial Reasoning, Moral Judgements, Moral Decisions, and Non-moral Judgements. Each run included 3 questions for each of the 10 total categories, and as in Experiment 1 no questions were repeated, resulting in 300 unique questions over the 10 runs. There was no change to the ToM tasks from Experiment 1.

The visual motor task consisted of three 40s task blocks, with two 18s blocks of fixation between them, 30s of fixation prior to the first task block, and 18s of fixation after the final task block. During the task blocks, the participants fixated at the center of a flickering, black and white circular checkboard. During 10 of the 40 1s-trials in each task block, red squares were superimposed for 0.5s on of the checkerboard to the left and right of the fixation point. In these presentation trials, the red squares were presented close to the fixation point 5 times, and the squares were presented further from the fixation point the remaining 5 times. Whenever the red squares were presented, participants were asked to indicate that the squares were closer to the fixation point by pressing with both their index fingers simultaneously, and that the squares were further from the fixation point by pressing with both their middle fingers simultaneously.

In the visual oddball task, participants were presented sequentially with upper case "K"s and "O"s in either black or red, and asked to indicate whenever a red upper case "K" was presented. Each of the 5 acquired runs started with 26s of passive fixation, followed by a 2s cue indicating that letter presentation was about to begin. This was followed by 300 1s trials, during which a letter was presented for 150ms, followed by passive fixation for 850ms. 30 trials presented the salient target letter (red "K"), 30 presented a salient non-target (red "O"), and the remaining 240 trials were evenly split between the non-salient non-target letters (black "K" and "O"). After the trials, a 2s cue indicated the end of the task, followed by 20s of passive fixation.

MRI Exclusion Criteria and Quality Control

As with Experiment 1, all data was examined for quality prior to analysis. Run-level exclusion criteria included: (1) maximum absolute motion exceeding 1.8mm (except for episodic projection runs), and (2) eyes closed during skipped or incorrect task trials, or poor task performance. Because each run of the episodic projection task was significantly longer than other tasks, a maximum absolute motion of 1.8mm was deemed too stringent to serve as a hard threshold. Instead, each episodic projection run above the 1.8mm threshold was evaluated on a case by case basis and included if the cumulative motion appeared to be the result of small movements accumulating over the longer run, rather than fewer unacceptably large movements. The largest maximum absolute motion deemed acceptable was 2.5mm. Across all participants, 17 fixation runs, 11 episodic projection runs, 2 theory of mind runs, 10 visual oddball runs, and 2 working memory runs were excluded. Of the 15 recruited individuals, three participants (P5, P10, and P11) were excluded from analyses due to a high number of excluded episodic projection runs or missed trials within the episodic projection task.

MRI Data Processing

Data was processed as in Experiment 1, using the same custom iProc pipeline. The only notable changes in processing is the use of a higher resolution, 0.8mm isotropic T1 image for registration, along with the inclusion of the matched T2 image when calculating pial and white matter boundary surface estimates using Freesurfer's "recon-all" command (Fischl et al. 1999). Because each participant's T1 structural image is converted to a resolution of 1mm isotropic as part of the recon-all process, use of a higher resolution T1 in Experiment 2 did not affect alignment and registration. For one participant (P12), the pial and white matter boundaries calculated based on the 0.8mm T1 resulted in misregistration of subject-specific surface data to the fsaverage6 template, which was identified after processing and analysis. As all analyses were done within the individual this misregistration would likely have had minimal to no impact on the results, but to

ensure consistency both within and across experiments this participant's data are not reported here.

Remote Behavioral Participants

329 participants aged 20-28 were recruited through Amazon Mechanical Turk using Cloud Research and paid for their participation. Inclusion criteria, compensation, and informed consent process were unchanged from Experiment 1.

Question and Strategy Probe Format

Online participants answered questions from the expanded episodic projection task. The subset of trials presented to participants was rotated such that at least 30 individuals gave strategy ratings for each trial question. 21 strategy ratings were collected for each question, including 13 strategies from Experiment 1 and 8 additional strategies. Strategy ratings for Significance, Specificity, and Recent_Thoughts were collected in Experiment 1 but not Experiment 2 to reduce the burden of including the 8 new strategies. Specificity was not included in any strategy composite, so its removal had no effect on subsequent analyses. Significance and Recent_Thoughts strategy ratings were included in the Experiment 1 Self-Relevant composite, but were deemed acceptable omissions because these ratings were highly correlated with the other two strategies in the Self-Relevant composite, and as such did not show evidence of contributing additional information to the overall Self-Relevant composite.

Remote Behavioral Exclusion Criteria and Quality Control

Participant responses were screened for engagement and compliance as in Experiment 1. 54 participants were excluded through this process, leaving 266 participants in the final set, with 25 or more participant responses for each question. Included participant were ages 18 to 27 (mean

age = 23.2 yr (SD = 1.9 yr), 51% identified as female), and spent between 22 and 185 min (mean = 49.5 min) completing the tasks. Consistent with Experiment 1 strategy collection, there was no effect of cohort on the ratings for control questions repeated across all 10 groups ($F(9,640) = 0.26$, $p = 0.98$).

Strategy Clustering

Strategy clustering was performed as in Experiment 1 (hclust function and ward.D2 amalgamation procedure in R v4.2.1) including only the 13 strategy ratings and 180 questions included in both experiments. Strategies which clustered together in Experiment 1 data were also closely clustered in Experiment 2 (see Results, Fig. 13). As such, the same 5 clusters were used for Experiment 2: Difficulty (Facts and Difficulty strategies); Scene Construction (Loc_Obj_Places and Visual_Imagery strategies); Autobiographical (Pers_Past_Experiences and Sequence_Events strategies); Others-Relevant (Others_Feelings and Other_Personality strategies); Self-Relevant (Pers_Feelings and Emotions strategies). Note that the Self-Relevant cluster has two fewer strategies than in Experiment 1 because strategy ratings for Significance and Recent_Thoughts were not collected, as discussed above (see Question and Strategy Probe Format).

Individualized Cerebral Surface Parcellation

For Experiment 2, cerebral networks were identified using a multi-session hierarchical Bayesian model approach (MS-HBM, Kong et al. 2019; Xue et al. 2021, Du et al. In Press; calculated in MATLAB version 2019a; MathWorks, Natick, MA; https://github.com/ThomasYeoLab/CBIG/tree/master/stable_projects/brain_parcellation/Kong2019_MSHBM). This new method for network identification was chosen prior to any analyses in the hippocampus, and was not informed by hippocampal results from Experiment 1. We decided to switch to an MS-HBM approach, rather than continue to use a k-means approach, for two reasons.

First, while k-means parcellation considers only the average correlation matrix, the MS-HBM accounts for correlation variability both within an individual (i.e. different runs of fixation) and between individuals. This improves the reliability of network estimates by preventing cases where noisy correlations or suboptimal amounts of data (causing high intra-subject variability) result in inappropriately idiosyncratic estimates for highly stereotyped networks (networks with low inter-subject variability like primary sensory networks). The second advantage of an MS-HBM parcellation is the ability to consistently identify all networks of interest. Because the model is initialized with a group parcellation (in our case a Human Connectome Project, HCP, 15-network parcellation), any network included in that parcellation will also be present in every individual, with topography determined by their data. This avoids situations where some individual's parcellations require more networks to be estimated to dissociate certain networks, which was common with the k-means approach. Importantly for hippocampal analyses, this ensured that both DN-A and SAL / PMN were identified in every participant.

In brief (for detailed description, see Du et al. In Prep), MS-HBM parcellations begin in each individual with Pearson's correlations calculated between the fMRI time course at each vertex on the fsaverage6 cerebral surface (40,962 vertices for each hemisphere) and each of 1,175 ROIs evenly distributed across the fsaverage5 surface mesh (Yeo et al. 2011). The highest 10% of correlation values within each hemisphere's 40,962 x 1,175 correlation matrix were kept and binarized to produce a functional connectivity profile (Yeo et al. 2011). Participants were split into three groups, each consisting of 5 individuals, for the purposes of estimating networks. Within each group, all the participant- and run-specific connectivity profiles were fed into a MS-HBM initialized using a 15-network group level parcellation estimated from the HCP S900 data release (Kong et al. 2019; Yeo et al. 2011). This method produced a 15 network parcellation for each individual, a solution which critically followed established literature by both dissociating DN-A from DN-B

(Braga et al. 2019; Braga and Buckner 2017) and SAL / PMN from the Cingulo-Opercular Network (CG-OP, see Seeley 2019).

Individualized Hippocampal Functional Connectivity, Region Creation, and Model Free Seed-Based Functional Connectivity

The procedure for creating hippocampal regions and quantifying hippocampal functional connectivity followed that of Experiment 1 exactly. In addition to these analyses, a model free seed-based approach (e.g. Braga and Buckner 2017) was used to assess the specificity of hippocampal functional connectivity to the hippocampus, rather than nearby cortical and sub-cortical structures. For this exploration, the pair-wise Pearson correlation was calculated between every voxel within an expanded hippocampal mask (59,343 – 68,354 voxels), based on an individual's freesurfer parcellation, to every vertex on the cortical surface (81,924 vertices). The resulting correlation matrix was calculated for each fixation run, Fischer z-transformed, and averaged across all of an individual's fixation runs to yield a single best estimate of that participant's correlation structure. This correlation structure was then explored using Connectome Workbench's wb_view software (Glasser et al. 2013; Marcus et al. 2011) by interactively choosing seed regions and visualizing the correlations from that seed using the Jet look-up table, excluding negative values. The correlations were threshold in order to better see the functional connectivity topography on the cerebral surface or in the hippocampus.

Task Analysis

Run- and trial-level analyses were completed as in Experiment 1 for episodic projection and ToM tasks. Only those 180 episodic projection questions included in both Experiment 1 and Experiment 2 were analyzed. Additional run-level analyses were completed for the visual oddball task which mirrored the run-level analyses for episodic projection and ToM. General linear models

for each run of the visual oddball task were created separately for each hemisphere of surface

projected data (whole-brain regressed, smoothed to 2mm FWHM) and the MNI111-registered

volume data (whole-brain regressed, not smoothed). The regressors included in the GLM were: task

cues (both onset and offset), salient targets (red "K"s), salient non-targets (red "O"s), and fixation

periods. Non-salient non-targets were not explicitly modelled. For this task, regressor β-values

were taken directly (rather than contrasted), z-transformed, and averaged across runs to create

task activation maps. Quantification was done by extracting z-values within cerebral networks and

hippocampal regions, as with the episodic projection and ToM tasks.

<div align="center">

Results

</div>

The Anterior and Posterior Hippocampus are Differentially Correlated with Cerebral DN-A

and SAL / PMN

Across the 9 participants in Experiment 1, functional connectivity analyses on fixation data

revealed consistently different patterns of the connectivity from cerebral Default Network A (DN-A)

and Salience Network / Parietal Memory Network (SAL / PMN) to the anterior and posterior

hippocampus. In all participants, voxels in the anterior hippocampus were nearly all more

correlated with DN-A than SAL / PMN, while voxels more correlated with SAL / PMN were virtually

only present in the posterior hippocampus (Fig. 3.3, right). The anterior-posterior border

placements and anterior-posterior network assignments reflect this dissociation: Across

participants the chosen border fell between MNI Y coordinates -22 and -31, and in all cases DN-A

was assigned to the region anterior to this border (henceforth referred to as the anterior

hippocampal region) while SAL / PMN was assigned to the region posterior to the border

(henceforth referred to as the posterior hippocampal region) (Fig. 3.3, left). After voxels belonging

to the non-assigned network were removed from each region, >73% of each network's total
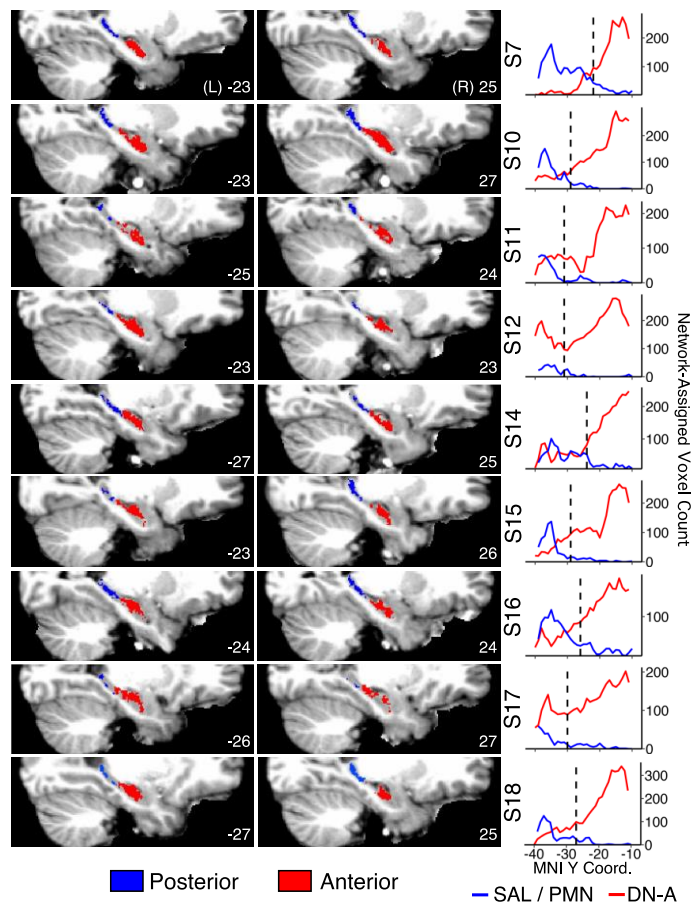
Figure 3.3 Cerebral SAL / PMN is preferentially correlated with the posterior hippocampus and DN-A is preferentially correlated with the anterior hippocampus in all Experiment 1 participants. For each participant a single representative sagittal slice for the left (L) and right (R) hemisphere is shown on the left, along with a plot of SAL / PMN and DNA assigned voxel counts along the hippocampal long axis. The MNI X coordinate for each slice is given in the bottom right of each image, and the location of the anterior / posterior border is shown by the black dashed line in the plots on the right. In all participants, SAL / PMN was the appropriate choice for defining the posterior hippocampal region (blue), while DN-A was appropriate for defining the anterior hippocampal region (red). While the size of the anterior and posterior regions varies between individuals, SAL / PMN correlated voxels were consistently almost only present in the posterior hippocampus, while DN-A correlated voxels were the majority of voxels in the anterior hippocampus. The anterior/posterior border defined for each participant were, from top to bottom, MNI Y = -22, -29, -31, -31, -24, -29, -26, -30, and -27.

155

assigned voxels remained. The anterior region included between 2691 (S16) and 4180 (S12) voxels (mean 3353), while the posterior region included between 276 (S12) and 1726 (S7) voxels (mean 778).

Given that the process for defining these regions was restricted to only two cerebral networks of interest, we sought to characterize the coupling of these hippocampal regions to cerebral networks more broadly by performing further functional connectivity analyses on each participant's fixation data, this time correlating activity within the individual-specific hippocampal regions with activity on the cerebral surface. In all participants, visual inspection of the pattern of correlations from the hippocampal regions to the cerebral surface suggested preferential coupling to the networks chosen to define each region. Posterior hippocampal regions were highly correlated with regions of SAL / PMN, such as posterior cingulate cortex, posteromedial cortex, and anterior insula (Figs. 3.4 and 3.5, left). In contrast, the anterior hippocampal regions were highly correlated with regions of DN-A, such as retrosplenial, parahippocampal, and dorso-lateral prefrontal cortices (Figs. 3.4 and 3.5, right).

We quantified the extent of this preferential coupling by extracting the average correlation from each hippocampal region within a subset of individually defined cerebral networks (Fig. 3.6). This quantification confirmed that among the identified cerebral networks, the posterior hippocampal region was most correlated with cerebral SAL / PMN, while the anterior hippocampal region was on average most correlated with DN-A. Some participants showed high correlations between the anterior hippocampus and Default Network B (DN-B), which may suggest additional variation in the anterior hippocampus not captured by the current approach, but all participants showed strong correlations between the anterior hippocampus and DN-A. To better understand these regions in aggregate, we averaged the individual-specific network correlation values across subjects (Fig. 3.7). The resulting group-level data further supports the conclusions from the individual level quantification: the posterior hippocampal region was preferentially correlated with

156

SAL / PMN | **DN-A**

S7 · S10 · S11 · S12 · S14

z(r) > 0.20
z(r) > 0.25
z(r) > 0.15
z(r) > 0.20
z(r) > 0.20

Posterior Correlation   Anterior Correlation
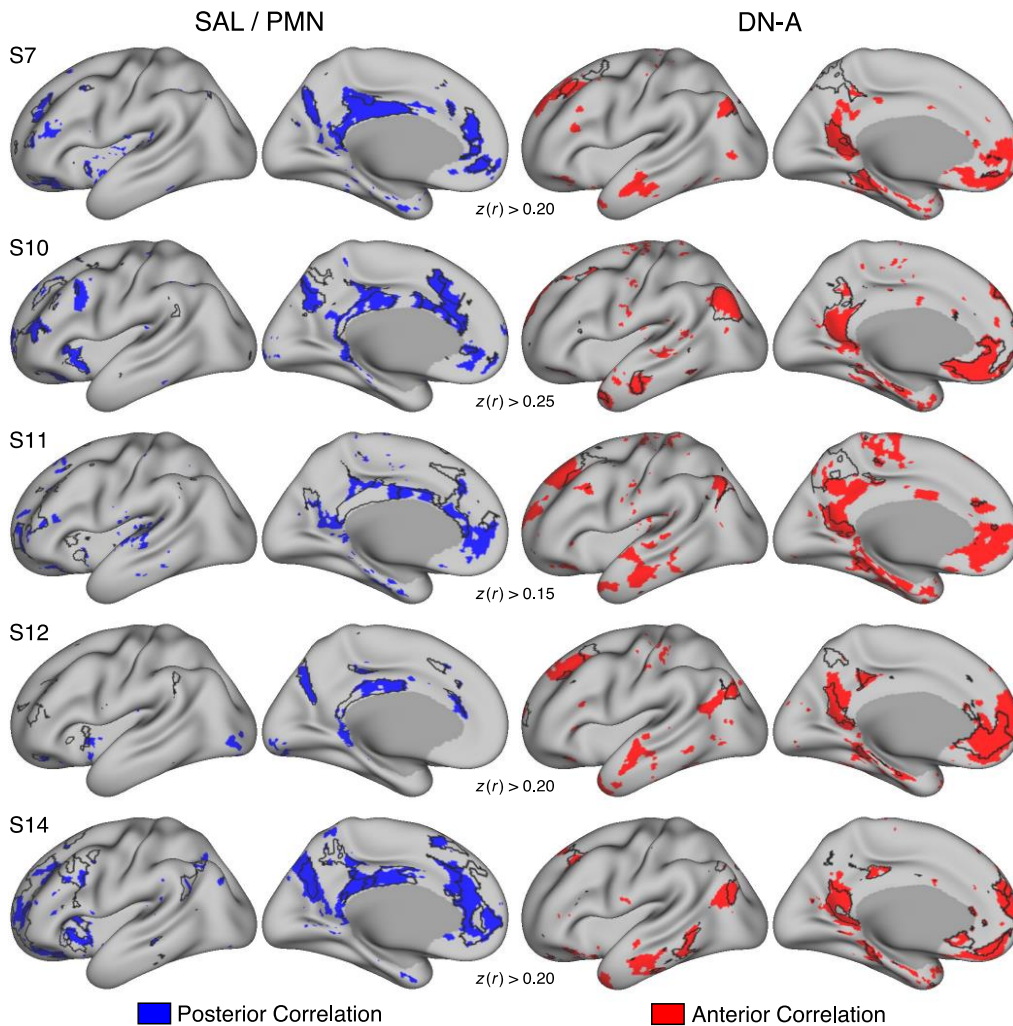
Figure 3.4 Functional connectivity from the posterior and anterior hippocampal regions consistently recapitulates diagnostic features of cerebral SAL / PMN and DN-A, respectively, in Experiment 1 participants (S7-S14). Correlations to the cerebral surface from the individual-specific hippocampal regions in Experiment 1 participants 7-14 followed the topography of the networks used to identify each region (SAL / PMN for the posterior region, DN-A for the anterior region). Left: correlations from an individual's posterior hippocampal region (blue) along with their k-means derived cerebral SAL / PMN (outline). Notable SAL / PMN regions include posteromedial and posterior cingulate cortex, as well as the anterior insula. Right: correlations from an individual's anterior hippocampal region (red) along with their k-means derived cortical DN-A (outline). Notable DN-A regions include retrosplenial, parahippocampal, and dorso-lateral prefrontal cortices. Correlations displayed as Fisher *z*-transformed Pearson's *r*, thresholded at the *z*-value indicated below each participant's maps.
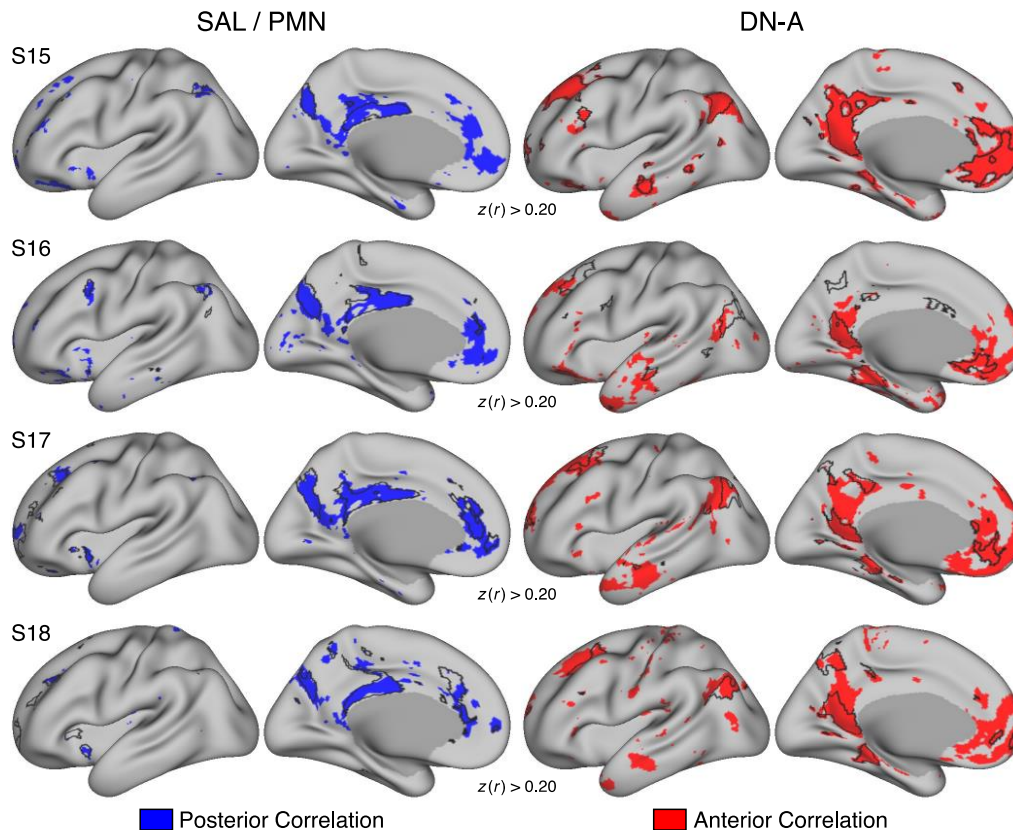
Figure 3.5. Functional connectivity from the posterior and anterior hippocampal regions consistently recapitulates diagnostic features of cerebral SAL / PMN and DN-A, respectively, in Experiment 1 participants (S15-S18). Correlations to the cerebral surface from the individual-specific hippocampal regions in Experiment 1 participants 15-18 followed the topography of the networks used to identify each region (SAL / PMN for the posterior region, DN-A for the anterior region). Left: correlations from an individual's posterior hippocampal region (blue) along with their k-means derived cortical SAL / PMN (outline). Notable SAL / PMN regions include posteromedial and posterior cingulate cortex, as well as the anterior insula. Right: correlations from an individual's anterior hippocampal region (red) along with their k-means derived cortical DN-A (outline). Notable DN-A regions include retrosplenial, parahippocampal, and dorso-lateral prefrontal cortices. Correlations displayed as Fisher z-transformed Pearson's r, thresholded at the z-value indicated below each participant's maps.

Figure 3.6 Individual-specific posterior and anterior hippocampal regions are preferentially correlated with SAL / PMN and DN-A, respectively. Quantification of the average correlations from Experiment 1 participants' posterior and anterior hippocampal regions to cerebral networks. In all participants the posterior hippocampal region was most correlated with cerebral SAL / PMN. The anterior hippocampal region was most correlated with DN-A in most participants, and some participants showed high correlations with DN-B. Correlation values are mean Fisher *z*-transformed Pearson's *r*, and error bars indicate the standard error around the mean *z*(*r*) across separate fixation scan runs. SAL / PMN = Salience Network / Parietal Memory Network; CG-OP = Cingular-Opercular Network; DN = Default Network; dATN = Dorsal Attention Network; LANG = Language Network; FPN = Frontoparietal Network. Networks were identified as outlined in Braga et al. 2020, and labeled according to convention in line with Xue et al. 2021 and Du et al. (In Prep). Note that these labels differ somewhat from those used in previous work (Braga et al. 2020; DiNicola et al. 2020, 2023). CG-OP was previously labeled SAL, FPN-A was previously labeled FPN-B, and similarly FPN-B was previously labeled FPN-A. These networks names and abbreviations are used similarly throughout the figures.

cerebral SAL / PMN (p < 0.001), with additional weaker correlation to DN-A ($p < 0.001$), while the anterior hippocampal region was preferentially correlated with DN-A ($p < 0.001$) and more weakly to DN-B ($p = 0.013$). Notably, the anterior hippocampus was not coupled to SAL / PMN ($p = 0.998$), and neither region was significantly coupled to the other cerebral networks we investigated (p range = 0.110 – 0.999, with most $p > 0.9$).
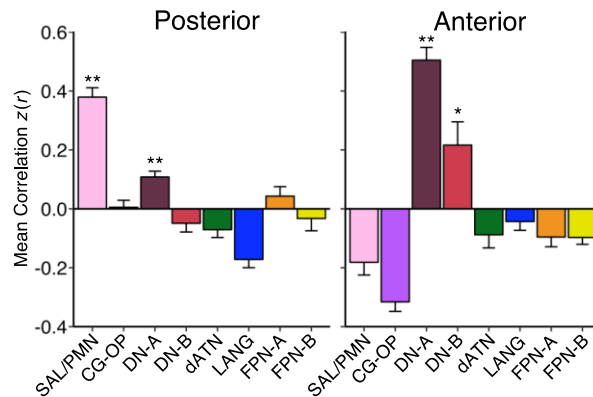
Figure 3.7 Across Experiment 1 participants, the posterior hippocampal region is significantly and preferentially correlated with SAL / PMN, while the anterior hippocampal region is more correlated with DN-A. Correlations between hippocampal regions and cerebral networks calculated within an individual were pooled across participants and averaged. In this pooled group average, the posterior hippocampal regions were significantly correlated with both SAL / PMN and DN-A, with a stronger correlation to SAL / PMN. In contrast, the anterior hippocampal regions were more strongly correlated with DN-A and did not show significant positive correlation with SAL / PMN. Correlation values are mean Fisher z-transformed Pearson's r and error bars indicate the standard error around the mean $z(r)$ across participants. Significance measured with a one-tailed t-test, H_o: $\mu = 0$, H_a: $\mu > 0$; ** = $p < 0.001$; * = $p < 0.05$

Run-Level Analyses Indicate Functional Coupling of the Anterior and Posterior Hippocampus to Correlated Cerebral Networks

After dissociating regions in the anterior and posterior hippocampus based on fixation-based functional connectivity, we could then ask if these regions had different task responses, and whether the responses within a hippocampal region mirrored activity within its coupled cortical network. Previous investigations into the functional response of cerebral DN-A during tasks found that DN-A was more strongly recruited in individuals during episodic projection tasks than ToM

160

tasks (DiNicola et al. 2020). That result held true in current cohort of participants, as quantified by averaging the mean z-value within individualized cerebral DN-A across participants (Fig. 3.8, Cohen's d range = 1.34 – 1.87). Just like its correlated cerebral network DN-A, the anterior hippocampal region showed higher activity during both episodic remembering (Fig. 3.8, EP PAST) and future projection (EP FUTURE) than during a ToM task about other's false belief (ToM BELIEF; Cohen's d EP PAST against ToM BELIEF = 1.66, EP FUTURE against ToM BELIEF = 1.83). Unlike DN-A, the anterior hippocampus showed a level of activity comparable to episodic projection when participants considered someone's level of emotional pain, contrasted against physical pain (ToM PAIN; Cohen's d EP PAST against ToM PAIN = -0.13, EP FUTURE against ToM PAIN = 0.22). In contrast to DN-A, cerebral SAL / PMN showed no significant increase in activity during ToM and episodic projection tasks (p range = 0.09 – 0.99). The SAL / PMN correlated posterior hippocampal region, however, showed significant activations during the EP PAST (p = 0.002) and EP FUTURE (p = 0.046) conditions, but not the two ToM condition. The departure of the posterior region from SAL / PMN likely reflects the weaker coupling of this region to DN-A (as observed in the functional connectivity results), which would be observable in tasks like episodic projection and ToM which do not engage the more strongly coupled network SAL / PMN.

Trial-Level Variation in Scene Construction Tracks Anterior Hippocampus Activity

Previous work (DiNicola et al. 2023) has identified that activity within cerebral DN-A during individual trials of the episodic projection task is highly correlated with the extent to which that question engages the process of scene construction (Hassabis and Maguire 2007). Motivated by this finding, we investigated the relationship between trial-level scene construction ratings and activity within the anterior hippocampal region, which in all subjects was defined based on functional connectivity to cerebral DN-A. The mean z value within the anterior hippocampal region for a given episodic projection trial, across subjects, had a strong positive correlation with the scene

161

construction rating of that trial (Fig. 3.9 left middle; $r = 0.47$, 95% CI [0.35 0.58], $p < 0.001$). The correlation with scene construction within the anterior hippocampus was somewhat weaker than in cerebral DN-A (Fig 3.9, left top; $r = 0.60$, 95% CI [0.50 0.69] $p < 0.001$), but stronger than the correlation in the posterior hippocampus (Fig. 3.9, left bottom; $r = 0.35$, 95% CI [0.21 0.47] $p < 0.001$). In their report, Zheng et al. (2021) postulated that the anterior hippocampal region may be involved in self-relevant processes, but we found a much weaker correlation with self-relevance than scene construction (Fig. 3.9, right middle; $r = 0.15$, 95% CI [0.00 – 0.29], $p = 0.046$). A multiple regression linear model including both scene construction and self-relevance composites as predictors significantly predicted activity in the anterior hippocampal region ($F(2, 177) = 27.7$, $p < 0.001$), and showed that scene construction both was a more significant explanatory variable, and accounted for more variance in anterior hippocampal region BOLD signal (Adjusted $R^2_{\text{Full Model}} = 0.23$, $p_{\text{Scene Construction}} < 0.001$, $p_{\text{Self Relevance}} = 0.039$; $R^2_{\text{Scene Construction}} = 0.22$; $R^2_{\text{Self Relevance}} = 0.02$).
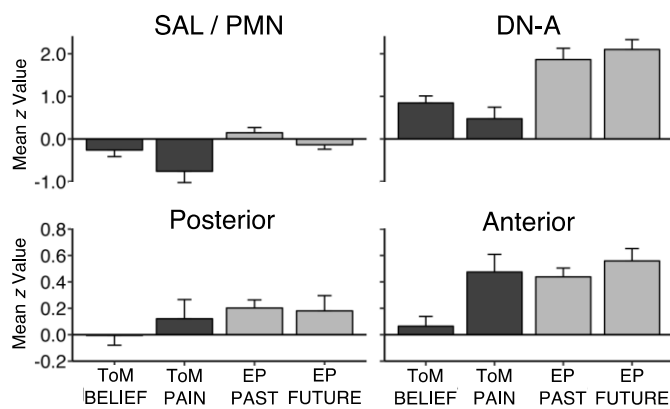
Figure 3.8 Run-level analyses replicate DN-A sensitivity to episodic projection and similarity in task response between hippocampal regions and associated cerebral networks. Condition contrasts from tasks targeting Theory of Mind (ToM) and episodic projection (EP), averaged across Experiment 1 participants, showed that both DN-A and the anterior hippocampal region were recruited when individual's recall their own past (EP PAST) or imagine their own future (EP FUTURE), and were not recruited when considering other's false beliefs (ToM BELIEF). In contrast, activity within SAL / PMN and the posterior hippocampal region was more muted during these tasks, suggesting less involvement. Plot values are mean z-transformed beta values, and error bars indicate standard error around the mean across participants.
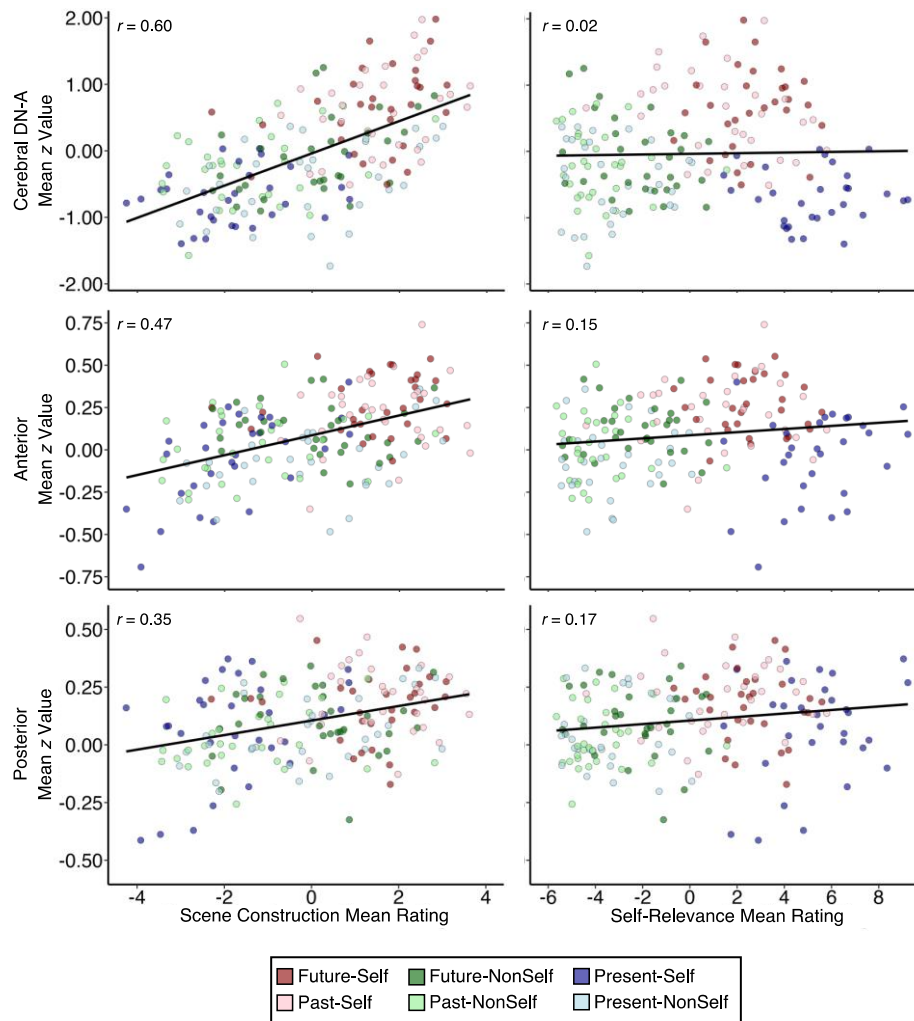
Figure 3.9 DN-A and hippocampal region activity tracks trial-level variations in scene construction more than self-relevance during the episodic projection task. Plots indicate activity within individual-specific DN-A and hippocampal regions, pooled across Experiment 1 subjects for each episodic projection trial. Mean trial-level activity is plotted against each trial's scene construction (left) or self-relevance (right) composite rating, as scored by at least 37 independent behavioral participants. The color of each trial indicates the condition to which that trial belonged. Future- and Past-Self trials (dark and light red) were originally designed to engage episodic projection, while the Present-Self (dark blue) condition served as the control. Note the variability in the composite scores for individual question within each condition, highlighting the utility of a trial-specific approach to explore variance not captured by the trial condition. While DN-A and both hippocampal regions displayed strong, highly significant ($p < 0.001$) correlations with scene construction, the posterior hippocampal region has the weakest correlation. In contrast, only the hippocampal regions showed significant ($p < 0.05$) correlations with self-relevance, and both regions displayed a weaker correlation with self-relevance than with scene construction.

In addition to being highly correlated with composite scene construction rating, activity within the anterior hippocampus was also highly correlated with each of individual strategy ratings that make that composite (Fig. 3.10, r range = 0.40 – 0.44), and less correlated with all other strategies. The notable exception are the autobiographical strategies ($r_{Pers\_Past\_Exper}$ = 0.35; $r_{Sequence\_Events}$ = 0.48), but the correlation with these strategies is confounded by the high correlation of the autobiographical and difficulty composites (r = -0.76) which is not present between scene construction and difficulty (r = -0.10). After correcting for difficulty, correlations to autobiographical strategies are lowered more ($r_{Pers\_Past\_Exper}$ = 0.20; $r_{Sequence\_Events}$ = 0.38) than correlations to scene construction (r range = 0.36 – 0.45).
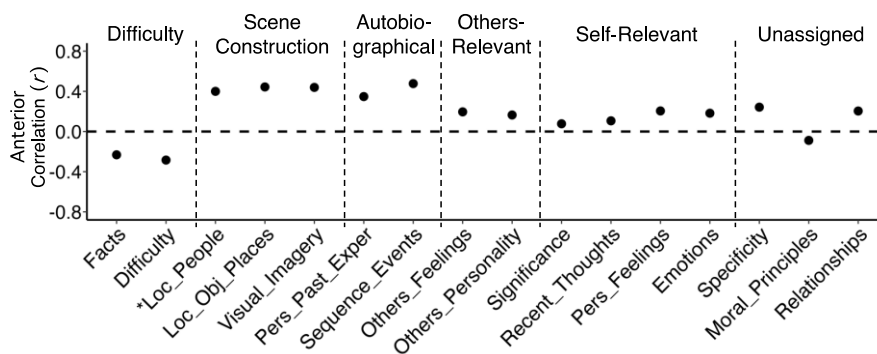
Figure 3.10 Activity within the anterior hippocampal region is highly correlated with trial-level scene construction and autobiographical strategies. Across all collected trial-level strategies, activity within the anterior hippocampal region was most correlated with strategies involved in the scene construction and considering autobiographical features. A trial's strategy rating for Locations of People (Loc_People) was highly correlated with that trials rating for the Locations of Objects and Places (Loc_Obj_Places) and Visual Imagery (Visual_Imagery) strategies but did not algorithmically cluster with the other two strategies. As such, it was not included in the scene construction composite score but is displayed here under scene construction due to conceptual similarity. Autobiographical, but not scene construction, strategy ratings were negatively correlated with difficulty strategy ratings across trials.

To assess the relative contributions of hypothesized hippocampal functions to activity within the anterior hippocampal region, we fit a multiple regression linear model including the composite ratings for scene construction, autobiographical, and self-relevant strategies, with all values corrected for trial difficulty. The model overall significantly predicted activity within the

anterior hippocampus ($F(3,176) = 16.83$, $p < 0.001$), and once again the scene construction

composite was the most significant predictor and largest contributor to overall model fit (Adjusted

$R^2_{\text{Full Model}} = 0.21$, $p_{\text{Scene Construction}} < 0.001$, $p_{\text{Autobiographical}} = 0.030$, $p_{\text{Self Relevance}} = 0.040$, ; $R^2_{\text{Scene Construction}} =$

0.19; $R^2_{\text{Autobiographical}} = 0.11$; $R^2_{\text{Self Relevance}} = 0.02$).

Our exploration of the relationship between scene construction and activity within cerebral

SAL / PMN and the posterior hippocampal region was less conclusive. On the cerebral surface,

activity within SAL / PMN was not correlated with the scene construction rating of a given trial, in

stark contrast to activity within DN-A (Fig. 3.11, top; $r_{\text{SAL/PMN}} = 0.09$, 95% CI [-0.05 0.24], $p = 0.22$;

$r_{\text{DN-A}} = 0.60$, 95% CI [0.50 0.69], $p < 0.001$; Scene Construction*Network interaction $F(1,178) =$

67.61, $p < 0.001$). In the hippocampus, activity within the posterior hippocampal region was still

correlated with scene construction, although significantly less correlated than the anterior

hippocampus (Fig. 3.11, bottom; $r_{\text{Posterior}} = 0.35$, 95% CI [0.21 0.47], $p < 0.001$; $r_{\text{Anterior}} = 0.47$, 95% CI

[0.35 0.58], $p < 0.001$; Scene Construction*Region interaction $F(1,178) = 17.55$, $p < 0.001$).

Importantly, this does not necessarily indicate that this region is primarily sensitive to scene

construction. Despite being primarily coupled to SAL / PMN, the posterior hippocampal region had

significant functional connectivity to DN-A (Figs. 3.6 and 3.7) and was also highly correlated with

activity in the anterior hippocampus during the episodic projection task ($r = 0.69$, 95% CI [0.60

0.76], $p < 0.001$). The correlation between activity in the anterior and posterior hippocampal

regions persisted for all strategies collected, with the posterior hippocampus often departing from

SAL / PMN (Fig. 3.12), notably showing more sensitivity to scene construction and less sensitivity

to self-relevance. In both cases, the posterior hippocampal region's correlation value for each

strategy resembled the anterior hippocampal region's correlation more so than cerebral SAL /

PMN. These features, together with a general lack of activity within SAL / PMN, suggests that the

episodic projection task is not particularly well suited to studying activity within SAL / PMN and

the posterior hippocampal region.
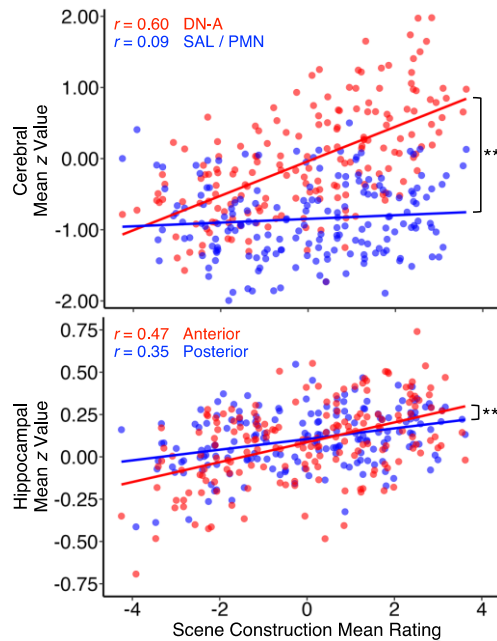
Figure 3.11 Cerebral DN-A is more sensitive to scene construction than SAL / PMN, and the anterior hippocampal region is similarly more sensitive than the posterior region. Combined scatter plots showing trial-level activity within cerebral networks (top) and hippocampal regions (bottom) against trial-level scene construction ratings. DN-A and the anterior hippocampal region had stronger correlations with scene construction than SAL / PMN and the posterior hippocampal region, respectively. A linear mixed effects model run separately on cerebral and hippocampal data revealed a highly significant interaction between cerebral network and scene construction rating ($F(1,178) = 67.607$), and between hippocampal region and scene construction rating ($F(1,178) = 17.552$) in predicting trial-level activation. ** = $p < 0.001$
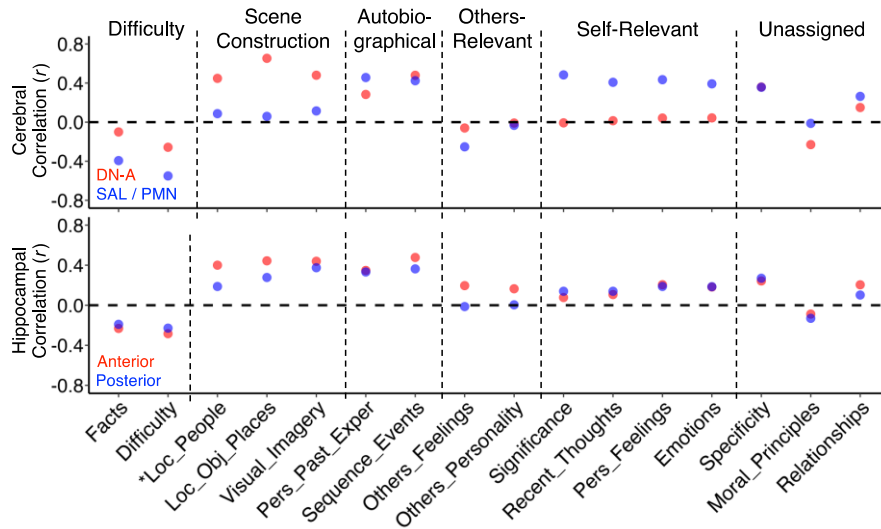
Figure 3.12 Posterior hippocampal region sensitivity to trial-level strategies deviates from cerebral SAL / PMN, and is similar to both the anterior hippocampal region and DN-A. Trial-level strategy correlations within cerebral DN-A and SAL / PMN (top) were notably different for scene construction and self-relevant strategies, while hippocampal regions (bottom) had more similar sensitivity for all strategies. This coherence is further reflected by a larger correlation between global activity in hippocampal regions ($r = 0.69$, $p < 0.001$) than cerebral networks ($r = 0.31$, $p < 0.001$).

Experiment 2 Behavioral Strategy Data Replicates Experiment 1 Results

For Experiment 2, an expanded version of the episodic projection task was presented to the in-scanner participants, and was also used to collect a new, independent set of online behavioral strategy data. Because the purpose of the present exploration was a replication of findings from Experiment 1, all analyses using this expanded episodic projection task included only those 180 questions and 13 strategy ratings that were included in both data sets. Hierarchical clustering performed on these newly collected strategy ratings showed robust convergence with the original strategy data (Fig. 3.13). The strategies which clustered together to form each of the 5 original strategy composites (difficulty, scene construction, others-relevant, self-relevant, and autobiographical) continued to cluster closely with each other in Experiment 2. In light of this, and in the interest of setting up a direct replication for Experiment 1, we carried forward these strategy composites, with the same component strategies, for all analyses in Experiment 2. One exception is the Self-Relevant composite, which did not include ratings for Personal Significance and Recent Thoughts in Experiment 2 as those strategies were not collected.

To evaluate the stability of these ratings across Experiments, which had independently acquired strategy ratings, we correlated the composite ratings between the two data sets for each question (Fig. 3.14). For every strategy composite, the rating for a question in the replication data set was very well correlated with the rating in the initial data set (r range = 0.89 – 0.95). For the difficulty, scene construction, and autobiographical composites, the average rating value for a particular question was also highly consistent between the two data sets, with slopes ≥ 0.90. For the self-relevant composite, values in the replication data set were roughly one half of the values in the initial data set (slope = 0.46), consistent with the inclusion of half the number of strategy ratings. Finally, the value of the others-relevant composite for each question in the replication data set was about two thirds of the value for the same question in the initial data set (slope = 0.67). This shift in ratings may be due to the inclusion of questions concerning the explicit judgement of other's moral
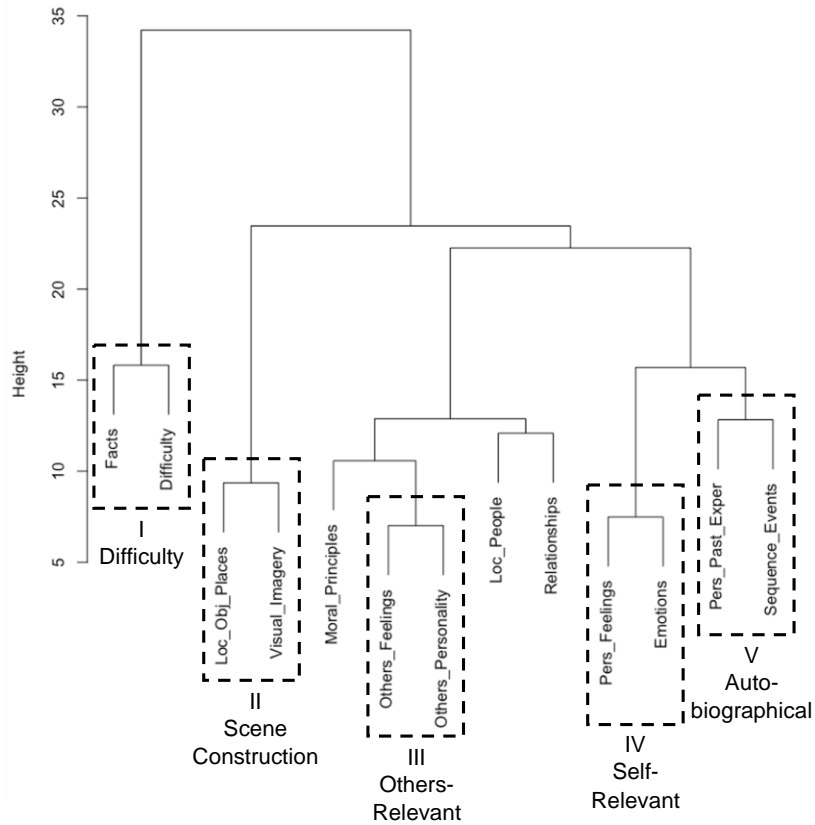
Figure 3.13 Expanded Experiment 2 strategy data clusters into five strategy composite scores. Hierarchical clustering of Experiment 2 strategy data using Ward's minimum variance method. The Experiment 2 replication included only those questions and strategies also acquired in Experiment 1 (see DiNicola et al. 2023). All five of the original clusters (difficulty, scene construction, others-relevant, self-relevant, and autobiographical) were also present in this new data set. The clusters were used as defined here for all Experiment 2 analyses.
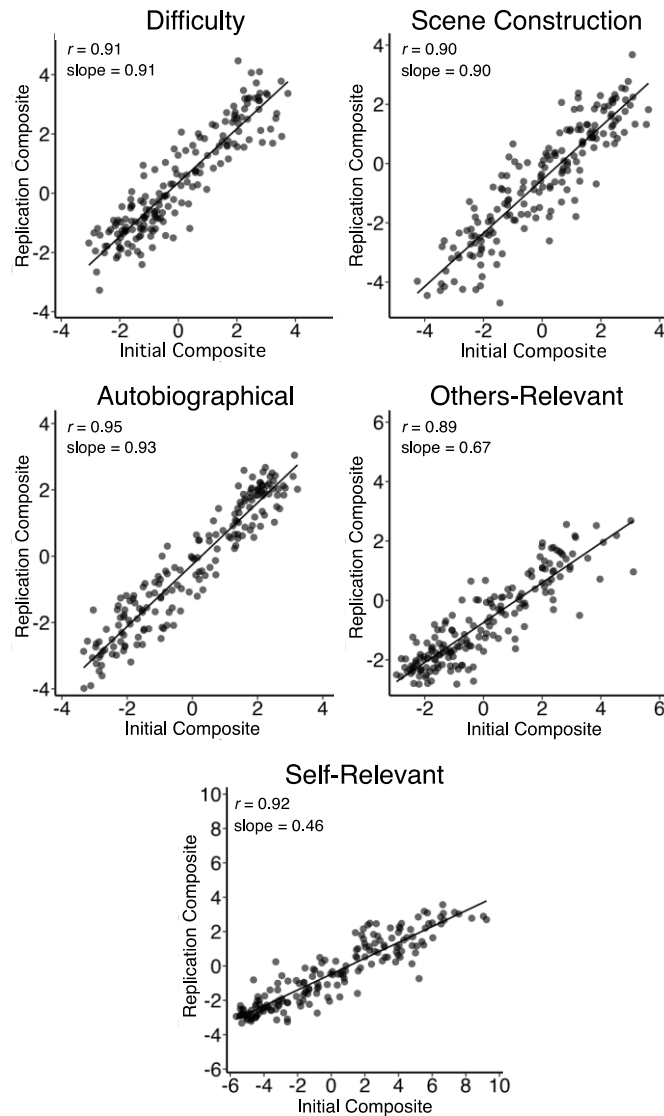
Figure 3.14 Trial-level composite strategy ratings are consistent between Experiments 1 and 2. Correlating the trial-level strategy composites calculated from Experiment 1 (≥ 37 participant responses per question) and Experiment 2 (≥ 25 participant responses per question) data reaffirmed the stability of these estimates. For all five composites, Experiment 1 and 2 data were highly correlated, and for most the slope of correlation was near one. The others-relevant and self-relevant composites alone had slopes below 0.90 (0.67 and 0.46 respectively). Two strategies from the self-relevant composite were not included in Experiment 2 (reducing the maximum possible composite by ½) so a slope of 0.46 indicates excellent consistency. The reduction in Experiment 2 others-relevant composite scores may be due to the inclusion of explicitly moral questions in Experiment 2.

or non-moral actions in the expanded task. Even though these questions were not included in our analysis, they collectively have the highest ratings for the others-relevant composite, and participants may have adjusted their ratings for other questions to compensate.

Experiment 2 Replicates Differential Cerebral Correlations in the Anterior and Posterior Hippocampus

In all 11 participants in Experiment 2, we replicated the finding that the anterior hippocampus is preferentially correlated with cerebral DN-A, while voxels highly correlated to cerebral SAL / PMN are only present in the posterior hippocampus (Fig. 3.15). The anterior-posterior border for each participant was placed between MNI Y coordinates -28 and -34, and as in Experiment 1 in every participant DN-A was assigned to the region anterior to the border and SAL / PMN to the region posterior to the border (Fig. 3.15, left). After network assignment and binarization, ≥ 73% of each networks total assigned voxels remained. The size of the anterior region ranged from 2274 (P1) to 4456 (P6) voxels (mean 3639), while the posterior region ranged from 181 (P8) to 685 (P7) voxels (mean 378). On average, the size of the posterior hippocampus in Experiment 2 was smaller than in Experiment 1, likely resulting from slight changes in the cerebral networks due to the use of a multi-session hierarchical Bayesian model, rather than k-means, for clustering. While the two clustering methods produce nearly identical patterns on the cerebral surface, there are slight differences in vertex assignment. Exploratory analyses performed later in which both clustering methods were used on the same data (not shown) indicated these changes were enough to increase the relative correlation of some hippocampal voxels to DN-A, which resulted in these voxels which maybe have been assigned to SAL / PMN using k-means networks either being removed as ambiguous, or assigned to DN-A instead.
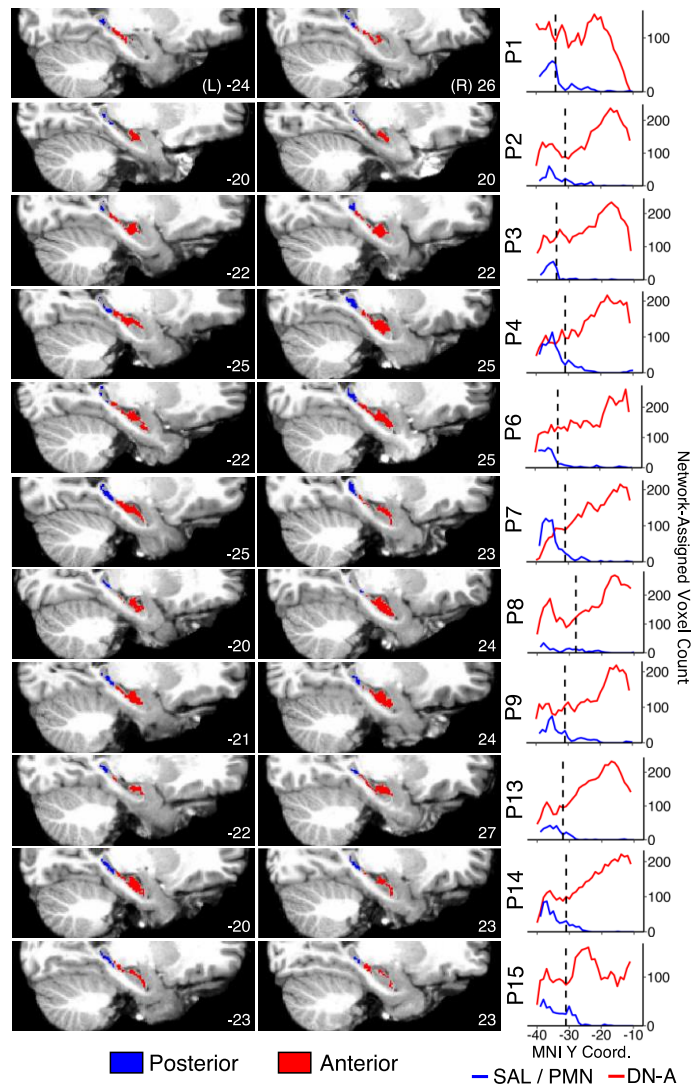
Figure 3.15 Experiment 2 replicates preferential functional connectivity of cerebral SAL / PMN with the posterior hippocampus and DN-A connectivity with the anterior hippocampus.
Paralleling Fig. 3.3, a single representative sagittal slice for the left (L) and right (R) hemisphere is shown on the left for each participant, along with a plot of SAL / PMN and DNA assigned voxel counts along the hippocampal long axis. The MNI X coordinate for each slice is given in the bottom right of each image, and the location of the anterior / posterior border is shown by the black dashed line on the right. In all participants, SAL / PMN was the appropriate choice for defining the posterior hippocampal region (blue), while DN-A was appropriate for defining the anterior hippocampal region (red). While the size of the anterior and posterior regions varies between individuals, SAL / PMN correlated voxels were consistently almost only present in the posterior hippocampus, while DN-A correlated voxels were the majority in the anterior hippocampus. The anterior/posterior border defined for each participant were, from top to bottom, MNI Y = -34, -31, -34, -31, -33, -31, -28, -31, -33, -32, -31, -31

172
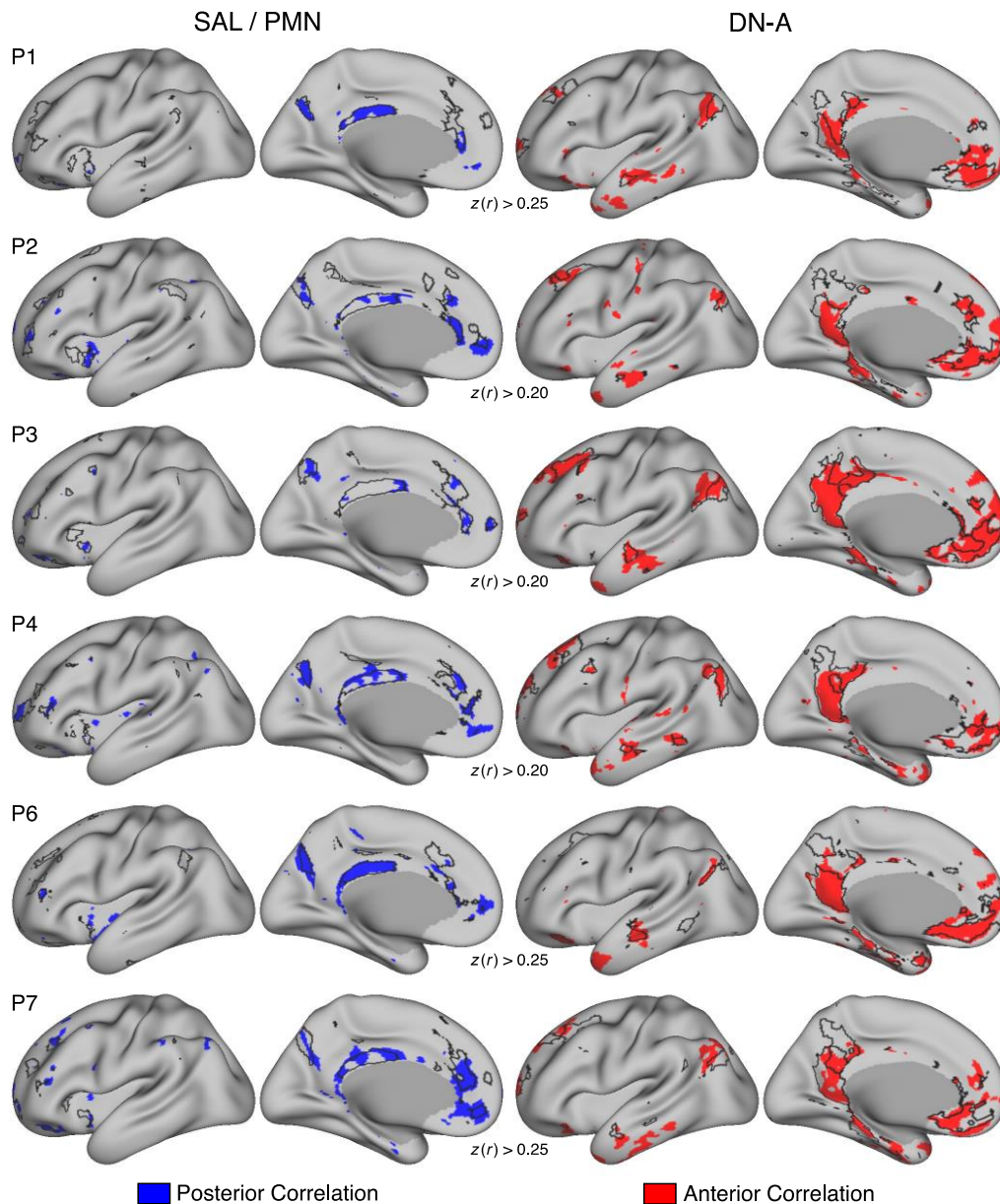
Figure 3.16 Connectivity from Experiment 2 participant's posterior and anterior hippocampal regions consistently recapitulates diagnostic features of cerebral SAL / PMN and DN-A, respectively (P1-P7). Paralleling Figs. 3.4 and 3.5, correlations to the cerebral surface from the individual-specific hippocampal regions in Experiment 2 participants 1-7 followed the topography of the networks used to identify each region (SAL / PMN for the posterior region, DN-A for the anterior region), replicating results from Experiment 1. Left: MS-HBM derived cortical SAL / PMN (outline) and correlations from posterior hippocampal region (blue). Notable SAL / PMN regions include posteromedial and posterior cingulate cortex, as well as the anterior insula. Right: MS-HBM derived cortical DN-A (outline) and correlations from anterior hippocampal region (red). Notable DN-A regions include retrosplenial, parahippocampal, and dorso-lateral prefrontal cortices. Correlations displayed as Fisher z-transformed Pearson's r, thresholded at the z-value indicated below each participant's map.

Figure 3.17 Connectivity from Experiment 2 participant's posterior and anterior hippocampal regions consistently recapitulates diagnostic features of cerebral SAL / PMN and DN-A, respectively (P8-P15). Paralleling Figs. 3.4 and 3.5, correlations to the cerebral surface from the individual-specific hippocampal regions in Experiment 2 participants 8-15 followed the topography of the networks used to identify each region (SAL / PMN for the posterior region, DN-A for the anterior region), replicating results from Experiment 1. Left: MS-HBM derived cortical SAL / PMN (outline) and correlations from posterior hippocampal region (blue). Notable SAL / PMN regions include posteromedial and posterior cingulate cortex, as well as the anterior insula. Right: MS-HBM derived cortical DN-A (outline) and correlations from anterior hippocampal region (red). Notable DN-A regions include retrosplenial, parahippocampal, and dorso-lateral prefrontal cortices. Correlations displayed as Fisher z-transformed Pearson's r, thresholded at the z-value indicated below each participant's map.

An investigation of the correlations from each of the hippocampal regions to the cerebral surface replicated preferential connectivity to the network used to define each region. The posterior hippocampal region was highly correlated with cerebral vertices within SAL / PMN, while the anterior hippocampal was highly correlated with vertices within DN-A (Figs. 3.16 and 3.17).

Quantification of this coupling confirmed that in every participant, the posterior hippocampal region was most correlated with cerebral SAL / PMN, while the anterior hippocampal region was most correlated with DN-A (Fig. 3.18). This pattern of preferential coupling continued to hold true when the correlations were averaged across participants to obtain a group estimate of the coupling from the posterior and anterior hippocampal regions to cerebral networks (Fig. 3.19). Correlations from the anterior hippocampus replicated the results from Experiment 1, with a strong correlation to DN-A ($p < 0.001$) and a weaker but still significant correlation to cerebral DN-B ($p < 0.001$). The posterior hippocampal region was preferentially correlated with cerebral SAL / PMN ($p < 0.001$) with an additional, smaller correlation to cerebral DN-A ($p < 0.001$), also mirroring Experiment 1. Interestingly, the posterior hippocampal region in this data set also had a highly significant correlation to the Cingulo-Opercular network (CG-OP; $p < 0.001$). This is most likely the result of slight changes network identification using MS-HBM clustering mentioned above. Our exploratory analyses revealed that voxels that would have been included in the posterior hippocampal region using k-means, but are excluded using MS-HBM, generally had strong positive correlations to cerebral DN-A, and strong negative correlations to CG-OP. The exclusion of these voxels seems to have, on both the individual and group level, reduced the correlation of the posterior hippocampal region to DN-A, and increased the correlation to CG-OP.
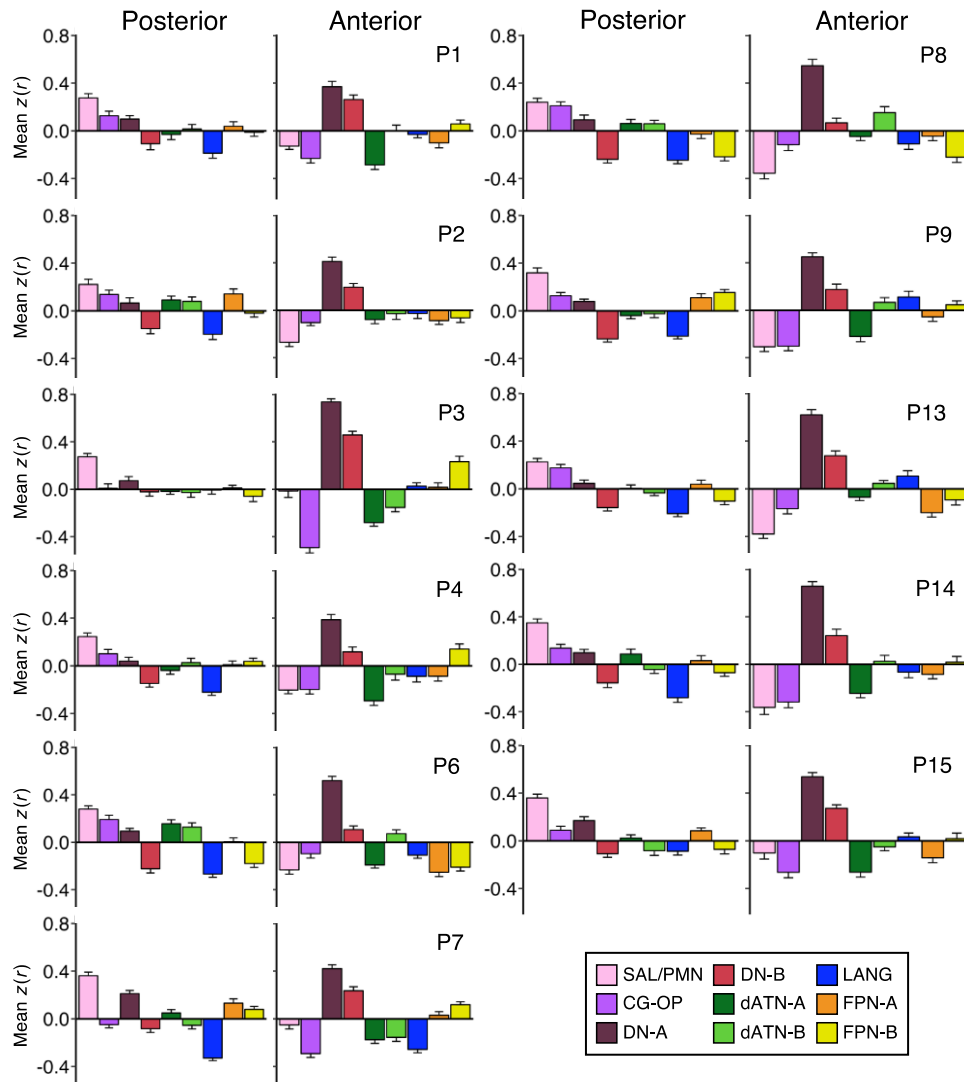
Figure 3.18 Individual-specific posterior and anterior hippocampal regions in Experiment 2 participants are preferential correlated with SAL / PMN and DN-A, respectively. Paralleling Fig. 3.6, the quantification of average correlations from Experiment 2 participant's posterior and anterior hippocampal regions to cerebral networks is shown. The posterior hippocampal region was primarily correlated with cerebral SAL / PMN and the anterior hippocampal region was primarily correlated with DN-A across most participants. Correlation values are mean Fisher z-transformed Pearson's *r*, and error bars indicate the standard error around the mean *z*(*r*) across separate fixation scan runs. Networks were clustered using a Multi-Session Hierarchical Bayesian Model (MS-HBM) as outlined in Du et al. (In Prep) and identified as described in Braga et al. 2020. All labels are consistent with Experiment 1, though note the identification of dATN-A and dATN-B in Experiment 2, in contrast to a single dATN in Experiment 1. These networks names and abbreviations are used similarly throughout upcoming figures.
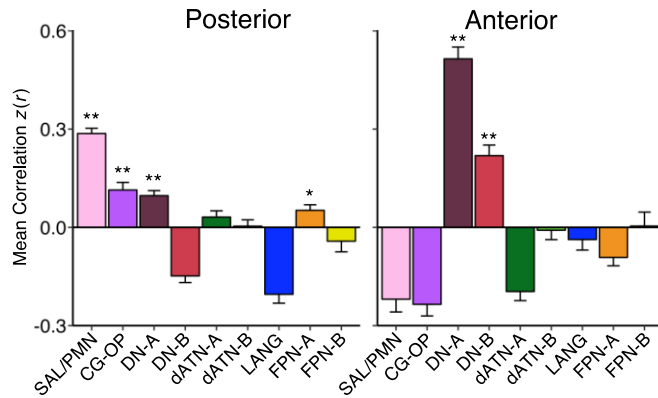
Figure 3.19 Average hippocampal region correlations in Experiment 2 replicates the preferential correlation of the posterior hippocampal region with SAL / PMN and the anterior hippocampal region with DN-A. Paralleling Fig. 3.7, correlations between hippocampal regions and cerebral networks calculated within an individual were pooled across Experiment 2 participants and averaged. In this pooled group average, the posterior hippocampal regions were significantly correlated with several cerebral networks, with the strongest correlation to SAL / PMN as in Experiment 1. A primary correlation to DN-A from anterior hippocampal regions similarly replicated results from Experiment 1. Correlations values are mean Fisher z-transformed Pearson's r and error bars indicate the standard error around the mean $z(r)$ across participants. Significance measured with a one-tailed t-test, H_o: $\mu = 0$, H_a: $\mu > 0$; ** = $p < 0.001$; * = $p < 0.05$

Model-free functional connectivity provides convergent evidence for DN-A and SAL / PMN coupling to the anterior and posterior hippocampus.

Winner-take-all parcellations, like those used here to define the hippocampal regions, are insensitive to correlation strengths beyond assigning each voxel to a network, and as a result have the potential to miss important nuances in functional connectivity topography. The large blood vessels on the surface of cerebral cortex generally have the largest changes in blood oxygenation, and the resulting change in magnetic properties can extend to nearby regions of the brain even if those regions have not had any local change in blood oxygenation. This manifests in fMRI, including functional connectivity correlations, as a signal peak at the actual location of increase blood oxygenation, surrounded by "bleed" which weakens further from the source. This signal bleed is particularly important to consider in subcortical structures like the hippocampus that generally have a weaker BOLD signal but are close to regions of cerebral cortex.

To assess whether our hippocampal segmentation was the result of signal bleed from nearby cerebral cortex (i.e. EC, PRC, and PHC), rather than signal within the hippocampus itself, we visualized correlations in the hippocampus from seed regions in cerebral cortex. A representative participant is shown here to highlight our findings (P3, Fig. 3.20), but the seed-based analysis was performed on all participants in Experiment 2 (Appendix Figs. A.1-A.10). Cerebral seed regions which reproduced the cerebral network topography were chosen within both the antero- and postero-medial portions of DN-A and SAL / PMN. Across all participants, both seeds in cerebral DN-A converged on correlation peaks within or near the hippocampus, and not surrounding cerebral cortex. In most cases, and in our example P3, cerebral DN-A seeds produced peak correlations unambiguously within the hippocampal formation (Fig. 3.20A, indicated by arrows). In addition, every participant had peaks in functional connectivity to DN-A along the medial portion of the hippocampus (Fig. 3.20A). While the resolution of our data is insufficient to conclusively localize these peaks within the hippocampus, these results are similar to previous work which identified functional connectivity between DN-A and the hippocampal subiculum using a higher resolution (7T) magnet (Braga et al. 2019). Finally, we noted in every participant a correlation peak near the dorso-medial edge of the hippocampus, most easily seen in a sagittal slice towards the middle of the hippocampal long axis (Fig. 3.20A). The origin of this signal is unclear at the resolution of this data, but it is in all participants distinct from the two other peaks.

Seeds within anterior and posterior SAL / PMN (Fig. 3.20B; Appendix Figs. A.1-A.10) produced convergent correlations within the posterior hippocampus (indicated by arrows). However, the extent and pattern of the hippocampal correlations was more sensitive to seed location than DN-A seeds. In six participants, including P3 used as a representative example here, a seed placed within antero-medial SAL / PMN resulted in larger correlations within the posterior hippocampus than seeds places within postero-medial SAL / PMN. In some cases (e.g. P14, Appendix Fig. A.9), only the anterior seed produced meaningful correlations in the hippocampus.

178
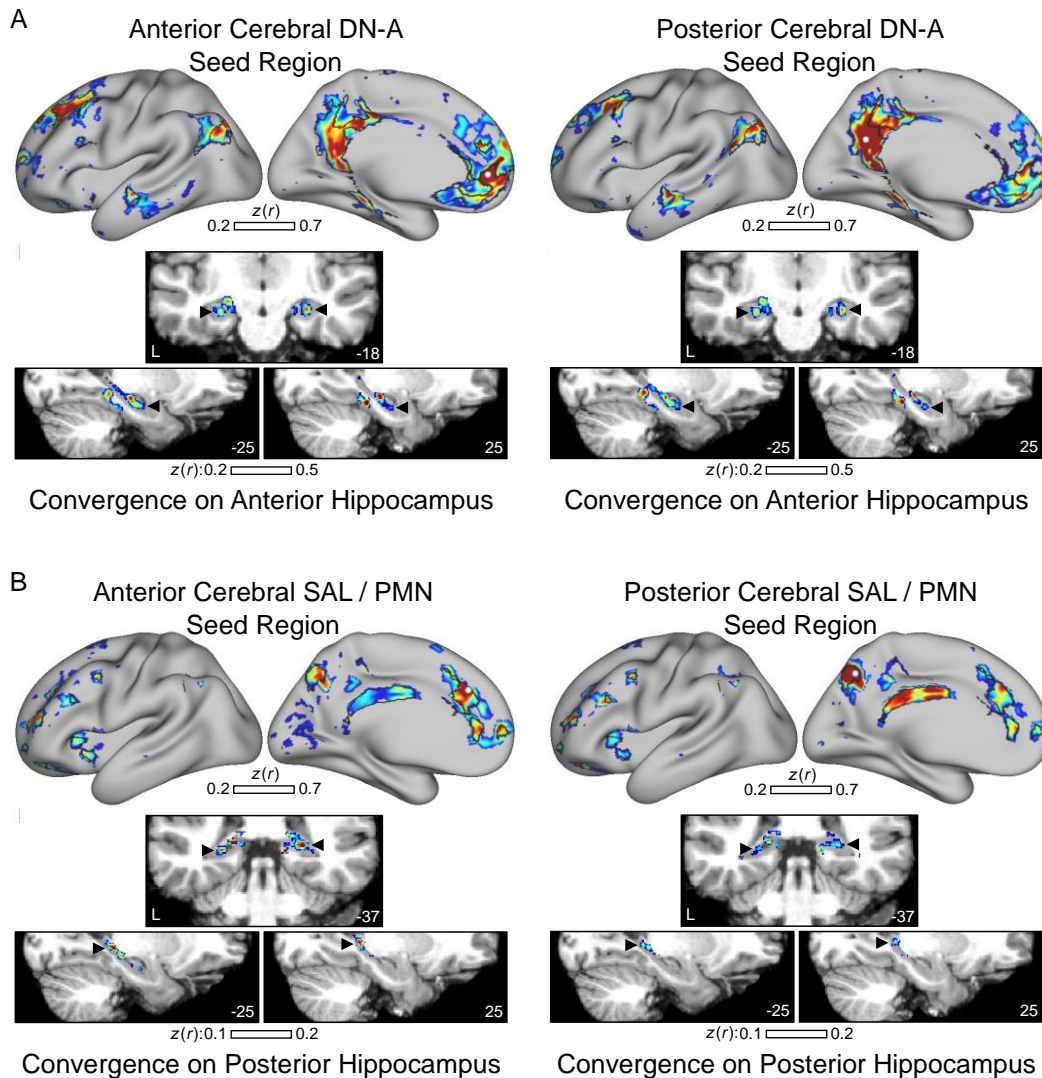
Figure 3.20 Unbiased seed-based functional connectivity shows convergent cerebral network coupling to voxels within the hippocampus. Functional connectivity from seed region on the cerebral surface to both the cerebral surface and the dilated hippocampal region, shown in a representative subject from Experiment 2. A: Seeds placed within the ventromedial prefrontal and retrosplenial portions of DN-A produced convergent patterns of functional connectivity in the anterior hippocampus (indicated by arrows). B: SAL / PMN seeds resulted in convergent functional connectivity within the posterior hippocampus (indicated by arrows).

Peak correlations were generally along the medial portion of the posterior hippocampus, and always distinct from nearby PHC. Peak correlations in the posterior hippocampus were also always separable from correlation within the thalamus. These results, along with those from cerebral DN-A seed regions, give us confidence that our functional connectivity parcellations are reflecting of activity within the hippocampus rather than neighboring regions, but our limited resolution leaves ambiguity around precise localization.

Trial-Level Estimates of Cerebral and Hippocampal Activity were Similar Between Experiments 1 and 2

Previous work (DiNicola et al. 2023), along with the behavioral data presented above, shows that the strategies individuals use to answer questions in the episodic projection task are remarkably consistent. This makes plausible a hypothesis that the functional response to a given question may also be similar across individual and data sets, to the extent allowed by differences in idiosyncratic biology. To assess this, we correlated the mean trial-level z values across all Experiment 1 participants with the mean trial-level z values from all Experiment 2 participants within each of the individual-specific networks and hippocampal regions (Fig. 3.21). Trial-level estimates on the cerebral surface were highly correlated across data sets within both DN-A ($r = 0.83$, 95% CI [0.78 0.87], $p < 0.001$, slope = 0.82) and SAL / PMN ($r = 0.60$, 95% CI [0.50 0.69], $p < 0.001$, slope = 0.63). In the hippocampus, mean trial-level z values within the anterior region were very consistent between the initial and replication data set ($r = 0.55$, 95% CI [0.44 0.65], $p < 0.001$, slope = 0.59), while in the posterior hippocampal region the association was weaker, but still significant ($r = 0.19$, 95% CI [0.05 0.33], $p = 0.010$, slope = 0.25). The low correlation between trial-level z values in the posterior hippocampal region may be due to the observed changes in that region described above.
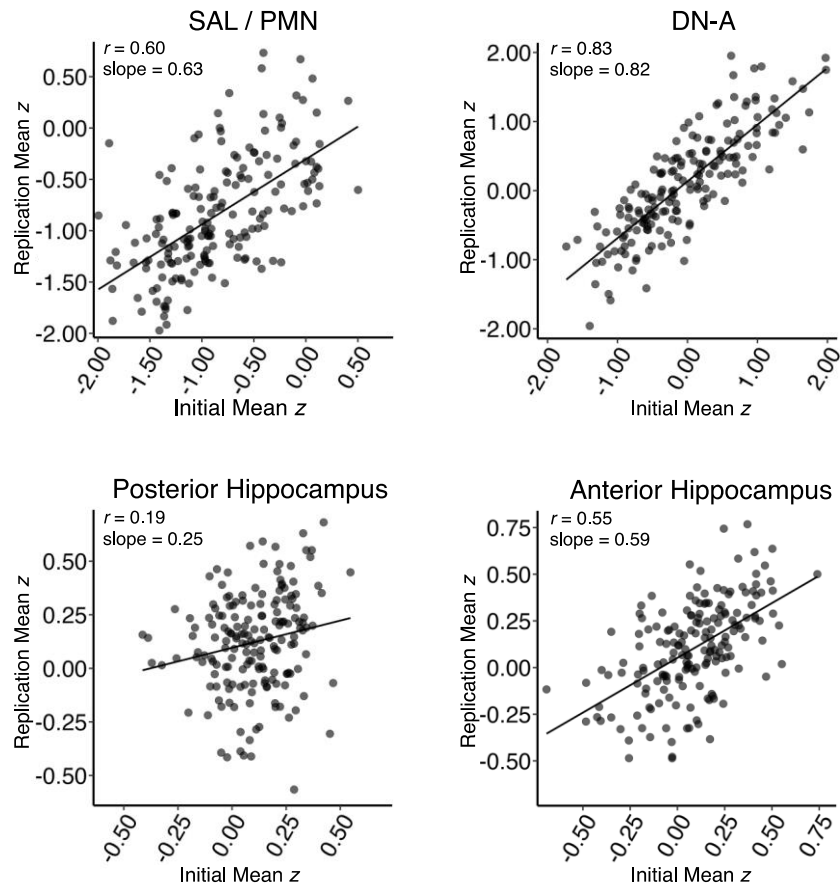
Figure 3.21 Trial-specific mean *z* values within cerebral networks and hippocampal regions are correlated across independent data sets. Correlating the trial level mean *z* values calculated across participants from Experiment 1 and Experiment 2 reaffirms the relative stability of these estimates, particularly within cerebral SAL / PMN and DN-A. In the hippocampus, mean *z* statistics for a given trial within individual-specific anterior hippocampal regions were well correlated between studies. The weaker correlation in posterior hippocampal regions may be due to the use of a different clustering method for identifying cerebral networks in Experiment 2 resulting in a change in how the posterior hippocampal region was defined.

To further verify the consistency of the BOLD response to questions during the episodic projection task, we sought to replicate the double dissociation on the cerebral surface between DN-A and Frontoparietal Network A (FPN-A) for scene construction and difficulty, as first reported by DiNicola et al. (2023). We found that cerebral DN-A showed a strong positive correlation with the scene construction rating of a question (Fig. 3.22, top left; $r = 0.58$, 95% CI [0.48 0.67], $p < 0.001$), but a weak negative correlation with the difficulty of a question (Fig. 3.22, top right; $r = -0.16$, 95% CI [-0.30 -0.02], $p = 0.029$). In contrast, activity within cerebral FPN-A was not correlated with scene construction (Fig. 3.22, bottom left; $r = 0.00$, 95% CI [-0.15 0.14], $p = 0.960$) but strongly correlated with difficulty (Fig. 3.22, bottom right; $r = 0.71$, 95% CI [0.63 0.78], $p < 0.001$), thus replicating the full double dissociation in independent behavioral and fMRI data.

Experiment 2 Run-Level Analyses Further Support Anterior – Posterior Functional Dissociation

Run-level analyses for the episodic projection and theory of mind tasks in the Experiment 2 yielded results consistent with a functional dissociation between cortical networks and hippocampal regions. Episodic projection contrasts resulted in more cerebral DN-A activity than ToM contrasts, although the difference in activity was smaller than in Experiment 1 (Fig. 3.23, Cohen's d range = 0.645 – 1.67). To include more conditions in each episodic projection run, the number of trials belonging to each condition was reduced from 5 to 3 per run, while ToM tasks were unchanged. This relative decrease in the run-level power of episodic projection task, while ToM power remained constant, may explain the reduced selectivity of cerebral DN-A for episodic projection. Exploratory analysis performed later calculated the contrasts using trial-level estimates for both tasks, thus equally reducing the power, and resulted in a difference in DN-A activity between the tasks more comparable to Experiment 1 (not shown, Cohen's d range = 1.22 - 2.11).
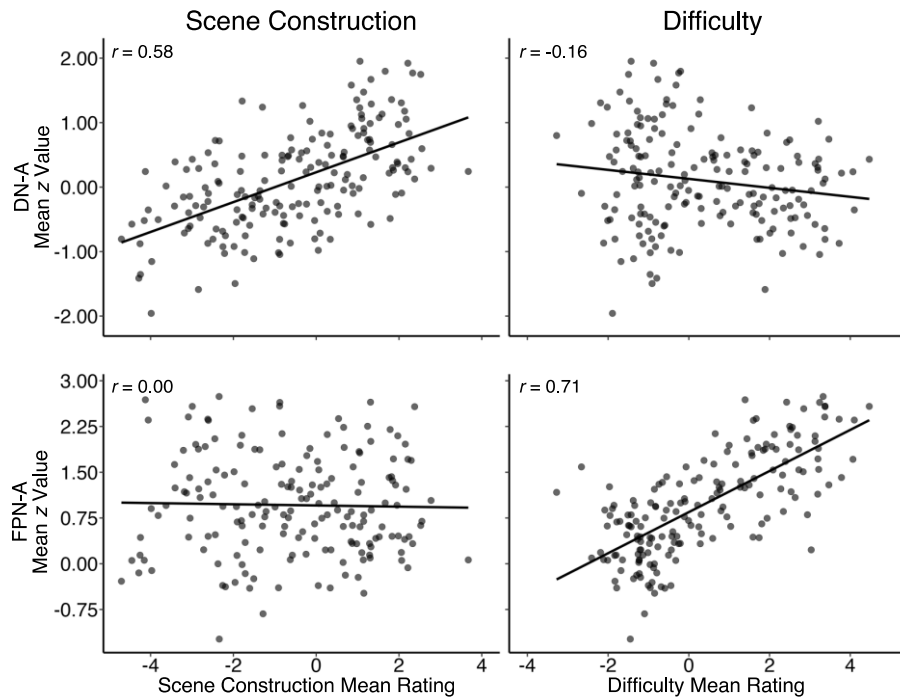
Figure 3.22 Experiment 2 replicates a double dissociation between scene construction and difficulty in cerebral DN-A and FPN-A. Correlations of trial-level mean betas values with cerebral DN-A and FPN-A with strategy composites for scene sonstruction and difficulty. DN-A is strongly correlated with scene construction but not difficulty, while FPN-A displays the opposite behavior: strong correlation with difficulty but not scene construction. This is a replication of findings from DiNicola et al. 2023 in an independent data set. Note that in DiNicola et al. 2023, FPN-A was labeled FPN-B.

The anterior hippocampal region contrast values departed from DN-A during Experiment 2 for reasons that are currently undetermined. However, anterior hippocampal activity was still notably different from activity within the posterior hippocampal area, which only showed a slightly significant increase in activity during the episodic projection future condition ($p = 0.034$).
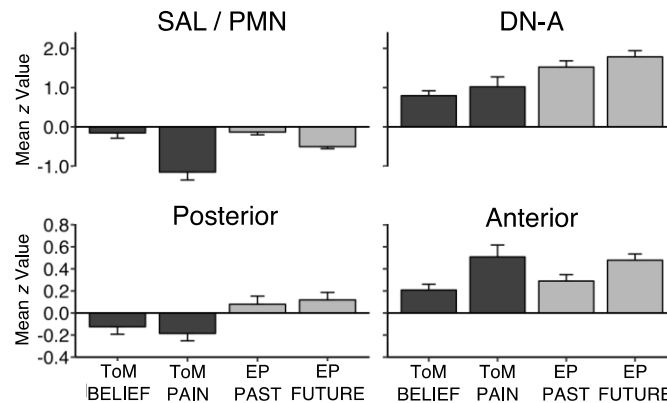
Figure 3.23 Run-level analysis in Experiment 2 replicates DN-A sensitivity to episodic projection, as well as the similarity in task response between hippocampal regions and associated cerebral networks. Paralleling Fig. 3.8, condition contrasts from tasks targeting Theory of Mind (ToM) and episodic projection (EP), averaged across Experiment 2 participants, showed that both DN-A and the anterior hippocampal region are recruited when individual's recall their own past (EP PAST) or imagine their own future (EP FUTURE). In contrast, activity within SAL / PMN and the posterior hippocampal region continues to be more muted during these tasks. The z values for episodic projection contrasts were lower in Experiment 2 than Experiment 1 because fewer questions belonging to a given contrast were included in each task run (5 questions in Experiment 1, 3 questions in Experiment 2). Plot values are Fisher mean z-transformed beta values, and error bars indicate standard error around the mean across participants.

Anterior Hippocampal Sensitivity to Scene Construction Replicates in Experiment 2

The expanded episodic projection task in Experiment 2, along with the new behavioral data set, allowed us to investigate the relationship between scene construction and activity within the anterior hippocampus in a completely independent, prospective data set. In this new data, the mean z value within the anterior hippocampal region during a single trial of the episodic projection task showed a strong positive correlation with extent to which that question used scene construction strategies (Fig. 3.24 left middle; $r = 0.40$, 95% CI [0.27 0.52], $p < 0.001$). This correlation, along with the finding that activity within the anterior hippocampal region is more weakly correlated with the

recruitment of self-relevant strategies (Fig. 3.24 right middle; $r = 0.17$, 95% CI [0.02 0.31], $p = 0.025$) are complete replications of the results of Experiment 1. A multiple regression linear model further replicated that while both strategies together significantly predicted anterior hippocampal activity ($F(2, 177) = 20.2$, $p < 0.001$), the scene construction rating of an individual question is more predictive of activation than the self-relevance rating (Adjusted $R^2_{Full\ Model} = 0.18$, $p_{Scene\ Construction} < 0.001$, $p_{Self\ Relevance} = 0.019$; $R^2_{Scene\ Construction} = 0.16$; $R^2_{Self\ Relevance} = 0.01$).

As in Experiment 1, anterior hippocampal activity was highly correlated with the individual strategy ratings included in both the scene construction composite (Fig. 3.25, r range $= 0.32 – 0.38$) and the autobiographical composite ($r_{Pers\_Past\_Exper} = 0.30$; $r_{Sequence\_Events} = 0.41$). After correction for difficulty, the correlations to scene construction strategies remained largely unchanged (r range $= 0.30 – 0.37$), while autobiographical strategies had reduced correlation ($r_{Pers\_Past\_Exper} = 0.19$; $r_{Sequence\_Events} = 0.34$). After difficulty correction, strategy composites for scene construction, autobiographical, and self-relevant strategies were used a predictors in a multiple regression linear model which was highly predictive of anterior hippocampal region activity ($F(3, 176) = 10.81$, $p < 0.001$). However, only scene construction contributed significantly to the model (Adjusted $R^2_{Full\ Model} = 0.14$, $p_{Scene\ Construction} < 0.001$, $p_{Autobiographical} = 0.134$, $p_{Self\ Relevance} = 0.857$). This replicated the contribution of scene construction observed in Experiment 1 with added specificity: in Experiment 1, autobiographical and self-relevant strategies were less predictive but still significant, whereas in Experiment 2 these strategies were not significant.

Activity within cerebral SAL / PMN and the posterior hippocampal region was not correlated with scene construction in Experiment 2 (Fig. 3.26; SAL / PMN: $r = -0.11$, 95% CI [-0.25 0.04], $p = 0.155$; Posterior Hippocampal Region: $r = 0.08$, 95% CI [-0.06 0.23], $p = 0.266$). The lack of a significant correlation in the posterior hippocampal region is in contrast to Experiment 1, where activity in the posterior hippocampus was correlated more weakly with scene construction. This may be another result of slight changes to the cerebral networks estimated using the MS-HBM.
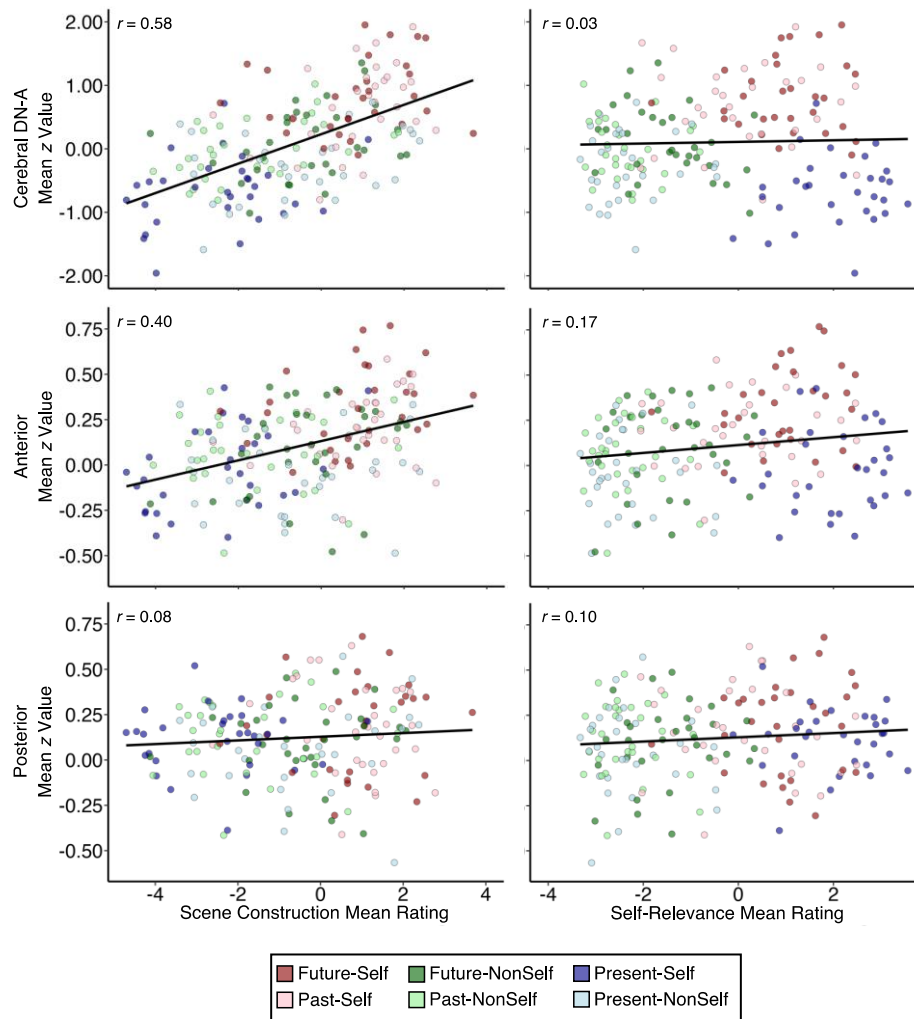
Figure 3.24 DN-A and anterior, but not posterior, hippocampal region activity tracks trial-level variations in scene construction more than self-relevance during the episodic projection task. Paralleling Fig. 3.9, plots indicate activity within individual-specific DN-A and hippocampal regions, pooled across Experiment 2 subjects for each episodic projection trials. Mean trial-level activity is plotted against each trial's scene construction (left) or self-relevance (right) composite, as scored by at least 25 independent behavioral participants. Both DN-A and the anterior hippocampal region displayed strong, highly significant ($p < 0.001$) correlations with scene construction, while in contrast to Experiment 1 the posterior hippocampal region was not significantly correlated with scene construction ($p = 0.266$). Similarly, only anterior hippocampal region activity was significantly correlated with self-relevance ($p < 0.05$), and that correlation was weaker than for scene construction.

Interestingly, the coupling between anterior and posterior hippocampal region activity is visible in

the correlation values for all individual strategies except scene construction strategies and the

sequence of events strategy (Fig. 3.27, bottom), while cerebral DN-A and SAL / PMN are not

coupled across nearly all strategy correlations (Fig. 3.27, top).
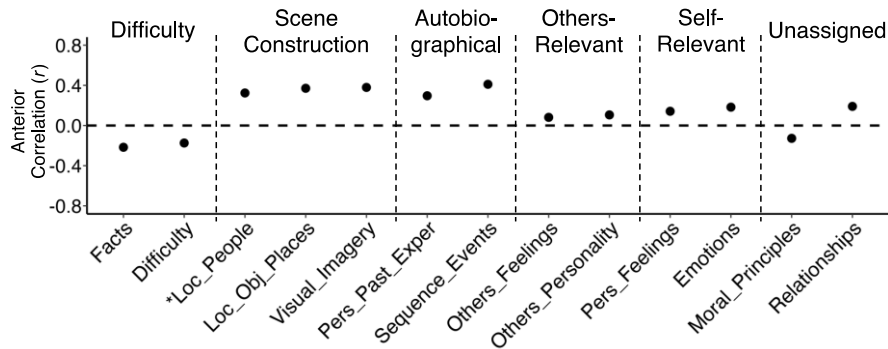
Figure 3.25 Activity within anterior hippocampal region is highly correlated with trial-level scene construction and autobiographical strategies in Experiment 2. Paralleling Fig. 3.10, across all collected trial-level strategies activity within the anterior hippocampal region was most correlated with strategies involved in the scene construction and considering autobiographical features. As in Experiment 1, the strategy rating for Locations of People (Loc_People) is included within scene construction due to a high correlation with Locations of Objects and Places (Loc_Obj_Places) and Visual Imagery (Visual_Imagery) strategies, but was not included in the scene construction composite. Autobiographical, but not scene construction, strategy ratings were negatively correlated with difficulty strategy ratings across trials, replicating the pattern from Experiment 1.

The Posterior Hippocampus, Along with SAL / PMN, is Transiently Activated at Block

Transitions in Both Experiment 1 and 2.

The lack of significant activity within cerebral SAL / PMN during the episodic projection

task suggested that this paradigm was not well suited to understanding activity within this

network, and by extension the posterior hippocampal region. However, the inclusion of regions in

the canonical salience network within SAL / PMN suggested a new avenue of exploration. Exploring

the BOLD percent signal change within our regions of interest in Experiment 1 during an N-back

working memory task with discrete task and fixation blocks revealed a dissociation both on the

cerebral surface and within the hippocampus. On the cerebral surface (Fig. 3.28A, top), SAL / PMN
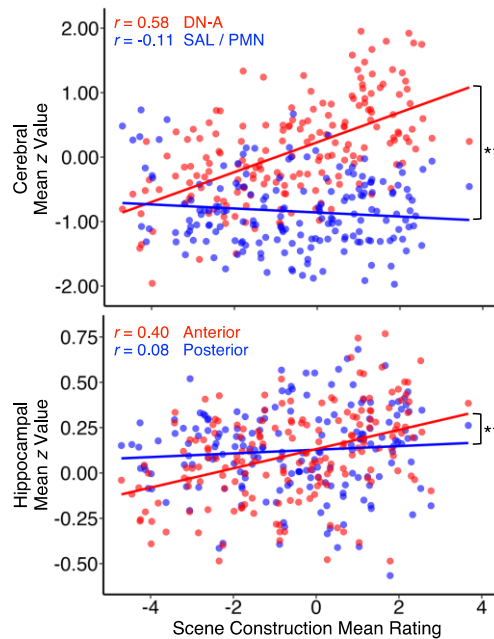
Figure 3.26 Experiment 2 replicates that DN-A and the anterior hippocampal region are significantly more sensitive scene construction than SAL / PMN and the posterior hippocampal region. Paralleling Fig.3.11, combined scatter plots showing trial-level activity within cerebral networks (top) and hippocampal regions (bottom) against scene construction ratings reveal stronger correlations in DN-A and the anterior hippocampal region than SAL / PMN and the posterior hippocampal region, respectively. A linear mixed effects model run separately on cerebral and hippocampal data revealed a highly significant interaction between cerebral network and scene construction rating ($F(1,178) = 65.239$), and between hippocampal region and scene construction rating ($F(1,178) = 36.537$) in predicting trial-level activation. ** = $p < 0.001$
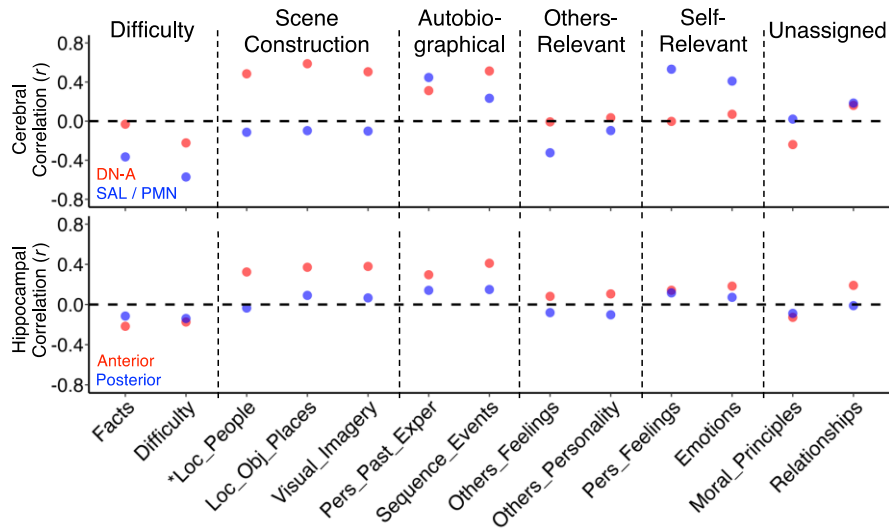
Figure 3.27 Posterior hippocampal region sensitivity to trial-level strategies deviates from the anterior hippocampal region and DN-A only for scene construction and autobiographical strategies. Paralleling Fig. 3.12, trial-level strategy correlations within cerebral DN-A and SAL / PMN (top) continued to be notably different for scene construction and self-relevant strategies in Experiment 2. Hippocampal regions (bottom) displayed more deviation within scene construction and autobiographical strategies, suggesting improved specificity in region definition. The lack of deviance within the hippocampus for other strategies reflects the high correlation in global activity between hippocampal regions (r = 0.67, p < 0.001) even while the correlation between cerebral networks was reduced compared to Experiment 1 (r = -0.05, p = 0.483).

showed a transient increase in BOLD signal after block onsets and offsets (dotted vertical lines), while DN-A did not show transient activity. Activity within the hippocampal regions followed the cerebral networks used to identify them (Fig. 3.28A, bottom): the posterior hippocampal region showed transient increases at task onset/offset, while the anterior hippocampus did not. To assist with visualizing these transients, and motivated by the secondary functional connectivity between the posterior hippocampus and cerebral DN-A, we regressed DN-A activity from both cerebral SAL / PMN activity (Fig. 3.28B, top), and posterior hippocampal activity (Fig. 3.28B, bottom). At three of the four task onset/offsets, the adjusted signal within both SAL / PMN and the posterior hippocampus increases for a time before decreasing (marked by inverted triangles). After one task onset (indicated by a question mark), adjusted activity within cerebral SAL / PMN increases, but remains high until the task offset. However, adjusted signal within the posterior hippocampus at that same time increased, mirroring other block onsets and offsets.

This unexpected, salience-like activity within the posterior hippocampus prospectively replicated in Experiment 2 within the visual motor task, which also included discrete fixation and task blocks. As in the N-back task from Experiment 1, activity within both cerebral SAL / PMN and the posterior hippocampal region transiently increased after block transitions, while activity within DN-A and the anterior hippocampal region did not (Fig. 3.29A), and these transients became clearer after regressing DN-A activity (Fig. 3.29B).

The Posterior Hippocampal Region and SAL / PMN are Transiently Active in Response to Salient Stimuli.

After observing the transient increase in activity within SAL / PMN and posterior hippocampal region at the onsets and offsets of blocks during the Experiment 1 N-back task, we chose to include a visual oddball task in Experiment 2 to test the hypothesis that SAL / PMN and the posterior hippocampus would also be sensitive to tasks shown to activate the canonical salience
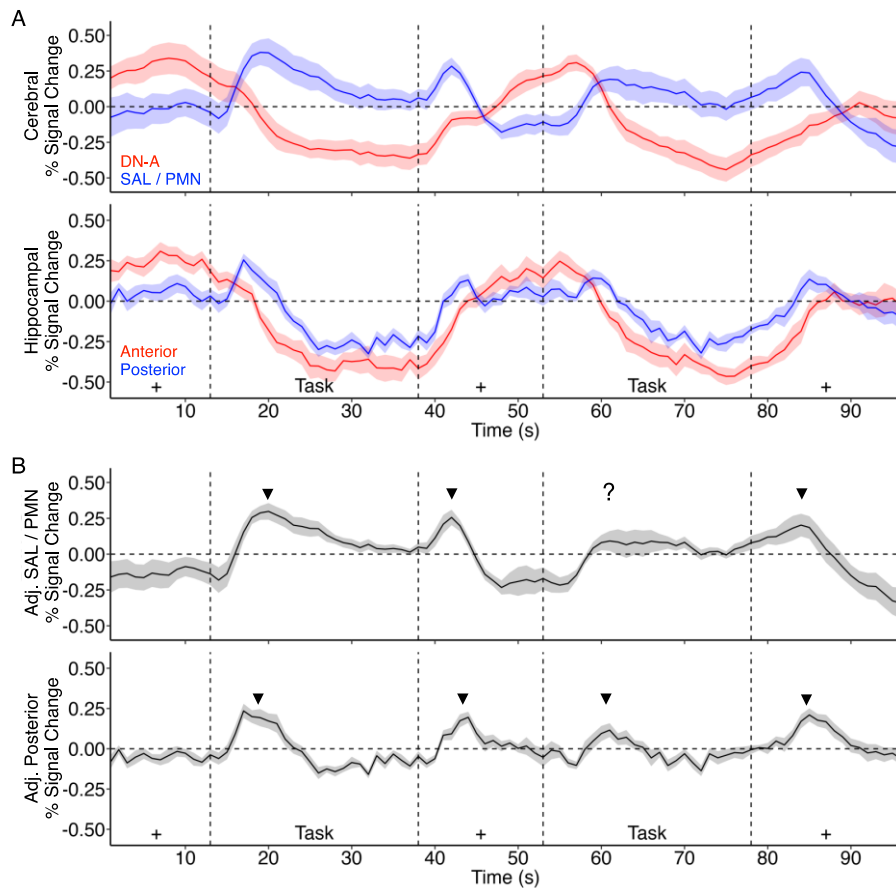
Figure 3.28 SAL / PMN and the posterior hippocampus are transiently recruited at task onsets and offsets in Experiment 1. Mean percent signal change within cerebral networks and hippocampal regions during the N-back task. A: Activity within both cerebral SAL / PMN (blue, top) and the posterior hippocampal region (blue, bottom) increased for several seconds after task onsets and offsets (vertical dotted lines) before reducing. Activity within cerebral DN-A (red, top) and the anterior hippocampal region (red, bottom) did not display these transients. B: Transients (indicated by inverse triangles) in the posterior hippocampal region (bottom), as well as in cerebral SAL / PMN (top), were more clearly visible after regressing out signal within DN-A. At one task onset, signal within SAL / PMN increased, but without a subsequent decrease (indicated by ?), but activity within the posterior hippocampal region followed the expected pattern. Shading on plot indicates standard error around the plotted mean across participants.
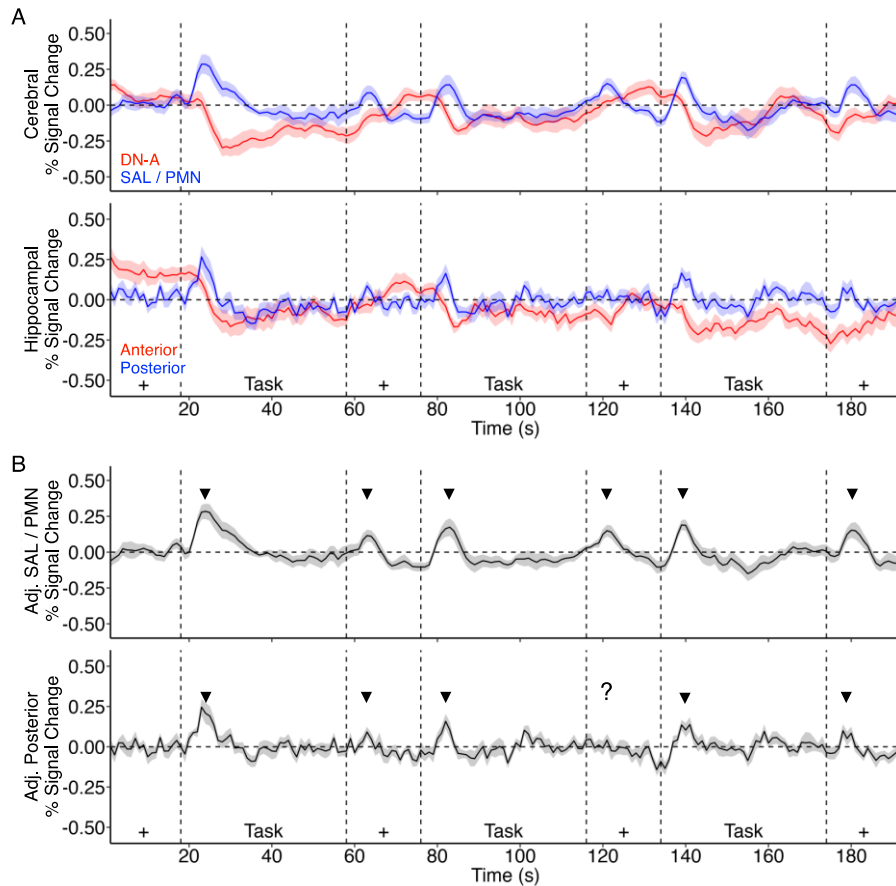
Figure 3.29 Experiment 2 replicates transient recruitment of SAL / PMN and the posterior hippocampus at block transitions. Paralleling Fig. 3.28, plots show mean percent signal change within cerebral networks and hippocampal regions during the visual motor task. A: Activity within both cerebral SAL / PMN (blue, top) and the posterior hippocampal region (blue, bottom) increased for several seconds after task onsets and offsets (vertical dotted lines) before reducing. Activity within cerebral DN-A (red, top) and the anterior hippocampal region (red, bottom) did not display these transients. B: Transients (indicated by inverse triangles) in the posterior hippocampal region (bottom), as well as in cerebral SAL / PMN (top), were more clearly visible after regressing out signal within DN-A. Transient responses within the posterior hippocampal region were more pronounced for task onsets than offsets, and for one task offset no transient increase is visible (indicated by ?). Shading on plot indicates standard error around the plotted mean across participants.

network. Run-level GLM analysis of the visual oddball task, done in each individual and then

averaged to produce a group map, showed a clean separation between default network-like regions

of brain (which showed deactivation in response to salient targets, Fig. 3.30 blue shading) and

nearby "salience-like" regions (which showed activation to salient targets, Fig 3.30 red shading). In

all 11 subjects, the set of regions activated by salient targets included SAL / PMN (Fig. 3.31).

Quantification of this activation (Fig. 3.32) confirms that activity to salient targets was primarily

within cerebral SAL / PMN ($p < 0.001$) and CG-OP ($p < 0.001$). Consistent with canonical default

mode network task deactivation (Buckner et al. 2008; Greicius et al. 2003; Raichle et al. 2001), we

also observed large deactivation in response to salient targets in both DN-A and DN-B (Fig. 3.32).
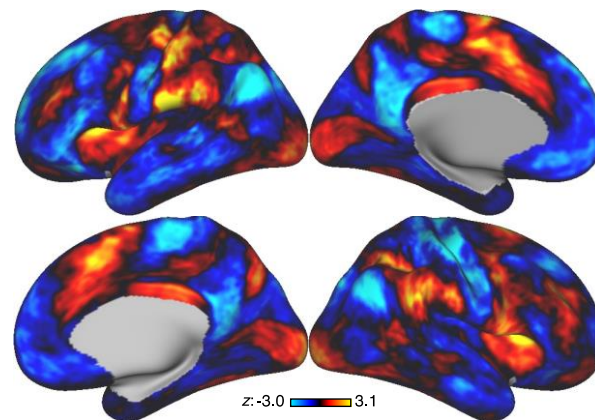
Figure 3.30 Group-averaged activity response to salient visual oddball targets dissociates SAL / PMN and associated networks from canonical Default Network regions. Activity on the cerebral surface in response to target letters in the visual oddball paradigm averaged across all Experiment 2 participants reveals positive activation in regions of SAL / PMN such as the anterior insula, anterior and posterior cingulate, and posteromedial cortex, as well as nearby regions that are often included in CG-OP. In contrast, target letters produce a pronounced deactivation within regions of the canonical Default Network, such as retrosplenial, ventral-medial prefrontal, and lateral parietal cortices.

In addition to activity within cortical networks, there was significantly more activity in the

posterior than the anterior hippocampal region in response to salient targets (Fig. 3.33A; $p <$

0.001). The observed lack of activity within the posterior hippocampal region, when considered in

the context of the observed coupling between anterior and posterior hippocampal activity during

the episodic projection task, may be the result of suppression from the large deactivation within the

anterior hippocampal region (mirroring cerebral DN-A). To test this hypothesis, we adopt the same approach we had used previously to better visualize block transients, and regressed DN-A activity. After regression (Fig. 3.33B), the posterior hippocampal region displayed significant positive activation ($p < 0.05$), while also remaining significantly more active than the anterior hippocampus ($p < 0.001$). When we averaged activity within the posterior hippocampal region (with cerebral DN-A activity regressed) after each of the target trials, we observed a canonical hemodynamic response (Fig. 3.33C). This shows the transience of the posterior hippocampal response to salient stimuli, and highlights how analyses over longer trials may miss this response.

Discussion

Within-individual precision analysis of the long axis of the hippocampus revealed differential functional connectivity to distinct cerebral networks, along with a functional double dissociation during tasks. Replicating Zheng et al. (2021), the anterior hippocampus is preferentially correlated to DN-A (and to a lesser degree DN-B), while the posterior hippocampus is primarily correlated with SAL / PMN. This difference in functional connectivity to anterior and posterior hippocampal regions underpins a double dissociation during tasks. The anterior hippocampus, like cerebral DN-A, responds when a task demands scene construction, while the posterior hippocampus, like cerebral SAL / PMN, responds to salient task transitions. The hippocampal regional assignments and task dissociations replicated across datasets. Hypothesis-driven exploration of the role of posterior hippocampus in salience processing was directly tested within a prospective study of visual oddball detection. The posterior hippocampus responded robustly to salient, transient target events. We discuss implications of these findings, and their limitations, for understanding heterogeneity along the long axis of the hippocampus.

194
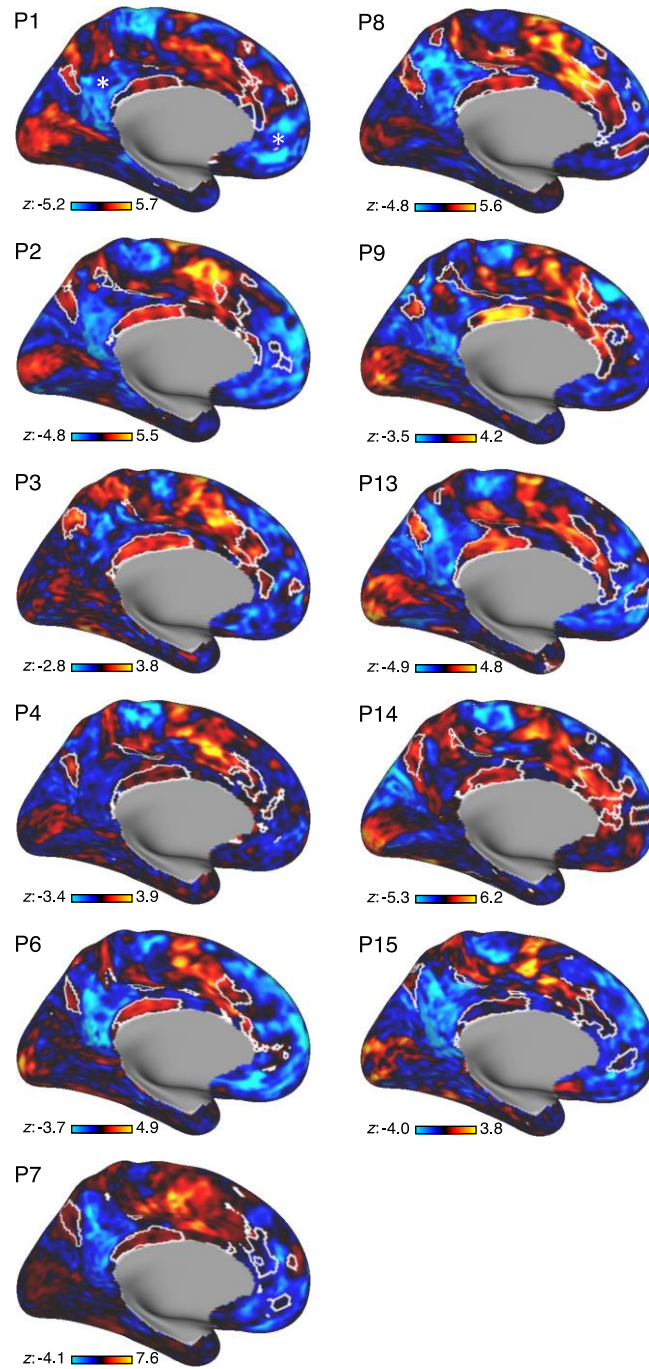
Figure 3.31 Within-individuals, responses to salient visual oddball targets recruits SAL / PMN and not nearby regions canonically included in the Default Network. Activity in response to target letters in the visual oddball paradigm is shown on the medial surface for individual Experiment 2 participants, along with an outline of the individual's SAL / PMN (in white). SAL / PMN is at least partially recruited in all participants, although the extent of that recruitment is variable. Notably not recruited in any subject are regions of the canonical Default Network (indicated by * on P1), which in individuals generally includes DN-A, DN-B, and LANG.
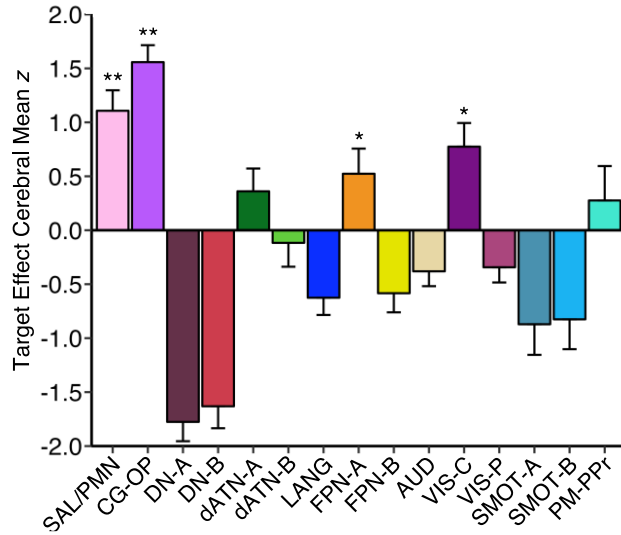
Figure 3.32 Salient visual oddball targets dissociate SAL / PMN and DN-A functional responses. Activity within individual's cerebral networks in response to visual oddball targets was pooled across Experiment 2 participants. Significant increases in activity were observed in SAL / PMN and spatially nearby CG-OP, as well the network encompassing centrally responsive visual cortex (VIS-C). In contrast, DN-A displayed a large decrease in activity level to these salient targets, consistent with its location within the canonical Default Network. Additional network abbreviations: AUD = Auditory; VIS-C = Visual-Central; VIS-P = Visual-Peripheral; SMOT = Somatomotor; PM = Premotor; PPr = Posterior Parietal Rostral. Significance statistics are a one-tailed t-test for each network/region (H_o: $\mu = 0$, H_a: $\mu > 0$) ** = $p < 0.001$.
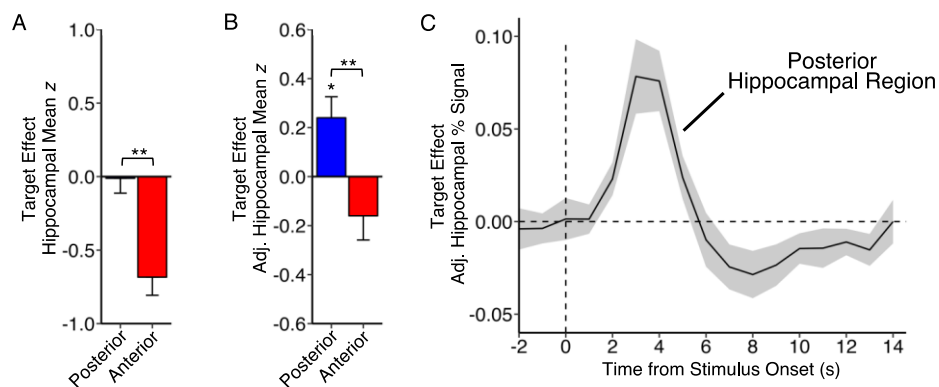
Figure 3.33 Salient visual oddball targets selectively and transiently recruit the posterior hippocampal region. Activity within individual's hippocampal regions in response to visual oddball target pooled across Experiment 2 participants. A: In response to salient targets, the anterior hippocampal region is strongly deactivated, and while the posterior region is significantly more active than the anterior, the overall activity is near baseline. B: Regressing out DN-A activity (as in Figs. 28 and 29) removed the influence of DN-A deactivation and allowed the positive activation in the posterior region to be seen. C: Plotting the mean percent signal change within the posterior hippocampal region immediately before and after each target letter presentation shows a transient, canonical hemodynamic response to salient targets. Significance statistics are either a one-tailed t-test for each hippocampal region (H_o: $\mu = 0$, H_a: $\mu > 0$), or a two-tailed paired t-test to assess for differences between the hippocampal regions (H_o: $\mu_1 = \mu_2$, H_a: $\mu_1 \neq \mu_2$). Error bars indicate standard error around the mean z across participants. ** = $p < 0.001$; * = $p < 0.0$

The Anterior Hippocampus is Coupled to DN-A and is Sensitive to Scene Construction

Functional connectivity analysis of the hippocampus identified a region of the anterior hippocampus which displayed strong coupling to cerebral DN-A. The consistency of this finding across two independent data sets, and its similarity to results recently described by Zheng and colleagues (2021), underscores the reliability of this observation. Previous group-level studies exploring differential functional connectivity along the hippocampal long axis identified correlations between the anterior hippocampus and distributed cerebral regions including parahippocampal cortex, retrosplenial cortex, ventromedial prefrontal cortex, posterior parietal cortex and dorsolateral prefrontal cortex (Barnett et al. 2021; Frank et al. 2019; Kahn et al. 2008). Because DN-A and DN-B are closely interdigitated within these regions (Braga and Buckner 2017), these studies likely reflect group-averaged blurring across both networks. Our results refine the hippocampal-cortical association by identifying preferential coupling of the anterior hippocampus to DN-A, and weaker coupling to DN-B.

By keeping our analyses within individuals, we were not only able to identify the region of the anterior hippocampus coupled to DN-A, but also precisely explore the function of this region. Zheng et al. (2021) supported a functional link between individual-specific DN-A (which they called DMN) and the anterior hippocampus by showing comparable levels of deactivation during externally directed tasks (which we also observed, see Fig. 3.28). Based on this shared functional response, as well as the presence of anterior hippocampal regions coupled to DN-B (their CAN), the authors proposed a role for the anterior hippocampus in integrating self-relevant information such as contextual and social associations (Zheng et al. 2021).

In contrast to the study by Zheng and colleagues (2021), the present work explored the function of the anterior hippocampus using hypothesis-directed tasks designed to engage specific cognitive functions. Specifically, we used an episodic projection task to probe anterior hippocampal function because cerebral DN-A is selectively recruited for episodic projection (DiNicola et al.

2020), and in particular is sensitive to the extent single trials of this task engage scene construction (DiNicola et al. 2023). Using the same trial-level approach used by DiNicola et al. (2023), we found that the portion of anterior hippocampus coupled to cerebral DN-A was also sensitive to participant's use of scene construction strategies (considering the locations of objects and places, and using visual imagery)(Hassabis and Maguire 2007), and notably less sensitive to self-relevant strategies (e.g. personal significance, evoking recent thoughts, considering personal preferences or feelings, and evoking emotions. See Figs. 3.9, 3.10, 3.24, and 3.25).

The anterior hippocampus has often been considered the less spatially involved counterpart to the posterior hippocampus, but these findings notably show in humans that the anterior hippocampus is more involved in mentally constructing scenes than the posterior hippocampus, even during control questions without explicit mnemonic demands. These findings complement studies that have suggested a role for the anterior hippocampus in learning spatial relationships (Woollett and Maguire 2012) and flexible wayfinding (Hartley et al. 2003). Further, cerebral activations when individuals see vs remember scenes shows a non-negligible amount of overlap in posterior cerebral cortex (Steel et al. 2021), notably PHC and retrosplenial cortex. This may indicate a role for DN-A, and potentially the anterior hippocampus, in scene perception, but further study is needed to assess the extent of anterior hippocampal involvement in non-constructive spatial tasks.

The Posterior Hippocampus is Coupled to SAL / PMN, and May Play a Role in Salience Processing

We identified in all participants a region in the posterior hippocampus coupled to SAL / PMN. Like with the anterior hippocampus, previous work in group-averaged data had described coupling of the posterior hippocampus to distributed cerebral regions (e.g. Barnett et al. 2021), but the lack of convergence across studies indicates that posterior hippocampal functional connectivity may be particularly hampered by blurring across participant's idiosyncratic cerebral and

hippocampal anatomy. Zheng et al. (2021) took an important step in improving our understanding of posterior hippocampal functional connectivity by identifying coupling to an individual-specific cerebral parcel which includes posteromedial cortex. The present work expanded this observation by establishing coupling between the posterior hippocampus and the entirety SAL / PMN as identified in each individual including the anterior cingulate and frontal insula, hallmark regions of the historically described SAL network (Seeley et al. 2007; see also Dosenbach et al. 2006; Seeley 2019).

Gilmore et al. (2015), given their focus on the posteromedial cortex, described the network's function in terms of classic mnemonic processes, without connection to the literature on the SAL network. The conflation may arise because of the SAL / PMN network is spatially adjacent to DN-A along the posterior midline, and easily confused. The present results suggest that the entirety of cerebral SAL / PMN is functionally aligned with salience processing rather than memory. The SAL / PMN responds to salient stimuli and tasks transitions. Past observations linking the posterior cingulate and posteromedial cortex to memory encoding and retrieval (Daselaar et al. 2009, 2004) may have been impacted by group-averaged blurring from nearby regions of the canonical default network, possibly resulting in the misattribution of mnemonic signals within the default network to these portions of SAL / PMN.

The role of SAL / PMN in salience processing holds true even within the hippocampus, as the posterior region coupled to SAL / PMN shows a transient increase in signal in response to salient stimuli, and either weaker (Experiment 1) or minimal (Experiment 2) sensitivity to scene construction. These findings are a departure from spatial framings of the posterior hippocampus, but are consistent with work describing a role for the hippocampus in processing novelty. In a study by Fyhn and colleagues, neurons in the dorsal rat hippocampus (homologous to the human posterior) displayed an increased response when the animal encountered a platform in a new place while swimming in a circular track (Fyhn et al. 2002). Critically, the firing rate did not increase as

much, or at all, on subsequent encounters with the platform in the same location, suggesting that these neurons were responding to the novelty of platform placement, rather than the new position itself (Fyhn et al. 2002). Despite this compelling response within the dorsal rat hippocampus, the inherently spatial nature of this task and others makes it difficult to fully disambiguate space and novelty in rodents.

Studies in humans allow for a much more diverse set of tasks independent from space, and add support for the role for the posterior hippocampus in assessing novelty. Notable among these are studies which use an oddball task like the one used in the present study. In general, during these tasks participants are presented with a string of similar or identical stimuli (visual, auditory, or tactile), punctuated at unpredictable times with unique oddball stimuli. When recording electrical potentials from the scalp of individuals doing this task using an electroencephalogram (EEG), these oddball stimuli consistently evoke a positive deflection around 300ms after presentation, referred to as the P300 event-related potential (ERP) (Sutton et al. 1965). In patients with damage to the posterior hippocampus, a portion of the P300 ERP is attenuated compared to control individuals, suggesting an impact to the brain's processing of novel stimuli (Knight 1996). Patients with hippocampal lesions also displayed a diminished skin conductance response when briefly given an electrical shocked, further implicating an impairment to novelty and salience processing resulting from hippocampal damage. Our results connect this work on hippocampal novelty responses to the literature on cerebral salience processing (e.g. Dosenbach et al. 2006; Seeley 2019; Seeley et al. 2007), and motivate further study of SAL / PMN and the posterior hippocampus in this context.

A Cross-Domain Double Dissociation in the Hippocampus

Our observed functional dissociation along the hippocampal long axis adds to an extensive literature on hippocampal specialization (for reviews, see Poppenk et al. 2013; Strange et al. 2014).

The recruitment of the anterior hippocampus for spatial processing and posterior hippocampus for salience processing have both been proposed previously, but to our knowledge never been studied simultaneously. In rodents, non-human primates, and humans, studies of hippocampal specialization generally remain within a single cognitive "domain", often spatial (e.g. Brunec et al. 2018; Jung et al. 1994; Kjelstrup et al. 2008; Maguire et al. 2000; Woollett and Maguire 2011) or mnemonic (e.g. Lepage et al. 1998; Poppenk and Moscovitch 2011; Schacter and Wagner 1999; Spaniol et al. 2009). The present study adopted a domain-agnostic approach to exploring hippocampal function, guided by the functional properties of coupled cerebral networks rather than previously described hippocampal functions. That this network-driven approach converged on previously described hippocampal functions, and that the observed network coupling and functional responses replicated across two independent data sets, is a testament to the robustness of this approach.

The cross-domain nature of our findings should be taken as an indication of how complex hippocampal processing is, and not evidence that previously described within-domain specialization does not exist. Notably, our results do not preclude posterior hippocampal involvement in spatial tasks like precise navigation, or anterior hippocampal involvement in processing of emotional salience. They do, however, encourage the exploration of hippocampal functional during tasks not designed to engage episodic memory: the tasks which evoked posterior hippocampal responses had no explicit mnemonic component, and anterior hippocampal sensitivity to scene construction persists even in control questions that minimize demands on episodic memory.

Limitations

Despite the improvements made possible by adopting a within-individual, network-based approach, our exploration of the hippocampus using fMRI was still limited by several technical

considerations. First among these is signal dropout in both the most anterior portions of the hippocampus and surrounding cortical regions. Beyond preventing the inclusion of these regions in our analyses (via screening for tSNR), the lack of signal in regions of the anterior parahippocampal gyrus makes it difficult to assess the possibility of signal bleed from this portion of cortex into included regions of the anterior hippocampus. It is possible that anterior PHC or EC activity, which we are unable to reliably measure due to dropout, is contributing to responses within the anterior hippocampus. In addition to dropout, the resolution of our BOLD acquisition (2.4 mm isotropic) becomes a notable hindrance when studying a structure as small as the hippocampus, resulting in ambiguity around the spatial location of activations and correlations (see Results, Fig. 3.20). Subsequent work would benefit from higher resolution acquisitions at high field to address this issue.

We approached the present study with an *a priori* hypotheses about the functional connectivity of the hippocampus to cerebral networks based on work by Zheng and colleagues (2021), and as such, we restricted our planned analyses to DN-A and SAL / PMN. Exploratory parcellation of hippocampus based on functional connectivity to all 15 identified cerebral networks (not shown here) supports our main finding of DN-A coupling to the anterior hippocampus and SAL / PMN coupling to the posterior hippocampus, but also shows additional correlation patterns to networks including DN-B in the anterior hippocampus and CG-OP in the posterior hippocampus. These correlations and their potential functional relevance are beyond the scope of the current paper, but warrant further exploration. In particular, while the DN-A coupling to the anterior hippocampus is consistent with functional tracking of processes related to scene construction, the lesser (but still prominent) coupling to DN-B may suggests a broader role that should be explored, especially in light of models of hippocampal function that extend beyond spatial representations.

Conclusions

The hippocampus can be robustly dissociated along its long axis based on connectivity to distributed cerebral networks. The anterior hippocampus is correlated with DN-A, while the posterior hippocampus is correlated with SAL / PMN. The network-defined anterior and posterior regions display a functional double dissociation, highlighting the functional relevance of this segmentation. The anterior hippocampus is sensitive to scene construction, and the posterior hippocampus responds transiently to salient stimuli. These findings motivate further study of the hippocampus in single individuals to characterize the extent of anterior and posterior hippocampal involvement in scene and salience processing, respectively.

Discussion

This dissertation has described the body of work to which I've contributed over the course of my graduate studies. **Chapters 1 and 2** focused on the cerebellum, characterizing cerebral-cerebellar organization and cerebellar function with the precision afforded by extensively studying single individuals rather than a group. The technical skills and experimental outlook I gained from these studies made possible work I led characterizing a functional double dissociation within the human hippocampus, which I presented and replicated in **Chapter 3**. There is relatively little in the way of an overarching theme to connect these chapters beyond methodological similarity and their contributions to my growth as a scientist. As such, this discussion will consist of thoughts primarily focusing on the hippocampus.

Our results showed that the anterior hippocampus is sensitive to the cognitive process of scene construction, while the posterior hippocampus is transiently responsive to salient changes and visual stimuli. It's important to note that while our findings in the anterior hippocampus directly relate to the ongoing debate on the spatial versus mnemonic hippocampus, our tools and approach were never meant to meaningfully resolve that debate. To highlight this, consider a recent proposal unifying the bodies of work on spatial and relational memory (Whittington et al. 2020) which relies on computational concepts to explain and predict activity on the level of cells, well beyond the resolution of our current neuroimaging methods. So instead of attempting to discuss our findings in the context of memory, I will instead stay within the cognitive domains for which we have experimental results, namely space and salience.

Of our observed functional double-dissociation in the hippocampus, the anterior hippocampal sensitivity to scene construction is the more straightforward, as the hippocampus has long been shown to be involved in spatial reasoning in both rodents (O'Keefe 1976; O'Keefe and Dostrovsky 1971) and humans (e.g. Maguire et al. 1997, 1998, 2000; Ryan et al. 2010). It is not

particularly concerning that the form of constructive scene processing we studied recruited the anterior hippocampus, rather than the posterior hippocampus implicated in many studies of human spatial navigation. Our interactions with the environment around us are multifaceted, and the processes required to navigate the world might be separate from those we use to consider it more generally. Indeed a representational gradient has been proposed within the hippocampus with precise representations of space in the posterior hippocampus, and coarser representations of space, like those one might spontaneously construct in their mind, in the anterior hippocampus (Brunec et al. 2018; Hirshhorn et al. 2012).

Recent studies on hippocampal activity when individuals construct and elaborate on an autobiographical scene further support this difference in granularity along the hippocampal long axis (Audrain et al. 2022; Gilmore et al. 2021). In the initial phase of their task, participants were shown two images and instructed to choose one of those images as a cue for an autobiographical scene. After selection, a brief delay was followed by the presentation of the chosen picture, and participants were asked to verbally describe the scene they associated with that image. During the initial phase, where individuals were asked to consider their constructed scene superficially in order to make a choice between pictures, only the anterior hippocampus displayed significant activation, consistent with a role for the anterior hippocampus in coarse scene construction (Audrain et al. 2022). However, the elaborative phase, when participants were required to engage with a mental scene in depth, recruited the posterior and not the anterior hippocampus (Gilmore et al. 2021). This suggests that our processing of mental scenes may be a two-pronged cognitive endeavor, of which the initial scene construction in the anterior hippocampus is only one part.

The role of the posterior hippocampus in the processing of salience could also be consistent with its involvement in humans with scene elaboration (Gilmore et al. 2021) and local navigation (e.g. Hartley et al. 2003; Woollett and Maguire 2011). It's possible that the posterior hippocampus is sensitive to salience and task-demands in not only the external world, as we have shown in

Chapter 3, but also in our internally constructed scenes. In the absence of any directed task, the posterior hippocampus may generally only be active if there is an inherently salient feature in the scene. However, if participants are given a task that requires elaboration of the scene (as Gilmore and colleagues did), then more details of the constructed scene become relevant, increasing posterior hippocampal involvement. A similar distinction might occur with navigation, which requires engaging with more specific details than general scene construction. For example, if I ask you to imagine the inside of your favorite restaurant, you might produce a general scene populated with inherently salient features like your favorite dish or the people you often eat with. If I were to then ask you to describe how you would get from that location to the street, now features you might not have originally focused on, like the location of the door, become important. When considering navigation as a demand required by specific tasks, rather than an inherent feature of representing space, its association with the posterior hippocampus become more consistent with our results.

As an additional point, I'd like to discuss how I conceptualize the hippocampus as part of broader brain networks. In cerebral cortex, the activation of entire networks for cognitive tasks suggests that while each portion of a network may be a node that performs a unique computation, these nodes are behaving as an ensemble to support cognitive processes. I believe the hippocampus should be considered as part of this network ensemble, rather than a separate "helper" structure to the cerebral network. Seminal work has described in detail the connectivity between the broad hippocampal region and cerebral cortex (e.g. Insausti and Amaral 2008; Squire 1992; Suzuki and Amaral 1994), but these connections are often contextualized as providing the hippocampus with different sources of information to synthesize, rather than an indication that the hippocampus and surrounding regions are nodes in a larger distributed network. Our results support considering the hippocampus as part of the broader brain network, and further suggest that different portions of the hippocampus are not only part of different networks but also functionally align with their associated network.

A distributed network view would predict that sufficiently extensive damage to any part of a network, including regions in cerebral cortex, would produce a deficit in the cognitive function that network supports. Despite that, lesion data has generally focused on hippocampus, likely due to a confluence of historical and biological factors. The circuitry of the hippocampus (notably the recurrent collaterals in CA3) makes this region particularly susceptible to epileptogenic runaway activation, which presented a compelling medical reason in H.M.'s case to remove it. Because H.M.'s lesion was done surgically, rather than through an accident or stroke as is common with lesions in cerebral cortex, it was a unique combination of being very large while remaining fairly specific (removing only the medial temporal lobe). This specific resection, and the resulting memory deficit, played a very large part in turning attention to hippocampus in humans, and was further reinforced by the susceptibility of hippocampal CA1 specifically to damage from ischemic stroke (e.g. Zola-Morgan et al. 1986). Additionally, given what we now know about the variability of individual-specific network topography, it's unsurprising that deficits resulting from lesions in cerebral cortex might be more difficult to pin down. Even given the extraordinary hypothetical of two individuals with lesions in the exact same location of cerebral cortex, these individuals could present with very different deficits depending on the networks which were damaged. Meanwhile, the hippocampus is a smaller structure with less potential separation between network-associated regions, and any separation that does exist becomes moot once the majority of the structure is removed as in H.M.'s case.

The focus in rats on the hippocampus rather than cerebral cortex is also understandable, as the rat simply does not have very much cerebral cortex. However, this presents an interesting problem: if in humans, hippocampal regions are functioning as part of broader brain networks, how does that translate to animals like the rat with significantly less association cortex? One possibility is that the rat does have distributed and specialized networks, but they are just less pronounced. However, it's also possible that the rat gives us a glimpse into an evolutionarily older role for the

hippocampus and surrounding cortical regions. Perhaps in a common ancestor shared between rats and primates, the hippocampus (or evolutionarily corresponding structure) was optimized for representing spatial relationships. Gradually, hippocampal function may have expanded, and by the time the rodent lineage split from primates included more general relational processing. To deal with the additional computations required by these expanded functions, the hippocampus could have begun incorporating surrounding cortex like PHC and PRC into a small local network.

After the rodent-primate evolutionary split, brain size continued to dramatically increase in the primate lineage, and association cortex in particular expanded much more than primary sensory or motor cortices (Chaplin et al. 2013; Krubitzer 2007). In macaque, these disproportionately expanded portions of cortex have connections not only to each other (Goldman-Rakic 1988), but also the hippocampal formation (Insausti and Amaral 2008; Suzuki and Amaral 1994), and possibly represent a shared evolutionary foundation for hippocampal-cortical networks. When these expanded cerebral regions fractionated and specialized into the closely interdigitated, distributed networks we see in humans (as proposed by DiNicola and Buckner 2021), a corresponding splitting likely occurred in the hippocampal formation. These newly created networks may have then continued to expand the functional role of the hippocampus by leveraging the circuitry of their connected portions of the hippocampal formation in different ways to support more complex cognitive processes.

To conclude this dissertation, I would encourage future investigations of hippocampal function to anchor to whole brain networks. The involvement of the anterior hippocampus in scene construction and the posterior hippocampus in salience processing are valuable leverage points for better understanding hippocampal function, but there is certainly still significant unknown complexity in the hippocampus. By studying the hippocampus in its network context, every improvement in our understanding of brain networks broadly holds the potential to translate into an improved understanding of the hippocampus and its function.

References

Addis DR, **Wong AT**, **Schacter DL**. Remembering the past and imagining the future: Common and distinct neural substrates during event construction and elaboration. *Neuropsychologia* 45: 1363–1377, 2007.

Adrian ED. Afferent areas in the cerebellum connected with the limbs. Brain 66: 289–315, 1943.

Amaral DG, **Witter MP**. The three-dimensional organization of the hippocampal formation: A review of anatomical data. *Neuroscience* 31: 571–591, 1989.

Amunts K, Malikovic A, Mohlberg H, Schormann T, Zilles K. Brodmann's areas 17 and 18 brought into stereotaxic space—where and how variable? NeuroImage 11: 66–84, 2000.

Andrews-Hanna JR, **Reidler JS**, **Sepulcre J**, **Poulin R**, **Buckner RL**. Functional-Anatomic Fractionation of the Brain's Default Network. *Neuron* 65: 550–562, 2010.

Andrews-Hanna JR, **Saxe R**, **Yarkoni T**. Contributions of episodic retrieval and mentalizing to autobiographical thought: Evidence from functional neuroimaging, resting-state connectivity, and fMRI meta-analyses. *NeuroImage* 91: 324–335, 2014.

Audrain S, **Gilmore AW**, **Wilson JM**, **Schacter DL**, **Martin A**. A Role for the Anterior Hippocampus in Autobiographical Memory Construction Regardless of Temporal Distance. *J Neurosci* 42: 6445–6452, 2022.

Barnett AJ, **Reilly W**, **Dimsdale-Zucker HR**, **Mizrak E**, **Reagh Z**, **Ranganath C**. Intrinsic connectivity reveals functionally distinct cortico-hippocampal networks in the human brain. *PLOS Biology* 19: e3001275, 2021.

Biswal B, Yetkin FZ, Haughton VM, Hyde JS. Functional connectivity in the motor cortex of resting human brain using echo-planar MRI. Magn Reson Med 34: 537–541, 1995.

Bliss TVP, **Lømo T**. Long-lasting potentiation of synaptic transmission in the dentate area of the anaesthetized rabbit following stimulation of the perforant path. *J Physiol* 232: 331–356, 1973.

Boillat Y, Bazin P-L, van der Zwagg W. Whole-body somatotopic maps in the cerebellum revealed with 7T fMRI. NeuroImage 211: 116624, 2020.

Brady RO, Gonsalvez I, Lee I, Öngür D, Seidman LJ, Schmahmann JD, Eack SM, Keshavan MS, Pascual-Leone A, Halko MA. Cerebellar-prefrontal network connectivity and negative symptoms in schizophrenia. Am J Psychiatry 176: 512-520, 2019.

Braga RM, Buckner RL. Parallel interdigitated distributed networks within the individual estimated by intrinsic functional connectivity. Neuron 95: 457-471.e5, 2017.

Braga RM, DiNicola LM, Becker HC, Buckner RL. Situating the left-lateralized language network in the broader organization of multiple specialized large-scale distributed networks. J Neurophysiol 124: 1415-1448, 2020.

Braga RM, Van Dijk KRA, Polimeni JR, Eldaief MC, Buckner RL. Parallel distributed networks resolved at high resolution reveal close juxtaposition of distinct regions. J Neurophysiol 121: 1513–1534, 2019.

Brissenden JA, Tobyn SM, Osher DE, Levin EJ, Halko MA, Somers DC. Topographic cortico-cerebellar networks revealed by visual attention and working memory. Curr Biol 28:3364-3372, 2018.

Broca P. Comparative anatomy of the cerebral convolutions: The great limbic lobe and the limbic fissure in the mammalian series. *J Comp Neurol* 523: 2501–2554, 2015.

Brunec IK, **Bellana B**, **Ozubko JD**, **Man V**, **Robin J**, **Liu Z-X**, **Grady C**, **Rosenbaum RS**, **Winocur G**, **Barense MD**, **Moscovitch M**. Multiple Scales of Representation along the Hippocampal Anteroposterior Axis in Humans. *Current Biology* 28: 2129-2135.e6, 2018.

Buckner RL. The cerebellum and cognitive function: 25 years of insight from anatomy and neuroimaging. Neuron 80: 807–815, 2013.

Buckner RL, **Andrews-Hanna JR**, **Schacter DL**. The Brain's Default Network: Anatomy, Function, and Relevance to Disease. *Annals of the New York Academy of Sciences* 1124: 1–38, 2008.

Buckner RL, **Carroll DC**. Self-projection and the brain. *Trends Cogn Sci* 11: 49–57, 2007.

Buckner RL, DiNicola LM. The brain's default network: Updated anatomy, physiology and evolving insights. Nat Rev Neurosci 20: 593–608, 2019.

Buckner RL, Krienen FM, Castellanos A, Diaz JC, Yeo BTT. The organization of the human cerebellum estimated by intrinsic functional connectivity. J Neurophysiol 106: 2322–2345, 2011.

Buckner RL, Krienen FM, Yeo BTT. Opportunities and limitations of intrinsic functional connectivity MRI. Nat Neurosci 16: 832-837, 2013.

Buckner RL, **Margulies DS**. Macroscale cortical organization and a default-like apex transmodal network in the marmoset monkey. *Nature Communications* 10, 2019.

Bushara KO, **Wheat JM**, **Khan A**, **Mock BJ**, **Turski PA**, **Sorenson J**, **Brooks BR**. Multiple tactile maps in the human cerebellum : NeuroReport. *Neuroreport* 12: 2483–2486, 2001.

Carr VA, **Rissman J**, **Wagner AD**. Imaging the Human Medial Temporal Lobe with High-Resolution fMRI. *Neuron* 65: 298–308, 2010.

Chaplin TA, **Yu H-H**, **Soares JGM**, **Gattass R**, **Rosa MGP**. A Conserved Pattern of Differential Expansion of Cortical Areas in Simian Primates. *J Neurosci* 33: 15120–15125, 2013.

Coffman KA, **Dum RP**, **Strick PL**. Cerebellar vermis is a target of projections from the motor areas

in the cerebral cortex. *Proc Natl Acad Sci U S A* 108: 16068–16073, 2011.

Cox RW. AFNI: Software for analysis and visualization of functional magnetic resonance neuroimages. Comput Biomed Res Int J 29: 162–173, 1996.

Cox RW. AFNI: What a long strange trip it's been. Neuroimage 62: 743–747, 2012.

Damadian R. Tumor Detection by Nuclear Magnetic Resonance. *Science* 171: 1151–1153, 1971.

Daselaar S, **Prince S**, **Dennis N**, **Hayes S**, **Kim H**, **Cabeza R**. Posterior midline and ventral parietal activity is associated with retrieval success and encoding failure [Online]. *Frontiers in Human Neuroscience* 3, 2009https://www.frontiersin.org/articles/10.3389/neuro.09.013.2009 [29 Jan. 2023].

Daselaar SM, **Prince SE**, **Cabeza R**. When less means more: deactivations during encoding that predict subsequent memory. *NeuroImage* 23: 921–927, 2004.

Desmond JE, Chen SA, Shieh PB. Cerebellar transcranial magnetic stimulation impairs verbal working memory. Ann Neurol 58: 553-560, 2005

DeYoe EA, **Carman GJ**, **Bandettini P**, **Glickman S**, **Wieser J**, **Cox R**, **Miller D**, **Neitz J**. Mapping striate and extrastriate visual areas in human cerebral cortex. *Proceedings of the National Academy of Sciences* 93: 2382–2386, 1996.

Diedrichsen J, King M, Hernandez-Castillo C, Sereno M, Ivry RB. Universal transform or multiple functionality? Understanding the contribution of the human cerebellum across task domains. Neuron 102: 918–928, 2019.

Diedrichsen J, Zotow E. Surface-based display of volume-averaged cerebellar imaging data. PLOS ONE 10: e0133402, 2015.

DiNicola LM, **Ariyo OI**, **Buckner RL**. Functional Specialization of Parallel Distributed Networks Revealed by Analysis of Trial-to-Trial Variation in Processing Demands. *Journal of Neurophysiology* 129: 17–40, 2023.

DiNicola LM, Braga RM, Buckner RL. Parallel distributed networks dissociate episodic and social functions within the individual. J Neurophysiol 123: 1144–1179, 2020.

DiNicola LM, **Buckner RL**. Precision estimates of parallel distributed association networks: evidence for domain specialization and implications for evolution and development. *Curr Opin Behav Sci* 40: 120–129, 2021.

Dobbins IG, **Rice HJ**, **Wagner AD**, **Schacter DL**. Memory orientation and success: separable neurocognitive components underlying episodic recognition. *Neuropsychologia* 41: 318–333, 2003.

Dolorfo CL, **Amaral DG**. Entorhinal cortex of the rat: Topographic organization of the cells of origin of the perforant path projection to the dentate gyrus. *Journal of Comparative Neurology* 398: 25–48, 1998.

Dosenbach NUF, **Koller JM**, **Earl EA**, **Miranda-Dominguez O**, **Klein RL**, **Van AN**, **Snyder AZ**, **Nagel BJ**, **Nigg JT**, **Nguyen AL**, **Wesevich V**, **Greene DJ**, **Fair DA**. Real-time motion analytics during brain MRI improve data quality and reduce costs. *NeuroImage* 161: 80–93, 2017.

Dosenbach NUF, **Visscher KM**, **Palmer ED**, **Miezin FM**, **Wenger KK**, **Kang HC**, **Burgund ED**, **Grimes AL**, **Schlaggar BL**, **Petersen SE**. A Core System for the Implementation of Task Sets. *Neuron* 50: 799–812, 2006.

Doucet G, **Naveau M**, **Petit L**, **Delcroix N**, **Zago L**, **Crivello F**, **Jobard G**, **Tzourio-Mazoyer N**, **Mazoyer B**, **Mellet E**, **Joliot M**. Brain activity at rest: a multiscale hierarchical functional organization. *J Neurophysiol* 105: 2753–2763, 2011.

Dow RS, **Anderson R**. Cerebellar action potentials in response to stimulation of proprioceptors in the rat. *J Neurophysiol* 5: 363–371, 1942.

Eichenbaum H. A cortical–hippocampal system for declarative memory. *Nat Rev Neurosci* 1: 41–50, 2000.

Eichenbaum H, **Cohen NJ**. Can We Reconcile the Declarative Memory and Spatial Navigation Views on Hippocampal Function? *Neuron* 83: 764–770, 2014.

Ekstrom AD, **Bazih AJ**, **Suthana NA**, **Al-Hakim R**, **Ogura K**, **Zeineh M**, **Burggren AC**, **Bookheimer SY**. Advances in high-resolution imaging and computational unfolding of the human hippocampus. *NeuroImage* 47: 42–49, 2009.

Elul R. Regional differences in the hippocampus of the cat. *Electroencephalogr Clin Neurophysiol* 16: 470–488, 1964.

Engel SA, **Glover GH**, **Wandell BA**. Retinotopic organization in human visual cortex and the spatial precision of functional MRI. *Cerebral Cortex* 7: 181–192, 1997.

Epstein R, **Harris A**, **Stanley D**, **Kanwisher N**. The Parahippocampal Place Area: Recognition, Navigation, or Encoding? *Neuron* 23: 115–125, 1999.

Epstein R, **Kanwisher N**. A cortical representation of the local visual environment. *Nature* 392: 598–601, 1998.

Epstein RA. Parahippocampal and retrosplenial contributions to human spatial navigation. *Trends Cogn Sci* 12: 388–396, 2008.

Esterman M, Thai M, Okabe H, DeGutis J, Saad E, Laganiere SE, Halko MA. Network-targeted cerebellar transcranial magnetic stimulation improves attentional control. NeuroImage 156: 190-198, 2017.

Evarts EV, **Thach WT**. Motor Mechanisms of the CNS: Cerebrocerebellar Interrelations. *Annu Rev Physiol* 31: 451–498, 1969.

Fedorenko E, Duncan J, Kanwisher N. Language-selective and domain-general regions lie side by side within Broca's area. Curr Biol 22: 2059–2062, 2012.

Fedorenko E, **Hsieh P-J**, **Nieto-Castañón A**, **Whitfield-Gabrieli S**, **Kanwisher N**. New Method for fMRI Investigations of Language: Defining ROIs Functionally in Individual Subjects. *Journal of Neurophysiology* 104: 1177–1194, 2010.

Feinberg DA, **Moeller S**, **Smith SM**, **Auerbach E**, **Ramanna S**, **Glasser MF**, **Miller KL**, **Ugurbil K**, **Yacoub E**. Multiplexed Echo Planar Imaging for Sub-Second Whole Brain FMRI and Fast Diffusion Imaging. *PLOS ONE* 5: e15710, 2010.

Fischl B. FreeSurfer. NeuroImage 62: 774–781, 2012.

Fischl B, Rajendran N, Busa E, Augustinack J, Hinds O, Yeo BTT, Mohlberg H, Amunts K, Zilles K. Cortical folding patterns and predicting cytoarchitecture. Cereb Cortex 18: 1973–1980, 2008.

Fischl B, **Salat DH**, **Busa E**, **Albert M**, **Dieterich M**, **Haselgrove C**, **van der Kouwe A**, **Killiany R**, **Kennedy D**, **Klaveness S**, **Montillo A**, **Makris N**, **Rosen B**, **Dale AM**. Whole brain segmentation: automated labeling of neuroanatomical structures in the human brain. *Neuron* 33: 341–355, 2002.

Fischl B, **Salat DH**, **van der Kouwe AJW**, **Makris N**, **Ségonne F**, **Quinn BT**, **Dale AM**. Sequence-independent segmentation of magnetic resonance images. *Neuroimage* 23 Suppl 1: S69-84, 2004.

Fischl B, Sereno MI, Dale AM. Cortical surface-based analysis. II: Inflation, flattening, and a surface-based coordinate system. NeuroImage 9: 195–207, 1999.

Fox MD, Raichle ME. Spontaneous fluctuations in brain activity observed with functional magnetic resonance imaging. Nat Rev Neurosci 8: 700–711, 2007.

Fox MD, **Snyder AZ**, **Barch DM**, **Gusnard DA**, **Raichle ME**. Transient BOLD responses at block transitions. *NeuroImage* 28: 956–966, 2005a.

Fox MD, **Snyder AZ**, **Vincent JL**, **Corbetta M**, **Van Essen DC**, **Raichle ME**. The human brain is intrinsically organized into dynamic, anticorrelated functional networks. *Proc Natl Acad Sci U S A* 102: 9673–9678, 2005b.

Fox PT, **Raichle ME**. Focal physiological uncoupling of cerebral blood flow and oxidative metabolism during somatosensory stimulation in human subjects. *Proc Natl Acad Sci* 83: 1140–1144, 1986.

Frank LE, **Bowman CR**, **Zeithamova D**. Differential Functional Connectivity along the Long Axis of the Hippocampus Aligns with Differential Role in Memory Specificity and Generalization. *Journal of Cognitive Neuroscience* 31: 1958–1975, 2019.

Fransson P. Spontaneous low-frequency BOLD signal fluctuations: An fMRI investigation of the resting-state default mode of brain function hypothesis. *Human Brain Mapping* 26: 15–29, 2005.

Fricke R, **Cowan WM**. An autoradiographic study of the commissural and ipsilateral hippocampo-dentate projections in the adult rat. *Journal of Comparative Neurology* 181: 253–269, 1978.

Fyhn M, **Molden S**, **Hollup S**, **Moser M-B**, **Moser EI**. Hippocampal Neurons Responding to First-Time Dislocation of a Target Object. *Neuron* 35: 555–566, 2002.

Fyhn M, **Molden S**, **Witter MP**, **Moser EI**, **Moser M-B**. Spatial Representation in the Entorhinal Cortex. *Science* 305: 1258–1264, 2004.

Gilmore AW, **Nelson SM**, **McDermott KB**. A parietal memory network revealed by multiple MRI methods. *Trends in Cognitive Sciences* 19: 534–543, 2015.

Gilmore AW, **Quach A**, **Kalinowski SE**, **González-Araya EI**, **Gotts SJ**, **Schacter DL**, **Martin A**. Evidence supporting a time-limited hippocampal role in retrieving autobiographical memories. *Proc Natl Acad Sci* 118: e2023069118, 2021.

Glasser MF, **Sotiropoulos SN**, **Wilson JA**, **Coalson TS**, **Fischl B**, **Andersson JL**, **Xu J**, **Jbabdi S**, **Webster M**, **Polimeni JR**, **Van Essen DC**, **Jenkinson M**. The minimal preprocessing pipelines for the Human Connectome Project. *NeuroImage* 80: 105–124, 2013.

Goldman-Rakic PS. Topography of Cognition: Parallel Distributed Networks in Primate Association Cortex. *Annu Rev Neurosci* 11: 137–156, 1988.

Gordon EM, Laumann TO, Adeyemo B, Huckins JF, Kelley WM, Petersen SE. Generation and evaluation of a cortical area parcellation from resting-state correlations. Cereb Cortex 26: 288–303, 2016.

Gordon EM, Laumann TO, Gilmore AW, Newbold DJ, Greene DJ, Berg JJ, Ortega M, Hoyt-Drazen C, Gratton C, Sun H, Hampton JM, Coalson RS, Nguyen AL, McDermott KB, Shimony JS, Snyder AZ, Schlaggar BL, Petersen SE, Nelson SM, Dosenbach NUF. Precision functional mapping of individual human brains. Neuron 95: 791-807.e7, 2017.

Gordon EM, Laumann TO, Marek S, Raut RV, Gratton C, Newbold DJ, Greene DJ, Coalson RS, Snyder AZ, Schlaggar BL, Petersen SE, Dosenbach NUF, Nelson SM. Default-mode network streams for coupling to language and control systems. Proc Natl Acad Sci U S A 117: 17308-17319, 2020.

Green JD. The Hippocampus. *Physiol Rev* 44: 561–608, 1964.

Greicius MD, **Krasnow B**, **Reiss AL**, **Menon V**. Functional connectivity in the resting brain: A network analysis of the default mode hypothesis. *Proceedings of the National Academy of Sciences* 100: 253–258, 2003.

Greicius MD, **Srivastava G**, **Reiss AL**, **Menon V**. Default-mode network activity distinguishes Alzheimer's disease from healthy aging: Evidence from functional MRI. *Proceedings of the National Academy of Sciences* 101: 4637–4642, 2004.

Grodd W, **Hülsmann E**, **Lotze M**, **Wildgruber D**, **Erb M**. Sensorimotor mapping of the human cerebellum: fMRI evidence of somatotopic organization. *Hum Brain Mapp* 13: 55–73, 2001.

Guell X, Gabrieli JDE, Schmahmann JD. Triple representation of language, working memory, social and emotion processing in the cerebellum: Convergent evidence from task and seed-

based resting-state fMRI analyses in a single large cohort. NeuroImage 172: 437–449, 2018a.

Guell X, Schmahmann JD, Gabrieli JDE, Ghosh SS. Functional gradients of the cerebellum. eLife 7: e36652, 2018b.

Guell X, Goncalves M, Kaczmarzyk JR, Gabrieli JDE, Schmahmann JD, Ghosh SS. LittleBrain: A gradient-based tool for the topographical interpretation of cerebellar neuroimaging findings. PLOS ONE 14: e0210028, 2019.

Habas C, Kamdar N, Nguyen D, Prater K, Beckmann CF, Menon V, Greicius MD. Distinct cerebellar contributions to intrinsic connectivity networks. J Neurosci 29: 8586–8594, 2009.

Hafting T, **Fyhn M**, **Molden S**, **Moser M-B**, **Moser EI**. Microstructure of a spatial map in the entorhinal cortex. *Nature* 436: 801–806, 2005.

Hartley T, **Maguire EA**, **Spiers HJ**, **Burgess N**. The well-worn route and the path less traveled: distinct neural bases of route following and wayfinding in humans. *Neuron* 37: 877–888, 2003.

Hassabis D, **Kumaran D**, **Maguire EA**. Using Imagination to Understand the Neural Basis of Episodic Memory. *J Neurosci* 27: 14365–14374, 2007a.

Hassabis D, **Kumaran D**, **Vann SD**, **Maguire EA**. Patients with hippocampal amnesia cannot imagine new experiences. *Proc Natl Acad Sci* 104: 1726–1731, 2007b.

Hassabis D, **Maguire EA**. Deconstructing episodic memory with construction. *Trends in Cognitive Sciences* 11: 299–306, 2007.

Hassabis D, **Spreng RN**, **Rusu AA**, **Robbins CA**, **Mar RA**, **Schacter DL**. Imagine All the People: How the Brain Creates and Uses Personality Models to Predict Behavior. *Cerebral Cortex* 24: 1979–1987, 2014.

Herzfeld DJ, Kojima Y, Soetedjo R, Shadmehr R. Encoding of action by the Purkinje cells of the cerebellum. Nature 526: 439-442, 2015.

Hirshhorn M, **Grady C**, **Rosenbaum RS**, **Winocur G**, **Moscovitch M**. Brain regions involved in the retrieval of spatial and episodic details associated with a familiar environment: An fMRI study. *Neuropsychologia* 50: 3094–3106, 2012.

Huang CM, **Liu G**. Auditory responses in the posterior vermis of the cat: The buried cerebellar cortex. *Brain Res* 553: 201–205, 1991.

Huntenburg JM, Bazin P-L, Margulies DS. Large-scale gradients in human cortical organization. Trends Cogn Sci 22: 21–31, 2018.

Huth AG, de Heer WA, Griffiths TL, Theunissen FE, Gallant JL. Natural speech reveals the semantic maps that tile human cerebral cortex. Nature 532: 453–458, 2016.

Insausti R, **Amaral DG**. Entorhinal cortex of the monkey: IV. Topographical and laminar organization of cortical afferents. *Journal of Comparative Neurology* 509: 608–641, 2008.

Insausti R, **Amaral DG**, **Cowan WM**. The entorhinal cortex of the monkey: II. Cortical afferents. *Journal of Comparative Neurology* 264: 356–395, 1987.

Jenkinson M, Beckmann CF, Behrens TEJ, Woolrich MW, Smith SM. FSL. NeuroImage 62: 782–790, 2012.

Johnston JM, **Vaishnavi SN**, **Smyth MD**, **Zhang D**, **He BJ**, **Zempel JM**, **Shimony JS**, **Snyder AZ**, **Raichle ME**. Loss of Resting Interhemispheric Functional Connectivity after Complete Section of the Corpus Callosum. *J Neurosci* 28: 6453–6458, 2008.

Jung MW, **Wiener SI**, **McNaughton BL**. Comparison of spatial firing characteristics of units in dorsal and ventral hippocampus of the rat. *J Neurosci* 14: 7347–7356, 1994.

Kahn I. Functional-Neuroanatomic Correlates of Recollection: Implications for Models of Recognition Memory. *J Neurosci* 24: 4172–4180, 2004.

Kahn I, **Andrews-Hanna JR**, **Vincent JL**, **Snyder AZ**, **Buckner RL**. Distinct Cortical Anatomy Linked to Subregions of the Medial Temporal Lobe Revealed by Intrinsic Functional Connectivity. *Journal of Neurophysiology* 100: 129–139, 2008.

Kelly RM, Strick PL. Cerebellar loops with motor cortex and prefrontal cortex of a nonhuman primate. J Neurosci 23: 8432-8444, 2003.

Keren-Happuch E, Chen SA, Ho MR, Desmond JE. A meta-analysis of cerebellar contributions to higher cognition from PET and fMRI studies. Hum Brain Mapp 35: 593–615, 2014.

King M, Hernandez-Castillo CR, Poldrack RA, Ivry RB, Diedrichsen J. Functional boundaries in the human cerebellum revealed by a multi-domain task battery. Nat Neurosci 22: 1371–1378, 2019.

Klüver H, **Bucy PC**. Preliminary Analysis of Functions of the Temporal Lobes in Monkeys. *Arch Neurol Psychiatry* 42: 979–1000, 1939.

Kjelstrup KB, **Solstad T**, **Brun VH**, **Hafting T**, **Leutgeb S**, **Witter MP**, **Moser EI**, **Moser M-B**. Finite Scale of Spatial Representation in the Hippocampus. *Science* 321: 140–143, 2008.

Knight RT. Contribution of human hippocampal region to novelty detection. *Nature* 383: 256–259, 1996.

Kong R, Li J, Orban C, Sabuncu MR, Liu H, Schaefer A, Sun N, Zuo X-N, Holmes AJ, Eickhoff SB, Yeo BTT. Spatial topography of individual-specific cortical networks predicts human cognition, personality, and emotion. Cereb Cortex 29: 2533–2551, 2019.

Konishi S, **Donaldson DI**, **Buckner RL**. Transient Activation during Block Transition. *NeuroImage* 13: 364–374, 2001.

Konishi S, **Wheeler ME**, **Donaldson DI**, **Buckner RL**. Neural Correlates of Episodic Retrieval Success. *NeuroImage* 12: 276–286, 2000.

Krienen FM, Buckner RL. Segregated fronto-cerebellar circuits revealed by intrinsic functional connectivity. Cereb Cortex 19: 2485–2497, 2009.

Krubitzer L. The Magnificent Compromise: Cortical Field Evolution in Mammals. *Neuron* 56: 201–208, 2007.

Kwong KK, Belliveau JW, Chesler DA, Goldberg IE, Weisskoff RM, Poncelet BP, Kennedy DN, Hoppel BE, Cohen MS, Turner R. Dynamic magnetic resonance imaging of human brain activity during primary sensory stimulation. Proc Natl Acad Sci U S A 89: 5675–5679, 1992.

Laumann TO, Gordon EM, Adeyemo B, Snyder AZ, Joo SJ, Chen M-Y, Gilmore AW, McDermott KB, Nelson SM, Dosenbach NUF, Schlaggar BL, Mumford JA, Poldrack RA, Petersen SE. Functional system and areal organization of a highly sampled individual human brain. Neuron 87: 657–670, 2015.

Lauterbur PC. Image Formation by Induced Local Interactions: Examples Employing Nuclear Magnetic Resonance. *Nature* 242: 190–191, 1973.

Leiner HC, Leiner AL, Dow RS. Does the cerebellum contribute to mental skills? Behav Neurosci 100: 443–454, 1986.

Leiner HC, Leiner AL, Dow RS. Reappraising the cerebellum: What does the hindbrain contribute to the forebrain? Behav Neurosci 103: 998–1008, 1989.

Leiner HC, Leiner AL, Dow RS. Cognitive and language functions of the human cerebellum. Trends Neurosci 16: 444–447, 1993.

Lepage M, **Habib R**, **Tulving E**. Hippocampal PET activations of memory encoding and retrieval: The HIPER model. *Hippocampus* 8: 313–322, 1998.

Litman L, **Robinson J**, **Abberbock T**. TurkPrime.com: A versatile crowdsourcing data acquisition platform for the behavioral sciences. *Behav Res* 49: 433–442, 2017.

Liu X, **Ramirez S**, **Pang PT**, **Puryear CB**, **Govindarajan A**, **Deisseroth K**, **Tonegawa S**. Optogenetic stimulation of a hippocampal engram activates fear memory recall. *Nature* 484: 381–385, 2012.

Lu J, Liu H, Zhang M, Wang D, Cao Y, Ma Q, Rong D, Wang X, Buckner RL, Li K. Focal pontine lesions provide evidence that intrinsic functional connectivity reflects polysynaptic anatomical pathways. J Neurosci 31: 15065–15071, 2011.

Maguire EA, Burgess N, **Donnett JG**, **Frackowiak RSJ**, **Frith CD**, **O'Keefe J**. Knowing Where and Getting There: A Human Navigation Network. *Science* 280: 921–924, 1998.

Maguire EA, **Frackowiak RSJ**, **Frith CD**. Recalling Routes around London: Activation of the Right Hippocampus in Taxi Drivers. *J Neurosci* 17: 7103–7110, 1997.

Maguire EA, **Gadian DG**, **Johnsrude IS**, **Good CD**, **Ashburner J**, **Frackowiak RSJ**, **Frith CD**. Navigation-related structural change in the hippocampi of taxi drivers. *PNAS* 97: 4398–4403, 2000.

Manni E, **Petrosini L**. A century of cerebellar somatotopy: A debated representation. *Nat Rev Neurosci* 5: 241–249, 2004.

Mansfield P. Multi-planar image formation using NMR spin echoes. *J Phys C Solid State Phys* 10: L55, 1977.

Marcus D, **Harwell J**, **Olsen T**, **Hodge M**, **Glasser M**, **Prior F**, **Jenkinson M**, **Laumann T**, **Curtiss S**, **Van Essen D**. Informatics and Data Mining Tools and Strategies for the Human Connectome Project [Online]. *Frontiers in Neuroinformatics* 5, 2011https://www.frontiersin.org/articles/10.3389/fninf.2011.00004 [5 Mar. 2023].

Marek S, Siegel JS, Gordon EM, Raut RV, Gratton C, Newbold DJ, Ortega M, Laumann TO, Adeyemo B, Miller DB, Zheng A, Lopez KC, Berg JJ, Coalson RS, Nguyen AL, Dierker D, Van AN, Hoyt CR, McDermott KB, Norris SA, Shimony JS, Snyder AZ, Nelson SM, Barch DM, Schlaggar BL, Raichle ME, Petersen SE, Greene DJ, Dosenbach NUF. Spatial and temporal organization of the individual human cerebellum. Neuron 100: 977-993.e7, 2018.

Margulies DS, Ghosh SS, Goulas A, Falkiewicz M, Huntenburg JM, Langs G, Bezgin G, Eickhoff SB, Castellanos FX, Petrides M, Jefferies E, Smallwood J. Situating the default-mode network along a principal gradient of macroscale cortical organization. Proc Natl Acad Sci U S A 113: 12574–12579, 2016.

Matsui T, Koyano KW, Tamura K, Osada T, Adachi Y, Miyamoto K, Chikazoe J, Power JD, Cohen AL, Nelson SM, Wig GS, Barnes KA, Church JA, Vogel AC, Laumann TO, Miezin FM, Schlaggar BL, Petersen SE. Functional network organization of the human brain. Neuron 72: 665–678, 2011.

Maunsell J, **van Essen D**. The connections of the middle temporal visual area (MT) and their relationship to a cortical hierarchy in the macaque monkey. *J Neurosci* 3: 2563–2586, 1983.

Mennes M, Jenkinson M, Valabregue R, Buitelaar JK, Beckmann C, Smith S. Optimizing full-brain coverage in human brain MRI through population distributions of brain size. NeuroImage 98: 513–520, 2014.

Middleton FA, **Strick PL**. Anatomical evidence for cerebellar and basal ganglia involvement in higher cognitive function. *Science* 266: 458–461, 1994.

Middleton FA, Strick PL. Cerebellar projections to the prefrontal cortex of the primate. J Neurosci 21: 700-712, 2001.

Miller MI, **Beg MF**, **Ceritoglu C**, **Stark C**. Increasing the power of functional maps of the medial temporal lobe by using large deformation diffeomorphic metric mapping. *Proceedings of the National Academy of Sciences* 102: 9685–9690, 2005.

Milner B, **Corkin S**, **Teuber H-L**. Further analysis of the hippocampal amnesic syndrome: 14-year follow-up study of H.M. *Neuropsychologia* 6: 215–234, 1968.

Mineroff Z, Blank IA, Mahowald K, Fedorenko E. A robust dissociation among the language, multiple demand, and default mode networks: Evidence from inter-region correlations in effect size. Neuropsychologia 119: 501–511, 2018.

Moeller S, **Yacoub E**, **Olman CA**, **Auerbach E**, **Strupp J**, **Harel N**, **Uğurbil K**. Multiband multislice GE-EPI at 7 tesla, with 16-fold acceleration using partial parallel imaging with application to high spatial and temporal whole-brain fMRI. *Magnetic Resonance in Medicine* 63: 1144–1153, 2010.

Moser E, **Moser MB**, **Andersen P**. Spatial learning impairment parallels the magnitude of dorsal hippocampal lesions, but is hardly present following ventral lesions. *J Neurosci* 13: 3916–3925, 1993.

Moser MB, **Moser EI**, **Forrest E**, **Andersen P**, **Morris RG**. Spatial learning with a minislab in the dorsal hippocampus. *Proceedings of the National Academy of Sciences* 92: 9697–9701, 1995.

Muller RU, **Kubie JL**. The effects of changes in the environment on the spatial firing of hippocampal complex-spike cells. *J Neurosci* 7: 1951–1968, 1987.

Murphy K, Birn RM, Bandettini PA. Resting-state fMRI confounds and cleanup. NeuroImage 80: 349-359, 2013.

Nadel L. Dorsal and ventral hippocampal lesions and behavior. *Physiology & Behavior* 3: 891–900, 1968.

Nasr S, **Liu N**, **Devaney KJ**, **Yue X**, **Rajimehr R**, **Ungerleider LG**, **Tootell RBH**. Scene-Selective Cortical Regions in Human and Nonhuman Primates. *J Neurosci* 31: 13771–13785, 2011.

Nielsen JA, Mair RW, Baker JT, Buckner RL. Precision brain morphometry: Feasibility and opportunities of extreme rapid scans. bioRxiv 530436, 2019.

Nitschke MF, **Kleinschmidt A**, **Wessel K**, **Frahm J**. Somatotopic motor representation in the human anterior cerebellum A high-resolution functional MRI study. *Brain* 119: 1023–1029, 1996.

O'Craven KM, **Kanwisher N**. Mental Imagery of Faces and Places Activates Corresponding Stimulus-Specific Brain Regions. *J Cogn Neurosci* 12: 1013–1023, 2000.

Ogawa S, **Lee TM**, **Kay AR**, **Tank DW**. Brain magnetic resonance imaging with contrast dependent on blood oxygenation. *Proc Natl Acad Sci* 87: 9868–9872, 1990.

Ogawa S, Tank DW, Menon R, Ellermann JM, Kim SG, Merkle H, Ugurbil K. Intrinsic signal changes accompanying sensory stimulation: Functional brain mapping with magnetic resonance imaging. Proc Natl Acad Sci U S A 89: 5951–5955, 1992.

O'Keefe J. Place units in the hippocampus of the freely moving rat. *Experimental Neurology* 51: 78–109, 1976.

O'Keefe J, **Burgess N**. Geometric determinants of the place fields of hippocampal neurons. *Nature* 381: 425–428, 1996.

O'Keefe J, **Dostrovsky J**. The hippocampus as a spatial map. Preliminary evidence from unit activity in the freely-moving rat. *Brain Research* 34: 171–175, 1971.

Okuda J, **Fujii T**, **Ohtake H**, **Tsukiura T**, **Tanji K**, **Suzuki K**, **Kawashima R**, **Fukuda H**, **Itoh M**, **Yamadori A**. Thinking of the future and past: the roles of the frontal pole and the medial temporal lobes. *NeuroImage* 19: 1369–1380, 2003.

Optican LM, Robinson DA. Cerebellar-dependent adaptive control of primate saccadic system. J Neurophysiol 44: 1058-1077, 1980.

Pandya DN, **Vignolo LA**. Intra- and interhemispheric projections of the precentral, premotor and arcuate areas in the rhesus monkey. *Brain Res* 26: 217–233, 1971.

Penfield W, **Boldrey E**. Somatic motor and sensory representation in the cerebral cortex of man as studied by electrical stimulation. *Brain* 60: 389–443, 1937.

Peters M, **Monjan AA**. Behavior after cerebellar lesions in cats and monkeys. *Physiol Behav* 6: 205–206, 1971.

Petersen SE, Fox PT, Posner MI, Mintun M, Raichle ME. Positron emission tomographic studies of the processing of single words. J Cogn Neurosci 1: 153-170, 1989.

Poppenk J, **Evensmoen HR**, **Moscovitch M**, **Nadel L**. Long-axis specialization of the human hippocampus. *Trends in Cognitive Sciences* 17: 230–240, 2013.

Poppenk J, **Moscovitch M**. A hippocampal marker of recollection memory ability among healthy young adults: contributions of posterior and anterior segments. *Neuron* 72: 931–937, 2011.

Power JD, Cohen AL, Nelson SM, Wig GS, Barnes KA, Church JA, Vogel AC, Laumann TO, Miezin FM, Schlaggar BL, Petersen SE. Functional network organization of the human brain. Neuron 72: 665–678, 2011.

Power JD, Schlaggar BL, Petersen SE. Studying brain organization via spontaneous fMRI signal. Neuron 84: 681-696, 2014.

Przeździk I, **Faber M**, **Fernández G**, **Beckmann CF**, **Haak KV**. The functional organisation of the hippocampus along its long axis is gradual and predicts recollection. *Cortex* 119: 324–335, 2019.

Quigley M, **Cordes D**, **Turski P**, **Moritz C**, **Haughton V**, **Seth R**, **Meyerand ME**. Role of the Corpus Callosum in Functional Connectivity. *American Journal of Neuroradiology* 24: 208–212, 2003.

Rabi II, **Zacharias JR**, **Millman S**, **Kusch P**. A New Method of Measuring Nuclear Magnetic Moment. *Phys Rev* 53: 318–318, 1938.

Rabin JS, **Gilboa A**, **Stuss DT**, **Mar RA**, **Rosenbaum RS**. Common and Unique Neural Correlates of Autobiographical Memory and Theory of Mind. *J Cogn Neurosci* 22: 1095–1111, 2010.

Racine R, **Rose PA**, **Burnham WM**. Afterdischarge Thresholds and Kindling Rates in Dorsal and Ventral Hippocampus and Dentate Gyrus. *Can J Neurol Sci* 4: 273–278, 1977.

Raichle ME, **MacLeod AM**, **Snyder AZ**, **Powers WJ**, **Gusnard DA**, **Shulman GL**. A default mode of brain function. *Proceedings of the National Academy of Sciences* 98: 676–682, 2001.

Ramirez S, **Liu X**, **Lin P-A**, **Suh J**, **Pignatelli M**, **Redondo RL**, **Ryan TJ**, **Tonegawa S**. Creating a False Memory in the Hippocampus. *Science* 341: 387–391, 2013.

Rijntjes M, **Buechel C**, **Kiebel S**, **Weiller C**. Multiple somatotopic representations in the human cerebellum. *Neuroreport* 10: 3653–3658, 1999.

Rolls ET, **Miyashita Y**, **Cahusac PM**, **Kesner RP**, **Niki H**, **Feigenbaum JD**, **Bach L**. Hippocampal neurons in the monkey with activity related to the place in which a stimulus is shown. *J Neurosci* 9: 1835–1845, 1989.

Ryan L, **Lin C-Y**, **Ketcham K**, **Nadel L**. The role of medial temporal lobe in retrieving spatial and nonspatial relations from episodic and semantic memory. *Hippocampus* 20: 11–18, 2010.

Saadon-Grosman N, **Angeli PA**, **DiNicola LM**, **Buckner RL**. A Third Somatomotor Representation in the Human Cerebellum. *Journal of Neurophysiology* 128: 1051–1073, 2022.

Saadon-Grosman N, Tal Z, Itshayek E, Amedi A, Arzy S. Discontinuity of cortical gradients reflects sensory impairment. Proc Natl Acad Sci 112: 16024–16029, 2015.

Schacter DL, **Addis DR**. The cognitive neuroscience of constructive memory: remembering the past and imagining the future. *Philos Trans R Soc B Biol Sci* 362: 773–786, 2007a.

Schacter DL, **Addis DR**. The ghosts of past and future. *Nature* 445: 27–27, 2007b.

Schacter DL, **Addis DR**, **Buckner RL**. Remembering the past to imagine the future: the prospective brain. *Nat Rev Neurosci* 8: 657–661, 2007.

Schacter DL, **Addis DR**, **Buckner RL**. Episodic Simulation of Future Events. *Ann N Y Acad Sci* 1124: 39–60, 2008.

Schacter DL, **Wagner AD**. Medial temporal lobe activations in fMRI and PET studies of episodic encoding and retrieval. *Hippocampus* 9: 7–24, 1999.

Schlerf JE, Verstynen TD, Ivry RB, Spencer RMC. Evidence of a novel somatopic map in the human neocerebellum during com plex actions. J Neurophysiol 103: 3330–3336, 2010.

Schmahmann JD, Guell X, Stoodley CJ, Halko MA. The theory and neuroscience of cerebellar cognition. Annu Rev Neurosci 42: 337–364, 2019.

Schmahmann JD, Pandya DN. The cerebrocerebellar system. Int Rev Neurobiol 41: 31–60, 1997.

Schmahmann JD, Sherman JC. The cerebellar cognitive affective syndrome. Brain 121: 561-579, 1998.

Scoville WB, **Milner B**. Loss of Recent Memory After Bilateral Hippocampal Lesions. *Journal of Neurology, Neurosurgery & Psychiatry* 20: 11–21, 1957.

Seeley WW. The Salience Network: A Neural System for Perceiving and Responding to Homeostatic Demands. *J Neurosci* 39: 9878–9882, 2019.

Seeley WW, **Menon V**, **Schatzberg AF**, **Keller J**, **Glover GH**, **Kenna H**, **Reiss AL**, **Greicius MD**. Dissociable Intrinsic Connectivity Networks for Salience Processing and Executive Control. *J Neurosci* 27: 2349–2356, 2007.

Sereno MI, Diedrichsen J, Tachrount M, Testa-Silva G, d'Arceuil H, De Zeeuw C. The human cerebellum has almost 80% of the surface area of the neocortex. Proc Natl Acad Sci U S A 117: 19538-19543, 2020.

Setsompop K, Gagoski BA, Polimeni JR, Witzel T, Wedeen VJ, Wald LL. Blipped-controlled aliasing in parallel imaging for simultaneous multislice echo planar imaging with reduced g-factor penalty. Magn Reson Med 67: 1210–1224, 2012.

Sheu Y, Liang Y, Desmond JE. Disruption of cerebellar prediction in verbal working memory. Front Hum Neurosci 13: 61, 2019.

Shirer WR, **Ryali S**, **Rykhlevskaia E**, **Menon V**, **Greicius MD**. Decoding Subject-Driven Cognitive States with Whole-Brain Connectivity Patterns. *Cereb Cortex* 22: 158–165, 2012.

Small SA, **Nava AS**, **Perera GM**, **Delapaz R**, **Stern Y**. Evaluating the function of hippocampal subregions with high-resolution MRI in Alzheimer's disease and aging. *Microscopy Research and Technique* 51: 101–108, 2000.

Smith SM, Beckmann CF, Andersson J, Auerbach EJ, Bijsterbosch J, Douaud G, Duff E, Feinberg DA, Griffanti L, Harms MP, et al. Resting-state fMRI in the Human Connectome Project. NeuroImage 80: 144-168, 2013.

Snider RS, **Eldred E**. Cerebro-cerebellar relationships in the monkey. *J Neurophysiol* 15: 27–40, 1952.

Snider RS, Stowell A. Receiving areas of the tactile, auditory, and visual systems in the cerebellum. J Neurophysiol 7: 331–357, 1944.

Soetedjo R, Kojima Y, Fuchs AF. How cerebellar motor learning keeps saccades accurate. J Neurophysiol 121: 2153-2162, 2019.

Sparks DL, Mays LE. Signal transformations required for the generation of saccadic eye movements. Ann Rev Neurosci 13: 309-336, 1990.

Spaniol J, **Davidson PSR**, **Kim ASN**, **Han H**, **Moscovitch M**, **Grady CL**. Event-related fMRI studies of episodic encoding and retrieval: Meta-analyses using activation likelihood estimation. *Neuropsychologia* 47: 1765–1779, 2009.

Squire LR. Memory and the Hippocampus: A Synthesis From Findings With Rats, Monkeys, and Humans. *Psychol Rev* 99: 195–231, 1992.

Stark CEL, **Okado Y**. Making Memories without Trying: Medial Temporal Lobe Activity Associated with Incidental Memory Formation during Recognition. *J Neurosci* 23: 6748–6753, 2003.

Steel A, **Billings MM**, **Silson EH**, **Robertson CE**. A network linking scene perception and spatial memory systems in posterior cerebral cortex. *Nat Commun* 12: 2632, 2021.

Stevens R, **Cowey A**. Effects of dorsal and ventral hippocampal lesions on spontaneous alternation, learned alternation and probability learning in rats. *Brain Research* 52: 203–224, 1973.

Stoodley CJ, Schmahmann JD. Functional topography in the human cerebellum: A meta-analysis of neuroimaging studies. NeuroImage 44: 489–501, 2009.

Strange BA, **Witter MP**, **Lein ES**, **Moser EI**. Functional organization of the hippocampal longitudinal axis. *Nat Rev Neurosci* 15: 655–669, 2014.

Strick PL. How do the basal ganglia and cerebellum gain access to the cortical motor areas? *Behav Brain Res* 18: 107–123, 1985.

Strick PL, Dum RP, Fiez JA. Cerebellum and nonmotor function. Annu Rev Neurosci 32:413–434, 2009.

Sultan F, Braitenberg V. Shapes and sizes of different mammalian cerebella. A study in quantitative comparative neuroanatomy. J Hirnforsch 34: 79–92, 1993.

Sutton S, **Braren M**, **Zubin J**, **John ER**. Evoked-Potential Correlates of Stimulus Uncertainty. *Science* 150: 1187–1188, 1965.

Suzuki WL, **Amaral DG**. Perirhinal and parahippocampal cortices of the macaque monkey: Cortical afferents. *The Journal of Comparative Neurology* 350: 497–533, 1994.

Takagi M, **Zee DS**, **Tamargo RJ**. Effects of lesions of the oculomotor vermis on eye movements in primate: Saccades. *J Neurophysiol* 80: 1911–1931, 1998.

Takanashi M, **Abe K**, **Yanagihara T**, **Sakoda S**, **Tanaka H**, **Hirabuki N**, **Nakamura H**, **Fujita N**. A functional MRI study of somatotopic representation of somatosensory stimulation in the cerebellum. *Neuroradiology* 45: 149–152, 2003.

Tootell RBH, **Hadjikhani NK**, **Mendola JD**, **Marrett S**, **Dale AM**. From retinotopy to recognition: fMRI in human visual cortex. *Trends in Cognitive Sciences* 2: 174–183, 1998.

Treves A, **Rolls ET**. Computational analysis of the role of the hippocampus in memory. *Hippocampus* 4: 374–391, 1994.

van der Kouwe AJW, Benner T, Fischl B, Schmitt F, Salat DH, Harder M, Sorensen AG, Dale AM. On-line automatic slice positioning for brain MR imaging. NeuroImage 27: 222–230, 2005.

van der Kouwe AJW, Benner T, Salat DH, Fischl B. Brain morphometry with multiecho MPRAGE. NeuroImage 40: 559–569, 2008.

van Es DM, van der Zwaag W, Knapen T. Topographic maps of visual space in the human cerebellum. Curr Biol 29: 1689-1694.e3, 2019.

Van Essen DC. Surface-based atlases of cerebellar cortex in the human, macaque, and mouse. Ann N Y Acad Sci 978: 468-479, 2002.

Vincent JL, **Patel GH**, **Fox MD**, **Snyder AZ**, **Baker JT**, **Van Essen DC**, **Zempel JM**, **Snyder LH**, **Corbetta M**, **Raichle ME**. Intrinsic functional architecture in the anaesthetized monkey brain. *Nature* 447: 83–86, 2007.

Vincent JL, **Snyder AZ**, **Fox MD**, **Shannon BJ**, **Andrews JR**, **Raichle ME**, **Buckner RL**. Coherent Spontaneous Activity Identifies a Hippocampal-Parietal Memory Network. *Journal of Neurophysiology* 96: 3517–3531, 2006.

Van Essen DC, Smith SM, Barch DM, Behrens TEJ, Yacoub E, Ugurbil K, WU-Minn HCP Consortium. The WU-Minn Human Connectome Project: An overview. NeuroImage 80: 62–79, 2013.

Wagner AD, **Shannon BJ**, **Kahn I**, **Buckner RL**. Parietal lobe contributions to episodic memory retrieval. *Trends Cogn Sci* 9: 445–453, 2005.

Wandell BA, **Dumoulin SO**, **Brewer AA**. Visual Field Maps in Human Cortex. *Neuron* 56: 366–383, 2007.

Wang D, Buckner RL, Liu H. Cerebellar asymmetry and its relation to cerebral symmetry estimated by intrinsic functional connectivity. J Neurophysiol 109: 46-57, 2013.

Weiskopf N, Hutton C, Josephs O, Deichmann R. Optimal EPI parameters for reduction of susceptibility-induced BOLD sensitivity losses: A whole-brain analysis at 3 T and 1.5 T. NeuroImage 33: 493–504, 2006.

Wheeler ME, **Buckner RL**. Functional Dissociation among Components of Remembering: Control, Perceived Oldness, and Content. *J Neurosci* 23: 3869–3880, 2003.

Whittington JCR, **Muller TH**, **Mark S**, **Chen G**, **Barry C**, **Burgess N**, **Behrens TEJ**. The Tolman-Eichenbaum Machine: Unifying Space and Relational Memory through Generalization in the Hippocampal Formation. *Cell* 183: 1249-1263.e23, 2020.

Wiestler T, McGonigle DJ, Diedrichsen J. Integration of sensory and motor representations of single fingers in the human cerebellum. J Neurophysiol 105: 3042–3053, 2011.

Wig GS, Laumann TO, Petersen SE. An approach for parcellating human cortical areas using resting-state correlations. NeuroImage 93: 276–291, 2014.

Witter MP. Organization of the entorhinal—hippocampal system: A review of current anatomical data. *Hippocampus* 3: 33–44, 1993.

Witter MP, **Amaral DG**. The entorhinal cortex of the monkey: VI. Organization of projections from the hippocampus, subiculum, presubiculum, and parasubiculum. *Journal of Comparative Neurology* 529: 828–852, 2021.

Witter MP, **Hoesen GV**, **Amaral DG**. Topographical organization of the entorhinal projection to the dentate gyrus of the monkey. *J Neurosci* 9: 216–228, 1989.

Woollett K, **Maguire EA**. Acquiring "the Knowledge" of London's Layout Drives Structural Brain Changes. *Current Biology* 21: 2109–2114, 2011.

Woollett K, **Maguire EA**. Exploring anterograde associative memory in London taxi drivers. *Neuroreport* 23: 885–888, 2012.

Xu J, **Moeller S**, **Auerbach EJ**, **Strupp J**, **Smith SM**, **Feinberg DA**, **Yacoub E**, **Uğurbil K**. Evaluation of slice accelerations using multiband echo planar imaging at 3T. *NeuroImage* 83: 991–1001, 2013.

Xu J, Moeller S, Strupp J, Auerbach EJ, Chen L, Feinberg DA, Ugurbil K, Yacoub E. Highly accelerated whole brain imaging using aligned-blipped-controlled-aliasing multiband EPI. Proc Int Soc Mag Reson Med 20: 2306, 2012.

Xue A, **Kong R**, **Yang Q**, **Eldaief MC**, **Angeli PA**, **DiNicola LM**, **Braga RM**, **Buckner RL**, **Yeo BTT**. The detailed organization of the human cerebellum estimated by intrinsic functional connectivity within the individual. *Journal of Neurophysiology* 125: 358–384, 2021.

Yamada J, Noda H. Afferent and efferent connections of the oculomotor cerebellar vermis in the macaque monkey. J Comp Neurol 265: 224-241, 1987.

Yeo BTT, Krienen FM, Sepulcre J, Sabuncu MR, Lashkari D, Hollinshead M, Roffman JL, Smoller JW, Zöllei L, Polimeni JR, Fischl B, Liu H, Buckner RL. The organization of the human cerebral cortex estimated by intrinsic functional connectivity. J Neurophysiol 106: 1125–1165, 2011.

Zeineh MM, **Engel SA**, **Bookheimer SY**. Application of Cortical Unfolding Techniques to Functional MRI of the Human Hippocampal Region. *NeuroImage* 11: 668–683, 2000.

Zeineh MM, **Engel SA**, **Thompson PM**, **Bookheimer SY**. Unfolding the human hippocampus with high resolution structural and functional MRI. *The Anatomical Record* 265: 111–120, 2001.

Zemanick MC, Strick PL, Dix RD. Direction of transneuronal transport of herpes simplex virus 1 in the primate motor system is strain-dependent. Proc Natl Acad Sci USA 88: 8048–8051, 1991.

Zheng A, **Montez DF**, **Marek S**, **Gilmore AW**, **Newbold DJ**, **Laumann TO**, **Kay BP**, **Seider NA**, **Van AN**, **Hampton JM**, **Alexopoulos D**, **Schlaggar BL**, **Sylvester CM**, **Greene DJ**, **Shimony JS**, **Nelson SM**, **Wig GS**, **Gratton C**, **McDermott KB**, **Raichle ME**, **Gordon EM**, **Dosenbach NUF**. Parallel hippocampal-parietal circuits for self- and goal-oriented processing. *Proc Natl Acad Sci USA* 118: e2101743118, 2021.

Zola-Morgan S, **Squire LR**, **Amaral DG**. Human amnesia and the medial temporal region: enduring memory impairment following a bilateral lesion limited to field CA1 of the hippocampus. *J Neurosci* 6: 2950–2967, 1986.
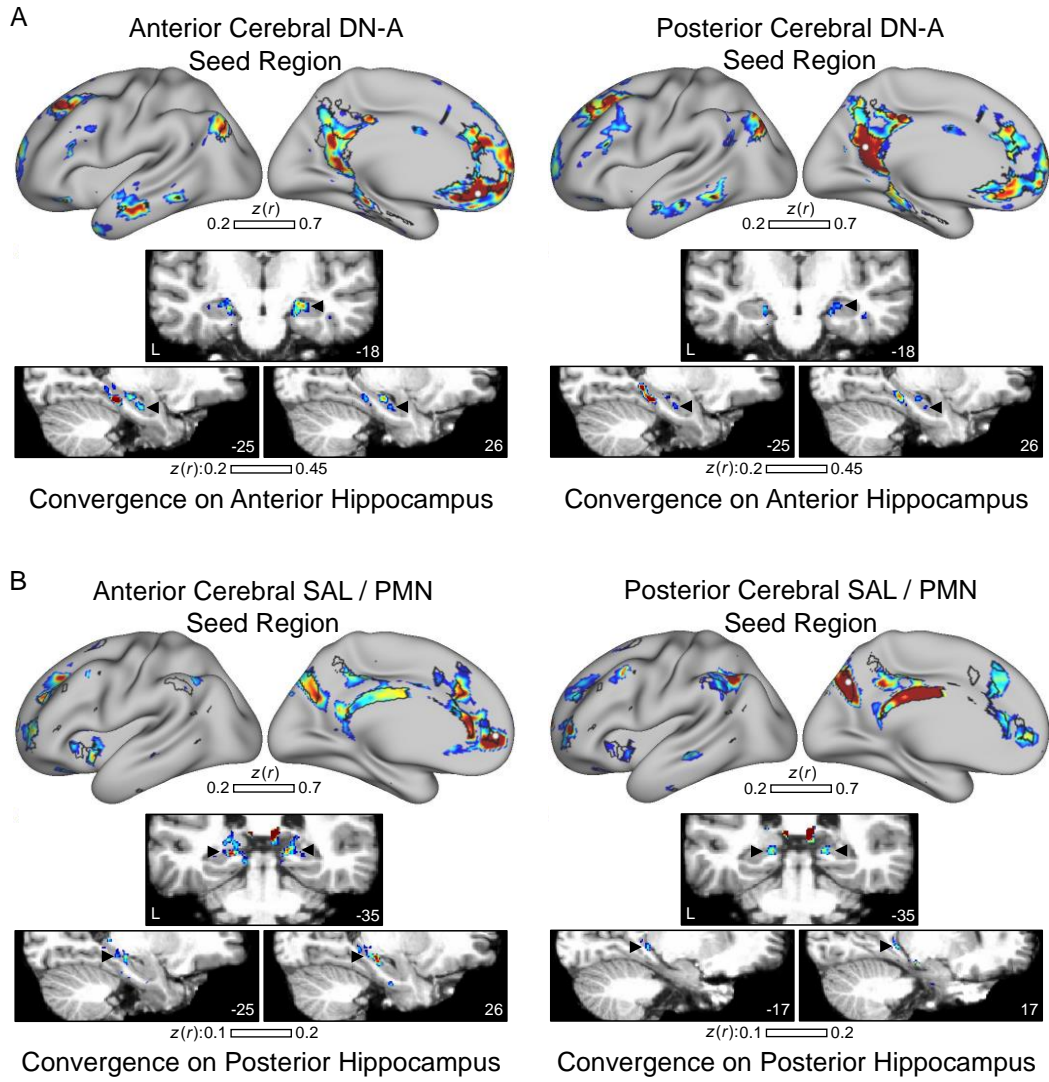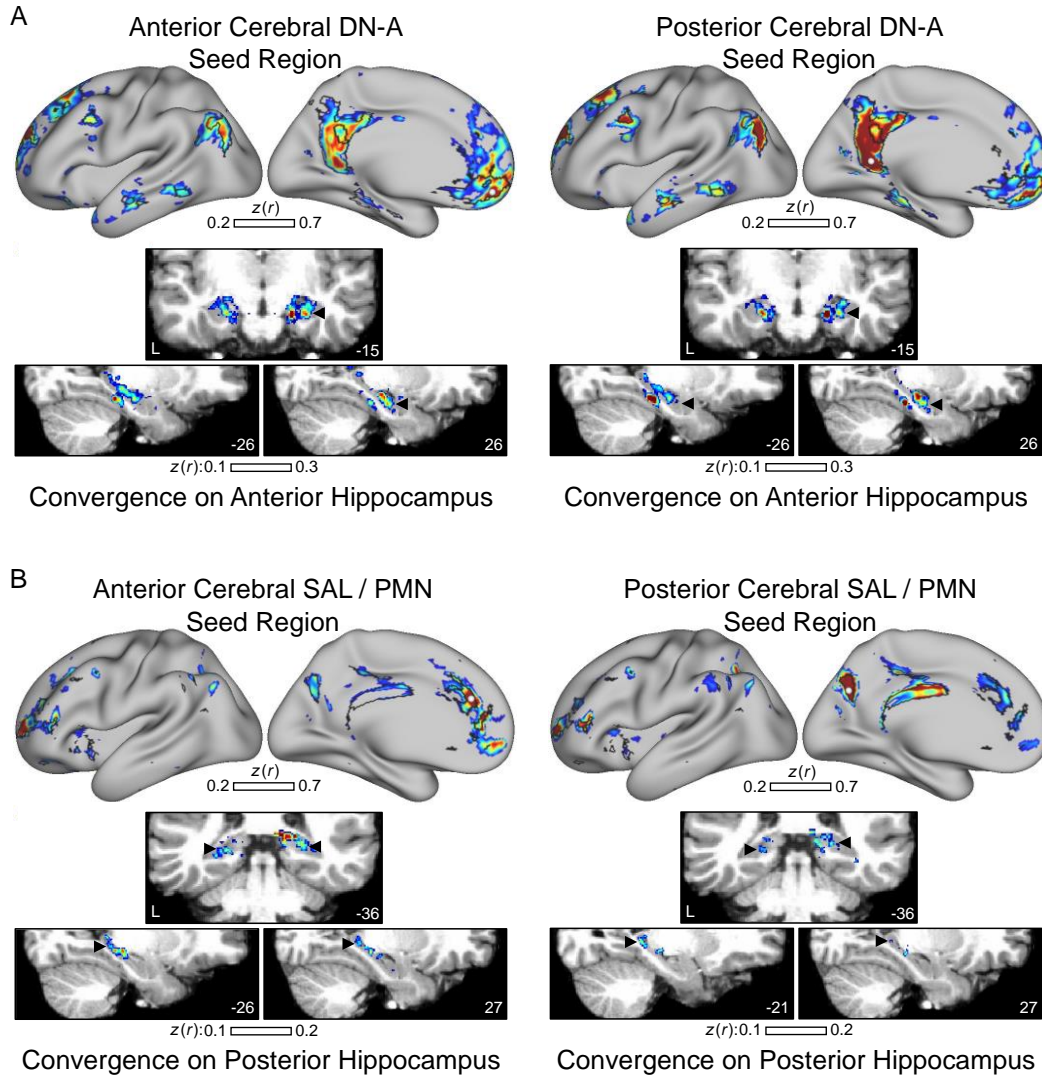
P1
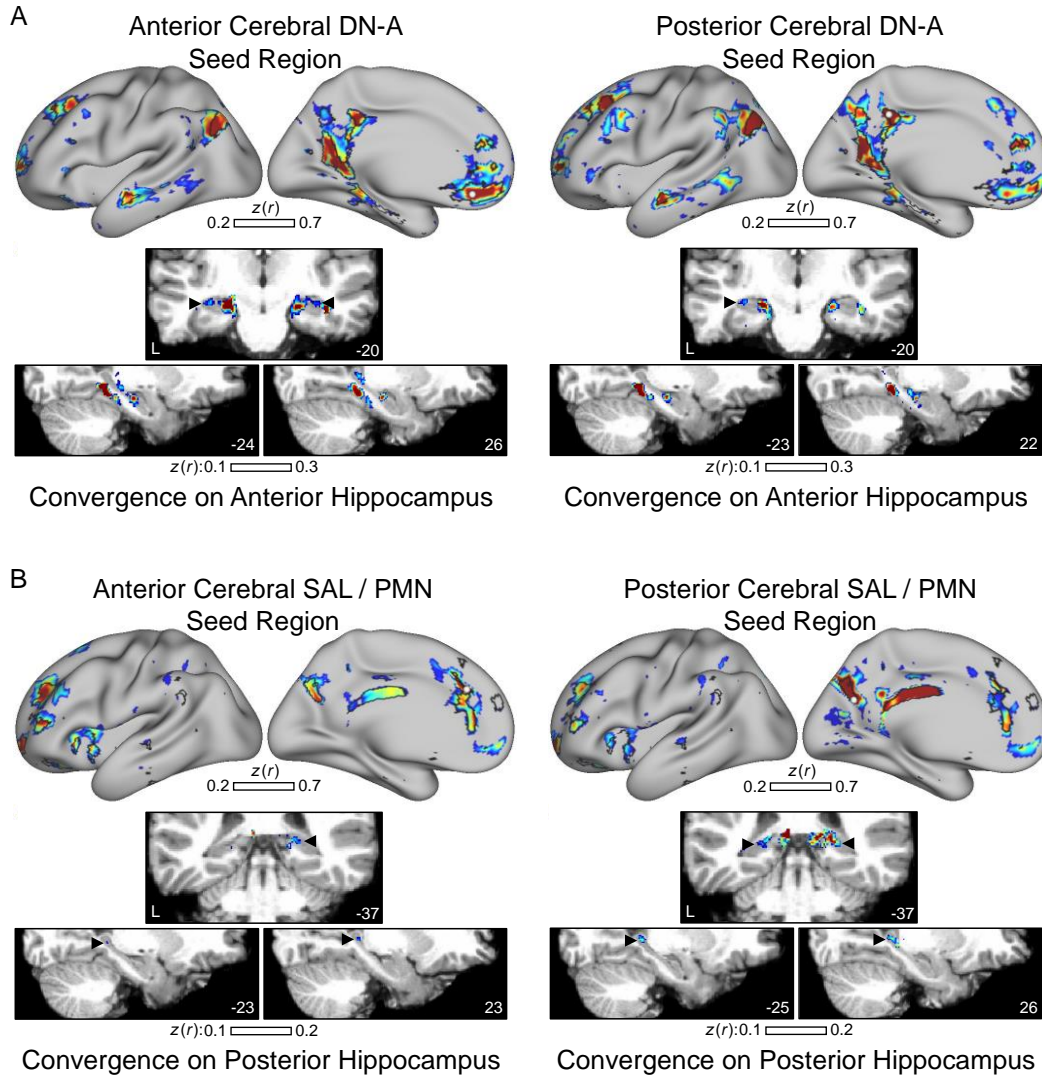
Figure A.1 Seed based functional connectivity, Experiment 2 Participant P1

Figure A.2 Seed based functional connectivity, Experiment 2 Participant P2

P4

A

Anterior Cerebral DN-A
Seed Region

Posterior Cerebral DN-A
Seed Region

Convergence on Anterior Hippocampus

Convergence on Anterior Hippocampus

B

Anterior Cerebral SAL / PMN
Seed Region

Posterior Cerebral SAL / PMN
Seed Region

Convergence on Posterior Hippocampus

Convergence on Posterior Hippocampus
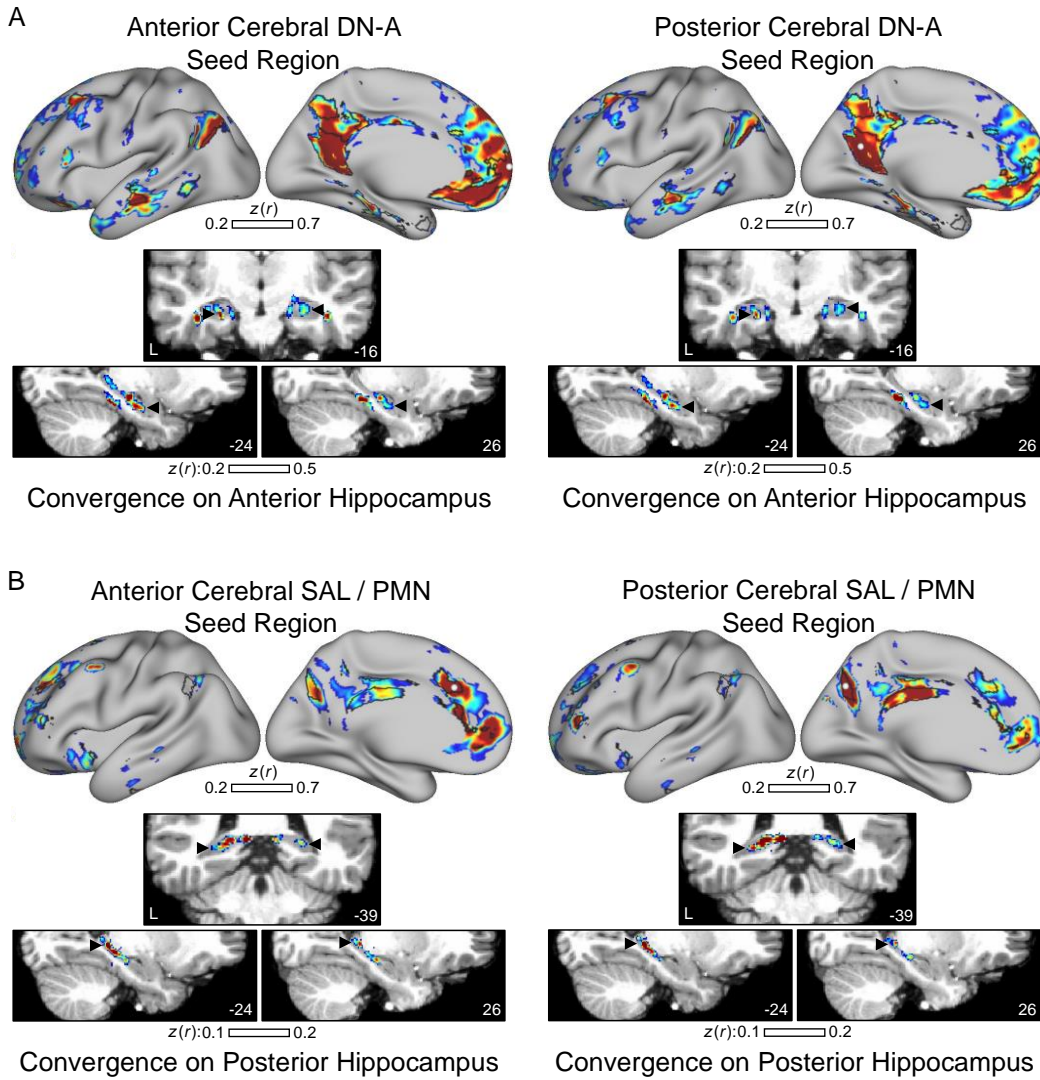
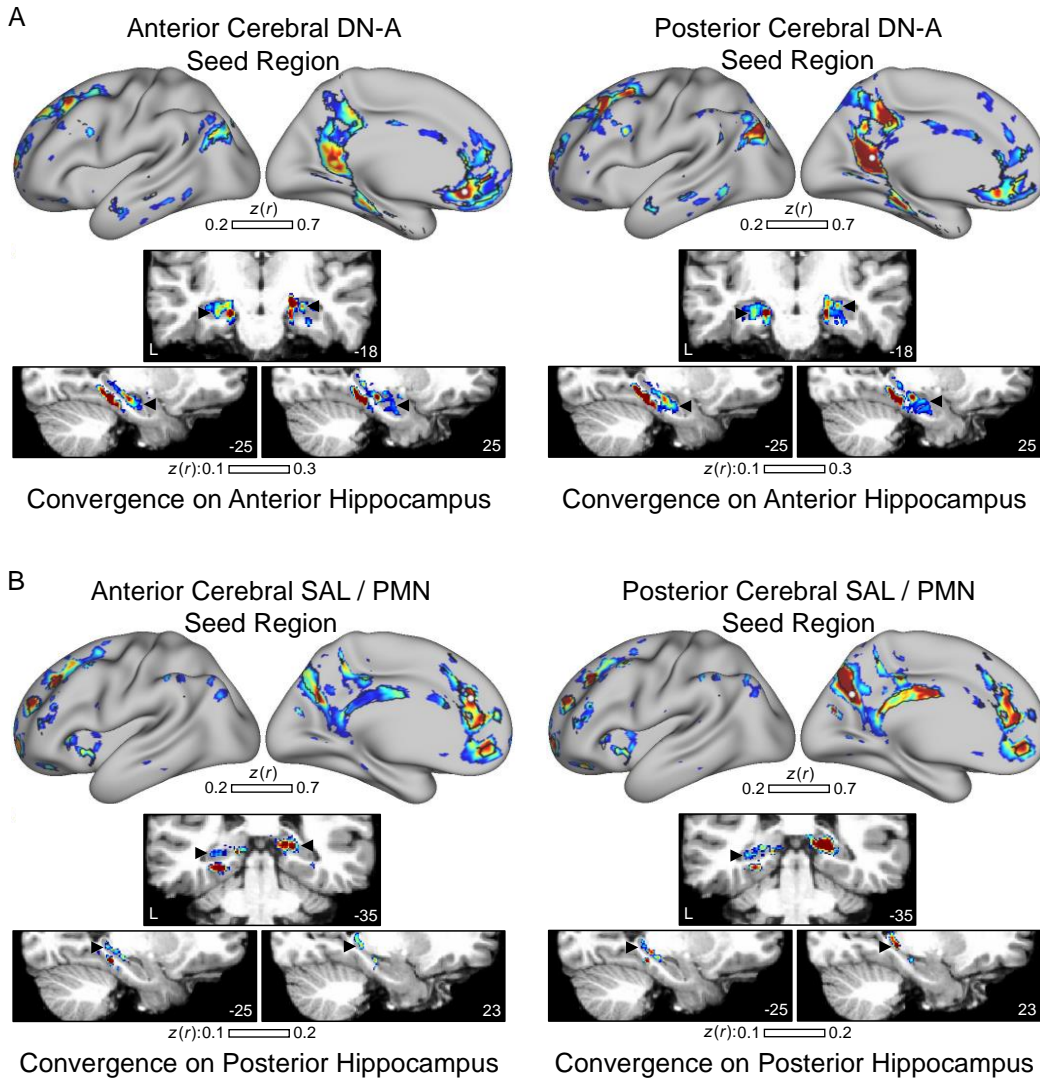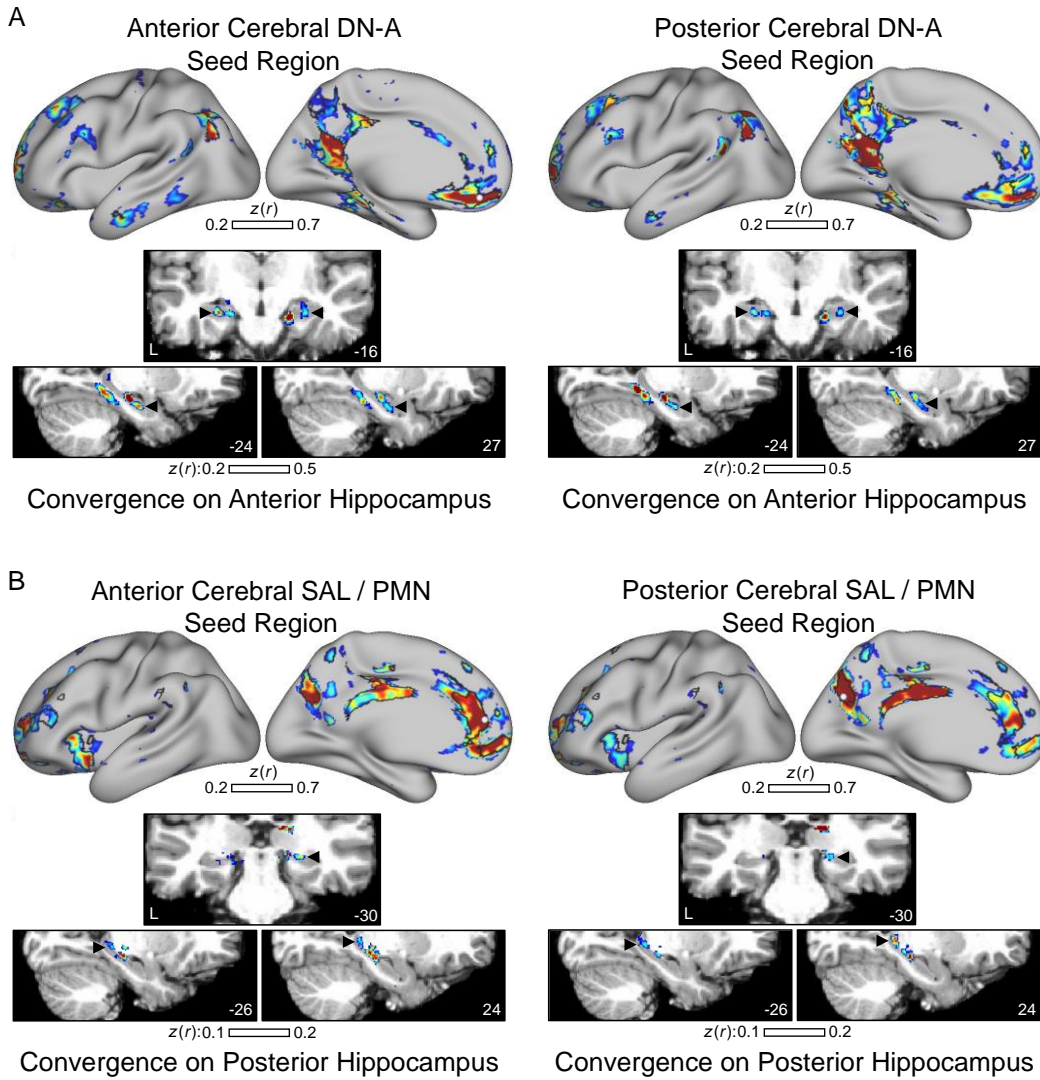**Figure A.3 Seed based functional connectivity, Experiment 2 Participant P4**

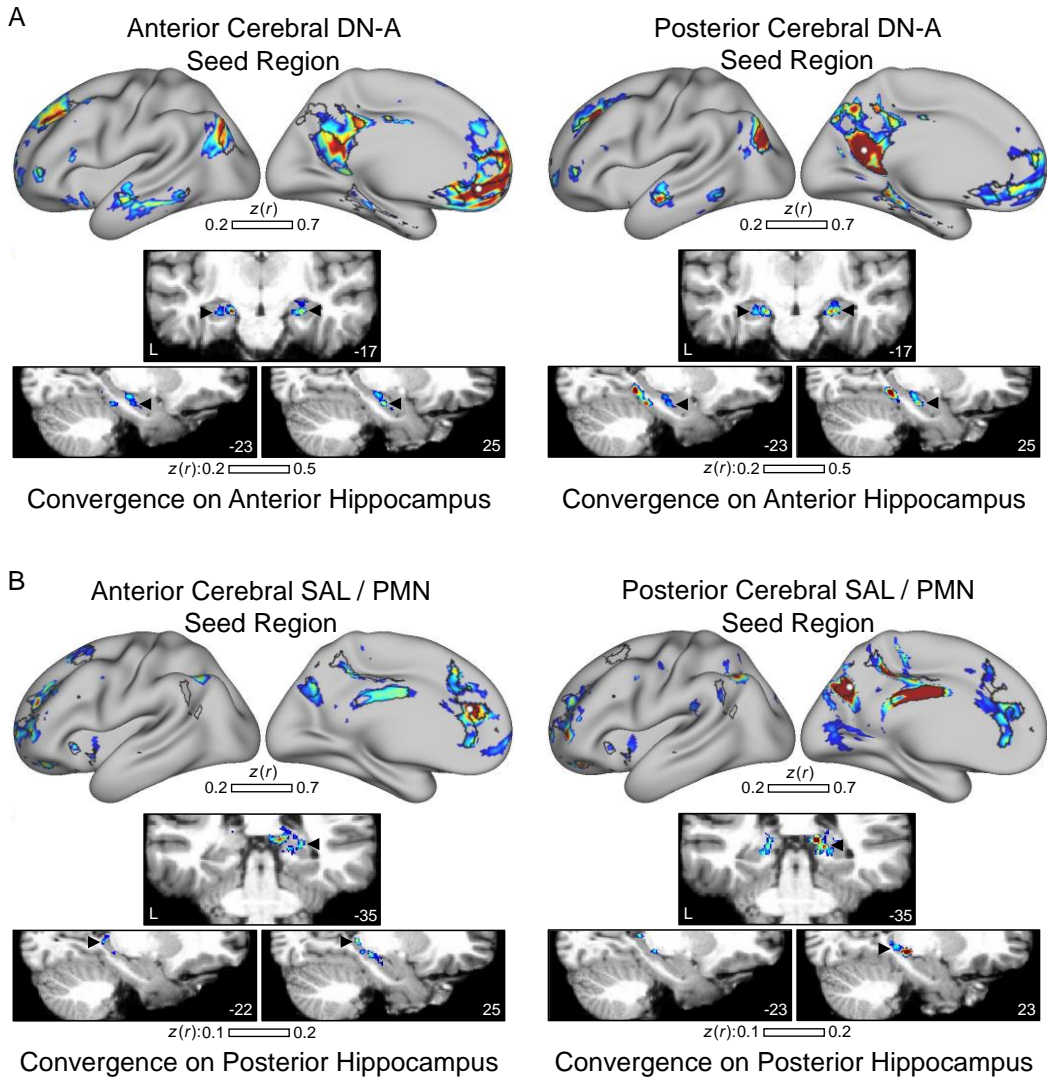**Figure A.4 Seed based functional connectivity, Experiment 2 Participant P6**

P7

A

Anterior Cerebral DN-A
Seed Region

Posterior Cerebral DN-A
Seed Region

Convergence on Anterior Hippocampus

Convergence on Anterior Hippocampus

B

Anterior Cerebral SAL / PMN
Seed Region

Posterior Cerebral SAL / PMN
Seed Region

Convergence on Posterior Hippocampus

Convergence on Posterior Hippocampus

Figure A.5 Seed based functional connectivity, Experiment 2 Participant P7

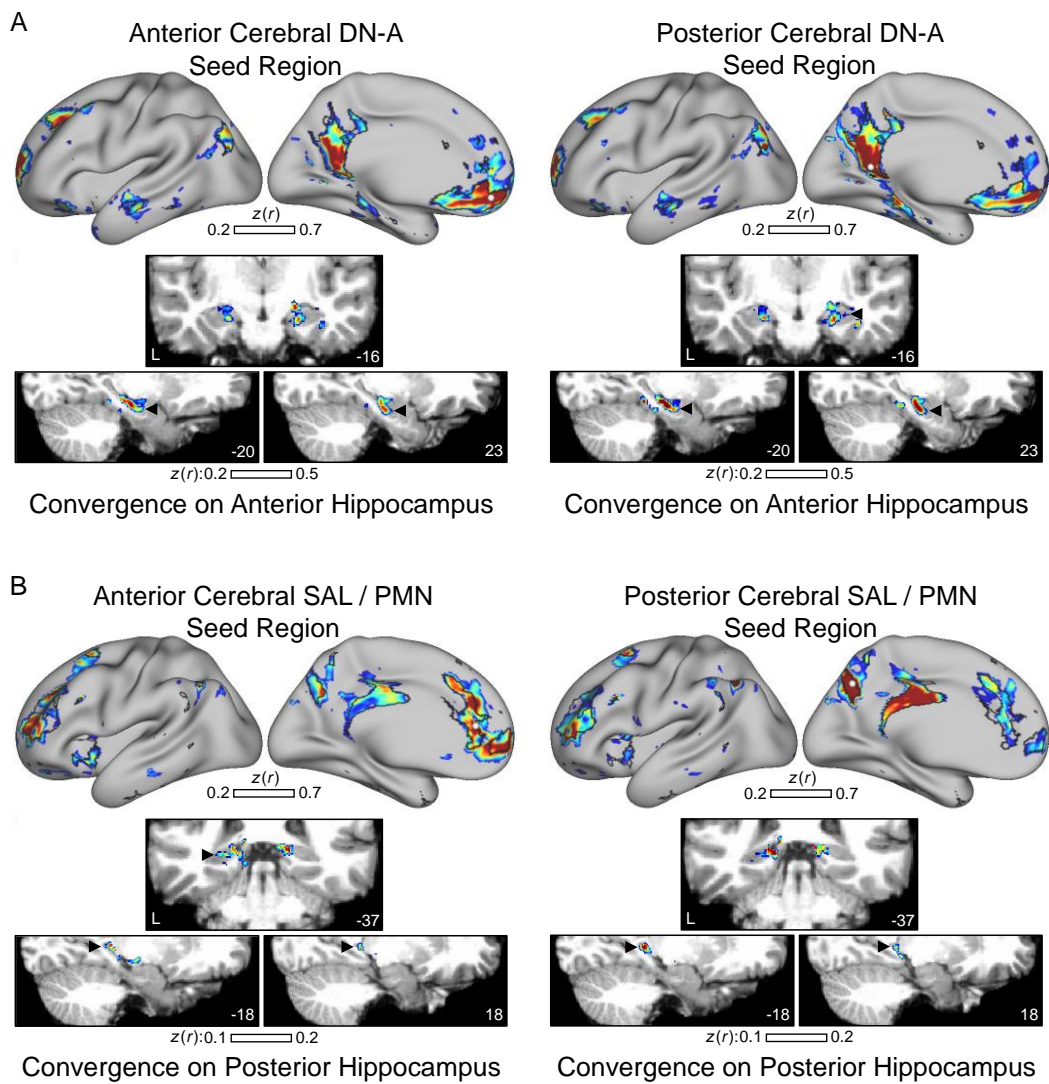Figure A.6 Seed based functional connectivity, Experiment 2 Participant P8

P9

A

Anterior Cerebral DN-A
Seed Region

Posterior Cerebral DN-A
Seed Region

Convergence on Anterior Hippocampus

Convergence on Anterior Hippocampus

B

Anterior Cerebral SAL / PMN
Seed Region

Posterior Cerebral SAL / PMN
Seed Region

Convergence on Posterior Hippocampus

Convergence on Posterior Hippocampus

Figure A.7 Seed based functional connectivity, Experiment 2 Participant P9

P13

A

Anterior Cerebral DN-A
Seed Region

Convergence on Anterior Hippocampus

Posterior Cerebral DN-A
Seed Region

Convergence on Anterior Hippocampus

B

Anterior Cerebral SAL / PMN
Seed Region

Convergence on Posterior Hippocampus

Posterior Cerebral SAL / PMN
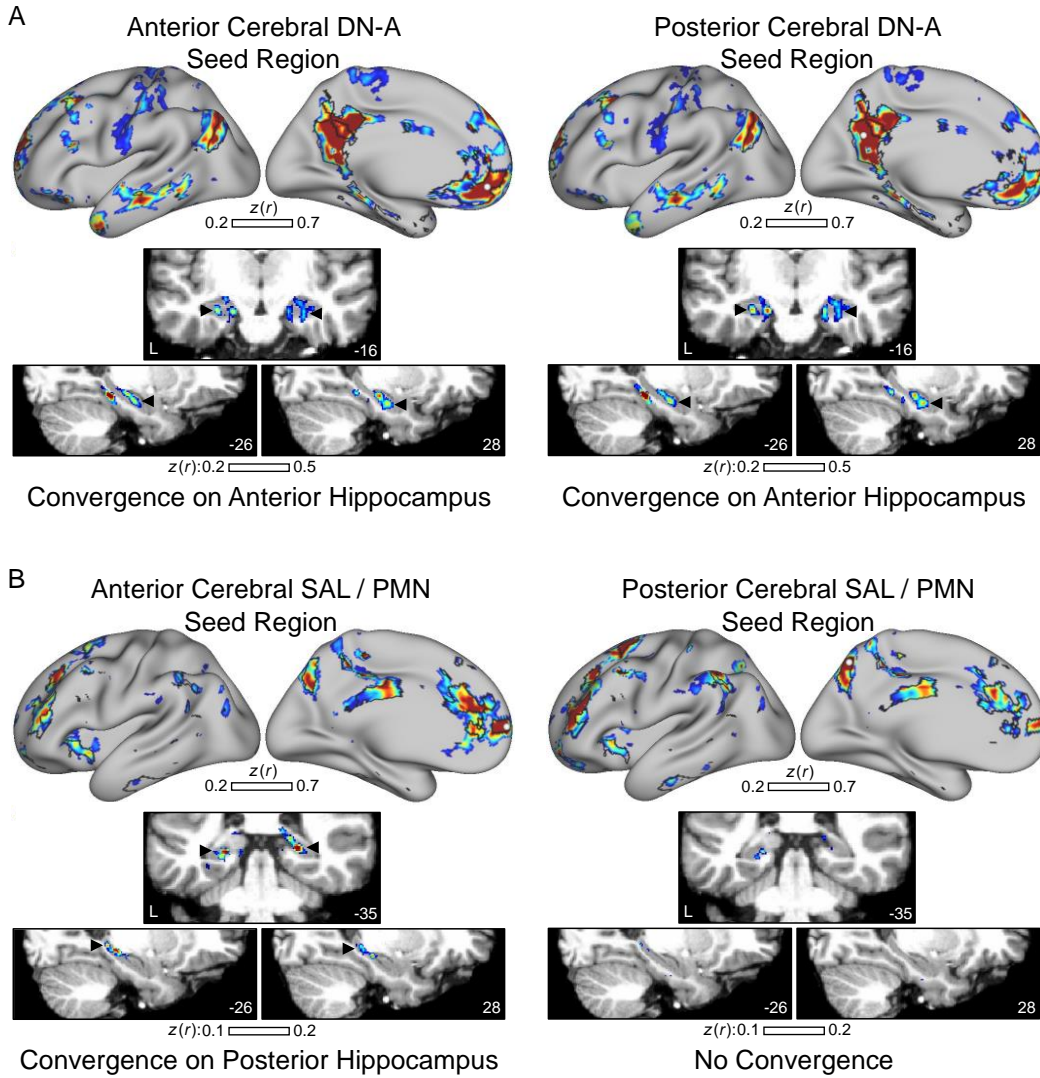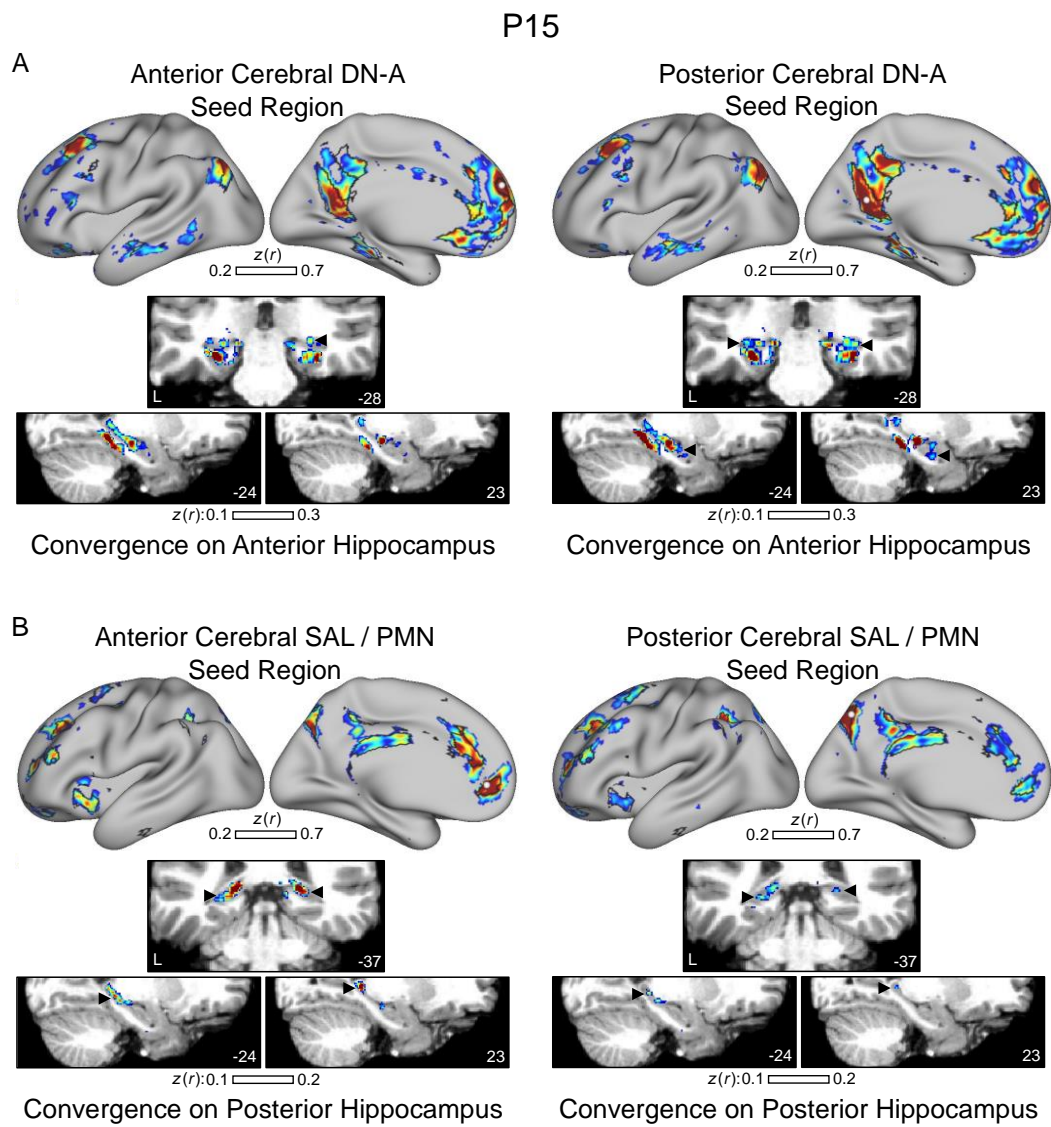Seed Region

Convergence on Posterior Hippocampus

Figure A.8 Seed based functional connectivity, Experiment 2 Participant P13

Figure A.9 Seed based functional connectivity, Experiment 2 Participant P14

Figure A.10 Seed based functional connectivity, Experiment 2 Participant P15